University of Alberta

EFFICIENT PERFORMANCE EVALUATION TECHNIQUES FOR DESIGN OF WIRELESS COMMUNICATIONS SYSTEMS

by

Pavel Loskot

A thesis submitted to the Faculty of Graduate Studies and Researcher in partial fulfillment of the requirements for the Degree of Doctor of Philosophy

Department of Electrical and Computer Engineering

Edmonton, Alberta

Spring 2008

Your file Votre référence
ISBN: 978-0-494-45559-3
Our file Notre référence
ISBN: 978-0-494-45559-3

Abstract

The ultimate goal in analysis of communications systems is to predict the performance of real communications systems as accurately and efficiently as possible in order to reduce the cost of the system development. However, there is a trade-off between accuracy and the time and effort required to obtain the performance estimate. Accurate performance prediction often requires complex system models that are, in general, difficult to analyze. Hence, if the efficiency of the performance evaluation techniques can be improved, then more complex system models can be analyzed and more accurate performance prediction is obtained. Also, for a given system model complexity, more efficient performance evaluation makes the analysis less complicated, and, in turn, such analysis is more likely to provide design guidelines, and support synthesis. Therefore, efficient performance evaluation techniques are always of high practical importance and interest.

In this thesis, performance evaluation techniques that improve efficiency of the existing techniques are proposed and investigated. The focus is on the efficient evaluation of the bit-error rates of wireless communications systems. The thesis can be divided into two parts. In the first part, novel performance evaluation techniques are proposed. Sample rejection is studied as a generally applicable and easy-to-implement computer simulation technique. Prony approximation is used for efficient semi-analytical evaluation of the average error rates of digital modulations over slowly fading channels. Channel models to simplify the analysis of diversity combining schemes over correlated fading channels are also investigated. In the second part, the proposed performance evaluation

techniques are employed to analyze the performance of several communication systems, and, in some cases, novel design guidelines are obtained. Particularly, coded MIMO-OFDM systems over arbitrary correlated generalized Ricean fading channels are analyzed. Binary Hamming codes are constructed recursively, and it is shown that their coding gain is not monotonic in signal-to-noise ratio. A class of multidimensional binary repetition codes having variable block length and variable minimum Hamming distance is proposed, and the applications are considered. Finally, a hypergeometry of objects in K dimensions is investigated. The results of hypergeometry are then used to optimize the signal-to-noise ratio adaptive receivers.

To my parents

Acknowledgment

I am especially grateful to my thesis supervisor Dr. Norman C. Beaulieu for giving me the opportunity to perform the research under his guidance. Clarity of my presentation, and scholarship rigorousness of my work improved enormously with his advice and valuable comments. My research would not be possible without the excellent research environment established in the *i*CORE Wireless Communication Laboratory.

I am indebted to Dr. John R. Barry from Georgia Institute of Technology, Atlanta, for his willingness to read my thesis and be an external examiner. His thorough proofreading provided further valuable insights into several problems considered in this thesis.

I would like to thank to all other members of my committee, namely Dr.'s Robert Fedosejevs, Chintha Tellambura, Doug Wiens, Hai Jiang and Sergiy Vorobyov.

I also want to express my thanks to Sharon Walker from *i*WCL for her help and support.

I appreciate the true friendship of Amir Rabiei and Tim Poon from *i*WCL. At all times, Amir has always been encouraging and supporting. Tim introduced me to the Canadian culture of tolerance and support, and he has always been ready to help.

I would like to mention my former colleagues and friends from Finland, Marcos Katz and Reijo Savola, currently with VTT, Technical Research Centre of Finland, and Kari Horneman and Roman Pichna from Nokia Siemens Networks. We had many fruitful discussions, and they provided me with industrial feedback on my research.

Lastly, I would like to thank my parents for their endless patience and many years of support.

This work was supported by the Alberta Ingenuity Scholarship and the *i*CORE Graduate Studentship which is greatly appreciated.

Contents

List of Figures

List of Tables

List of Acronyms

1D	one-dimensional
2D	two-dimensional
2G	2nd generation
3D	three-dimensional
3G	3rd generation
4G	4th generation
AF	amplify-and-forward
AMR	adaptive multirate
AP	access point
APP	a posteriori probability
AWGN	additive white Gaussian noise
BCH	Bose, Ray-Chaudhuri, Hocquenghem
BER	bit error rate
BICM	bit-interleaved coded modulation
BPSK	binary phase-shift keying
BRC	binary repetition code
BS	base station
BSC	binary symmetric channel
cBPSK	coherent BPSK
CC	convolutional code
CDF	cumulative distribution function
CDP	codeword decoding probability
CHF	characteristic function
CRC	cyclic redundancy check

DBPSK	differential BPSK
DCS	diversity combining scheme
DF	decode-and-forward
DMC	discrete memoryless channel
EGC	equal gain combining
FD	feedback decoding
FEC	forward error correction, forward error control
FER	frame error rate
FIR	finite impulse response
GCQ	Gauss-Chebyshev quadrature
GF	Galois field
GSM	global system for mobile communications
HS/MRC	hybrid selection/maximum ratio combining
ICI	intercarrier-interference
IID	independent and identically distributed
IOWE	input-output weight enumerator
IRWE	input-redundancy weight enumerator
IS	importance sampling
ISI	intersymbol interference
LDPC	low density parity check
LLR	long-likelihood ratio
LUT	look-up table
MC	Monte Carlo
mFD	modified feedback decoding
MAP	maximum a posteriori
MGF	moment generating function
MIMO	multiple-input multiple-output
ML	maximum-likelihood
MLSD	maximum-likelihood sequence decoding
MRC	maximum ratio combining
MT	mobile terminal
mtVA	modified truncated Viterbi algorithm

nBPSK	noncoherent BPSK
OFDM	orthogonal frequency division multiplexing
PAM	pulse amplitude modulation
PCC	principal components combining
PDF	probability density function
PEP	pairwise error probability
PER	packet error rate
PMF	probability mass function
PSK	phase-shift keying
QAM	quadrature amplitude modulation
RMS	root mean square
RV	random variable
SC	selection combining
SD	sphere decoding
SER	symbol error rate
SISO	single-input single-output, soft-input soft-output
SNR	signal-to-noise ratio
SPC	single parity check
SPCPC	SPC product code
SR	sample rejection
SS	subscriber station
STBC	space-time block code
STC	space-time code
SUI	Stanford University Interim
SVD	singular value decomposition
tVA	truncated Viterbi algorithm
TPC	turbo product code
UB	union bound
VA	Viterbi algorithm
WSS	wide-sense stationary

List of Symbols

$\lvert\cdot\rvert$	absolute value, cardinality of the set
$\lfloor\cdot\rfloor$	floor function
$\lceil\cdot\rceil$	ceil function
$\lfloor\cdot\rceil$	rounding function
$(\cdot)!$	factorial
$(\cdot)^*$	complex conjugate of a complex number
$\varnothing$	empty set
$\otimes$	Kronecker matrix product
$\odot$	Hadamard matrix product
$\oplus$	modulo 2 summation
$\mathbf{0}$	all-zero matrix or vector
$\mathbf{1}$	all-ones matrix or vector
$\mathbf{A}, \mathbf{a}$	matrix, column vector
$\mathbf{A}^\dagger$	matrix pseudoinverse
$\mathbf{A}^H, \mathbf{a}^H$	matrix and vector conjugate transpose
$\mathbf{A}^T, \mathbf{a}^T$	matrix and vector transpose
$\lVert\mathbf{A}\rVert$	Frobenius norm of the matrix $\mathbf{A}$
$\lVert\mathbf{a}\rVert$	Euclidean norm of the vector $\mathbf{a}$
$\lVert\mathbf{a}\rVert_p$	p-th vector norm of the vector $\mathbf{a}$
$a^{\mathbf{b}}$	column vector $(a^{b_0}, a^{b_1}, \cdots)^T$ where $\mathbf{b} = (b_0, b_1, \cdots)^T$
$a \vert b$	a divides b
$\binom{a}{b}$	binomial coefficient
$\arg(\cdot)$	argument of a complex number
$\mathbb{C}$	set of complex numbers

$\mathscr{C}$	code, codebook
$\mathrm{cov}[\cdot]$	covariance
d	differential
dB	decibel
d_{e}	Euclidean distance
$\det(\mathbf{A})$	determinant of the matrix $\mathbf{A}$
$\mathrm{diag}(\mathbf{A})$	column vector of the diagonal elements of the matrix $\mathbf{A}$
$\mathrm{diag}(\mathbf{a})$	diagonal matrix having diagonal elements $\mathbf{a}$
$d_{\min}$	minimum Hamming distance
$\mathrm{dom}(\cdot)$	domain
$\mathrm{E}[\cdot]$	expectation
e	$2.7182818284\ldots$
E_b	average energy per bit
$\mathrm{erfc}(\cdot)$	complementary error function
E_s	average energy per symbol
$\eta(\cdot)$	Heaviside step function
$\mathrm{etr}\{\cdot\}$	exponent trace
${}_nF_m(\cdot,\cdots,\cdot)$	hypergeometric function
$F_X(x)$	CDF of the random variable X
$f_X(x)$	PDF of the random variable X
$\Gamma(\cdot)$	Gamma function
$\gamma_b = E_b/N_0$	SNR per bit
$\mathrm{GF}(2)$	binary Galois field
$\mathbf{I}$	identity matrix
$\mathrm{Im}\{\cdot\}$	imaginary part of a complex number
$I_n(\cdot)$	n-th order modified Bessel function of the first kind
$\mathrm{j} = \sqrt{-1}$	imaginary unit
$\mathcal{L}$	log-likelihood function
l_p	p-th vector norm
λ	eigenvalue, likelihood ratio
$\mathrm{mod}_a(b)$	b modulo a
N_0	noise one-sided power spectral density

$\mathcal{O}$	complexity
$\Phi_X(t)$	MGF of the random variable X
$\phi_X(t,x)$	upper incomplete MGF of the random variable X
π	$3.1415926535\ldots$
$\Pr(\cdot)$	probability
$Q(\cdot)$	Q-function
$Q_n(\cdot,\cdot)$	n-th order Marcum Q-function
$\mathbb{R}$	set of real numbers
R	code rate
$\mathrm{Re}\{\cdot\}$	real part of a complex number
σ_w^2	noise variance
$\mathrm{sign}(\cdot)$	signum function
$\mathrm{tr}\{\mathbf{A}\}$	trace of the matrix $\mathbf{A}$
$\mathrm{var}[\cdot]$	variance
$\mathrm{w_H}(\cdot)$, $\mathrm{w_H}(\cdot,\cdot)$	Hamming weight, Hamming distance
$\mathbb{Z}$	set of integers
$\mathbb{Z}_Q$	set $\{0,1,\cdots,Q-1\}$

Chapter 1

Introduction

"Nothing is as practical as a good theory."

Kurt Lewin

The Ph.D. research project described in this thesis has been motivated by the following facts.

- In spite of more than ten years of intensive research and development of the 3rd generation (3G) cellular systems, and having skills and knowledge obtained from building the immensely successful 2nd generation (2G) cellar network, deployment of the 3G cellular networks experienced serious technical difficulties.
- Many algorithms and technical solutions have been proposed for the 4th generation (4G) cellular systems. However, only a small subset of the proposed algorithms and solutions can be included in the 4G standards; their selection requires extensive performance evaluations.
- Robert Lucky commented in [1] that "...without a grounding of reality supplied by industry, academic papers can tend to drift off into imaginary spaces."
- In the Kailath Lecture and Colloquium [2], Robert Gallager suggested that, "Universities, governments, and industries should encourage more Shannon style research. It is focused on simplification."

Each fact has its own merits, however, all four facts have a common focus. In particular, many technical difficulties in deploying the 3G cellular networks could have been prevented if more complex system models had been used for prediction of the system performance. Design of the 4G networks

could be improved if the performance of larger number of system configurations can be evaluated and compared. Also, performance evaluation techniques that are sufficiently simple, and, at the same time, can accurately predict the performance of communications systems are helpful to bridge the gap between academia and industry. Hence, in this thesis, efficient performance evaluation techniques that can improve prediction of the performance of communications systems are investigated. Noteworthy, the keyword 'efficient' is now frequently appearing in the literature. In general, efficiency becomes important whenever the available resources are limited. In this thesis, efficiency is related to the difficulty in obtaining a performance estimate of given accuracy. Thus, efficiency can be expressed in terms of the time and effort required to obtain the performance estimate of given accuracy. Efficient performance evaluation is then developed to complement the research in efficient signal processing where efficiency corresponds to the implementation complexity of algorithms. Note also that, in this thesis, complexity is used in two contexts. First, it is required that the complexity of performance evaluation techniques is reduced, so that the performance analysis is simplified and is more easily applicable. Second, it is desirable to consider more complex system models in order to model the real systems more accurately.

Furthermore, in order to clarify "theoretical" and "practical" research, consider Fig. 1.1; this figure is inspired by the cover page of book [3]. The top most level of the pyramid in Fig. 1.1 corresponds to the most general theory of information transmission [4]. The lowest level of the pyramid in Fig. 1.1 represents actual implementation of the communication system in hardware. Hence, moving from a general theory towards hardware implementation requires that the communication system is described using more specific (i.e., less general) system models of increasing complexity having larger number of parameters, and being more difficult to analyze.

1.1 Background and Research Area Identification

Rapid development of technology over the past 100 years led our society to information revolution in the break of the twenty first century. Acquired knowledge and understanding of diverse natural phenomena enabled manufacturing of sophisticated technological systems. Given the complex nature of today's technical devices, the system design has become more challenging than ever before. The system design requires various levels of abstraction of the system description. Such abstraction is referred to as the system model. The system is then described using the system model inputs, outputs, and the state space of latent (hidden) variables often referred to as the system model pa-

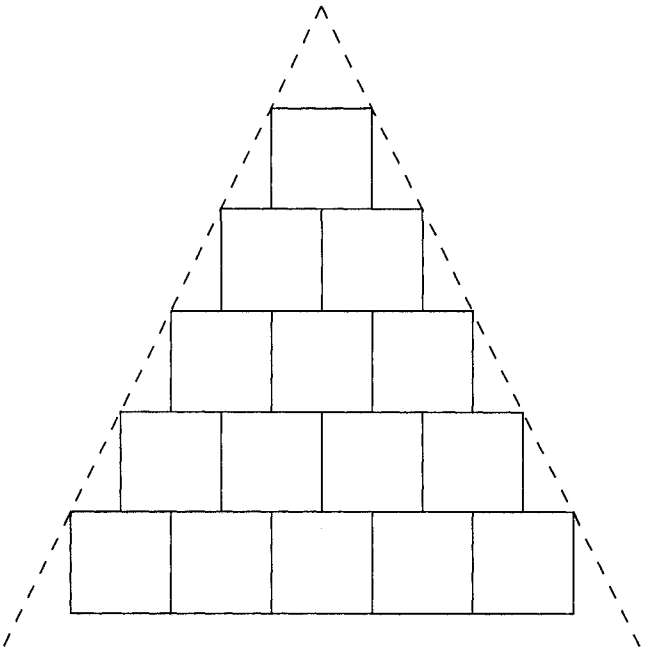

Figure 1.1: "Theoretical" versus "practical".

rameters. Assumptions are considered to be a part of the system model, and they represent the system model constraints (limitations). In general, improving the performance of any system appears to be directly related to the system (model) dimensionality; for example, the number of system inputs and outputs can be increased to improve the system performance. The systems are then described using the system models of large dimension and large number of parameters; this, in turn, significantly complicates the system design and analysis. Therefore, technological progress must be accompanied by advancements of designing methods that are suitable for system models of large dimension.

A general system design process is shown in Fig. 1.2. The design process is usually performed in two design cycles. The upper design cycle corresponds to iterative modifications of the initial design until the desired performance can be expected. In the lower design cycle, a prototype is synthesized, and implemented in hardware. The prototype is then operated in a series of field tests to determine its real performance. If the real performance of the prototype does not meet the design requirements (i.e., the desired performance), the design process must resume with further modifications of the design, and estimation of its performance in the upper design cycle. Note that the upper cycle can be used not only to design a system having the desired performance, but also, it can be used to optimize the system performance (i.e., to achieve the best possible performance for

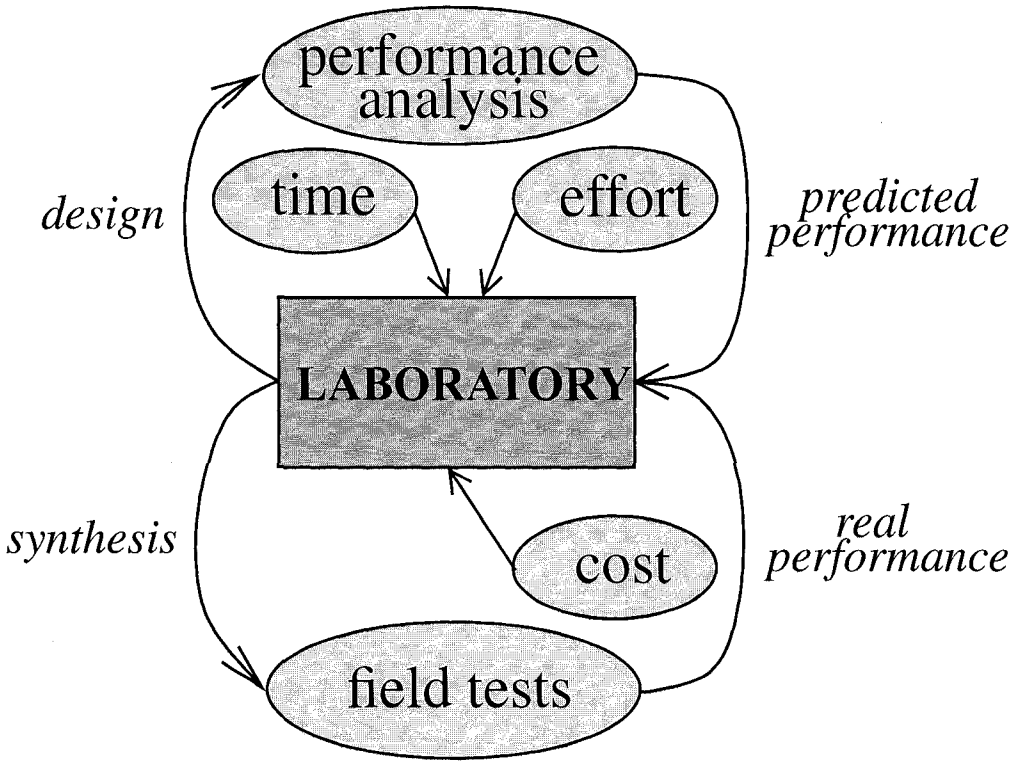

Figure 1.2: A general process of system design.

given design constraints).

The time, effort and cost are the three main resources that are being consumed during the design process until a prototype of the desired performance has been obtained. The more cycles in Fig. 1.2 are enclosed during the design process the more resources have been consumed. Since majority of the resources are consumed when the hardware implementation of the prototype has to be modified, it is desirable to confine the design process to the upper design cycle as much as possible. Avoiding unnecessary lower design cycles makes the design process much more efficient, and thus, less resources demanding. Correspondingly, the lower design cycles can be avoided if the performance analysis obtained in the upper design cycle is sufficiently accurate, i.e., the predicted performance is a good approximation of the real performance.

The relative error of the performance analysis can be defined as,

$$\text{'analysis error'} = (\text{'predicted performance'} - \text{'real performance'}) \Big/ \text{'real performance'}$$

and the relative accuracy of the performance analysis can be defined as,

$$\text{'analysis accuracy'} = 1 \Big/ \text{'analysis error'}.$$

Thus, more accurate prediction of the real system performance requires smaller number of lower design cycles, and less resources are going to be consumed.

There are three categories of the performance evaluation techniques.

- mathematical and statistical theoretic analysis
- computer simulations
- semi-analytical methods

The semi-analytical methods are combination of mathematical analysis and computer simulations. Selection of the performance evaluation technique depends on the particular system being investigated. The following factors have to be considered.

- required accuracy, e.g., the value of the target probabilities to be estimated
- required efficiency, e.g., the total time and effort available to evaluate the performance
- amount of knowledge about the system and its model
- the system model complexity

These factors are interrelated by the following rules.

- there is a trade-off between accuracy and efficiency of the performance analysis, i.e., more time and effort is required to obtain more accurate analysis
- more efficient performance evaluation techniques allow more complex, and thus, more realistic system models to be investigated
- more realistic system models improve accuracy of the performance prediction

For example, realistic modeling of communications systems requires that the system model takes into account subsystems interdependence, various sources of interference, non-ideal synchronization, finite precision numbers representation, non-ergodic observations etc.

Analytical tools are usually applicable only when the system model is simplified and some realistic assumptions are omitted. In some cases, analytical approach can be useful to obtain initial design guidelines. More realistic system models are often mathematically intractable which necessitates computer simulation. However, the system model complexity can exceed the computing power available, and the simulation run-times become excessive. In this case, more efficient computer simulation techniques must be used. Provided that some parts of the system model can be described analytically, semi-analytical methods achieve good trade-off between accuracy and efficiency, since significant amount of computations can be avoided to reduce the simulation run-times.

In general, the performance analysis should have the following properties.

- be accurate to predict the real performance
- be efficient to minimize the resources consumed
- be verifiable, so that it can be reproduced
- be trustable, so that it has a high level of confidence

Hence, performance analysis should be as simple as possible, and also, be sufficiently generic in order to be applicable to a variety of scenarios and system models. For example, a minor change in the assumptions or the parameters should be readily incorporated without major changes in the existing performance analysis. Furthermore and importantly, performance analysis that is sufficiently simple and generic can often provide design guidelines for system synthesis. On the other hand, complicated performance analysis is more likely to be incorrect, and such analysis is also more difficult to be verified, and even reproduced for the same system model under the same assumptions.

The probability of error and the error rate are the two performance measures primarily considered in this thesis. Whether the transmitted bits, symbols or sequences of symbols and the corresponding probabilities of bit, symbol and sequence of symbols error, respectively, are investigated in the performance analysis of a communication system is application dependent. Provided that the observations of bits, symbols or sequences and occurrences of their errors at the receiver are ergodic, the probability of a particular error is defined as,

$$\text{'probability of error'} = \mathrm{E}[\text{'error'}]$$

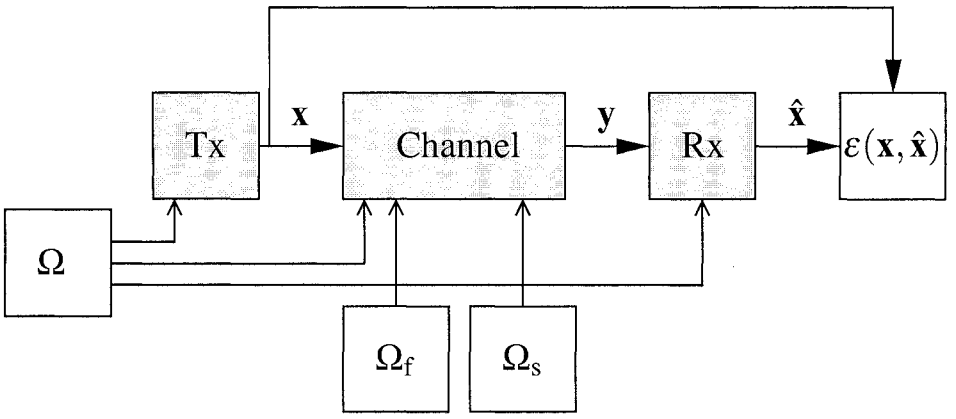

Figure 1.3: A generic transmission system and the error rate measurement.

where E[·] denotes expectation, and E['error'] is expectation of a particular error event where

$$\text{'error'} = \begin{cases} 1 & \text{transmission error occurred} \\ 0 & \text{transmission error did not occur.} \end{cases}$$

The error rate is defined as the ratio,

$$\text{'error rate'} = \frac{\text{'number of error occurrences'}}{\text{'total number of occurrences'}}.$$

Hence, the error rate corresponds to the average probability of error. If the probability of bit error and symbol error in the transmitted sequence is independent of a particular location of the bit and the symbol in the transmitted sequence, the probability of bit and symbol error is equal to the bit error rate (BER) and symbol error rate (SER), respectively. The probability of sequence of symbols error is always equal to the sequence error rate, and it is referred to as the frame error rate (FER) or the packet error rate (PER).

A generic transmission system and the measurement of the transmission error rate are shown in Fig. 1.3. The transmitted bits, symbols or sequences, $\mathbf{x}$, are transformed by the channel into the received bits, symbols or sequences, $\mathbf{y}$. The receiver outputs the decisions, $\hat{\mathbf{x}}$, on the transmitted bits, symbols or sequences. In general, properties of the transmission systems are described using three sets of system model parameters. The symbol, Ω, is used to denote the set of fixed (time-invariant) parameters. The channel parameters changing slowly compared to a symbol duration are denoted as Ω_s. The set, Ω_f, contains the parameters having the rate of change comparable to the

symbol duration. Then, the received signal can be written as,

$$\mathbf{y} = \mathbf{y}\left(\mathbf{x}, \Omega, \Omega_{\mathrm{s}}, \Omega_{\mathrm{f}}\right).$$

Note that the transmitted signal, $\mathbf{x}$, is a function of Ω, i.e., $\mathbf{x}(\Omega)$. The decision, $\hat{\mathbf{x}}$, is a function of the received signal and the receiver, i.e., $\hat{\mathbf{x}} = \hat{\mathbf{x}}(\mathbf{y}) = \hat{\mathbf{x}}(\mathbf{x}, \Omega, \Omega_{\mathrm{s}}, \Omega_{\mathrm{f}})$. An error event occurs when the receiver decides erroneously about the transmitted bit, symbol or sequence of symbols. Provided that the parameters, Ω_{s}, and, Ω_{f}, are ergodic and stationary processes, the first-order moment of the random error-event is typically considered to be sufficient description of the system error properties. Let $\epsilon(\mathbf{x}, \hat{\mathbf{x}})$ be an error event that the decision, $\hat{\mathbf{x}}$, is not equal to $\mathbf{x}$; thus, $\epsilon(\mathbf{x}, \hat{\mathbf{x}}) = \epsilon(\mathbf{x}, \Omega, \Omega_{\mathrm{s}}, \Omega_{\mathrm{f}})$, and $\epsilon = 1$, if $\mathbf{x} \neq \hat{\mathbf{x}}$, and $\epsilon = 0$, otherwise. Then, the conditional probability of error event, conditioned on realization of the transmitted sequence, $\mathbf{x}$, and the parameters, Ω_{s}, is defined as,

$$\mathrm{P}_{\epsilon}(\Omega|\mathbf{x}, \Omega_{\mathrm{s}}) = \int_{\mathrm{dom}(\Omega_{\mathrm{f}})} \epsilon(\mathbf{x}, \Omega, \Omega_{\mathrm{s}}, \Omega_{\mathrm{f}})\, f_{\Omega,\Omega_f}(\Omega, \Omega_{\mathrm{f}})\, \mathrm{d}\Omega_{\mathrm{f}}$$

where $\mathrm{dom}(\cdot)$ denotes the domain of its argument, and $f_{\Omega,\Omega_f}(\Omega, \Omega_{\mathrm{f}})$ is the joint probability density function (PDF) of Ω and Ω_{f}. The conditional error rate corresponds to the average conditional probability of error event, i.e.,

$$\mathrm{P}_{\epsilon}(\Omega|\Omega_{\mathrm{s}}) = \sum_{\mathbf{x}} \mathrm{Pr}(\mathbf{x})\, \mathrm{P}_{\epsilon}(\Omega|\mathbf{x}, \Omega_{\mathrm{s}})$$

where $\mathrm{Pr}(\mathbf{x})$ is the probability of transmitting $\mathbf{x}$. Correspondingly, the average probability of the error event is,

$$\bar{\mathrm{P}}_{\epsilon}(\Omega|\mathbf{x}) = \int_{\mathrm{dom}(\Omega_{\mathrm{s}})} \mathrm{P}_{\epsilon}(\Omega|\mathbf{x}, \Omega_{\mathrm{s}})\, f_{\Omega,\Omega_s}(\Omega, \Omega_{\mathrm{s}})\, \mathrm{d}\Omega_{\mathrm{s}}$$

where $f_{\Omega,\Omega_s}(\Omega, \Omega_{\mathrm{s}})$ is the join PDF of Ω and Ω_{s}, and the average error rate is evaluated as,

$$\bar{\mathrm{P}}_{\epsilon}(\Omega) = \sum_{\mathbf{x}} \mathrm{Pr}(\mathbf{x})\, \bar{\mathrm{P}}_{\epsilon}(\Omega|\mathbf{x}).$$

1.2 Thesis Outline

This thesis consists of nine chapters. Introductory Chapter 1 is followed by seven chapters where the main contributions of the thesis are presented. The thesis outcomes and results are summarized and suggestions for future work are given in Chapter 9.

The seven chapters of the main contributions can be divided into two parts. The first part is covered by Chapter 2–Chapter 4, and it introduces novel performance evaluation techniques that improve the performance analysis, so that the analysis becomes simpler, and more efficient. Some of the proposed efficient performance evaluation techniques are employed in the second part which consists of Chapter 5–Chapter 8. Furthermore, in the second part, novel design guidelines and principles are obtained. In particular, a sample rejection (SR) technique for efficient Monte Carlo (MC) computer simulations is proposed in Chapter 2. The SR simulation technique is also used in Chapter 7 to estimate the minimum Hamming distance, and to simulate the bit error rate of the proposed codes. Prony and polynomial approximations for semi-analytical evaluation of the average error rates over slowly fading channels are investigated in Chapter 3. The Prony approximation method is then used in chapters 4–7 to evaluate the average error rates. Channel models that can simplify the performance analysis of diversity combining receivers having correlated fading branches are considered in Chapter 4. In Chapter 5, coded multiple-input multiple-output orthogonal frequency division multiplexing (MIMO-OFDM) systems over arbitrary correlated generalized Ricean fading channels are analyzed. Binary Hamming codes are studied in Chapter 6. Binary repetition codes in multiple dimensions are proposed and analyzed in Chapter 7. Finally, a hypergeometric view on diversity combining schemes and the optimum receiver dimension are considered in Chapter 8.

In general, the problem background and literature survey are provided at the beginning of each chapter. The problems are formulated as general as practically possible. Then, the system model is presented, and the problem is solved using mathematical theoretic analysis. It is followed by numerical examples to illustrate the solution. The main results are summarized and discussed at the end of each chapter.

In the sequel of this subsection, the contents of Chapters 2–8 are outlined.

Chapter 2 In the first part of this chapter, we reexamine sample rejection (SR) introduced previously as an easy-to-implement efficient simulation technique. Since the decoding operation often represents a major part of the required simulation time, SR can be used to avoid decoding of the received sequences that are known beforehand to be decoded error-free. Previous work seems to indicate that SR may be effective only for simulations having small dimension, less than 10. We assume estimation of decoded bit-error probabilities for a general coding scheme of finite block-length transmitted over an additive white Gaussian noise (AWGN) channel with quantized output using binary antipodal signaling and maximum-likelihood sequence decoding (MLSD). We show

that knowledge of the minimum Hamming distance of the code and conditioning on the transmitted sequence can be exploited to form the rejection regions. In particular, we investigate hypersphere, hypercube and hyperquadrant rejection regions. Our analysis shows that SR can be effective for some systems with dimension of the order of hundreds with soft-decision decoding, and some systems with dimension more than a thousand with hard-decision decoding if the rejection regions are properly chosen.

In the second part of Chapter 2, we generalize a SR scheme for the simulation of multidimensional communication systems. We consider the use of SR for efficient simulation of uncoded continuous transmission with periodic trellis-termination over static intersymbol interference (ISI) channels and MLSD. The hypersphere, hypercube and hyperquadrant rejection regions proposed in the first part of Chapter 2 are applicable only for finite lattices with rectangular or circular symmetries and moderate dimension. However, these regions are not applicable or are inefficient if the dimension is increased for large block-lengths, or if the lattice symmetries are absent because of the ISI. Hence, we investigate sliding-window near-MLSD to resolve the dimension problem. In particular, we study the truncated Viterbi algorithm (tVA) and feedback decoding (FD). We propose several modifications to these two algorithms using SR principles to improve the simulation efficacy for the conventional Viterbi algorithm (VA) while achieving near MLSD performance. Finally, numerical examples confirm that FD and its modifications can be more efficient for simulations of ISI channels and near-MLSD than the VA.

Chapter 3 We propose a novel remarkably simple semi-analytical method for evaluation of the average probability of transmission error for digital communication systems operating over slowly fading channels. The proposed method applies a sum of exponentials fit known as the Prony approximation to the conditional probability of error. Hence, knowledge of the moment generating function (MGF) of the instantaneous signal-to-noise ratio (SNR) at the detector input can be used to compute the average probability of error. Numerical results show that knowledge of the conditional probability of error at only a small number of points, and the sum of only two exponentials are sufficient to achieve very high accuracy; the relative approximation error of the exact average probability of error is less than 6% in most of the cases considered. Furthermore, we investigate a piecewise polynomial approximation of the conditional probability of error as an alternative to the sum of exponentials fit. In this case, knowledge of the partial moments of the instantaneous SNR at the detector input, or equivalently, knowledge of the derivatives of the incomplete MGF can be

used to obtain the average probability of error. Numerical results indicate that in order to achieve good accuracy, the method based on the polynomial approximation requires that the product of the polynomial degree and the number of approximation sub-intervals are much larger than, 10.

Chapter 4 We investigate the average BER performance of one-stage and two-stage diversity combining schemes (DCS's) operating over correlated fading channels. We consider two channel models that can significantly simplify the performance analysis of DCS's in correlated fading. In particular, a linear correlation channel model having equal branch variances can be decorrelated at the receiver, so that the branches become independent. We show that, in general, employing diversity combining schemes for decorrelated or orthogonalized branches can recover some of the diversity gain lost due to the branch correlations. This is observed, for example, for the case of hybrid selection/maximum ratio combining (HS/MRC) operating over decorrelated and orthogonalized non-zero mean Gaussian fading channels. Furthermore, we propose a fading amplitude channel model assuming vector norm superposition of the impinging plane waves. This channel model is well-suited for the performance analysis of MRC and equal gain combining (EGC) diversity schemes operating over correlated fading channels. The average BER of DCS's are evaluated analytically using the Prony approximation method and using computer simulation.

Chapter 5 We establish a framework for analyzing the performance of coded MIMO-OFDM systems operating over arbitrary correlated generalized Ricean fading channels. We investigate orthogonal space-time block codes (STBC's), and transmitter beamforming to maximize SNR at the detector. We derive the MGF of the SNR at the input to the channel decoder assuming correlated transmitter and receiver antennas and correlated paths in frequency selective channels. We apply the MGF method to obtain the probability of outage, the pairwise error probability (PEP), and the BER. We also derive diversity gain and coding gain for the systems being considered. Furthermore, we prove that the rank and determinant design criteria for space-time-frequency block coding are valid for the exact PEP. We assume bit-interleaved and iteratively decoded turbo product codes, Gray encoded M-ary quadrature amplitude modulation (QAM), and other parameters of the IEEE 802.16 Standard to illustrate numerical results. Finally, we confirm that Prony approximation is a numerically efficient fading averaging method with excellent accuracy.

Chapter 6 We show that binary Hamming codes can be constructed recursively. The recursive structure is used to efficiently enumerate the input-output weights. Hence, the BER of binary Hamming codes with antipodal signaling and hard-decision demodulation used on AWGN channels can

be evaluated exactly. Furthermore, the numerically computed coding gain of Hamming codes reveals a surprising fact that the coding gain is not monotonically increasing with signal-to-noise ratio.

Chapter 7 In the first part of this chapter, we construct a family of linear binary block codes from ordinary block repetition codes using cyclic shifts of the input information bits. Such codes have variable block length and variable minimum Hamming distance and are referred to as improved binary repetition codes (IBRC's). We study the properties of binary cyclic matrices, and then, extend the code construction employing cyclic shifts of binary codewords in multiple dimensions. We consider two design criteria for multidimensional IBRC's assuming the code constraint length and constraint weight. An efficient algorithm to search for good codes is presented. The construction is illustrated using examples of the proposed IBRC's in one, two and three dimensions. Applications of the proposed codes are considered and their BER performance is analyzed using a union bound (UB). In particular, we show that the IBRC's are good candidates for adaptive coding, turbo product coding, retransmission and multihop routing, and block differential encoding. Also, multidimensional IBRC's are shown to be well-suited as an inner encoding scheme for concatenated one-dimensional outer codewords to increase their minimum Hamming distance without increasing the transmission bandwidth. A non-recursive block differential encoder is found to arbitrarily increase the code rate with the block length while the minimum Hamming distance of the code remains constant. Finally, we use a UB on the BER to optimize the transmission energy distribution over the codewords to improve the transmission reliability.

In the second part of Chapter 7, we consider further applications of IBRC's. In particular, we investigate a network consisting of an access point and N terminal nodes. We propose a three stage network protocol for uplink and downlink packet transmission. The proposed network protocol implements coded and cooperative diversity to improve packet transmission reliability and extend network coverage. In Stage 1 of the protocol, a cyclic redundancy check (CRC) code is used to detect erroneous packets. IBRC's and single parity check (SPC) codes are used in Stage 2 to obtain coding gain for forward diversity. Node cooperation in Stage 3 provides additional coding and diversity gains, and it is implemented using random SPC's distributed across the nodes. We evaluate the PER for specific network realizations assuming coherent and non-coherent binary modulation schemes over Gaussian channels with attenuation of the transmitted signals determined by the free-space path loss. We use a link budget analysis to calculate the receiver SNR for a given distance

between the transmitter and receiver antennas, and also, to evaluate the network coverage. We then optimize the transmitter powers for IBRC's to improve their PER. We also show using numerical examples that the network coverage for a target value of the PER is improved in all three protocol stages. Finally, we observe that the cooperation gains are strongly dependent on the particular network realization and less on the number of cooperating nodes.

Chapter 8 In general, many practical problems involve K-dimensional entities. Such entities can be described using a hypergeometry of objects in K dimensions. Hence, in this chapter, we consider a hypergeometry of objects in K dimensions, and then, we use the results of hypergeometry to optimize multidimensional receivers. In particular, we study the K-dimensional sphere, polytope, cube, scaled polytope and the scaled cube. We prove that the volume and the surface area of these objects reach a maximum for a particular value of dimension, and then, decrease towards zero. We obtain the dimension corresponding to the maximum volume and to the maximum surface area as a function of the radius. We also show that the p-norm of a vector in K dimensions is monotonically increasing in K, and monotonically decreasing in p. The general results of hypergeometry are then used to optimize SNR adaptive receivers employing a bank of subchannel detectors and employing a K branch diversity combining front-end. We also use the results of hypergeometry to prove that the average performance measures of detectors operating over erasure subchannels reach a maximum for a particular dimension and SNR partitioning. Theory and numerical examples confirm that the average probability of error corresponding to a particular subchannel, the probability of selecting a particular subchannel, and the information theoretic average subchannel capacity are maximized for a particular value of dimension. Finally, we show that the results of hypergeometry are relevant for determining an optimum number of receiver antennas and overall receiver complexity.

1.3 Thesis Contributions

In this subsection, thesis contributions are listed chapter by chapter.

Chapter 2

- Sample rejection is established as an easy-to-implement computer simulation technique for coded systems operating over quantized AWGN channels and ISI channels.
- Hypersphere, hypercube and hyperquadrant are proposed as the rejection regions well-suited for efficient simulations of coded systems over quantized AWGN channels.

- Sliding-window FD is modified using SR principles and is shown to be more efficient for simulations of ISI channels and near-MLSD than the VA.

Chapter 3

- The Prony approximation method is proposed as a remarkably simple semi-analytical technique for evaluation of the average probability of transmission error for digital communication systems operating over slowly fading channels.
- The Prony approximation method is shown to be a generalization of the Chernoff bound and the MGF method.
- A piecewise polynomial approximation of the conditional probability of error is investigated as an alternative to Prony approximation.

Chapter 4

- It is shown that decorrelation and orthogonalization of branches prior to employing DCS's can recover some of the diversity gain lost due to the branch correlations. This is observed, for example, for the case of HS/MRC operating over decorrelated and orthogonalized non-zero mean Gaussian fading channels.
- The performance analysis of DCS's operating over correlated fading channels can be greatly simplified if a linear correlation channel model having equal branch variances is decorrelated prior to employing diversity combining since the branches become independent.
- A fading amplitude channel model assuming vector norm superposition of the impinging plane waves is proposed. Such channel model can greatly simplify the performance analysis of DCS's having correlated fading branches.

Chapter 5

- The turbo product coded MIMO-OFDM systems operating over arbitrary correlated Ricean fading channels are analyzed. Particularly, the probability of outage, the BER, and the theoretically achievable diversity gain and coding gain are derived for two transmitter diversity schemes.
- It is proved that the rank and determinant design criteria of space-time-frequency block codes used over Gaussian channels are also valid for the exact PEP.

Chapter 6

- It is shown that binary Hamming codes can be constructed recursively.
- The recursive structure is used to efficiently enumerate the input-output weights of binary Hamming codes.
- The exact BER of binary Hamming codes with antipodal signaling and hard-decision demodulation used on AWGN channels is evaluated exactly.
- The coding gain is shown not to be monotonically increasing with SNR.

Chapter 7

- A family of IBRC's having variable block length and variable minimum Hamming distance is constructed.
- The construction of IBRC's is extended to multiple dimensions.
- Two design criteria of multidimensional IBRC's are given assuming the code constraint length and the code constraint weight.
- An efficient algorithm to search for good codes is presented.
- The IBRC's are shown to be good candidates for adaptive coding, turbo product coding, retransmission schemes and multihop routing.
- A non-recursive block differential encoder of IBRC's is found to arbitrarily increase the code rate with the block length while the minimum Hamming distance of the code remains constant.
- Multidimensional IBRC's are shown to be also well-suited as an inner encoding scheme for concatenated one-dimensional outer codewords to increase their minimum Hamming distance without increasing the transmission bandwidth.
- The transmission energy distribution over the codewords of IBRC's is optimized to improve the BER.
- A three stage network protocol employing IBRC's and the distributed random SPC codes is proposed for the uplink and downlink packet transmission.

- The PER is evaluated for all three protocol stages assuming particular network realizations and coherent and non-coherent binary modulation schemes.
- A link budget analysis is used to calculate the receiver SNR.
- It is found that the cooperation gains in the network are strongly dependent on the particular network realization and less on the number of cooperating nodes.

Chapter 8

- The K-dimensional sphere, polytope, cube, scaled polytope and the scaled cube are studied.
- It is proved that the volume and the surface area of these objects reach a maximum for a particular value of dimension, and then, decrease towards zero.
- The dimension corresponding to the maximum volume and to the maximum surface area is obtained as a function of the radius.
- The l_p norm of a vector in K dimensions is shown to be monotonically increasing in K, and monotonically decreasing in p.
- The SNR adaptive receivers employing a bank of subchannel detectors and employing a K branch diversity combining front-end are investigated.
- The average performance measures of detectors operating over erasure subchannels are shown to reach a maximum for a particular dimension and SNR partitioning.
- It is shown that there exists optimum receiver dimension.

Chapter 2

Efficient Computer Simulation Techniques

This chapter considers efficient computer simulation techniques. In particular, the SR simulation technique is proposed and investigated in Section 2.1 for MLSD and quantized AWGN channels, and in Section 2.2 for MLSD and ISI channels.

2.1 Sample Rejection for Simulations of Binary Coded Schemes and MLSD over Quantized AWGN Channels

2.1.1 Background

The use of coding to approach channel capacity is a topic of renewed great research interest. However, theoretical performance analysis of sophisticated coding schemes is often mathematically intractable, particularly for finite values of SNR. Several techniques have been developed for efficient estimation of BER's of communication systems. Among them, a modified MC simulation method based on importance sampling (IS) (proposed in [5]) is the most frequently used in practice. A discussion of the state-of-the-art of IS used for efficient simulation of communication systems can be found in [6]. In general, the application of IS to systems with large dimensionality (sometimes referred to as the memory of the system) is rather problematic [7]. Furthermore, the IS technique must be often tailored to a specific system under consideration, and the variance reduction of the BER estimator is not always guaranteed. For example, the optimum IS biasing scheme for a system operating over an AWGN channel and using Viterbi decoding depends on the particular coding

scheme employed, the received signal quantization, and the SNR [8]. While the dimensionality problem for systems over quantized AWGN channels with Viterbi decoding can be relieved using, for example, an error-event IS simulation technique proposed in [9], the necessity to customize the IS biasing scheme for the system considered remains. Therefore, the main focus of this section is to investigate an IS technique which is easy to implement, universally applicable, and sufficiently robust regarding the system dimensionality. We will show that these requirements can be fulfilled by SR.

The use of IS may require determining the simultaneous biases of a large number of noise processes which can be an arduous task, especially for complex systems. Therefore, SR was proposed in [10] as a special case of IS to significantly alleviate the implementation requirements. The SR technique is based on the following idea. In the course of simulation, decoding of the received sequence is almost always the most time consuming operation since the decoder typically searches over a large set of possible transmitted sequences to select the best candidate. Hence, the elapsed simulation time can be reduced if we avoid decoding of the received sequences which are known beforehand to be decoded error-free. The potential simulation time-savings were analyzed in [10] for the case of a perfectly quantized (i.e., unquantized) AWGN channel and a hypersphere rejection region (i.e., all noise vectors with magnitude less than half the minimum Euclidean distance are rejected without decoding). The conclusions in [10], however, seem to indicate that SR may be effective only for systems with dimensionality less than 10. The idea of SR was also applied independently in [11] for a system with intersymbol-interference and Viterbi decoding, in [12] where a rejection region was designed for trellis-coded modulation with stack sequential decoding, and in [9] as an error-event IS simulation; see also [6, p. 609] and references therein. Nevertheless, the use of SR in [9], [11] and [12] is limited for a specific problem at hand whereas the discussion in [10] and this section aims at a broader perspective on SR.

In this section, the SR technique is investigated for binary antipodal signaling over quantized AWGN channels and MLSD. The analysis of the SR technique is valid for any coding scheme of finite block length. A discrete memoryless channel (DMC) model derived from the AWGN channel with quantized output is introduced in Section 2.1.2. We present the structure of the MLSD for different levels of channel quantization and the corresponding probability of a decoded bit error. In Section 2.1.3, we discuss codeword decoding probability (CDP) estimation using IS and SR techniques, and define the gain of SR as a reduction of the estimator variance with respect to conventional MC simulation. In Section 2.1.4, rejection regions for an AWGN channel with quantized

output are compared. In addition to a hypersphere rejection region considered in [10] for perfectly quantized decisions, we propose and analyze hypercube and hyperquadrant rejection regions for quantized AWGN channels. While hypersphere SR typically gives greater gains than hyperquadrant and hypercube SR at large SNR, it is shown that the proposed rejection regions can have gains as large as several orders of magnitude greater than hypersphere SR when the number of dimensions is large and the SNR is finite. In Section 2.1.5, a numerical example is given, and run-time issues are considered. Summary is given in Section 2.1.6.

2.1.2 System Model

Assume baseband equivalent signals represented as vectors in a n-dimensional signal space. The k independent and identically distributed (IID) equally probable information bits are encoded into a length n binary codeword $\mathbf{x} = (x_1, x_2, \cdots, x_n)$, $x_i \in \{0, 1\}$, from a codebook $\mathscr{C}$. The size of the codebook is $|\mathscr{C}| = 2^k$ and the code rate is $R = k/n$. The codebook can be either a binary block code or a binary convolutional code with trellis termination or trellis truncation. The dimensionality is equal to the number of samples that affects a single symbol decision. For a simulation model using one sample per data symbol, the codeword length, n, corresponds to the dimensionality of the system. The codeword, $\mathbf{x}$, is mapped onto a modulated signal vector, $\mathbf{s}$, using binary phase-shift keying (BPSK), i.e., $s_i = (-1)^{x_i}$, $i = 1, 2, \cdots, n$. This implies that the minimum squared Euclidean distance at the output of the modulator is $d_{\mathrm{e}}^2 = 4d_{\min}$ where $d_{\min}$ is the minimum Hamming distance of the code (i.e., the squared Euclidean distance is directly proportional to the Hamming distance). The transmitted signal vector, $\mathbf{s}$, is corrupted by a zero-mean AWGN vector, $\mathbf{w}$, with variance, $\sigma_w^2 = N_0/2$, per dimension where N_0 is the one-sided noise power spectral density. The noise and the transmitted signal are uncorrelated. The energy of the encoded modulated symbols is assumed, without loss of generality, to be unity, i.e., $\mathrm{E}\left[|s_i|^2\right] = 1$, $i = 1, 2, \cdots, n$. Therefore, the energy of an uncoded modulated symbol is $E_b = 1/R$, and the SNR per uncoded modulated symbol is $\gamma_b = E_b/N_0 = (2R\sigma_w^2)^{-1}$. The received signal, $\mathbf{y}$, quantized into Q levels is,

$$\mathbf{y} = \mathscr{Q}_Q(\mathbf{s} + \mathbf{w}) \tag{2.1}$$

where transformation $\mathscr{Q}_Q(\cdot)$ quantizes each component of its vector argument, and hence, $\mathbf{y} \in \mathbb{Z}_Q^n$ where $\mathbb{Z}_Q = \{0, 1, \cdots, Q-1\}$. When $Q \to \infty$, the receiver processes perfectly quantized soft-decisions while $Q = 2$ corresponds to a hard-decision decoding. The Q quantization intervals that

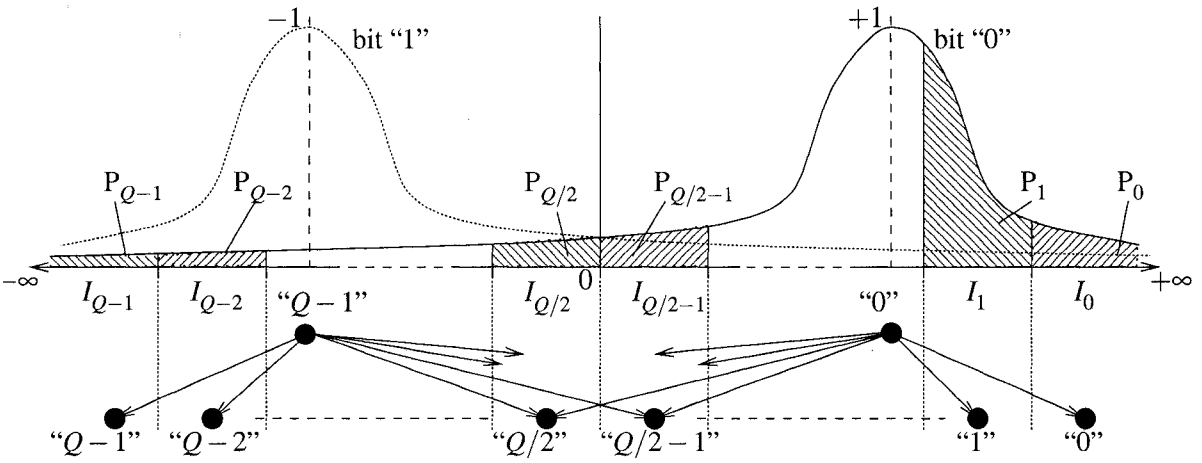

Figure 2.1: The Q-ary quantization of BPSK in AWGN with quantization intervals I_i, an equivalent symmetric DMC model with binary input $\{0,1\}$ and Q-ary output $i \in \{0,1,\cdots,Q-1\}$ and the transition probabilities P_i.

partition the real axis are defined as,

$$I_j = \begin{cases} [(\frac{Q}{2}-1)\Delta, \infty] & j = 0 \\ [(\frac{Q}{2}-j-1)\Delta, (\frac{Q}{2}-j)\Delta] & j = 1,2,\cdots,(Q-2) \\ [-\infty, (1-\frac{Q}{2})\Delta] & j = (Q-1) \end{cases} \tag{2.2}$$

assuming Q is even and Δ is the width of the quantization intervals except the outermost intervals I_{Q-1} and I_0 which extend to infinity. Each quantization interval is assigned a value from the set $\mathbb{Z}_Q$; see Fig. 2.1. Optimum quantization for AWGN channels is well-studied in the literature; see, for example, [13] and references therein. Note that a heuristic approach to quantizer design is often sufficient and may yield a negligible performance loss [14].

It is useful to represent the quantized AWGN channel by an equivalent DMC if $Q < \infty$ (cf. Fig. 2.1). The DMC input is a binary codeword, $\mathbf{x}$, and the output is a Q-ary received word, $\mathbf{y}$. In the case of BPSK signaling, AWGN with zero mean and quantization intervals symmetric about the origin (cf. Fig. 2.1), the DMC is symmetric. The transition probabilities of the symmetric DMC are given in Table 2.1. Define a binary operator, $\oplus$, between two vectors, $\mathbf{a}$ and $\mathbf{b}$, such that $\mathbf{a} \oplus \mathbf{b} = |\mathbf{a} - \mathbf{b}| = (|a_1 - b_1|, \cdots, |a_n - b_n|)$ where $|\cdot|$ is the absolute value (i.e., the operator is related to the distance between vectors). Then, the DMC model is,

$$\mathbf{y} = (Q-1)\mathbf{x} \oplus \mathbf{e} \tag{2.3}$$

Table 2.1: Transitions of the symmetric DMC for given values of discrete noise samples.

noise sample	transitions		probability
0	$0 \rightarrow 0$	$(Q-1) \rightarrow (Q-1)$	P_0
1	$0 \rightarrow 1$	$(Q-1) \rightarrow (Q-2)$	P_1
2	$0 \rightarrow 2$	$(Q-1) \rightarrow (Q-3)$	P_2
$\vdots$	$\vdots$	$\vdots$	$\vdots$
$Q-1$	$0 \rightarrow (Q-1)$	$(Q-1) \rightarrow 0$	P_{Q-1}

where scalar multiplication of vector, $\mathbf{x}$, by $(Q-1)$ is introduced for convenience, and $\mathbf{e} \in \mathbb{Z}_Q^n$ represents the noise, i.e., forces the transitions of the input coded bits within the DMC. Note that if $\mathbf{e} = (0, 0, \cdots, 0)$, no noise is present and the output is equal to the input. Note also that the operator $\oplus$ corresponds to modulo 2 summation if $Q = 2$. One can show that (2.3) is equivalent to,

$$\mathbf{e} = (Q-1)\mathbf{x} \oplus \mathbf{y}. \tag{2.4}$$

Recall that the DMC is symmetric. Therefore, the channel transition probability between the channel input, $i \in \{0, 1\}$, and output, $j \in \mathbb{Z}_Q$, can be designated using a single subscript, i.e., $\mathrm{P}_{ij} = \mathrm{P}_{(Q-1)i \oplus j}$; see (2.4), Table 2.1 and Table 2.2 (note that in Table 2.1 the transitions are shown for the channel input $\{0, Q-1\}$). If X is a Gaussian random variable with mean m and variance σ^2, the probability $\Pr(a \leq X < b) = Q\big(\frac{a-m}{\sigma}\big) - Q\big(\frac{b-m}{\sigma}\big)$ where $Q(\cdot)$ denotes the Q-function; see (A-2). Therefore, the transition probabilities are computed as,

$$\mathrm{P}_{(Q-1)i \oplus j} = Q\left(\frac{I_j^{(l)} - (-1)^{x_i}}{\sigma_w}\right) - Q\left(\frac{I_j^{(u)} - (-1)^{x_i}}{\sigma_w}\right)$$

where $I_j^{(l)}$ and $I_j^{(u)}$ is the lower and upper bound of the quantization interval I_j, respectively, and x_i is a symbol at the channel input.

The channel is assumed to be stationary with conditional probability mass function (PMF) $f(\mathbf{y}|\mathbf{x}) = \prod_{i=1}^{n} f(y_i|x_i)$ having the multinomial distribution given by [15],

$$f(\mathbf{y}|\mathbf{x}) = \frac{n!}{m_0! m_1! \ldots m_{Q-1}!} P_0^{m_0} P_1^{m_1} \ldots P_{Q-1}^{m_{Q-1}}$$

where m_i is the number of occurrences of the transitions with probability P_j, $\sum_{j=0}^{Q-1} m_j = n$ and $\sum_{j=0}^{Q-1} P_j = 1$. It follows from (2.4) that the noise vector, $\mathbf{e}$, conditioned on the transmitted

Table 2.2: DMC transition probabilities.

$\Pr(j\|i)$	0		1
0	P_0	$>$	P_{Q-1}
1	P_1	$>$	P_{Q-2}
$\vdots$	$\vdots$		$\vdots$
$Q/2-1$	$\mathrm{P}_{Q/2-1}$	$>$	$\mathrm{P}_{Q/2}$
$Q/2$	$\mathrm{P}_{Q/2}$	$<$	$\mathrm{P}_{Q/2-1}$
$\vdots$	$\vdots$		$\vdots$
$Q-1$	P_{Q-1}	$<$	P_0

codeword, $\mathbf{x}$, also has a multinomial distribution.

Optimum Detector

The optimum decoder partitions the space $\mathbb{Z}_Q^n$ of all possible received sequences, $\mathbf{y}$, in order to minimize the probability of making an incorrect sequence decision. Assuming IID equally probable input information bits, the codewords, $\mathbf{x} \in \mathscr{C}$, are equally likely and the optimum decoder performs ML sequence decoding [16]. The decision (Voronoi) region [17] for transmitted codeword $\mathbf{x}$ is denoted as $\mathscr{D}(\mathbf{x})$, i.e., $\forall \mathbf{x} \neq \mathbf{x}' : \mathscr{D}(\mathbf{x}) \cap \mathscr{D}(\mathbf{x}') = \varnothing$ and $\cup_{\mathbf{x}\in\mathscr{C}} \mathscr{D}(\mathbf{x}) = \mathbb{Z}_Q^n$. The Voronoi regions are determined as [9],

$$\mathscr{D}(\mathbf{x}) = \left\{\mathbf{y} \in \mathbb{Z}_Q^n : m(\mathbf{x},\mathbf{y}) = \max_{\min \mathbf{x}' \in \mathscr{C}} m(\mathbf{x}',\mathbf{y})\right\}$$

where $m(\mathbf{x},\mathbf{y})$ is the metric to be maximized or minimized over all possible transmitted codewords. The specific form of the metric depends on the number of quantization levels, Q.

For perfectly quantized soft-decisions, $Q \to \infty$, and the detector minimizes the squared Euclidean distance [16],

$$m(\mathbf{x},\mathbf{y}) = \min_{\mathbf{x}'\in\mathscr{C}} \left\|\mathbf{y} - (-1)^{\mathbf{x}'}\right\|^2 = \min_{\mathbf{x}'\in\mathscr{C}} \sum_{i=1}^{n} -y_i(-1)^{x_i'} \tag{2.5}$$

where $\|\cdot\|$ is the Euclidean norm of the vector, and $(-1)^{\mathbf{x}'} = ((-1)^{x_1'}, (-1)^{x_2'}, \cdots, (-1)^{x_n'})$.

For quantized soft-decisions, $2 < Q < \infty$, the detector maximizes [18],

$$m(\mathbf{x},\mathbf{y}) = \max_{\mathbf{x}'\in\mathscr{C}} \prod_{i=1}^{n} f(y_i|x_i') = \max_{\mathbf{x}'\in\mathscr{C}} \prod_{i=1}^{n} \mathrm{P}_{e_i} = \max_{\mathbf{x}'\in\mathscr{C}} \prod_{j=0}^{Q-1} \mathrm{P}_j^{m_j} \tag{2.6}$$

where $e_i = (Q-1)x_i' \oplus y_i$. For equally probable codewords, the metric (2.6) is proportional to the *a posteriori* probability (APP) of the transmitted sequence, and hence, the reliability of the decision [17]. Owing to quantization (2.2), we have always $\mathrm{P}_j > \mathrm{P}_{Q-1-j}$ for $j = 0, 1, \cdots, Q/2-1$ (cf. Table 2.2), and thus, the metric (2.6) is bounded as,

$$\left(\min_{j=Q/2,\cdots,Q-1} \mathrm{P}_j\right)^n \le \prod_{i=1}^{n} \mathrm{P}_{e_i} \le \left(\max_{j=0,\cdots,Q/2-1} \mathrm{P}_j\right)^n.$$

Finally, for hard-decisions, $Q = 2$, and the metric (2.6) can be simplified to minimize the Hamming distance, i.e.,

$$m(\mathbf{x},\mathbf{y}) = \min_{\mathbf{x}'\in\mathscr{C}} \sum_{i=1}^{n} x_i' \oplus y_i. \tag{2.7}$$

Probability of Decoded Bit Error

The probability of erroneously decoding a bit (the BER) is an important performance measure of a communication system. The BER can be evaluated as [9],

$$\Pr(e) = \frac{1}{k}\mathrm{E}[e(\mathbf{x},\mathbf{x}')] = \frac{1}{k}\sum_{\mathbf{x}\in\mathscr{C}}\sum_{\mathbf{x}'\in\mathscr{C}} e(\mathbf{x},\mathbf{x}')\Pr(\mathbf{x}'|\mathbf{x})\Pr(\mathbf{x}) = \sum_{\mathbf{x}\in\mathscr{C}} \Pr(e|\mathbf{x})\Pr(\mathbf{x}) \tag{2.8}$$

where $e(\mathbf{x},\mathbf{x}')$ is the number of information bit-errors when the two codewords are interchanged, and the BER is a weighted sum of CDP's, $\Pr(\mathbf{x}'|\mathbf{x})$. Note that owing to one-to-one mapping of input information bits onto codewords, the summations in (2.8) can be done equivalently over input information vectors. For equally probable codewords, $\Pr(\mathbf{x}) = 1/2^k$. In general, the conditional probabilities $\Pr(e|\mathbf{x}) = \frac{1}{k}\sum_{\mathbf{x}'\in\mathscr{C}} e(\mathbf{x},\mathbf{x}')\Pr(\mathbf{x}'|\mathbf{x})$ differ depending which codeword was transmitted. For linear codes that are regular, i.e., the distance spectrum is independent of the selected codeword [19], the conditional bit-error probabilities are independent of the transmitted codeword, and the all-zero sequence can be exclusively considered as the transmitted sequence saving simulation efforts. On the other hand, for example, trellis termination of convolutional codes violates the code regularity, and the conditional bit-error probabilities are not independent of the transmitted

codeword. The CDP's can be expressed as [9], [17],

$$\Pr(\mathbf{x}'|\mathbf{x}) = \sum_{\mathbf{y}\in\mathscr{D}(\mathbf{x}')} f(\mathbf{y}|\mathbf{x}) = \sum_{\mathbf{y}\in\mathbb{Z}_Q^n} I_{\mathbf{x}'}(\mathbf{y}) f(\mathbf{y}|\mathbf{x}) \tag{2.9}$$

where the indicator function $I_{\mathbf{x}'}(\mathbf{y}) = 1$ for $\mathbf{y} \in \mathscr{D}(\mathbf{x}')$ and 0, otherwise.

The double summation over all pairs of codewords in (2.8) may be overwhelming even for codes of moderate block length. Another difficulty is that knowledge of the decision region, $\mathscr{D}(\mathbf{x}')$, is often missing, and hence, the CDP (2.9) cannot be evaluated analytically. Therefore, simulation is usually used to determine the performance of coded systems. The estimator of the BER (2.8) has the form,

$$\hat{\mathrm{P}}(e) = \frac{1}{k} \sum_{\mathbf{x}\in\mathscr{C}} \sum_{\mathbf{x}'\in\mathscr{C}} e(\mathbf{x},\mathbf{x}') \hat{\mathrm{P}}(\mathbf{x}'|\mathbf{x}) \Pr(\mathbf{x}) \tag{2.10}$$

where $\hat{\mathrm{P}}(\mathbf{x}'|\mathbf{x})$ is the estimator of CDP (2.9). The variance of the estimator (2.10) is,

$$\begin{aligned} \mathrm{var}\left[\hat{\mathrm{P}}(e)\right] &= \sum_{\mathbf{x}} \sum_{\mathbf{x}'} \sum_{\mathbf{x}''} \sum_{\mathbf{x}'''} \left(\frac{\Pr(\mathbf{x})}{k}\right)^2 e(\mathbf{x}'|\mathbf{x}) e(\mathbf{x}'''|\mathbf{x}'') \,\mathrm{cov}\left[\hat{\mathrm{P}}(\mathbf{x}'|\mathbf{x}), \hat{\mathrm{P}}(\mathbf{x}'''|\mathbf{x}'')\right] \\ &\approx \sum_{\mathbf{x}} \sum_{\mathbf{x}'} \left(\frac{\Pr(\mathbf{x})\, e(\mathbf{x}'|\mathbf{x})}{k}\right)^2 \mathrm{var}\left[\hat{\mathrm{P}}(\mathbf{x}'|\mathbf{x})\right] = \sigma_B^2 \end{aligned} \tag{2.11}$$

since CDP's are conditionally uncorrelated (for $\mathbf{x} = \mathbf{x}''$ and $\mathbf{x}' \neq \mathbf{x}'''$) and other covariances are neglected (for $\mathbf{x} \neq \mathbf{x}''$ and $\mathbf{x}' = \mathbf{x}'''$). Assuming further that the variance of the CDP estimator is approximately constant for all pairs of codewords, one has $\sigma_B^2 \approx \text{constant} \times \mathrm{var}\left[\hat{\mathrm{P}}(\mathbf{x}'|\mathbf{x})\right]$.

2.1.3 Estimation of CDP

Using simulation to estimate $\Pr(e)$ may require excessively or prohibitively long computer run-times. In some cases, the IS technique can be employed to reduce the excessive simulation times required to estimate CDP (2.9) (and consequently to estimate BER (2.10)). We review IS first, and then, proceed to SR as a special form of IS.

Importance Sampling

The computation of CDP (2.9) can be rewritten using another channel transition PMF, $f^*(\mathbf{y}|\mathbf{x})$, as [9],

$$\Pr(\mathbf{x}'|\mathbf{x}) = \sum_{\mathbf{y}\in\mathbb{Z}_Q^n} I_{\mathbf{x}'}(\mathbf{y}) \underbrace{\frac{f(\mathbf{y}|\mathbf{x})}{f^*(\mathbf{y}|\mathbf{x})}}_{w(\mathbf{y}|\mathbf{x})} f^*(\mathbf{y}|\mathbf{x})$$

where $w(\mathbf{y}|\mathbf{x})$ is a weighting function. Then, the unbiased estimator of the CDP for L simulation trials is,

$$\hat{\mathrm{P}}(\mathbf{x}'|\mathbf{x}) = \frac{1}{L}\sum_{l=1}^{L} w(\mathbf{y}^{(l)}|\mathbf{x}) I_{\mathbf{x}'}(\mathbf{y}^{(l)}) \tag{2.12}$$

where the superscript indicates the l-th simulation trial. For independent errors, the estimator variance is,

$$\begin{aligned}\mathrm{var}\left[\hat{\mathrm{P}}(\mathbf{x}'|\mathbf{x})\right] &= \frac{1}{L}\mathrm{var}\left[w(\mathbf{y}^{(l)}|\mathbf{x}) I_{\mathbf{x}'}(\mathbf{y}^{(l)})\right] \\ &= \frac{1}{L}\left\{\sum_{\mathbf{y}\in\mathscr{D}(\mathbf{x}')}\left(\frac{f(\mathbf{y}|\mathbf{x})}{f^*(\mathbf{y}|\mathbf{x})}\right)^2 f^*(\mathbf{y}|\mathbf{x}) - \Pr(\mathbf{x}'|\mathbf{x})^2\right\}. \end{aligned} \tag{2.13}$$

Observe that if $w(\mathbf{y}|\mathbf{x}) = 1$, eq. (2.12) becomes an ordinary MC estimator.

Sample Rejection

The SR method was proposed in [10] as an IS technique for which no weights need to be computed. Provided that we can find an arbitrary region, $\mathrm{R}_{\mathbf{x}} \subseteq \mathscr{D}(\mathbf{x})$, inside the decision region of the codeword $\mathbf{x}$, the CDP can be expanded as [10],

$$\Pr(\mathbf{x}'|\mathbf{x}) = \underbrace{\Pr(\mathbf{x}'|\mathbf{x}, \mathbf{y}\in\mathrm{R}_{\mathbf{x}})}_{0}\Pr(\mathbf{y}\in\mathrm{R}_{\mathbf{x}}) + \Pr(\mathbf{x}'|\mathbf{x}, \mathbf{y}\notin\mathrm{R}_{\mathbf{x}})\Pr(\mathbf{y}\notin\mathrm{R}_{\mathbf{x}}). \tag{2.14}$$

Eq. (2.14) suggests that we may *a priori* reject the error-free received samples that fall into the region $\mathrm{R}_{\mathbf{x}}$. It is important to ensure that the region $\mathrm{R}_{\mathbf{x}}$ is fully inside the region $\mathscr{D}(\mathbf{x})$, otherwise, the estimator $\hat{\mathrm{P}}(\mathbf{x}'|\mathbf{x})$ will be biased. Note that $\mathbf{y}\in\mathrm{R}_{\mathbf{x}}$ ensures that $\mathbf{x}' = \mathbf{x}$, i.e., $e(\mathbf{x},\mathbf{x}') = 0$ in (2.8) and $\hat{\mathrm{P}}(\mathbf{x}'|\mathbf{x})$ is unbiased. If $\mathrm{R}_{\mathbf{x}}$ is sufficiently large, the probability $\Pr(\mathbf{y}\notin\mathrm{R}_{\mathbf{x}})$ is small and consequently probability $\Pr(\mathbf{x}'|\mathbf{x}, \mathbf{y}\notin\mathrm{R}_{\mathbf{x}})$ is large and easier to simulate. It is of interest since typically larger $\mathrm{R}_{\mathbf{x}}$ can be chosen for higher values of SNR corresponding to lower values of BER which are more difficult to simulate.

When the samples are being rejected, the channel transition PMF is biased according to,

$$f^*(\mathbf{y}|\mathbf{x}) = \begin{cases} \frac{f(\mathbf{y}|\mathbf{x})}{1-\Pr(\mathrm{R}_\mathbf{x})} & \mathbf{y} \notin \mathrm{R}_\mathbf{x} \\ 0 & \mathbf{y} \in \mathrm{R}_\mathbf{x} \end{cases} \tag{2.15}$$

where the probability mass of region $\mathrm{R}_\mathbf{x}$ is $\Pr(\mathrm{R}_\mathbf{x}) = \Pr(\mathbf{y} \in \mathrm{R}_\mathbf{x}) = \sum_{\mathbf{y}\in\mathrm{R}_\mathbf{x}} f(\mathbf{y}|\mathbf{x})$. Strictly speaking, rejecting the samples introduces memory into the channel [9]; however, the channel remains block-wise memoryless, and the simulation result is unaffected.

There are two ways to obtain biasing function (2.15). We may generate all the received vectors $\mathbf{y}$ according to $f(\mathbf{y}|\mathbf{x})$ and discard the samples that fall inside the region $\mathrm{R}_\mathbf{x}$. This approach may be viewed as a fast decoding rule [10]. The second method is to generate the received vectors directly according to $f^*(\mathbf{y}|\mathbf{x})$, i.e., a hole corresponding to the region $\mathrm{R}_\mathbf{x}$ is carved within $f(\mathbf{y}|\mathbf{x})$ [10]. However, care must be exercised in removing mass in the n-dimensional event space because if mass is removed from regions that are inside the error event volume, the estimator $\hat{\mathrm{P}}(\mathbf{x}'|\mathbf{x})$ will be biased. The direct method is, in general, difficult to implement, particularly for biasing functions that are not circularly symmetric [20]. Moreover, in most practical situations, the time taken to generate the samples is insignificant compared to the time taken to execute the decoding. In this case, the simulation gains of the two approaches are similar.

Variance Reduction of SR

The efficiencies of accelerated simulation methods are usually measured in terms of variance reduction relative to conventional MC simulation, or equivalently, the reduction in the number of simulation trials required to achieve a given estimator variance. In particular, the gain of SR in estimation of the CDP $\hat{\mathrm{P}}(\mathbf{x}'|\mathbf{x})$ is,

$$G_{\hat{\mathrm{P}}(\mathbf{x}'|\mathbf{x})} = \left.\frac{\sigma^2_{\mathrm{mc}}}{\sigma^2_{\mathrm{sr}}}\right|_{L_{\mathrm{mc}}=L_{\mathrm{sr}}} = \left.\frac{L_{\mathrm{mc}}}{L_{\mathrm{sr}}}\right|_{\sigma^2_{\mathrm{mc}}=\sigma^2_{\mathrm{sr}}} \tag{2.16}$$

where σ^2_{mc}, σ^2_{sr}, L_{mc} and L_{sr} is the variance of the MC estimator, the variance of the SR estimator and the number of simulation trials for MC and SR simulation, respectively. One has from (2.13)

that,

$$\sigma_{\mathrm{sr}}^2 = \mathrm{var}\left[\hat{\mathrm{P}}(\mathbf{x}'|\mathbf{x})\right] = \frac{1}{L_{\mathrm{sr}}} \left((1 - \Pr(\mathrm{R}_{\mathbf{x}})) \underbrace{\sum_{\mathbf{y} \in \mathscr{D}(\mathbf{x}')} f(\mathbf{y}|\mathbf{x})}_{\Pr(\mathbf{x}'|\mathbf{x})} - \Pr(\mathbf{x}'|\mathbf{x})^2 \right) \tag{2.17}$$

since by the definition of error-free region, $\mathrm{R}_{\mathbf{x}} \cap \mathscr{D}(\mathbf{x}') = \varnothing$, and the summands in (2.13) are independent. Similarly, the variance of the MC estimator (2.12) when $w(\mathbf{y}|\mathbf{x}) = 1$ is,

$$\sigma_{\mathrm{mc}}^2 = \frac{1}{L_{\mathrm{mc}}} \left(\Pr(\mathbf{x}'|\mathbf{x}) - \Pr(\mathbf{x}'|\mathbf{x})^2 \right). \tag{2.18}$$

It is worth noting that the variance of the CDP estimators (2.17) and (2.18) reach their respective maximum for certain (different) values of CDP, $\Pr(\mathbf{x}'|\mathbf{x})$. We can substitute (2.17) and (2.18) into (2.16) to obtain the gain of the SR method,

$$G_{\hat{\mathrm{P}}(\mathbf{x}'|\mathbf{x})} = \frac{1 - \Pr(\mathbf{x}'|\mathbf{x})}{1 - \Pr(\mathrm{R}_{\mathbf{x}}) - \Pr(\mathbf{x}'|\mathbf{x})}. \tag{2.19}$$

The numerator in (2.19) equals the probability of not decoding $\mathbf{x}'$ when $\mathbf{x}$ was transmitted, and the denominator equals this probability reduced by the probability mass of $\mathrm{R}_{\mathbf{x}}$. Intuitively, if the decision region is known *a priori* (for example, it is for the case of perfect codes [18]), $\mathrm{R}_{\mathbf{x}} = \mathscr{D}(\mathbf{x})$, and the gain $G_{\hat{\mathrm{P}}(\mathbf{x}'|\mathbf{x})} \to \infty$. On the contrary, if no rejections are performed, $\mathrm{R}_{\mathbf{x}} = \varnothing$, and the gain $G_{\hat{\mathrm{P}}(\mathbf{x}'|\mathbf{x})} = 1$. Note that the variances of the MC and SR estimators, and consequently the gain (2.19) are functions of the SNR.

For any value of $\Pr(\mathbf{x}'|\mathbf{x})$, the gain (2.19) can be lower bounded as $G_{\hat{\mathrm{P}}(\mathbf{x}'|\mathbf{x})} \geq (1 - \Pr(\mathrm{R}_{\mathbf{x}}))^{-1}$. Assuming $1 - \Pr(\mathbf{x}'|\mathbf{x}) \gg \Pr(\mathrm{R}_{\mathbf{x}})$, this lower bound is tight, and using (2.11) and (2.16), the gain of SR over MC method for the BER estimator, $\hat{\mathrm{P}}(e)$, can be well approximated as,

$$G_{\hat{\mathrm{P}}(e)} \approx \frac{1}{1 - \Pr(\mathrm{R}_{\mathbf{x}})}. \tag{2.20}$$

The approximation of the gain $G_{\hat{\mathrm{P}}(e)}$ in (2.20) is valid provided that $\Pr(\mathrm{R}_{\mathbf{x}})$ is constant, independent of the specific codeword, $\mathbf{x}$. We may interpret the result as the ratio of space masses that must be searched in the course of simulation without or with the implemented rejection rule, respectively.

2.1.4 Rejection Regions for Quantized AWGN Channels

It is clear from the previous discussion that the rejection region $\mathrm{R}_{\mathbf{x}}$ must be determined such that for any transmitted codeword, $\mathbf{x}$, it is easy to determine whether the received vector $\mathbf{y}$ is inside this region. In general, the greater the (probability) mass of the rejection region, the higher the achievable gain (cf. (2.20)). The influence of the shape of rejection region on the gain achievable by SR was briefly considered in [10]; a hypersphere was analyzed for perfectly quantized soft-decision decoding while a hypercube was only conjectured (but neither defined nor analyzed) to possibly be better for hard-decision decoding.

We can form rejection regions of different shapes depending on what knowledge about the error-free region $\mathscr{D}(\mathbf{x})$ is available. The use of a n-dimensional hypersphere for an AWGN channel is motivated by the fact that a hypersphere of radius $d_{\mathrm{e}}/2$ centered about the transmitted codeword in a signal space cannot contain error events. In problems having rectangular symmetries, it may be possible to use a n-dimensional hypercube. If the hypercube contains the hypersphere, the gain is improved. If one conditions the shape of a rejection region on the transmitted codeword, it is possible to remove probability mass from regions that are not centered on the origin. For example, one can reject a block of noise samples if, for each bit in the block, the noise sample is less than 1 when the transmitted symbol is -1 and greater than -1 when the transmitted symbol is $+1$. This creates a hyperquadrant conditioned on the transmitted sequence in the n-dimensional noise space. While it is clear that this scheme is "safe" for hard-decision decoding, it is not clear that this scheme will not bias the estimator for soft-decision decoding.

Perfectly Quantized Soft-Decisions

For perfectly quantized soft-decisions, $Q \to \infty$, and the decoder minimizes the Euclidean distance (2.5). For illustration and clarity, we consider the one-dimensional case first which corresponds to an uncoded system. Then, the received signal is $y_1 = s_1 + w_1$ (cf. (2.1)). For BPSK signaling with symbols ± 1, no errors occur if the noise sample $|w_1| < 1$, i.e., the noise samples inside $\mathrm{R}_1 = \{w_1 : |w_1| < 1\}$ can be rejected (cf. Fig. 2.1). The probability mass of R_1 is $\Pr(\mathrm{R}_1) = 1-2p$ where $p = Q\left(\sqrt{2\gamma_b}\right)$ is the BER of BPSK over an AWGN channel. The rejection region can be enlarged if we condition the rejections on the transmitted symbol, s_1. Then, the rejection region is $\mathrm{R}_1(s_1) = \{w_1 : s_1 w_1 > -1\}$, and since $\mathrm{R}_1 \subset \mathrm{R}_1(s_1)$, the probability mass is increased to $\Pr(\mathrm{R}_1(s_1)) = 1 - p$ and the gain (2.20) is doubled. Importantly, note that, in this case, the

theoretically computed gain of the one-dimensional SR technique neglects the fact that the time to reject the sample is approximately equal to the time to decode the sample. In general, we will show in the next subsection that the probability of rejection in the theoretically computed gain of SR is scaled by the ratio of times to reject and decode the received sequence. In this subsection, it is assumed that the time to reject the received sequence can be neglected. Even though such assumption is well justified for longer sequences, for sequences of smaller block length, the time to reject the sequence cannot be neglected and the gain of SR will be reduced. Hence, one should use the IS simulation for sequences of block length, say, less than 10, and the SR simulation for sequences of block length larger than 10.

To illustrate further, consider a transmission in two dimensions as depicted in Fig. 2.2. The rectangle centered in the origin corresponds to an uncoded transmission when the rejection region is independent of the transmitted bits. The rectangle illustrates a hypercube in 2D. The circle around the rectangle is a 2D hypersphere rejection region for the repetition code with codewords $(0,0)$ and $(1,1)$ (modulated $\mathbf{s}_1 = (1,1)$ and $\mathbf{s}_2 = (-1,-1)$, respectively) with $d_{\min} = 2$, i.e., $d_{\mathrm{e}} = 2\sqrt{2}$. The dashed line in Fig. 2.2 corresponds to the decision boundary for codewords $\mathbf{s}_1$ and $\mathbf{s}_2$. In this case, the hypersphere is defined as $\mathrm{R}_2 = \{w_1, w_2 : |w_1|^2 + |w_2|^2 < d_{\mathrm{e}}^2/4\}$. The circle inside the rectangle is a hypersphere for the case when $d_{\min}$ of the code is unknown; then it is safe to assume $d_{\min} = 1$, i.e., $d_{\mathrm{e}} = 2$. Finally, the lines E_1 and E_2 enclosing the shaded area are the error boundaries when the codeword $(1,1)$ (modulated signal $\mathbf{s}_2 = (-1,-1)$) is transmitted. This rejection region is a hyperquadrant in 2D.

The general case of n dimensions applies when coding of codeword length n is used. The rejection region suggested in [10] is a hypersphere of radius $\sqrt{T_n}$, $T_n = d_{\mathrm{e}}^2/4 = 4d_{\min}/4 = d_{\min}$. The hypersphere effectively restricts the energy of the noise which is related to the squared Euclidean distance between the transmitted and received codewords (cf. (2.5)). In addition to a hypersphere, an equilateral hypercube is readily applicable. For noise samples inside the hypercube, it is ensured that the noise does not alter the sign of *every* transmitted symbol in a block; regardless whether the symbol $+1$ or -1 is transmitted. The hyperquadrant exploits knowledge of the particular transmitted block of symbols to increase the volume of the hypercube. In this case, for *every* symbol in a block, the noise sample can be less than 1 if the symbol -1 is transmitted or greater than -1 if the symbol $+1$ is transmitted. In the following claim, we prove that all three regions are inside the (error-free) decision region $\mathscr{D}(\mathbf{x})$ for any transmitted codeword $\mathbf{x}$.

Claim 2.1 *Consider the hypersphere* $\mathrm{R}_s(d_{\min}) = \{w_i, i = 1, 2, \cdots, n : \sum_{i=1}^{n} w_i^2 \leq d_{\min}\}$, *the*

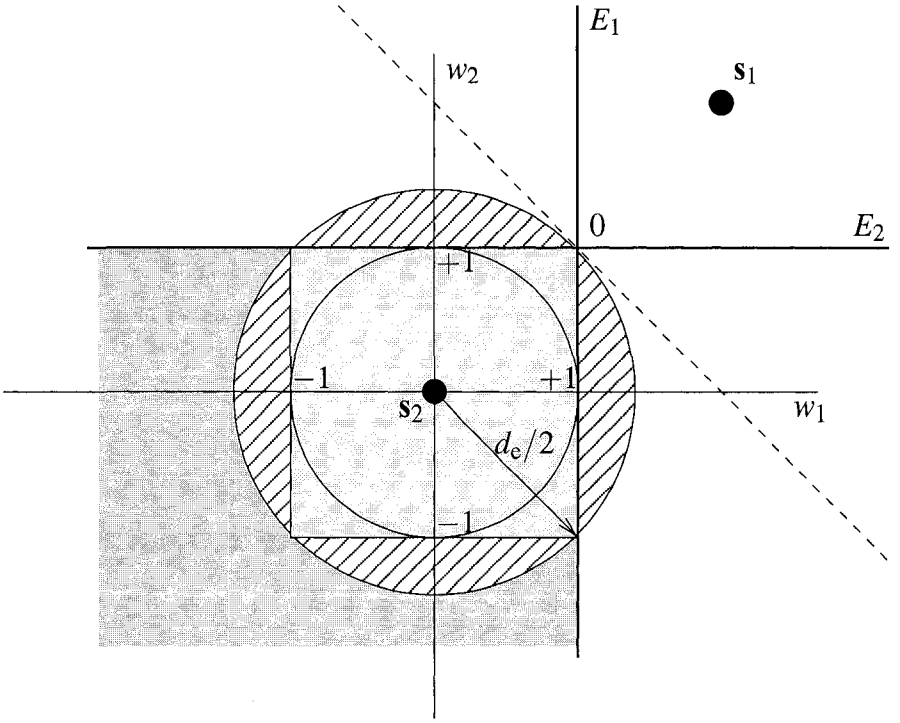

Figure 2.2: Rejection regions for a repetition code in $n = 2$ dimensions with decision boundaries E_1 and E_2 assuming $(1, 1)$ was transmitted which corresponds to signal point $\mathbf{s}_2 = (-1, -1)$.

hypercube $\mathrm{R}_c = \{w_i, i = 1, 2, \cdots, n : |w_i| < 1\}$ *and the hyperquadrant* $\mathrm{R}_q(\mathbf{x}) = \{w_i, i = 1, 2, \cdots, n : w_i(-1)^{x_i} > -1\}$. *For perfectly quantized soft-decisions, if the noise vector* $\mathbf{n}$ *is inside* $\mathrm{R}_s(d_{\min})$, R_c *or* $\mathrm{R}_q(\mathbf{x})$, *the optimum detector selects the correct transmitted codeword.*

Proof: The optimum detector selects the transmitted codeword minimizing the metric (2.5). The coding scheme guarantees that the squared Euclidean distance between any two transmitted sequences is at least $d_e^2 = 4d_{\min}$. Therefore, the detector can tolerate noise energy less than $(d_e/2)^2 = d_{\min}$ which is a definition of the hypersphere. By definition of the hypercube and the hyperquadrant, the noise does not change the sign of any symbol in a transmitted block, i.e., $\mathrm{sign}(y_i) = (-1)^{x_i}$, $i = 1, 2, \cdots, n$. Since this is also a condition for which the minimum of (2.5) is obtained, the detector must select the correct transmitted codeword and no error occurs. ■

The probability mass contained in the hypersphere is [10],

$$\Pr(\mathrm{R}_s(d_{\min})) = \Pr\Big(\|\mathbf{n}\|^2 < T_n\Big) = F_{\|\mathbf{n}\|^2}(T_n) = \tag{2.21}$$

$$= \begin{cases} 1 - \mathrm{e}^{-R\gamma_b d_{\min}} \sum_{k=0}^{\frac{n}{2}-1} \frac{1}{k!} \left(d_{\min} R\gamma_b\right)^k & n \text{ is even} \\ 1 - 2\left(Q\left(\sqrt{2R\gamma_b d_{\min}}\right) + \frac{\mathrm{e}^{-d_{\min} R\gamma_b}}{\sqrt{2\pi}} \sum_{k=1}^{\frac{n-1}{2}} \frac{\left(\sqrt{2R\gamma_b d_{\min}}\right)^{2k-1}}{1 \cdot 3 \cdot 5 \cdots (2k-1)}\right) & n \text{ is odd} \end{cases}$$

where $F_{\|\mathbf{n}\|^2}(T_n)$ is the cumulative distribution function (CDF) of multivariate chi-square distribution with n degrees of freedom. The probability mass of the hypercube is,

$$\Pr(\mathrm{R}_c) = (1-2p)^n \tag{2.22}$$

and of the hyperquadrant is,

$$\Pr(\mathrm{R}_q(\mathbf{x})) = (1-p)^n \tag{2.23}$$

where $p = Q\left(\sqrt{2R\gamma_b}\right) < 1/2$ is the probability of bit-error before decoding for BPSK signaling over an AWGN channel. One can use eqs. (2.20) – (2.23) to determine the potential gains of SR for any coding scheme with binary antipodal signaling and maximum-likelihood sequence detection over a quantized AWGN channel. Note that the probability masses (2.21) – (2.23) are constant (independent of $\mathbf{x}$), and that $\Pr(\mathrm{R}_c) < \Pr(\mathrm{R}_q(\mathbf{x}))$ for any $\mathbf{x}$ and n.

Claim 2.1 ensures that an appropriate hypersphere, hypercube or hyperquadrant can be carved from the noise hyperspace. In the absence of any additional knowledge regarding the error event volume, one cannot use a hypersphere that has squared radius greater than $d_{\min} = 1$ without risk of removing mass from the error event region and creating a biased estimator. The hypersphere of squared radius $d_{\min} = 1$ is always contained inside the corresponding hypercube and hyperquadrant (cf. Fig. 2.2). Hence, as shown in Fig. 2.3 using (2.20) – (2.23), the hypercube and hyperquadrant will provide greater gains than the hypersphere while knowledge of the transmitted codeword increases the volume of the hyperquadrant relative to the hypercube. In Fig. 2.3, we assume a hypothetical rate $1/2$ code. In general, we assume the Singleton bound to lower-bound the block length, n, of a hypothetical code of rate, R, and the minimum Hamming distance, $d_{\min}$, i.e.,

$$n \geq \frac{d_{\min} - 1}{1 - R}.$$

Note that we can also use other lower-bounds of the block length of the hypothetical code, for example, the Plotkin bound [21]. Also, in order to simplify evaluation of the theoretically achievable SR gain, we assume that a hypothetical rate $1/2$ code can be an odd number if we append, for

example, a trailing overall-parity symbol.

Additional knowledge of $d_{\min}$ of the code permits using a hypersphere of greater volume than the hypercube or the hyperquadrant without biasing the estimator. This is shown in Fig. 2.4 assuming again a hypothetical rate $1/2$ code, and an optimistic lower bound of the block length, $n \geq d_{\min}$. We observe that the use of the hypersphere is restricted to lower values of dimensionality, say, $n \leq 100$, while the hypercube and the hyperquadrant can provide value of SR gain at least as large as 2 for dimensionality as large as 400 and 900, respectively, when the SNR $\gamma_b = 10\,\mathrm{dB}$. Note that the gain is the code rate dependent; for example, the change of the code rate from $R = 1/2$ to $R = 1/3$ reduces equivalently the SNR by $1.76\,\mathrm{dB}$. Observe from Fig. 2.4 that the gain of the hypersphere of constant radius decreases much more rapidly with increasing dimensionality than the gains of the hypercube and the hyperquadrant. This is explained as follows.

Fig. 2.5 shows the probability mass contained in the hypersphere of dimension n computed using (2.21) for $d_{\min} R\gamma_b = \{1/2, 1, 2\}$. These values are chosen so that $(d_{\min} R\gamma_b)^k$ decreases, remains constant, or increases as k increases. Observe that the probability mass in the hypersphere is strictly decreasing as n increases for all three cases. There are two reasons for this. First, the mode of the multivariate chi-square PMF moves out to larger and larger values of argument as n increases (see [21, Fig. 2-1-9]). Second, and perhaps much less known than the former fact, the volume of the n-dimensional hypersphere increases with n, attains a maximum at a finite value of n, and then decreases to zero as n increases further. This is seen by plotting the volume of the n-dimensional hypersphere which can be found in [22] and [23]. Fig. 2.6 presents the volume of the n-dimensional hypersphere given by $V_n(r) = \frac{\pi^{n/2} r^n}{\Gamma(n/2+1)}$ where $\Gamma(\cdot)$ is the Gamma function for $r = 1/2, 1$ and 2, demonstrating this behavior.

On the other hand, while the probability mass of the hypercube and the hyperquadrant do decrease to zero as n increases according to (2.22) and (2.23), the volume of the hyperquadrant, and the hypercube when the edge length is greater than one, grows to infinity as n increases. In consequence, the gains of hyperquadrant and hypercube SR suffer far less from increase in dimensionality than does the gain of the hypersphere. In summary, although the gain of the hypersphere can be greater than the gain of the hyperquadrant and the hypercube for small values of n, it will always be smaller for sufficiently large values of n. This discussion and the results presented in Fig. 2.3 establish that the potential gains of SR for moderate to large values of n are much more optimistic than suggested by the results in [10] obtained for hypersphere SR.

Finally, note that the radius of the hypersphere used in SR is constant if $d_{\min}$ of the code is

constant, independent of the block length, n; this is the case, for example, for convolutional codes and some block codes (e.g., Hamming codes). If $d_{\min}$ of the code can grow with the block length (e.g., BCH codes), the hypersphere may outperform the other two regions. In any particular case, one can use (2.20) – (2.23) to compare the gains of the three rejection regions for the problem at hand.

Quantized Soft-Decisions

For quantized soft-decisions, $2 < Q < \infty$, and the rejection regions have to be defined for the DMC model (2.3). The detector maximizes the metric (2.6). The notion of distance between the received sequences is not well-defined, and thus, a hypersphere is not applicable for the DMC. In principle, hypercube SR can be used for the DMC if some of the quantization intervals (2.2) are fully contained inside the interval $(-1, 1)$. The hyperquadrant for the DMC, $\tilde{\mathrm{R}}_q(\mathbf{x})$ (tilde distinguishes the hyperquadrant for the DMC from the hyperquadrant for the AWGN channel), conditioned on the transmitted codeword, $\mathbf{x}$, can be defined noting the even-symmetry of the quantization intervals (2.2). Since the hyperquadrant provides better SR gain, and is more readily applicable for the DMC than the hypercube, we prove the following claim for the hyperquadrant.

Claim 2.2 *Consider the hyperquadrant* $\tilde{\mathrm{R}}_q(\mathbf{x}) = \{e_i, i = 1, 2, \cdots, n : (-1)^{x_i}(e_i - \frac{Q-1}{2}) < 0\}$ *for quantized soft-decisions with* $2 < Q < \infty$. *If the noise vector* $\mathbf{e}$ *is inside* $\tilde{\mathrm{R}}_q(\mathbf{x})$, *the optimum detector always selects the correct transmitted codeword.*

Proof: The optimum detector selects the transmitted codeword in order to maximize the metric (2.6). The metric (2.6) is maximized by choosing the larger from a pair of transition probabilities for every received symbol. If the noise vector is inside $\tilde{\mathrm{R}}_q(\mathbf{x})$, then the channel transition for every symbol in a block is such that the correct transmitted symbol conditioned on the received symbol is more likely than the incorrect one; see Table 2.2. Therefore, the detector must select the correct transmitted codeword and no error occurs. ■

It can be shown that $\Pr\Big(\tilde{\mathrm{R}}_q(\mathbf{x})\Big) = \Pr(\mathrm{R}_q(\mathbf{x}))$ where in (2.23), we substitute the probability of error for a single symbol in a block (before decoding), i.e., $p = \sum_{j=Q/2}^{Q-1} \mathrm{P}_j$ (cf. Fig. 2.2).

Hard-Decisions

For hard-decision decoding, the DMC model (2.3) corresponds to a binary symmetric channel (BSC). The decoder minimizes the metric (2.7). The notion of Hamming distance between the

received sequences is well-defined. Recognizing that up to t errors are corrected by the decoder where $t = \lfloor \frac{d_{\min}-1}{2} \rfloor$, a hypersphere rejection region for the BSC can be defined as $\tilde{\mathrm{R}}_s(d_{\min}) = \{e_i, i = 1, 2, \cdots, n : \sum_{i=1}^{n} e_i^2 \leq t\}$. The probability mass of the hypersphere for the BSC is,

$$\Pr\Big(\tilde{\mathrm{R}}_s(d_{\min})\Big) = \sum_{i=0}^{\lfloor \frac{d_{\min}-1}{2} \rfloor} \binom{n}{i} p^i (1-p)^{n-i} \tag{2.24}$$

where $p = P_1 = 1 - P_0 = Q\big(\sqrt{2\gamma_b}\big)$. Note that for $d_{\min} < 3$ (i.e., $t = 0$), $\Pr\Big(\tilde{\mathrm{R}}_s(d_{\min})\Big) = \Pr(\mathrm{R}_q(\mathbf{x}))$ (cf. (2.23)). A hypercube for the BSC is not possible, since none of the quantization intervals, I_0 and I_1, is inside the interval $(-1, 1)$. Nor is a hyperquadrant for the BSC defined.

The gain of the hypersphere for the BSC for a hypothetical rate $1/2$ code is plotted in Fig. 2.7 using (2.20) and (2.24) for $d_{\min} = 1$ (uncoded transmission), $d_{\min} = 5$ and $d_{\min} = 11$. We assume an optimistic lower bound on the block length, $n \geq d_{\min}$. Comparing Fig. 2.4 with Fig. 2.7, we observe that, for $d_{\min} > 1$, the dimensionality problem is much less severe for hard-decisions than for soft-decision decoding. For example, for SNR $\gamma_b = 8\,\mathrm{dB}$ and $d_{\min} = 11$, a worthwhile hypersphere SR gain of 2 is obtained for a block length of 70 for soft-decisions and 1000 for hard-decision decoding.

2.1.5 Numerical Examples

The actual simulation time savings achievable with SR depends mainly on the ratio of the time required for generation of a received block of samples, t_g, and the time required for decoding such a block, t_d. It is obvious that necessarily $t_g/t_d \ll 1$ in order for the time savings due to SR to be significant. If t_g and t_d can be estimated, one can estimate the total simulation time as [10],

$$\begin{aligned} T_{\mathrm{mc}} &\doteq (t_g + t_d) L_{\mathrm{mc}} \\ T_{\mathrm{sr}} &\doteq (t_g + (1 - \Pr(\mathrm{R}_{\mathbf{x}}))t_d)\, L_{\mathrm{sr}} \end{aligned} \tag{2.25}$$

where T_{mc} is the time required for the MC simulation and T_{sr} is the time required for the simulation using SR. For the same number of simulation trials, i.e., $L_{\mathrm{mc}} = L_{\mathrm{sr}}$, and assuming $t_g/t_d \ll 1$, time savings of the order $T_{\mathrm{mc}}/T_{\mathrm{sr}} \approx 1/(1 - \Pr(\mathrm{R}_{\mathbf{x}}))$ are obtained (cf. (2.20)).

The practical applicability of SR was evaluated using four "real-life" examples of convolutionally coded schemes with hard-decision Viterbi decoding. Schemes I and II are the protection of the most sensitive (class A) bits of the AMR-wideband speech codec in the 3^{rd} generation systems

using a convolutional code of rate $1/3$ and $1/2$, respectively; see [24, Table 2] and [25, Sec. 4.2.3.1]. Schemes III and IV are the convolutionally coded full-rate speech and data channels for the GSM Phase 2+ system; see [26, Sec. 3.1] and [26, Sec. 3.3]. The simulation results obtained using Matlab and Care summarized in Table 2.3 where k is the number of input information data bits, $n = (k + K)/R$ is the length of the codeword including K zero bits to terminate the trellis where K is the constraint length of the convolutional code, g.p. are the generator polynomials of the code in octal notation, $G_{\hat{\mathrm{P}}(e)}$ is the SR gain according to (2.20) and (2.24), and R, $d_{\min}$, γ_b, T_{mc}, T_{sr}, t_g and t_d were defined previously. We observe reductions in simulation run-times by factors from 3.35 to 52.03 for Matlab and 1.43 to 21.23 for the C implementation. The estimated times, t_g and t_d, for the examples in Table 2.3 confirm that the gain of SR depends on the t_g/t_d ratio. The condition $t_g/t_d \ll 1$ is well-satisfied for the simulations in Matlab and the gains realized in simulations are in good-to-fair agreement with the predicted gains. However, the condition $t_g/t_d \ll 1$ is not satisfied for the simulations in C. In particular, for $R = 1/2$, the gain achievable in C is approximately half of the theoretically predicted gain, but nonetheless valuable. The different gains of the SR simulation technique for Matlab and C implementations can be explained as follows. In Matlab, the time to decide whether the received sequence will be rejected is much smaller than the time to decode this sequence. On the other hand, in C, and especially for smaller sequence length, the time to reject the sequence can be comparable to the sequence decoding time. In general, the ratio of times to decode and reject the received sequence is increasing with the sequence length for both Matlab and C implementations. There are other factors that influence the total required simulation time and these are machine and compiler specific, precluding more accurate estimation of the SR gains.

Table 2.3: Simulation results for four convolutionally coded schemes with trellis termination and hard-decision Viterbi decoding implemented in Matlab and in C, respectively.

scheme	I		II			III			IV	
(n,k)	$(210,62)$		$(176,80)$			$(378,185)$			$(488,240)$	
g.p.	$0557,0663,0711$		$0561,0753$			$023,035$			$023,035$	
$R,K,d_{\min}$	$1/3,8,18$		$1/2,8,12$			$1/2,4,7$			$1/2,4,7$	
γ_b [dB]	7.0		7.0			8.0			8.0	
$G_{\mathrm{f(e)}}$	3.56		40.33			5.15			2.97	
script	Matlab									
errors	6	6	6	5	11	8	6	6		
blocks	5309734	4118050	1127315	787997	74620	57679	39576	37023		
rej. blocks	—	2961702	—	768653	—	46337	—	24701		
BER	$1.82\text{x}10^{-8}$	$2.35\text{x}10^{-8}$	$6.65\text{x}10^{-8}$	$7.93\text{x}10^{-8}$	$7.97\text{x}10^{-7}$	$7.50\text{x}10^{-7}$	$6.32\text{x}10^{-7}$	$6.75\text{x}10^{-7}$		
$T_{\mathrm{mc}}, T_{\mathrm{sr}}$ [s]	211341	63182	68837	1323	4505	695	3248	955		
$T_{\mathrm{mc}}/T_{\mathrm{sr}}$	3.35		52.03		6.48		3.40			
t_g [s]	$3.78\text{x}10^{-4}$		$3.36\text{x}10^{-4}$		$4.17\text{x}10^{-4}$		$4.55\text{x}10^{-4}$			
t_d [s]	$5.77\text{x}10^{-2}$		$5.86\text{x}10^{-2}$		$6.20\text{x}10^{-2}$		$7.72\text{x}10^{-2}$			
script	C-language									
errors	33	30	100	101	102	102	100	102		
blocks	32930688	27344824	17953710	16706926	797928	700742	612911	790578		
rej. blocks	—	19655085	—	16291855	—	564996	—	523945		
BER	$1.61\text{x}10^{-8}$	$1.77\text{x}10^{-8}$	$6.96\text{x}10^{-8}$	$7.56\text{x}10^{-8}$	$6.91\text{x}10^{-7}$	$7.87\text{x}10^{-7}$	$6.80\text{x}10^{-7}$	$5.38\text{x}10^{-7}$		
$T_{\mathrm{mc}}, T_{\mathrm{sr}}$ [s]	93540	25754	44247	2084	457	165	489	343		
$T_{\mathrm{mc}}/T_{\mathrm{sr}}$	3.63		21.23		2.77		1.43			
t_g [s]	$1.40\text{x}10^{-4}$		$1.25\text{x}10^{-4}$		$2.05\text{x}10^{-4}$		$3.37\text{x}10^{-4}$			
t_d [s]	$3.18\text{x}10^{-3}$		$2.75\text{x}10^{-3}$		$3.80\text{x}10^{-4}$		$5.00\text{x}10^{-4}$			

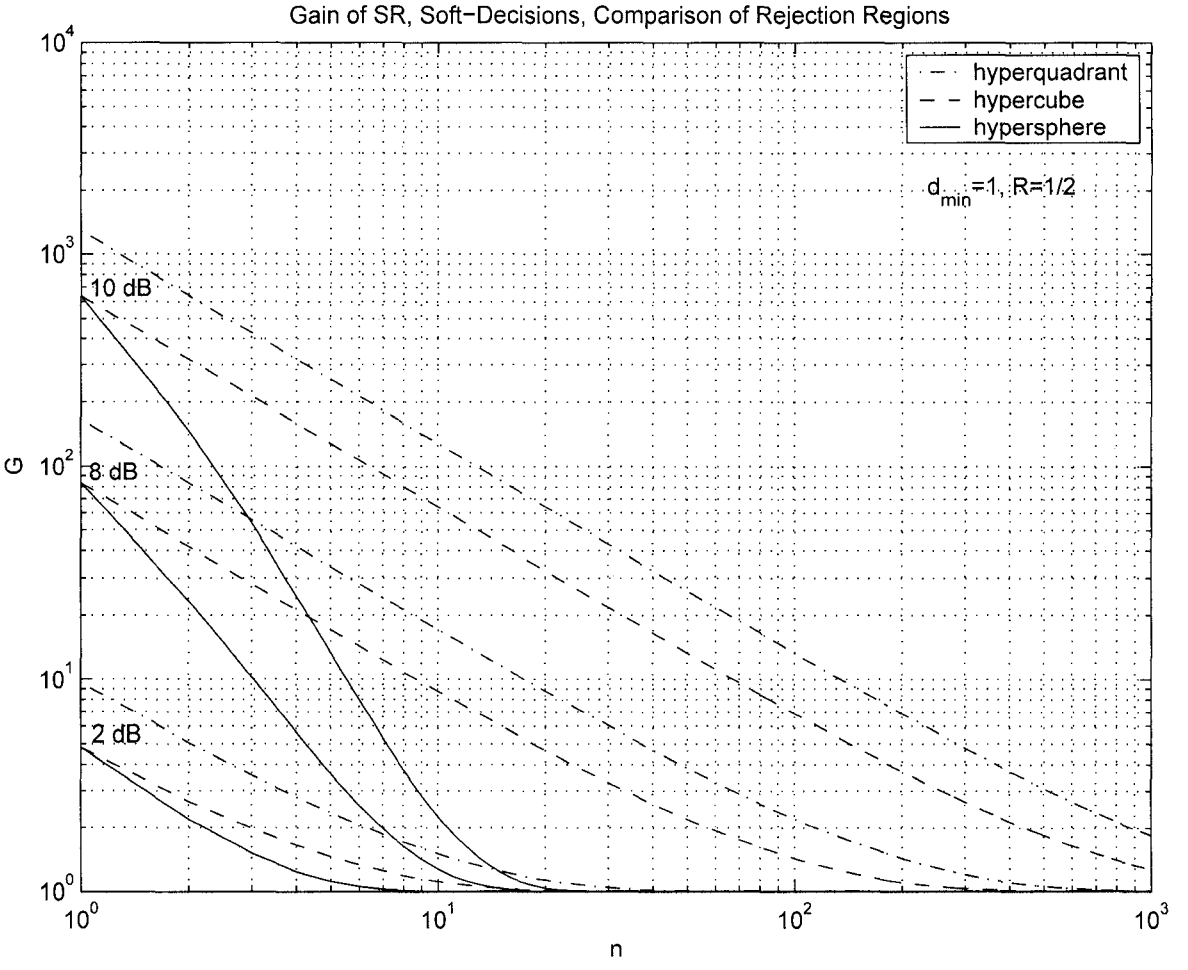

Figure 2.3: The gain of SR versus dimensionality n with perfectly quantized soft-decision decoding and the hypersphere, hypercube and hyperquadrant rejection regions with SNR per uncoded modulated symbol $\gamma_b = 2, 8$ and $10\,\mathrm{dB}$, minimum Hamming distance $d_{\min} = 1$ and code rate $R = 1/2$.

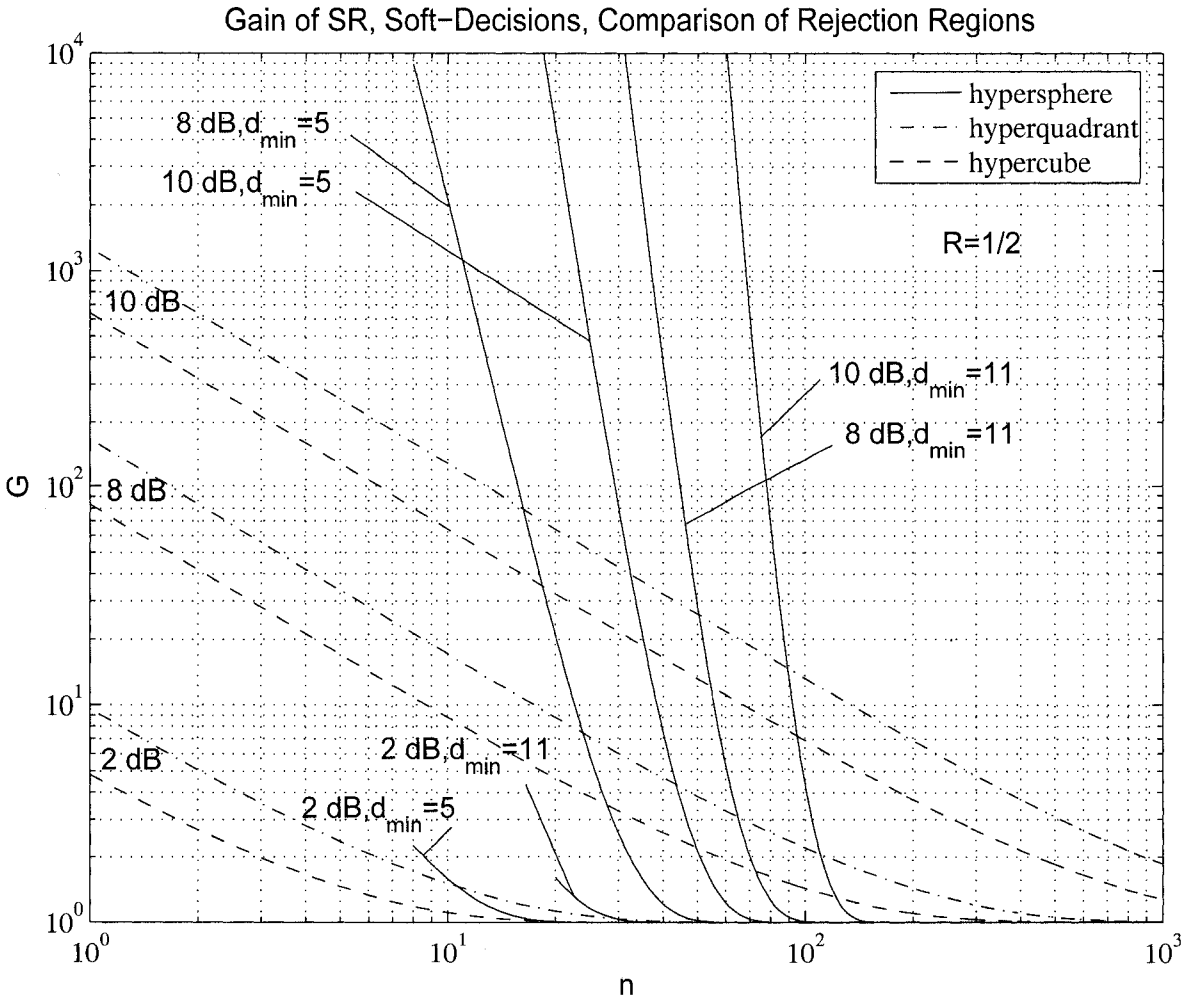

Figure 2.4: The gain of SR versus dimensionality n with perfectly quantized soft-decision decoding and the hypersphere, hypercube and hyperquadrant rejection regions with SNR per uncoded modulated symbol $\gamma_b = 2, 8$ and $10\,\mathrm{dB}$, minimum Hamming distance $d_{\min} = 5, 11$ and code rate $R = 1/2$.

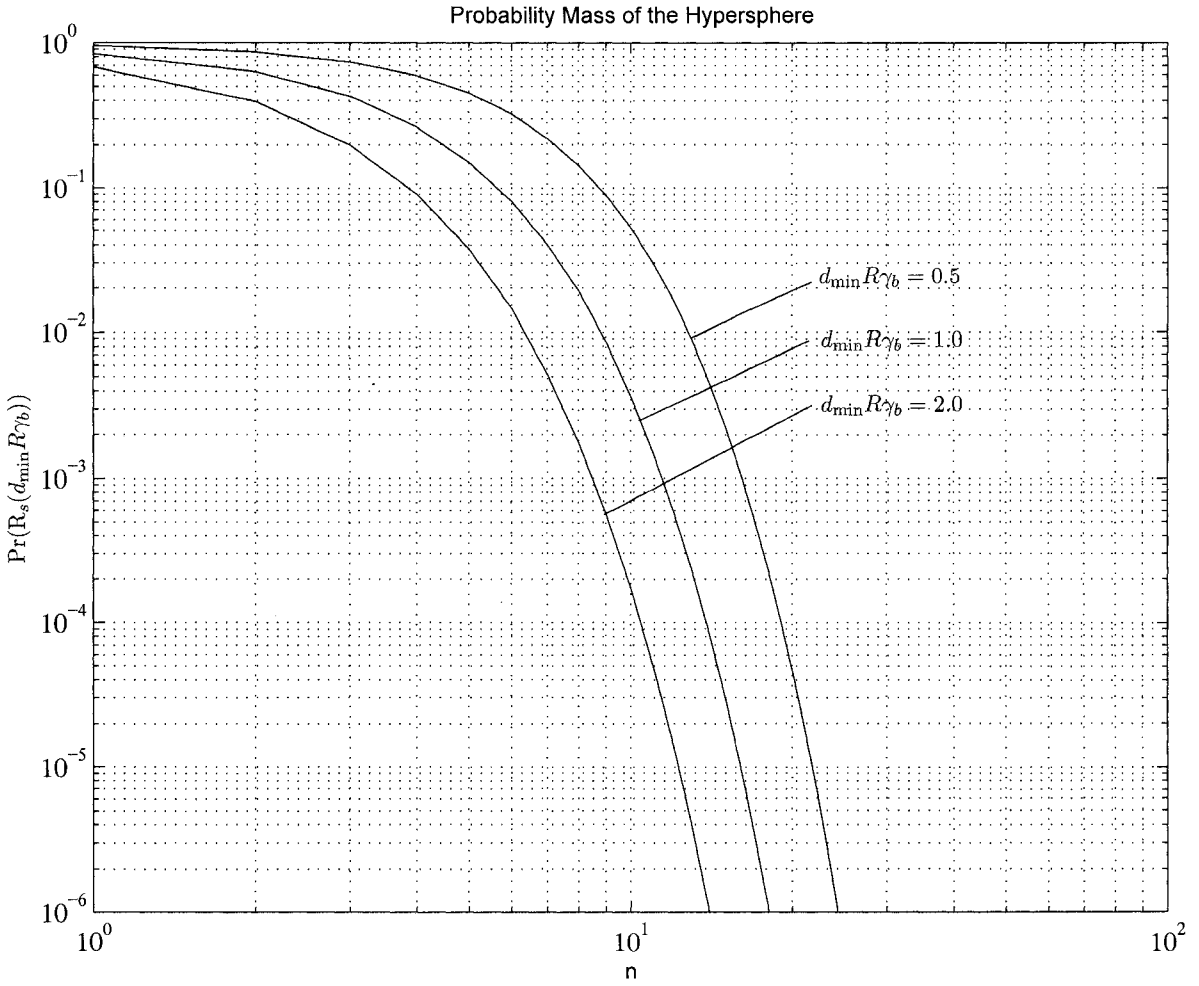

Figure 2.5: The probability mass of the hypersphere versus dimensionality n for perfectly quantized soft-decision decoding.

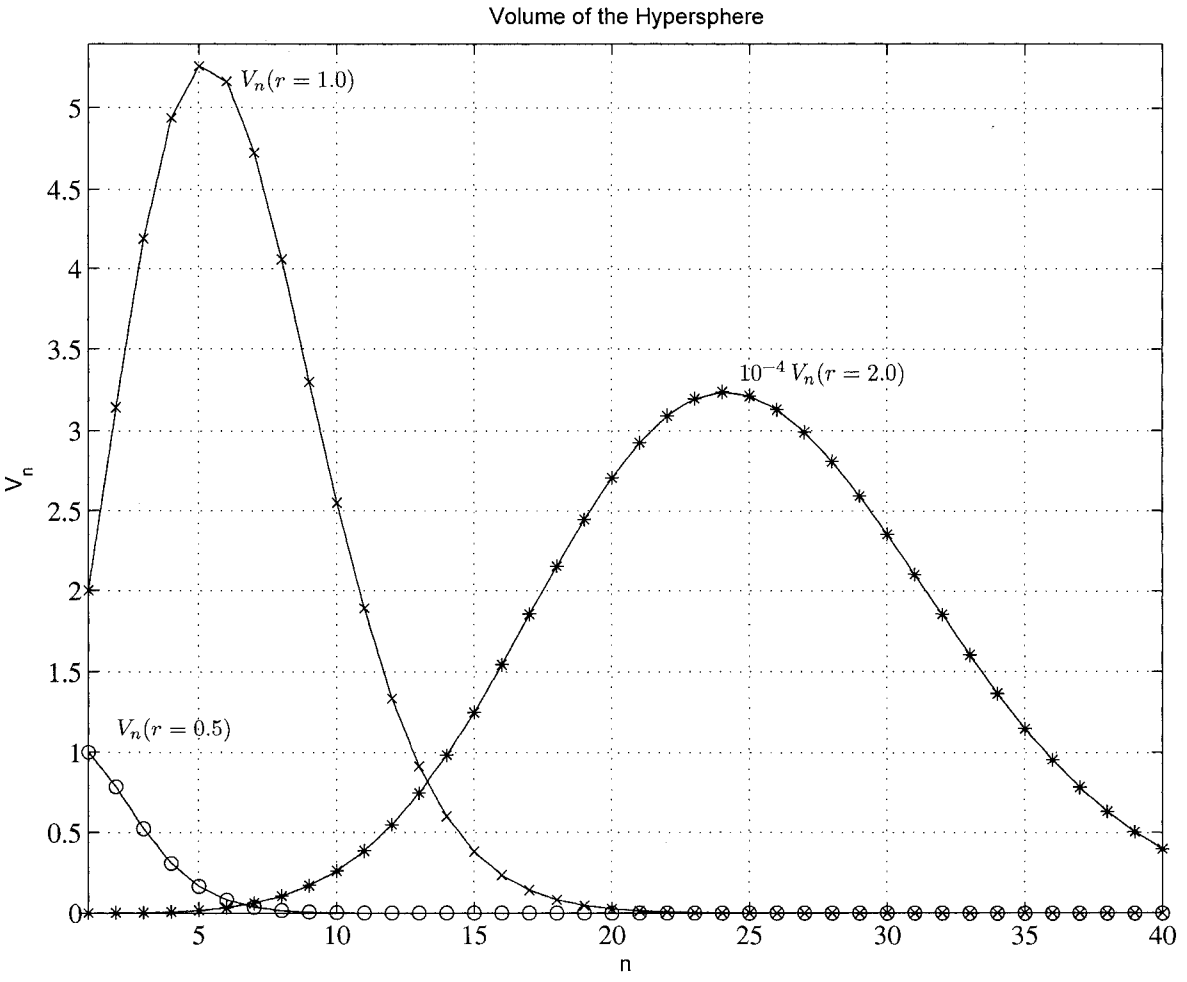

Figure 2.6: The volume of the n-dimensional hypersphere.

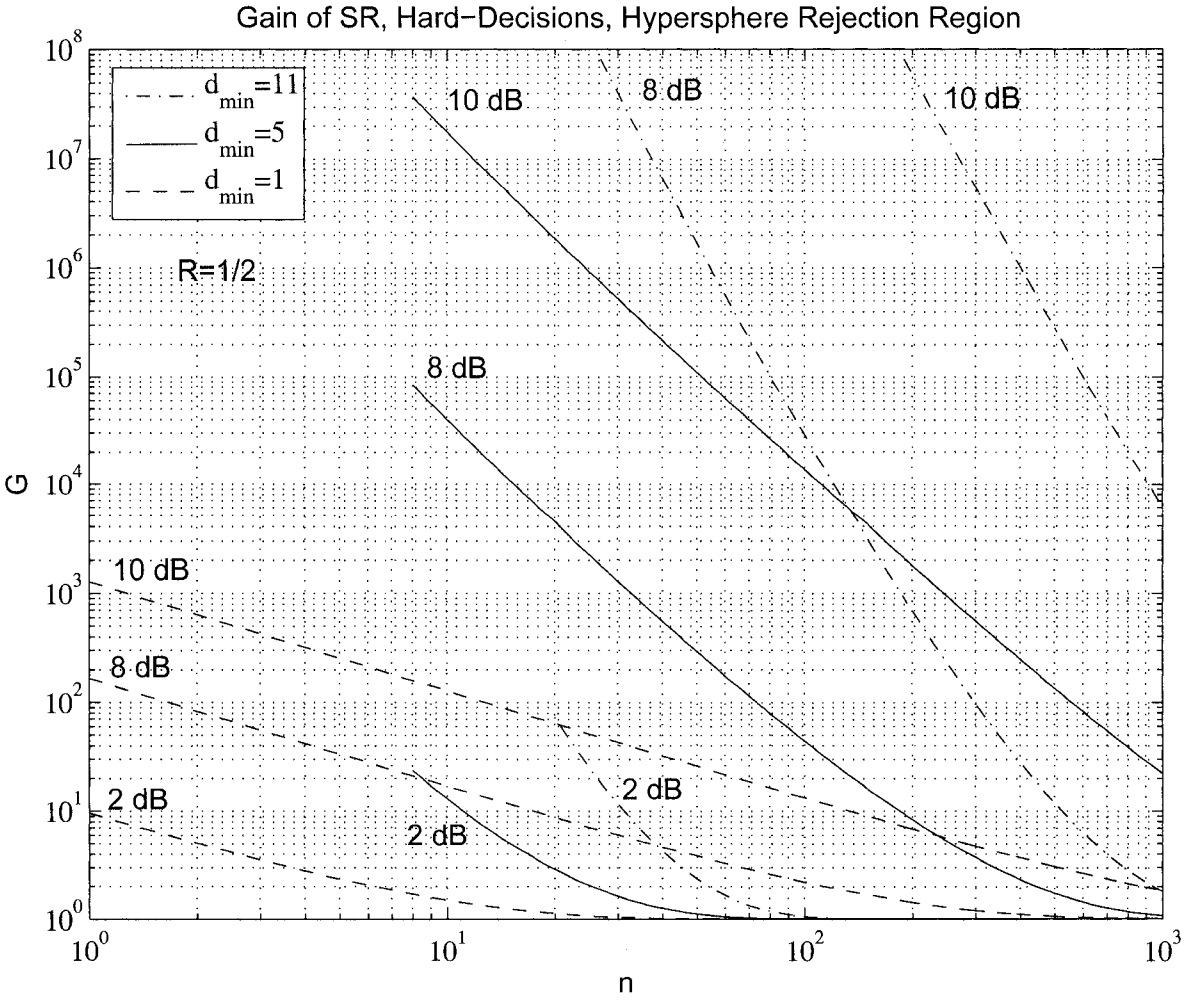

Figure 2.7: The gain of SR versus dimensionality n for hard-decision decoding and the hypersphere rejection region for a BSC with SNR per uncoded modulated symbol $\gamma_b = 2, 8$ and 10 dB, minimum Hamming distance $d_{\min} = 1, 5$ and 11 and code rate $R = 1/2$.

2.2 Sample Rejection for Simulations of Binary Coded Schemes and near-MLSD over ISI Channels

2.2.1 Background

The SR simulation technique biases the channel transitional probability distribution by discarding the received sequences that are known beforehand to be decoded error-free. For the case of binary block-coded transmission over a quantized AWGN channel and MLSD using the VA, a hypersphere, hypercube and hyperquadrant rejection regions were considered in the previous section. However, for ISI channels, the lattice observed at the detector input is skewed, and neither hypercube nor hyperquadrant are applicable. Furthermore, the minimum Euclidean distance between the transmitted sequences in the case of uncoded transmission over an ISI channel is typically small. Then, especially for large block-lengths (i.e., large dimensionality), a hypersphere rejection region is inefficient. Therefore, we investigate the sliding-window MLSD to resolve the dimensionality problem as well as to mitigate the problem of the small Euclidean distance between the transmitted sequences. The length of the observation window (i.e., to what extent the channel memory is ignored) determines how closely we can approach the MLSD performance. In particular, we study the truncated VA (tVA) [21], and FD [21, p. 505], [27] which is a special case of the stack sequential decoding [28], [29]. The combination of the VA and FD to decode high-rate convolutional codes was proposed in [30]. Sliding-window FD for MIMO detection was considered in [31]. For ISI channels, the multiple path sequential stack algorithm is considered in [32], and the Fano sequential decoder was studied in [33]. The complexity of the VA for MLSD of ISI channels is reduced by periodically inserting zeros in [34]. The SR principles for the Zigangirov-Jelinek sequential decoder are independently considered in [12]. An error-event simulation method introduced in [9] can be also considered as a form of SR. A general discussion of improving the efficacy of MC estimators can be found in [35].

In this section, we generalize the idea of SR for efficient simulations of multidimensional communication systems. In particular, conditioning the sequence decisions at the receiver on knowledge of the transmitted sequence and on knowledge of the finite impulse response (FIR) of the channel and the noise realization, we modify the tVA and the FD algorithm to obtain the MLSD solution in shorter time than required using the conventional VA. Both the modified tVA (mtVA) and the modified FD (mFD) are more robust against error propagation than the tVA and FD which results in reduced simulation run-times. However, it is important that the mtVA and the mFD estimators

remain unbiased with respect to the tVA and FD. Next, we propose the hypersphere SR for use in FD to further improve the simulation efficiency.

This section is organized as follows. The system model and MLSD are described in Section 2.2.2. The SR principle is generalized and then applied to MLSD in Section 2.2.3. In Section 2.2.4, we discuss FD, the tVA, the modified FD, the modified tVA and the FD/SR algorithm for efficient simulation of ISI channels and near MLSD. Finally, numerical examples and discussion are given in Section 2.2.5.

2.2.2 System Model

Assume that information symbol, d_k, is mapped to a M-ary pulse amplitude modulation (PAM) data symbol, $u_k \in \{M-1-2d_k, d_k = 0, 1, \cdots, M-1\}$, at the symbol time interval, k. The PAM symbols are continuously transmitted over a static multipath channel with FIR, $\mathbf{a} = (a_0, a_1, \cdots, a_K)$, where K is the channel memory; see Fig. 2.8. The sequence of transmitted data symbols is periodically terminated after every n symbols. Let the row vector of $(n+2K)$ data symbols be denoted as $\mathbf{u} = (u_{-K}, \cdots, u_{-1}, u_0, \cdots, u_{n-1}, u_n, \cdots, u_{n+K-1})$. Hence, without loss of generality, let $u_{-K} = \cdots = u_{-1} = 1$ and $u_n = \cdots, u_{n+K-1} = 1$. The carrier, time and block synchronization is assumed to be perfect, and the received signal is sampled once every symbol period at the output of an ideal whitening and matched filter. Then, the received $(n+K)$-dimensional vector, $\mathbf{r}$, can be written as,

$$\mathbf{r} = \mathbf{x} + \mathbf{w} = \mathbf{uA} + \mathbf{w} \tag{2.26}$$

where the channel matrix, $\mathbf{A} \in \mathbb{R}^{(n+2K, n+K)}$, is,

$$\mathbf{A} = \begin{bmatrix} a_K & & & \\ a_{K-1} & a_K & & \\ \vdots & a_{K-1} & \ddots & a_K \\ a_0 & \vdots & & a_{K-1} \\ & a_0 & \ddots & \vdots \\ & & & a_0 \end{bmatrix}.$$

The vector, $\mathbf{w}$, represents a zero-mean AWGN, i.e., we assume that the elements of $\mathbf{w}$ are uncorrelated, and thus, independent, with variance, $\sigma_w^2 = N_0/2$, per dimension. The noise and the transmitted signal are uncorrelated. Assume symbols, u_k, are equiprobable, $\mathrm{E}[u_k u_l] = 0$

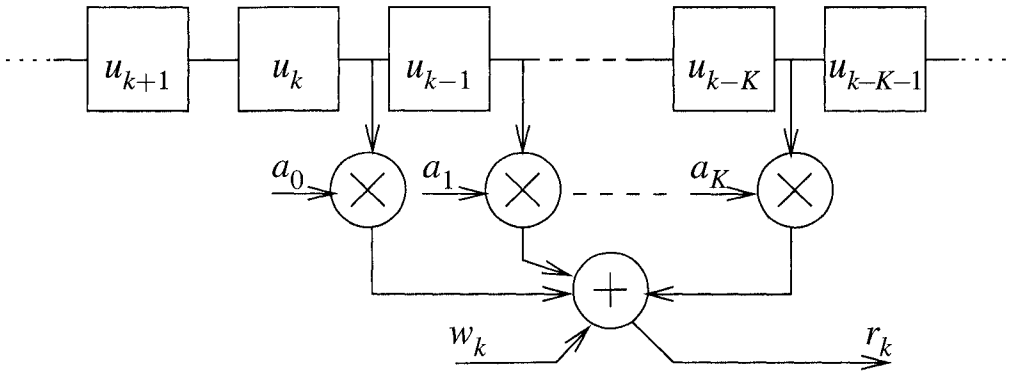

Figure 2.8: The FIR channel model with AWGN.

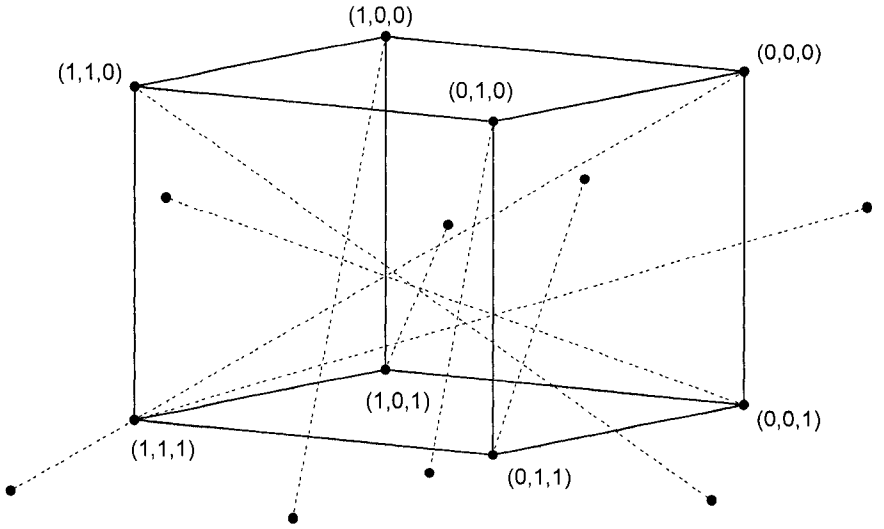

Figure 2.9: An example of the transmitted and the received lattices.

for $k \neq l$, and $\mathrm{E}\left[|u_k|^2\right] = E_s$ is the average energy per symbol. The channel FIR is assumed to be normalized so that the squared Euclidean norm, $\|\mathbf{a}\|^2 = 1$. Thus, the SNR per bit is $\gamma_b = E_s(N_0 \log_2 M)^{-1} = E_s(2\sigma_w^2 \log_2 M)^{-1}$.

To illustrate the effect of ISI at the output of the channel on the transmitted lattice, assume $M = 2$ where the bits-to-symbol mapping, '0' $\rightarrow -1$, and, '1' $\rightarrow +1$, and $\mathbf{a} = (0.79, 0.62)$, i.e., $K = 1$. The transformed $(n = 3)$-dimensional input vectors (corresponding to the vertexes of the 3D-cube) are indicated by dashed lines in Fig. 2.9. Hence, the ISI may result in a severe distortion of the transmitted lattice which significantly complicates the design of rejection regions for use in SR.

2.2.3 MLSD

The MLSD detector is optimum in the sense of minimizing the probability of incorrect sequence decision. In a zero-mean AWGN channel, MLSD is equivalent to the least-squares problem [36, p. 187]. In particular, the MLSD detector minimizes the log-likelihood function [21],

$$\mathcal{L}_{i,j:k,l} = \min_{\mathbf{u}_i^{k-K-1}:s_i=S_j,s_k=S_l} \sum_{p=i}^{k-1} \left| r_p - \sum_{q=0}^{K} a_q u_{p-q} \right|^2 \tag{2.27}$$

where $\mathbf{u}_i^{k-K-1} = (u_i, u_{i+1}, \cdots, u_{k-K+1})$, and $\mathcal{L}_{i,j:k,l}$ is the minimum metric for all sequences originating from the state, S_j, at time, i, and terminating at the state, S_l at time, k. The channel states are defined as $s_k \in \{S_0, \cdots, S_{M_s-1}\}$ where $M_s = M^K$, or equivalently, the states, $\mathbf{s}_k = (u_{k-K}, \cdots, u_{k-1})$. We denote $\mathcal{L}_{0,0:k,l} \equiv \mathcal{L}_{k,l}$, and note that it is assumed, $\mathbf{s}_0 = (1, 1, \cdots, 1) = \mathbf{1}_{(1,K)} = \mathbf{s}_{n+K}$. If the block, $\mathbf{u}$, is transmitted, the MLSD finds $\hat{\mathbf{u}}_{\mathrm{ML}} = \arg\min_{l=0,1,\cdots,M_s-1} \mathcal{L}_{k,l}$. The VA is often used to find the MLSD solution efficiently if the transmitted sequences are described using a trellis. Note that the complexity of the VA does not decrease with SNR. Hence, the complexity of the VA can be reduced if the increased SNR is taken into account.

2.2.4 Generalization of SR Simulation Technique

Recall that typically the time, t_g, to generate the received sequence, $\mathbf{r}$, is negligible compared to the time to decode such a sequence, t_d, since the optimum decoder must search over the whole space of possible transmitted sequences, $\mathbf{u}(\mathbf{d})$. Hence, significant simulation run-time savings can be obtained if the decoded sequence at the receiver can be obtained more efficiently, for example, conditioned on knowledge of the transmitted sequence, and knowledge of the channel FIR and AWGN realizations. It is important that the decisions, $\hat{\mathbf{d}}$, conditioned on such knowledge do not bias the BER estimator. In particular, consider the block diagram for the SR simulation of a generic communication system in Fig. 2.10. A block labeled, 'SR', is inserted between the received signal and the receiver, 'Rx'. Note that all the simulation random inputs (provided by the random generators, 'RG') are fed also into the 'SR' block. The BER counter is updated with an estimate of the most likely transmitted sequence, $\hat{\mathbf{d}}$, either from the 'SR' block or from the receiver.

The efficiency of the SR simulation technique is measured in terms of the variance reduction of the BER estimator. Also, the gain of SR, G, is approximately equal to the ratio of the number of simulation trials without SR and with SR for a given variance of the BER estimator. Let the MC

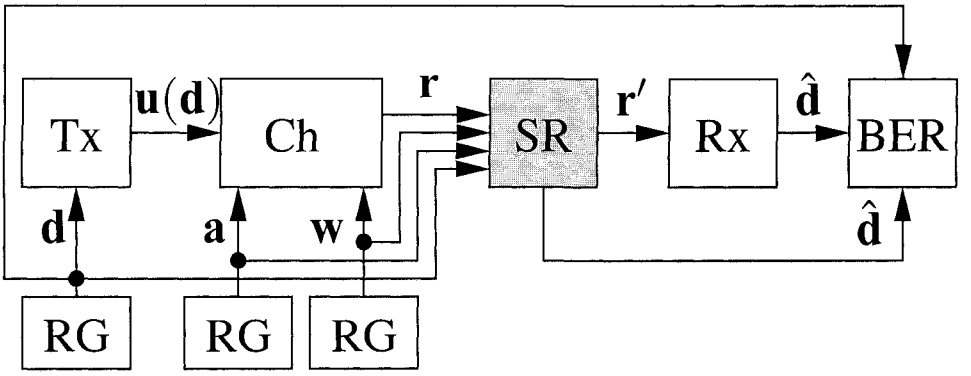

Figure 2.10: The SR simulation of a generic communication system.

simulation run-time be, $T_{\rm mc} = (t_g + t_d)N$, and the SR simulation run-time be, $T_{\rm sr} = (t_g + t_d(1 - \mathrm{P}_r) + t_r\mathrm{P}_r)N$, where t_r is the time required to reject the received sequence and decide on $\hat{\mathbf{d}}$, P_r is the probability of rejecting the received sequence, and N is the number of simulation trials. The SR gain is,

$$G \approx \frac{T_{\rm mc}}{T_{\rm sr}} = \frac{1}{1 - \epsilon \mathrm{P}_r} \tag{2.28}$$

where $\epsilon = \frac{t_d - t_r}{t_d + t_g}$ is implementation dependent, and it is required that $t_g \ll t_d$ and $t_r \ll t_d$, i.e., the added complexity of the SR block must be minimized. The probability, P_r, is a function of the SNR, the system dimensionality and the rejection region chosen.

We can elaborate on the SR simulation technique further. In particular, consider simulation of a communication system in Fig. 2.11. Observation, $y(t, \mathbf{d}, \mathbf{p})$, at time, t, is a function of data symbols, $\mathbf{d}$, and parameters, $\mathbf{p}$. The detector DET decides on the most likely transmitted symbols using the ML rule,

$$\hat{\mathbf{d}} = \underset{\tilde{\mathbf{d}}}{\operatorname{argmin}}\, p\big(y(t, \tilde{\mathbf{d}}, \mathbf{p})|\tilde{\mathbf{d}}\big).$$

The SR simulation technique consists of a detector DET_1 and the rejection rule that is used to select either the detector DET or detector DET_1 for processing the received samples, y. In order to maximize the simulation run-time reduction of the SR technique (i.e., the SR gain), it is required that the complexity, $\mathcal{O}(\mathrm{DET})$, of the detector, and, $\mathcal{O}(\mathrm{DET}_1)$, of the SR detector 1 are such that,

$$\mathcal{O}(\mathrm{DET}) \gg \mathcal{O}(\mathrm{DET}_1)$$

and the detector 1 is selected as many times as possible, i.e., with the probability, $\mathrm{P}_r \to 1$. Further-

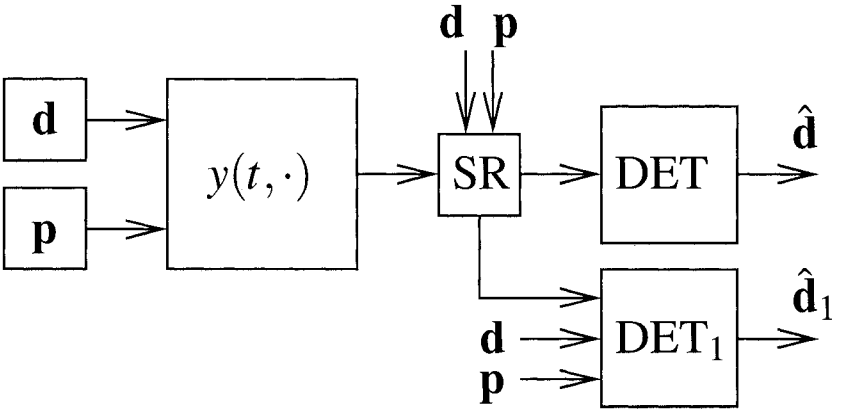

Figure 2.11: The SR simulation principle.

more and importantly, it is required that,

$$\Pr\left(\mathbf{d} \neq \hat{\mathbf{d}}\right) = \Pr\left(\mathbf{d} \neq \hat{\mathbf{d}}_1\right)$$

so that the SR detector provides an unbiased estimate of the probability of error, $\Pr\left(\mathbf{d} \neq \hat{\mathbf{d}}\right)$. Generalization of the SR simulation in Fig. 2.11 to more than two detectors is straightforward.

SR and MLSD

We can rewrite the squared Euclidean norm (cf. (2.26)) as,

$$\|\mathbf{r} - \tilde{\mathbf{x}}\|^2 = \|\mathbf{x} - \tilde{\mathbf{x}} + \mathbf{w}\|^2 = \|\Delta_{\mathbf{x}\tilde{\mathbf{x}}} + \mathbf{w}\|^2 \tag{2.29}$$

where $\mathbf{x}$ is the transmitted sequence at the channel output, $\tilde{\mathbf{x}}$ is a candidate solution, and the components of $\Delta_{\mathbf{x}\tilde{\mathbf{x}}}$ are conditioned on knowledge of the components of $\mathbf{x}$, i.e., $[\Delta_{\mathbf{x}\tilde{\mathbf{x}}}]_i \in \{2(d' - d) : d' = 0, 1, \cdots, M-1 \text{ and } d : x_i = (M - 1 - 2d)\}$. Hence, the components of $\Delta_{\mathbf{x}\tilde{\mathbf{x}}}$ are from the set of cardinality, M, and minimization of $\|\Delta_{\mathbf{x}\tilde{\mathbf{x}}} + \mathbf{w}\|^2$ has the same complexity as minimization of $\|\mathbf{r} - \tilde{\mathbf{x}}\|^2$. We can prove that the MLSD solution, $\mathbf{x}_{\mathrm{ML}}$, minimizing (2.29) results in an unbiased BER estimator; see Fig. 2.12. Since we have that, $\arg\min_{\Delta_{\mathbf{x}\tilde{\mathbf{x}}}} \|\Delta_{\mathbf{x}\tilde{\mathbf{x}}} + \mathbf{w}\|^2 = \arg\min_{\Delta_{\mathbf{x}\tilde{\mathbf{x}}}} \left(\|\Delta_{\mathbf{x}\tilde{\mathbf{x}}}\|^2 + 2\Delta_{\mathbf{x}\tilde{\mathbf{x}}} \cdot \mathbf{w}\right) \leq \|\mathbf{w}\|^2$ where the dot denotes the inner product, it is necessary that the term, $\|\Delta_{\mathbf{x}\tilde{\mathbf{x}}}\|^2$, is minimized. This suggests to search for the MLSD solution among sequences in the vicinity of $\mathbf{x}$. Thus, we restrict the search over the set of sequences about $\mathbf{x}$ that can differ only for $L < n$ consecutive symbols (or equivalently, we search over L consecutive dimen-

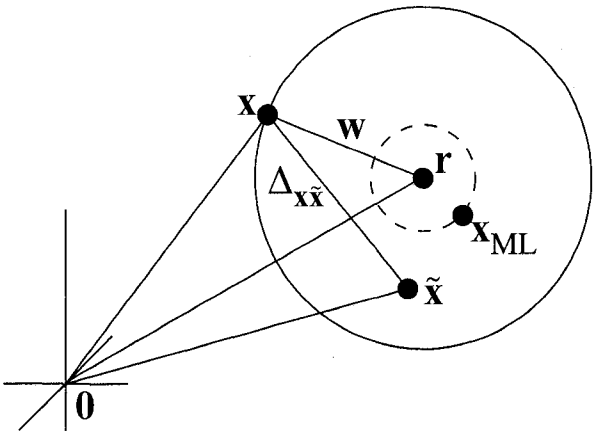

Figure 2.12: Geometric interpretation of the MLSD.

sions) which leads to the decoding algorithm known as FD. Since typically $L \ll n$, an important consequence of FD is the reduction of the effective system dimensionality, from $L_{\text{eff}} = n + K$ to $L_{\text{eff}} = L + K$, and thus, the potential gains of SR are improved (cf. (2.28)).

Sliding-Window Decoding

The transmitted sequence, $\mathbf{x}$, at the channel output can be described using the tree or using the trellis (if the same states are merged). The MLSD receiver searches the tree or the trellis to find the sequence minimizing the squared Euclidean norm (2.29). For example, the VA searches the trellis discarding all but M_s most likely transmitted sequences. The decoding based on a finite-length observation window is clearly suboptimal; information outside the observation window is neglected, however, the decoding delay is reduced as is also the decoding complexity in the case of the tree search. The sliding-window decoder of length $(L + K)$ samples makes the decisions, $\hat{u}_k$, $k = 0, 1, \cdots, n - L + 1$, using the received samples, $\mathbf{r}_k^{k+L+K-1}$, and knowledge of the state, $\mathbf{s}_k = S_j$, at time k. In particular, the decision, $\hat{u}_k$, is evaluated as,

$$\hat{u}_k = \underset{l=0,1,\cdots,M_s-1}{\operatorname{argmin}} \mathcal{L}_{k,j:k+L+K-1,l} \tag{2.30}$$

while the decisions on the remaining symbols in the block, $\hat{u}_k$, $k = n-L+2, \cdots, n$, are determined, for example, using the sequence minimizing the metric (2.30) for $k = n - L + 1$. If $M = 2$ (binary

signaling), the log-likelihood ratio [21],

$$\Lambda_k = \frac{\min\limits_{l=0,1,\cdots,M_s-1} \mathcal{L}_{k,j:k+L+K-1,l}(u_k = +1)}{\min\limits_{l=0,1,\cdots,M_s-1} \mathcal{L}_{k,j:k+L+K-1,l}(u_k = -1)}$$

provides the reliability of the estimate (2.30). Note that since the metric (2.30) depends on the state, s_k, an incorrect decision of $\hat{u}_k$ may cause erroneous decisions in the subsequent symbols. Hence, error propagation sets the lower limit on the minimum length of the observation window, L, [29, Sec. 4.7, Sec. 5.6]. The smaller values of L are possible for larger values of SNR and for the smaller block-lengths, n, which reduces the complexity of the decoder.

The value of L is selected to achieve desired accuracy of the MLSD. Let $\mathrm{P_{ML}}$ be the unbiased BER estimate corresponding to MLSD. Let p be the probability that the sliding-window decoder will find the MLSD solution, and the biased BER estimate of the suboptimum sliding-window decoder will be in the interval $(0.1\mathrm{P_{ML}}, 10\mathrm{P_{ML}})$. Then, the average BER of the sliding-window decoder, P, is bounded as,

$$(0.1 + 0.9p)\mathrm{P_{ML}} < \mathrm{P} < (10 - 9p)\mathrm{P_{ML}}. \tag{2.31}$$

Truncated VA

The most likely transmitted sequence is searched in the trellis having M^K states. For every received sample, the M^K candidate sequences are extended by one symbol, and the final decision is made about the symbol L epochs back in the history using the current estimate of the most likely transmitted sequence. Since typically $M^K < M^L$, a smaller number of candidate sequences are stored using the tVA than using FD. Thus, the tVA requires, in general, a longer observation window; error-propagation can be neglected if $L \approx 5(K+1)$ [21].

FD

The FD technique was proposed for decoding the convolutional codes in [27]. At every step, FD searches the tree of depth, L, symbols, and makes the final decision on the first symbol of the tree corresponding to the root. Then, the tree search advances one symbol forward. In general, error-propagation can be neglected if $(K+1) \leq L \leq 2(K+1)$ [21, p. 505]. There are M^L paths to be searched for every received symbol, and thus, the search must be done efficiently. The available tree-search strategies are the following.

Look-up-table (LUT): For moderate values of M and L, a brute-force search is possible.

M-algorithm, T-algorithm [28], [37]: These algorithms are preferable if the brute-force search becomes inefficient.

Sphere decoding (SD): The structure of the matrix, $\mathbf{A}$, in (2.26) can be exploited to search for the lattice points inside the sphere about the received point, and thus, the usual QR-decomposition can be avoided [38].

Sample rejection (SR): Conditioned on the transmitted sequence, $\mathbf{u}$, FIR, $\mathbf{a}$, and the noise, $\mathbf{w}$, we may directly decide on the sequence minimizing the metric, and thus, completely avoid the computationally expensive tree-search.

Modified tVA and Modified FD

Error propagation decreases with the length of the observation window, L, however, complexity (e.g., the storage requirements) is increased. Assume the search for the closest lattice point, $\mathbf{x}_{\mathrm{ML}}$, is performed using the metric, $\|\Delta_{\mathbf{x}\tilde{\mathbf{x}}} + \mathbf{w}\|^2$ (cf. (2.29)). In particular, the decoder makes the decisions,

$$\hat{u}_k = u_k - \underset{\tilde{\Delta}_{\mathbf{x}\tilde{\mathbf{x}}}}{\operatorname{argmin}} \sum_{i=k}^{k+L+K-1} |[\tilde{\Delta}_{\mathbf{x}\tilde{\mathbf{x}}}]_i + w_i|^2$$

where $\tilde{\Delta}_{\mathbf{x}\tilde{\mathbf{x}}} = \mathbf{x}_{i=k}^{k+L+K-1} - (\hat{\mathbf{s}}_k, \tilde{u}_k, \cdots, \tilde{u}_{k+L-1}, \mathbf{0}_{(1,K)})\mathbf{A}'$, $\hat{\mathbf{s}}_k$ is the estimate of the state at time, k, $\mathbf{0}_{(1,K)}$ is the all-zero vector, and $\mathbf{A}'$ is the corresponding channel matrix. Hence, the initial state for decoding the symbol, $\hat{u}_k$, is given as a difference, $\mathbf{s}_k - \hat{\mathbf{s}}_k$. Therefore, the modified search is more robust against error propagation if the estimate of $\hat{\mathbf{s}}_k$ is incorrect, and thus, the values of L can be reduced. The sliding-window search of the vector, $\Delta_{\mathbf{x}\tilde{\mathbf{x}}}$, minimizing the metric (2.29), will be referred to as the modified FD (mFD) and the modified tVA (mtVA).

The window length, L, could be reduced further if the search is done iteratively. In particular, the estimate, $\hat{\mathbf{u}}\mathbf{A}$, is used as the transmitted sequence in the repeated search. Then, the noise vector in the second iteration is $\mathbf{w}' = \mathbf{r} - \hat{\mathbf{u}}\mathbf{A}'$, and $\|\mathbf{w}'\|^2 \leq \|\mathbf{w}\|^2$. However, note that reducing the noise energy does not necessarily mean that the Hamming distance, $\mathrm{w_H}(\hat{\mathbf{u}}, \mathbf{u}_{\mathrm{ML}})$, is decreased. Furthermore, every iteration increases t_d, the time to decode the received block; this may eliminate any benefits of the iterative search.

FD and SR

Let the minimum Euclidean distance between any two transmitted sequences, $\mathbf{x}$ and $\tilde{\mathbf{x}}$, be denoted d_{e}. Then, if $\|\mathbf{w}\|^2 \leq d_{\mathrm{e}}^2/4$, the MLSD decides $\mathbf{x}_{\mathrm{ML}} = \mathbf{x}$, i.e., if the noise energy is less than $d_{\mathrm{e}}^2/4$, the received sequence can be rejected avoiding the computationally expensive MLSD. This technique is referred to as hypersphere SR [10]. The probability of rejecting the received sequence, $\mathrm{P_r}$, is evaluated as the probability mass inside the hypersphere of radius, $d_{\mathrm{e}}/2$, about the transmitted sequence, $\mathbf{x}$. In particular, assume $L \geq K$, and the states, $\mathbf{s}_k$, $\mathbf{s}_{k+L+K}$ and $\hat{\mathbf{s}}_k$ are known, and denote the matrices,

$$\mathbf{A}' = \begin{bmatrix} a_K & & \cdots & 0 \\ a_{K-1} & a_K & & \vdots \\ \vdots & \vdots & \ddots & \\ a_1 & a_2 & \cdots & a_K \end{bmatrix} \mathbf{A}'' = \begin{bmatrix} a_0 & a_1 & \cdots & a_{K-1} \\ & a_0 & & a_{K-2} \\ \vdots & & \ddots & \vdots \\ 0 & \cdots & & a_0 \end{bmatrix}.$$

Let the received signal in the observation window be $\mathbf{r}_k^{k+L+K-1} = (u_k, \cdots, u_{k+L-1})\mathbf{A} + \mathbf{m} + \mathbf{w}_k^{k+L+K-1}$ where $\mathbf{m} = ((\mathbf{s}_k - \hat{\mathbf{s}}_k)\mathbf{A}', \mathbf{0}_{(1,L)}, \mathbf{s}_{k+L+K}\mathbf{A}'')$. Then, $\left\|\mathbf{m} + \mathbf{w}_k^{k+L+K-1}\right\|^2$ is conditionally noncentral chi-square distributed with $(L+K)$ degrees-of-freedom, and $\mathrm{P_r}$ is evaluated as,

$$\mathrm{P_r}(\alpha) = \frac{1}{M^{3K}} \sum_{i=0}^{M^{3K}-1} F\left(\frac{(\alpha d_{\mathrm{e}})^2}{4} \middle| m_i^2\right) \tag{2.32}$$

where

$$F\left(\frac{(\alpha d_{\mathrm{e}})^2}{4} \middle| m_i^2\right) = \int_0^{(\alpha d_{\mathrm{e}})^2/4} \gamma_b \left(\frac{u}{m_i^2}\right)^{(n-2)/4} \mathrm{e}^{-(m_i^2+u)\gamma_b} I_{n/2-1}(2\sqrt{u m_i^2}\gamma_b)\mathrm{d}u$$

is the CDF [21, eq. (2-1-121)], $\mathbf{s}_k$ and $\hat{\mathbf{s}}_k$ are assumed independent, $m_i^2 = \|\mathbf{m}\|^2$ is the noncentrality parameter conditioned on the values of $\mathbf{s}_k$, $\mathbf{s}_{k+L+K}$ and $\hat{\mathbf{s}}_k$, and $\alpha \geq 1$ is a constant.

For uncoded transmission and given FIR, $\mathbf{a}$, the value of d_{e} is typically small, and so is $\mathrm{P_r}(\alpha)$. Therefore, we may consider the N_{nb} nearest neighbors of the transmitted sequence, $\mathbf{x}$, to increase $\mathrm{P_r}(\alpha)$; see Fig. 2.13. It is straightforward to show that always $N_{\mathrm{nb}} \leq L$. If $\alpha = 1$, we can show that the SR estimator is unbiased, but $\mathrm{P_r}(1)$ is typically small and so is the SR gain (2.28). Since at large SNR, with a high probability, the transmitted sequence is also the MLSD solution, we propose the following modification to the hypersphere SR. If $1 < \alpha < 3$ *and* $\|\mathbf{r} - \mathbf{x}\|^2 < \left\|\mathbf{r} - \tilde{\mathbf{x}}_{(i)}\right\|^2$ for $\forall i = 1, 2, \cdots, N_{\mathrm{nb}}$, then, with a high probability, $\mathbf{x}$ is the MLSD solution. However, if the received signal is, for example, inside the shaded area in Fig. 2.13, and $\alpha > 3/2$, this procedure incorrectly

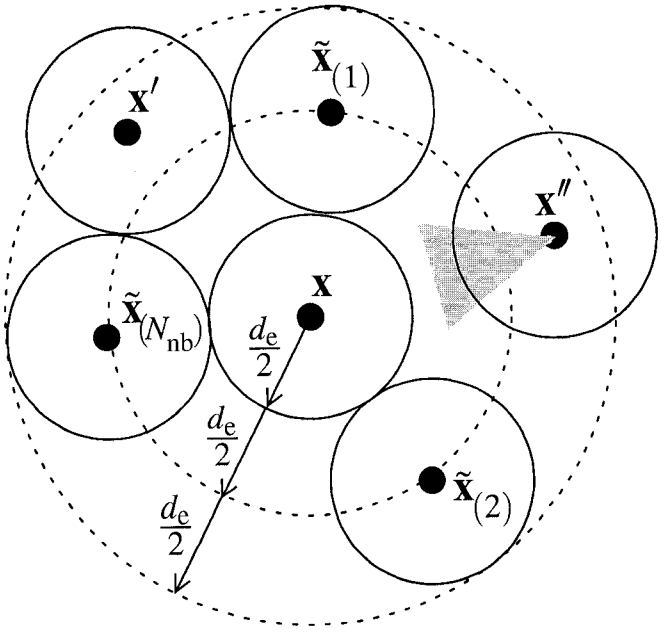

Figure 2.13: The nearest neighbors of the transmitted sequence, $\mathbf{x}$.

decides $\mathbf{x}$ as the MLSD solution, and the SR estimator will be biased. In general, the larger the SNR, the larger α can be (thus, increasing the probability, $\mathrm{P_r}$), however, always $\alpha < 3$.

2.2.5 Numerical Results and Discussion

Assume $M = 2$ (i.e., binary antipodal signaling), and the two static channels with FIR given as the average multipath delay profile specified in [39] for outdoor to indoor transmissions and pedestrian mobility, respectively, i.e.,

$$\begin{aligned} \mathbf{a}_A &= (0.9431, 0.3087, 0.1034, 0.0683) \\ \mathbf{a}_B &= (0.6369, 0.5742, 0.3623, 0.2536, 0.2595, 0.0407). \end{aligned}$$

The channel A has $K = 3$, $d_{\rm e}^2 = 4.00$, and the i-th nearest neighbor of $\mathbf{x}$ is $\tilde{\mathbf{x}}_{(i)} = (\mathbf{u} - 2\mathbf{u}_{(i)})\mathbf{A}$ where $\mathbf{u}_{(i)} = (\mathbf{0}_{(1,i-1)}, u_{i-1}, \mathbf{0}_{(1,n+K-i)})$ for $1 \leq i \leq n$, and $N_{\rm nb} = n$. The channel B has $K = 5$, $d_{\rm e}^2 = 2.06$, and if $u_{i-1} \neq u_i$, $\mathbf{u}_{(i)} = (\mathbf{0}_{(1,i-1)}, u_{i-1}, u_i, \mathbf{0}_{(1,n+K-i-1)})$ for $1 \leq i < n$, and $u_{(i)}$ is not defined if $u_{i-1} = u_i$, and $N_{\rm nb} = n - 1$.

Let $p = 0.9$ in (2.31), i.e., the sliding-window detector finds the MLSD solution with 90% probability. Empirically obtained minimum observation window length for different detectors and different values of SNR are summarized in Table 2.4 for $n = 500$ and $n = 50$, respectively. We

Table 2.4: Minimum length of the observation window for $p = 0.90$.

γ_b [dB]	0	1	2	3	4	5	6	7	8	9	10	n
channel	A											
tVA	8	8	7	6	6	6	6	6	6	5	5	500
	6	6	6	6	6	6	6	6	6	6	6	50
mtVA	8	7	7	6	5	5	4	3	2	1	1	500
	5	5	5	4	4	4	3	2	1	1	1	50
FD	8	8	8	8	7	7	7	7	5	5	5	500
	7	7	7	7	6	5	5	5	5	4	4	50
mFD	6	6	6	5	5	5	4	3	3	2	2	500
	4	4	3	3	3	3	2	2	1	1	1	50
channel	B											
tVA	21	21	21	21	20	20	18	14	13	12	10	500
	16	15	15	15	14	13	13	12	11	11	10	50
mtVA	21	21	20	20	18	18	15	12	11	8	6	500
	14	14	13	12	12	11	8	7	6	4	2	50
FD	20	19	19	18	17	14	12	11	10	9	8	500
	11	9	8	8	7	7	7	6	6	5	4	50
mFD	15	13	13	12	11	9	6	4	3	2	1	500
	8	6	6	5	5	4	3	2	2	1	1	50

observe from Table 2.4 that modification of the tVA and FD significantly reduces the minimum required length of the observation window, L.

The probability of rejection, $\mathrm{P_r}(\alpha)$, computed using (2.32) is depicted in Fig. 2.14. For $\alpha > 1$, $\mathrm{P_r}(\alpha)$ given in (2.32) is an upper-bound since recall that only the received sequences closest to the transmitted sequence, $\mathbf{x}$, are rejected.

The simulation results are in Table 2.5. The BER values in Table 2.5 are averaged over 5 simulation runs. There are N_{blocks} blocks per simulation run which corresponds to approximately 100 (50) erroneously decoded blocks at 8 dB (10 dB) using the VA. The asterisk at some values of L indicates that the value of L from Table 2.4 must be increased (i.e., the parameter, p, is increased) to improve the BER estimator accuracy. The value, T_{total}, is the total simulation run-time, $\bar{t}_d$ is the average time to decode the received block, and $\log_n F$ is the complexity exponent [38]. For FD/SR, $\hat{\mathrm{P}}_{\mathrm{r}}(\alpha)$ denotes the empirically obtained probability of the received sequence rejection.

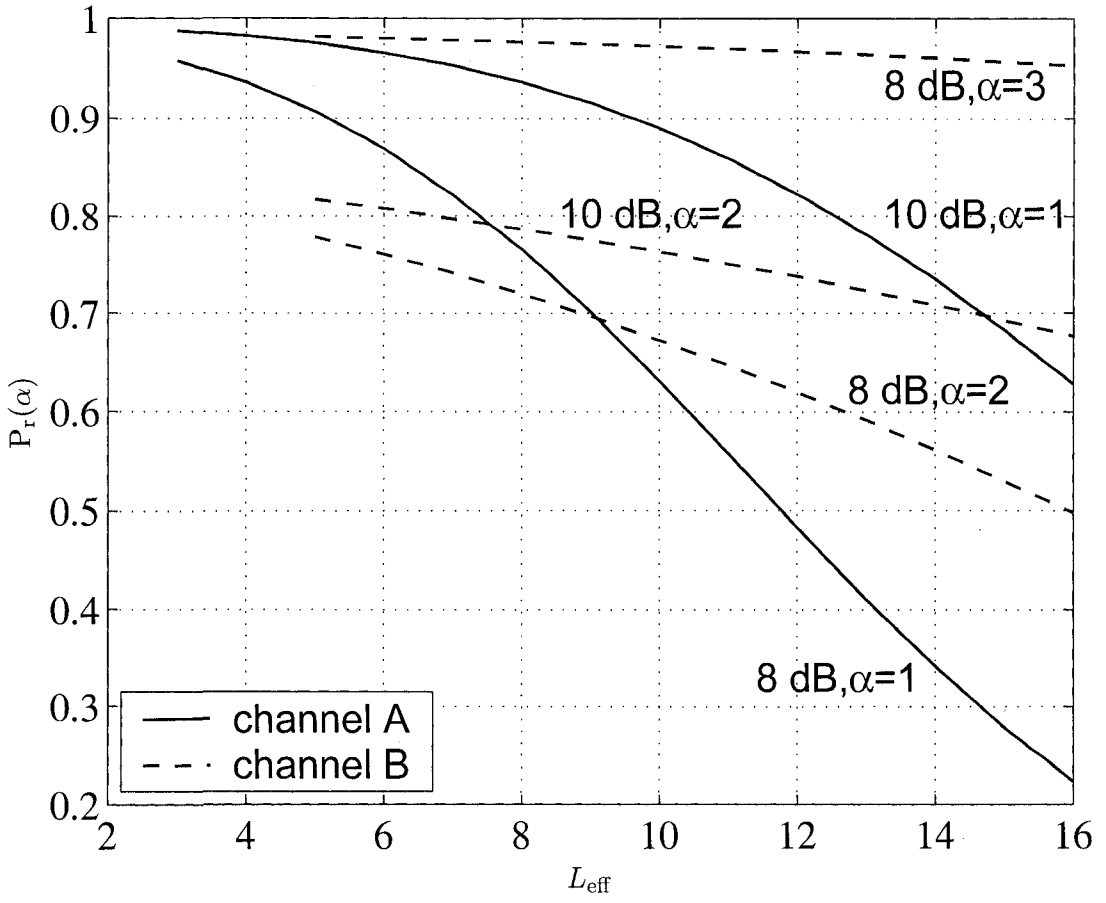

Figure 2.14: The theoretical probability of rejection, $\mathrm{P_r}(\alpha)$, versus effective dimensionality, $L_{\text{eff}} = L + K$, for $\alpha = 1, 2$ and 3, and SNR 8 and 10 dB.

Table 2.5: Examples of the simulation results.

channel	A				B			
n	500		50		500		50	
γ_b [dB]	8	10	8	10	8	10	8	10
N_{blocks}	1500	2×10^4	1×10^4	1×10^5	200	500	1000	3000
det.	VA							
BER	2.04×10^{-4}	3.40×10^{-6}	2.02×10^{-4}	4.20×10^{-6}	6.25×10^{-3}	5.04×10^{-4}	6.72×10^{-3}	5.80×10^{-4}
T_{total} $[s]$	176	2763	122	1216	53	157	20	118
$\bar{t}_d$ $[s]$	0.1392	0.1434	0.0117	0.0098	0.2680	0.2065	0.0227	0.0183
$\log_n F$	1.9800	1.9800	2.5698	2.5698	2.2606	2.2606	3.0227	3.0227
det.	tVA							
L	6	5	6	6	13	10	11	14*
BER	2.23×10^{-4}	3.75×10^{-6}	2.26×10^{-4}	6.20×10^{-6}	6.62×10^{-3}	6.56×10^{-4}	6.14×10^{-3}	7.87×10^{-4}
T_{total} $[s]$	365	4272	215	2072	51	102	22	65
$\bar{t}_d$ $[s]$	0.2550	0.2540	0.0268	0.0144	0.2980	0.1975	0.0215	0.0214
$\log_n F$	1.9822	1.9822	2.5733	2.5733	2.2615	2.2613	3.0237	3.0239
det.	mtVA							
L	2	1	1	1	11	6	6	6*
BER	2.25×10^{-4}	4.76×10^{-6}	3.40×10^{-4}	5.20×10^{-6}	6.35×10^{-3}	6.40×10^{-4}	6.18×10^{-3}	8.00×10^{-4}
T_{total} $[s]$	867	8155	599	4063	146	388	56	71
$\bar{t}_d$ $[s]$	0.4110	0.2820	0.0769	0.0596	0.7840	0.7800	0.0471	0.1935
$\log_n F$	2.0156	2.0153	2.6246	2.6246	2.2816	2.2815	3.0544	3.0544
det.	FD							
L	5	5	5	4	10	9*	8*	7*
BER	1.85×10^{-4}	5.10×10^{-6}	2.34×10^{-4}	3.88×10^{-6}	6.83×10^{-3}	6.64×10^{-4}	5.86×10^{-3}	7.95×10^{-4}
T_{total} $[s]$	74	102	48	457	109	104	10	28
$\bar{t}_d$ $[s]$	0.0441	0.0434	0.0045	0.0043	0.5260	0.1965	0.0091	0.0097
$\log_n F$	2.0955	2.0955	2.7252	2.5301	2.7455	2.6246	3.3581	3.1697
det.	mFD							
L	3	2	1	1	3	2*	2	2*
BER	1.95×10^{-4}	3.60×10^{-6}	2.61×10^{-4}	6.20×10^{-6}	5.98×10^{-3}	5.96×10^{-4}	5.60×10^{-3}	7.27×10^{-4}
T_{total} $[s]$	68	996	38	420	15	21	5	14
$\bar{t}_d$ $[s]$	0.0437	0.0406	0.0036	0.0035	0.0870	0.0413	0.0044	0.0045
$\log_n F$	1.8569	1.7472	2.0372	2.0372	1.9039	1.7973	2.2650	2.2650
det.	FD/SR							
L	5	5	5	4	10	9*	8*	7*
α	1	1	1	1	3	2	2	2
N_{nb}	0	0	0	0	9	8	7	6
$\mathrm{P_r}(\alpha)$	0.7650	0.9361	0.7650	0.9526	0.9570	0.7084	0.5914	0.7369
$\hat{\mathrm{P}}_{\mathrm{r}}(\alpha)$	0.7661	0.9377	0.7615	0.9532	0.8298	0.6762	0.5604	0.6811
BER	2.00×10^{-4}	4.00×10^{-6}	2.38×10^{-4}	4.80×10^{-6}	5.18×10^{-3}	5.44×10^{-4}	5.30×10^{-3}	8.20×10^{-4}
T_{total} $[s]$	41	771	34	297	32	54	7	17
$\bar{t}_d$ $[s]$	0.0252	0.0312	0.0034	0.0033	0.1928	0.1410	0.0086	0.0050
$\log_n F$	1.9242	1.8253	2.4675	2.1748	2.4870	2.4552	3.1523	2.9210

2.3 Summary

In this chapter, the SR technique was generalized for simulations of multidimensional communication systems. It was shown that the system model can strongly influence the simulation efficacy. Particularly, the MLSD detector can be replaced by the SR MLSD detector to significantly reduce the simulation run-times.

The SR method was proposed in [10] for the case of the hypersphere rejection region and AWGN channel with perfectly quantized soft decisions. The SR was reported to be applicable only for simulations of systems with small dimensionality, less than 10. In this section, the SR method was demonstrated to be applicable for simulations of coded schemes with a finite block length, binary antipodal signaling and ML sequence decoding over quantized AWGN channels. Our analysis indicates that applicability of SR is dependent upon the SNR, the region employed in the particular application, and also crucially upon the amount of knowledge about the system. In contrast to the results presented in [10], the newly proposed SR regions presented in this section can achieve gain at least 2 for dimensionality of the order of hundreds.

For perfectly quantized soft decisions, three rejection regions, hypersphere, hypercube and hyperquadrant, have been compared. The hypercube and hyperquadrant proposed in this section outperform the hypersphere for all values of dimensionality when there is no information available about the minimum Hamming distance of the code. The hyperquadrant exploits additional knowledge of the transmitted codeword, and thus, is always superior to the hypercube. The efficiency of the hypersphere can be improved significantly with additional knowledge of the minimum Hamming distance of the code. Importantly, the hypercube and hyperquadrant regions suffer substantially smaller gain degradation with increasing dimensionality than the hypercube which is always poorer for large dimensionality (assuming the minimum Hamming distance does not grow with dimensionality). We explained this behavior of the SR gain by comparing the volumes of the rejection regions under consideration over all values of the dimensionality, n. For quantized decisions, in general, a hyperquadrant rejection region is the most readily applicable for the DMC, while hypersphere rejection region should be used for the BSC.

The SR method is a special form of IS [10], so that more general IS might provide better simulation gains than SR. However, the strong advantage of SR is that it does not require any IS weights to be determined regardless of the system complexity. Moreover, SR can be easily combined with other techniques for improving simulation efficiency. In general, if the time to generate and decode

a single block of data can be estimated, one can estimate the expected simulation run-times and the gain of SR using eq. (2.20).

The SR method was also investigated for binary coded transmission over ISI channels. Several modifications of FD and VA were proposed to improve their simulation efficacy. The complexity of (m)FD is smaller than the complexity of the VA if $L \leq (K+1)$. The LUT tree search implementation of FD is more efficient than the VA in all but one example studied. The mtVA simulation run-times are worse than the simulation run-times of the tVA because of the associated overhead of the mtVA. The modification of FD is effective especially for channel A. In general, the time to perform the rejection, t_r, can be further reduced if the SR implementation is optimized so that $t_r \ll t_d$ (e.g., if $L = 1$, no tree search is necessary). Note also that a simulation run-time reduction of 2 is considered valuable (e.g., 2 days simulation reduces to 1 day). Hence, for given simulation parameters, the FD, mFD and FD/SR simulation techniques appear to reduce the simulation run-times of the VA while achieving good, near MLSD accuracy. In particular, we observe from Table 2.4 that the mFD has the shortest simulation runtimes for channel B, however, for channel A, the shortest simulation run-times are achieved by the FD/SR simulation technique.

Chapter 3

Efficient Semi-Analytical Techniques

In this chapter, we propose and analyze the Prony and polynomial approximation methods for semi-analytical evaluation of the average probabilities of error and the average error rates for digital modulations in slowly fading channels.

3.1 Background

The probability of a detection error is often considered as the most important performance measure in the receiver design for the communication system. In this chapter, we consider the probabilities of transmission bit, symbol and frame errors and the corresponding BER, SER and FER, respectively. Recall also that the probability of error and the error rate are defined for stationary and ergodic channels. On fading (time-varying) channels, the probability of error is a random variable, and its first moment is typically assumed to be a sufficient performance measure provided that the observations are long enough to consider the channel as ergodic. The first moment (average) of the probability of error is obtained by averaging the conditional probability of error over the channel SNR distribution at the input to the detector. Numerous methods have been developed to accomplish averaging of the conditional probability of error over the SNR distribution. In particular, the MGF method [40], and the characteristic function (CHF) [41] method are appealing since the Laplace or Fourier transform of the SNR distribution is usually known even for multichannel reception with correlated and non-identically distributed branches while, in general, the SNR distribution is often unknown or difficult to obtain. The CHF can be also obtained using the statistical moments of the SNR [42]. The SNR distribution is estimated from known moments in [43]. The method of residues [44], the Gauss-Chebyshev quadrature (GCQ) [45], saddle-point integration [46], and Beaulieu series [47]

can be used to invert the CHF and obtain the SNR distribution. Overview and further description of these methods can be found, for example, in [46], and in [48].

Even though, in many cases, an exact expression for the average probability of error can be found, especially for higher-order modulations, the result is often cumbersome to plot and to analyze further [48]. When the closed form expression cannot be obtained, we can use numerical methods to evaluate the probability of error. However, numerical integration can be impaired by semi-finite ranges of integration, possible singularities of the integrand, oscillatory behavior, and convergence problems for small values of the integrand. Also, many bounding techniques exist, but usually these bounds are not very tight; see, for example, the Chernoff bound [21]. A relationship between the saddlepoint integration and the modified Chernoff bound is investigated in [49]. Hence, semi-analytical (or, semi-numerical) methods appear to be the most appealing providing a good trade-off between evaluation complexity and the numerical accuracy.

We propose a new semi-analytical method to evaluate the average probability of error for a wide class of modulations and fading distributions. The proposed method fits a sum of exponentials to the conditional probability of error. Fitting a sum of exponentials into the measured data is a difficult, frequently occurring, and numerically rather ill-conditioned problem of applied data analysis known as the Prony approximation [50–52]. The parameters of the Prony approximation are obtained non-iteratively in [50]. A uniqueness of the Prony approximation assuming a least squares approximation error is investigated in [51]. In our case, once the conditional probability of error is approximated by a sum of exponentials, averaging over the fading distribution can be readily obtained using knowledge of the MGF of the SNR. Importantly, knowledge of the conditional probability of error at only a small number of points is sufficient to obtain the exponential fit. These points can be obtained either analytically or using a computer simulation. Hence, using the Prony approximation, we have a simple universal and highly accurate semi-analytical tool for evaluations of the average probability of error.

The rest of the chapter is organized as follows. In Section 3.2, we present the system model and fading statistics. Prony approximation of the conditional probability of error and the corresponding optimization problems are introduced in Section 3.3. The Prony approximations are given for several frequently used modulation formats. Piecewise polynomial approximation as an alternative to the sum of exponentials fit is investigated in Section 3.4. Numerical examples to determine the accuracy of the Prony and polynomial approximations for single as well as multichannel receptions are given in Section 3.5. The chapter is summarized in Section 3.6.

3.2 System Model

Assume a multichannel reception and postcombining detection of the K diversity branches as shown in Fig. 3.1. Linear memoryless modulation is used to transmit independent and IID symbols, $x \in X$, where $X = \{(2i-\sqrt{M}+1)+\mathrm{j}(2j-\sqrt{M}+1); i,j = 0,1,\cdots,\sqrt{M}-1\}$ for the M-ary square QAM where $\mathrm{j} = \sqrt{-1}$, $X = \{\mathrm{e}^{\mathrm{j}\,2\pi i/M}; i = 0,1,\cdots,M-1\}$, for M-ary phase-shift keying (PSK), and $m = \log_2 M$ is the number of IID information bits per modulation symbol [21]. Using equivalent complex-valued representation of the signals in the baseband, the received signals corresponding to the transmitted symbol, x, are written as, $y_i = \alpha g_i \,\mathrm{e}^{\mathrm{j}\phi_i} x + w_i$, where $\alpha = 1/\sqrt{\mathrm{E}[|x|^2]}$ sets the average energy, E_S, per transmitted symbol, x, to unity, $i = 1,2,\cdots,K$, and g_i is the i-th channel fading amplitude, ϕ_i is the channel fading phase, and w_i is a zero-mean complex AWGN having the variance, $\mathrm{E}[|w_i|^2] = 2\sigma_w^2 = N_0$, where $|\cdot|$ denotes the absolute value, and N_0 is the one-sided noise power spectral density. For an arbitrary joint PDF, $f_{\mathbf{g}}(g_1,\cdots,g_K)$, and assuming coherent detection and linear combining of the received branch signals, the decision variable at the detector input for MRC, EGC, and SC, respectively, is [16],

$$\begin{aligned} y &\overset{\text{(MRC)}}{=} \alpha x\left(\sqrt{\textstyle\sum_{i=1}^{K} g_i^2}\right) + w \\ y &\overset{\text{(EGC)}}{=} \alpha x\left(\tfrac{1}{\sqrt{K}}\textstyle\sum_{i=1}^{K} g_i\right) + w \\ y &\overset{\text{(SC)}}{=} \alpha x\left(\max_{i=1,\cdots,K} g_i\right) + w. \end{aligned}$$

Note that the average energy per transmitted bit, $E_b = E_S/m = 1/m$, and, $\alpha = \sqrt{3/(2M-2)}$, for M-ary square QAM, and, $\alpha = 1$, for M-ary PSK. In general, denote the received signal at the input to the detector as, $y = \alpha x\, g + w$. We define the SNR at the input of the detector as, $\gamma = g^2\gamma_b$, and $\gamma_b = E_b/N_0 = 1/(mN_0)$.

3.2.1 Fading Statistics

Let the channel fading amplitudes be the Euclidean norms of Gaussian random vectors having n components of equal variance, σ_i^2, $i = 1,2,\cdots,K$. Hence, the channel amplitudes, g_i, follow a generalized Rayleigh or Ricean distribution, respectively, with n degrees of freedom and non-centrality parameter, $s_i^2 \geq 0$; see Appendix C. Then, the PDF of squared amplitudes, g_i^2, corresponds to the central or non-central chi-square distribution, respectively; see Appendix C. For $s_i > 0$, we define the Ricean factor, $K_{\mathrm{R}_i} = s_i^2/(n\sigma_i^2)$. Using the infinite series (A-5b), one can

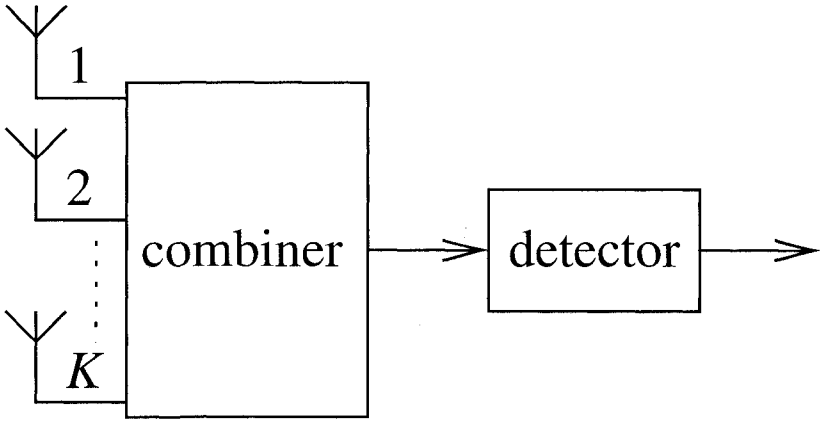

Figure 3.1: A generic digital communication system.

express the CDF of g_i^2 ; see Appendix C. Note that the summands in the infinite sum representation (A-5b) of the function $I_n(u)$ diminish quickly for all practical values of n and u. Using (C-1a) and (C-1b), one can obtain the MGF's, $\Phi_{g_i}(t) = \mathrm{E}\left[\mathrm{e}^{g_i t}\right]$, and, $\Phi_{g_i^2}(t) = \mathrm{E}\left[\mathrm{e}^{g_i^2 t}\right]$, of the random variables, g_i, and, g_i^2; see Appendix C.

For simplicity, assume that the channel fading amplitudes are independent, i.e., $f_{\mathbf{g}}(g_1, \cdots, g_K) = \prod_{i=1}^{K} f_{g_i}(g_i)$, and $\sigma_i = \sigma$, $\forall i = 1, 2, \cdots, K$. We obtain the PDF of the fading amplitude, g, at the combiner output. In particular, the MRC output fading amplitude, $g = \sqrt{\sum_{i=1}^{K} g_i^2}$, follows a generalized Ricean fading with nK degrees of freedom, non-centrality parameter, $s^2 = \sum_{i=1}^{K} s_i^2$, and variance, σ^2, per dimension; see (C-1b). The PDF of the EGC fading amplitude, $g = \sum_{i=1}^{K} g_i/\sqrt{K}$, is obtained by inverting the MGF, i.e., [53],

$$f_g(g) \overset{\text{(EGC)}}{=} \frac{\sqrt{K}}{2\pi \mathrm{j}} \int_{c-\mathrm{j}\infty}^{c+\mathrm{j}\infty} \prod_{i=1}^{K} \Phi_{g_i}(t)\, \mathrm{e}^{-t\sqrt{K}g} \mathrm{d}t = \frac{\sqrt{K}}{2\pi} \int_{-\infty}^{\infty} \prod_{i=1}^{K} \Phi_{g_i}(c+\mathrm{j}\omega)\, \mathrm{e}^{-(c+\mathrm{j}\omega)\sqrt{K}g} \mathrm{d}\omega \quad (3.1)$$

where c is chosen in the region of convergence. The inversion (3.1) can be performed, for example, using the GCQ rule [46] obtained in Appendix B. Hence, we can rewrite (3.1) as,

$$f_g(g) \overset{\text{(EGC)}}{=} \frac{\sqrt{K}}{2\pi} \int_{-1}^{1} \prod_{i=1}^{K} \Phi_{g_i}\left(c + \mathrm{j}\frac{c\sqrt{1-x^2}}{x}\right) \mathrm{e}^{-c\left(1+\mathrm{j}\frac{\sqrt{1-x^2}}{x}\right)\sqrt{K}g} \frac{c\,\mathrm{d}x}{x^2\sqrt{1-x^2}}$$

and using the GCQ rule, one has that,

$$f_g(g) = \frac{\sqrt{K}c}{2\nu} \sum_{l=1}^{\nu} \mathrm{e}^{-c(1+\mathrm{j}\tau_l)\sqrt{K}g}(1+\tau_l^2) \prod_{i=1}^{K} \Phi_{g_i}(c(1+\mathrm{j}\tau_l))$$

where $\tau_l = \tan((l-1/2)\pi/\nu)$.

When SC is employed, the combiner output PDF is [53],

$$f_{g^2}(g^2) \overset{(\mathrm{SC})}{=} \sum_{i=1}^{K} f_{g_i^2}(g^2) \prod_{\substack{j=1 \\ j\neq i}}^{K} F_{g_j^2}(g^2) \tag{3.2}$$

and we substitute (C-1b) and (C-2b) to (3.2). Since $\gamma = g^2\gamma_b$, the PDF of the SNR at the input to the detector is [53],

$$f_\gamma(\gamma) = (1/\gamma_b) f_{g^2}(\gamma/\gamma_b). \tag{3.3}$$

Finally, assuming knowledge of the conditional probability, $\mathrm{P}_\epsilon(\gamma)$, we evaluate the average probability,

$$\bar{\mathrm{P}}_\epsilon(\gamma_b) = \int_0^\infty \mathrm{P}_\epsilon(g^2\gamma_b)\, f_{g^2}(g^2)\mathrm{d}g^2. \tag{3.4}$$

3.3 Prony Approximation

We efficiently evaluate the average probability of error (3.4). Consider a random variable, X, and let, $g(X) = \eta(X - \tilde{x})$, where $\eta(\cdot)$ denotes the unit-step (Heaviside) function; see (A-15). Hence, let $\tilde{x}$ be a real positive constant, $\tilde{x} \geq 0$. Then, the probability, $\Pr(X \geq \tilde{x}) = \mathrm{E}[g(X)]$. Let, $\tilde{B}_i \geq 0$, and, $\tilde{b}_i \geq 0$, are non-negative real constants, $i = 1, 2, \cdots, p$, and let, $h(X) = \sum_{i=1}^{p} \tilde{B}_i \,\mathrm{e}^{\tilde{b}_i(X-\tilde{x})}$, so that $h(X)$ is the increasing function of X. Thus, if $\sum_{i=1}^{p} \tilde{B}_i \geq 1$, then $g(X) \leq h(X)$. Applying the expectation operation, we have that,

$$\mathrm{E}[g(X)] \leq \sum_{i=1}^{p} \tilde{B}_i \,\mathrm{e}^{-\tilde{b}_i\tilde{x}} \Phi_X(\tilde{b}_i)$$

where $\Phi_X(\tilde{b}_i) = \mathrm{E}\left[\mathrm{e}^{\tilde{b}_i X}\right]$ is the MGF. Note that the case, $p = 1$, and the case, $\tilde{b}_i = \tilde{b}\ \forall i$, correspond to the Chernoff bound of $\Pr(X \geq \tilde{x})$; cf. [21, Sec. 2-1-5]. Denote the bounding error, $e_p(\tilde{B}_1, \cdots, \tilde{B}_p, \tilde{b}_1, \cdots, \tilde{b}_p) = e_p(\tilde{\mathbf{B}}, \tilde{\mathbf{b}}) = \sum_{i=1}^{p} \tilde{B}_i \Phi_X(\tilde{b}_i)\,\mathrm{e}^{-\tilde{b}_i\tilde{x}} - \mathrm{E}[g(X)]$, and assume the fol-

lowing convex optimization problem having the convex constraints [54, Ch. 4],

$$\begin{aligned} \{\tilde{\mathbf{B}}, \tilde{\mathbf{b}}\} &= \text{argmin } e_p(\tilde{\mathbf{B}}, \tilde{\mathbf{b}}) \\ \text{s.t.} \quad \tilde{B}_i > 0,\ \tilde{b}_i \geq 0,\ \textstyle\sum_{i=1}^{p} \tilde{B}_i \geq 1,\ i &= 1, 2, \cdots, p. \end{aligned} \tag{3.5}$$

Thus, given, $\tilde{x} \geq 0$, and, p, the $2p$ coefficients, $\tilde{B}_i$, and, $\tilde{b}_i$, are the solution of the problem (3.5), and, $e_p \geq 0$. In general, one can reduce the bounding error, $e_p(\tilde{\mathbf{B}}, \tilde{\mathbf{b}})$, if the constraint, $\sum_{i=1}^{p} \tilde{B}_i \geq 1$, in (3.5) is relaxed, i.e., $\sum_{i=1}^{p} \tilde{B}_i \geq 0$, and thus, $h(X)$ is no longer an upper-bound of $g(X)$. In this case, let the bounding error be defined as,

$$e_p(\tilde{\mathbf{B}}, \tilde{\mathbf{b}}) = |\sum_{i=1}^{p} \tilde{B}_i \Phi_X(\tilde{b}_i)\, \mathrm{e}^{-\tilde{b}_i \tilde{x}} - \mathrm{E}[g(X)]\,|$$

so that,

$$\mathrm{E}[g(X)] = \Pr(X \geq \tilde{x}) \approx \sum_{i=1}^{p} \tilde{A}_i\, \mathrm{e}^{-\tilde{a}_i \tilde{x}}$$

where $\tilde{A}_i = \tilde{B}_i \Phi_X(\tilde{b}_i)$, and, $\tilde{a}_i = \tilde{b}_i$. In general, for non-negative constants, $\tilde{x}$, and, q, let the conditional probability of error, $\mathrm{P}_\epsilon(\gamma) \equiv \Pr(X \geq \tilde{x})$, and let, $\tilde{x} = \gamma^{\,q}$, and thus,

$$\mathrm{P}_\epsilon(\gamma) \approx \sum_{i=1}^{p} \tilde{A}_i\, \mathrm{e}^{-\tilde{a}_i \gamma^{\,q}}. \tag{3.6}$$

The approximation (3.6) will be referred to as the Prony approximation. Denote the approximation error of (3.6) as,

$$e_p(\gamma) = w(\gamma) \left(\sum_{i=1}^{p} \tilde{A}_i\, \mathrm{e}^{-\tilde{a}_i \gamma^{\,q}} - \mathrm{P}_\epsilon(\gamma) \right)^{q_1} \tag{3.7}$$

where $w(\gamma)$ is the weighting function, and $q_1 > 0$ is a real constant. A sensible choice of the weighting function is, $w(\gamma) = 1/\mathrm{P}_\epsilon(\gamma)$; then, $e_p(\gamma)$ in (3.7) corresponds to the relative approximation error. Importantly, approximation (3.6) is accurate over the interval, $\gamma \in (\tilde{\gamma}_{\min}, \tilde{\gamma}_{\max})$, and it can diverge for $\gamma < \tilde{\gamma}_{\min}$, and, $\gamma > \tilde{\gamma}_{\max}$. However, since $\sum_{i=1}^{p} \tilde{A}_i\, \mathrm{e}^{-\tilde{a}_i \gamma^q}$ is finite, for $\gamma \to 0$, and, 0, for $\gamma \to \infty$, approximation error, $e_p(\gamma)$, is always finite. Note also that the k-th derivative, $k \geq 0$, in the limit of infinite SNR, $\lim_{\gamma \to \infty} \frac{\mathrm{d}^k}{\mathrm{d}\gamma^k} \sum_{i=1}^{p} \tilde{A}_i\, \mathrm{e}^{-\tilde{a}\gamma^q} = 0$. It is useful to constrain minimization of the error, $e_p(\gamma)$, to a set of n points, $\tilde{\gamma}_{\min} < \gamma_1 < \gamma_2 < \cdots < \gamma_n < \tilde{\gamma}_{\max}$, rather than trying to minimize the error over a continuous range of γ. Hence, given, p, and, q, the optimization problem

to find the coefficients, $\tilde{A}_i$, and, $\tilde{a}_i$, minimizes the error,

$$\bar{e}_p = \sum_{j=1}^{n} |e_p(\gamma_j)|^{q_1} \tag{3.8}$$

and let the weights, $\tilde{w}_j = w(\gamma_j)$. Note that the case, $q_1 = 2$, corresponds to the least-squares curve-fitting, and, the error, $\bar{e}_p = \max_{j=1,\cdots,n} |e_p(\gamma_j)|$, becomes the min-max curve fitting, for $q_1 = \infty$. In general, Prony approximation minimizing the error (3.8) corresponds to the sum of exponentials interpolation. Thus, knowledge of $\mathrm{P}_\epsilon(\gamma)$ at n distinct SNR values is sufficient. It is required that $n \geq 2p$, and we solve an overdetermined system of exponential interpolation equations. The interpolation points, γ_j, can be selected with respect to some decomposition basis of the curve, $\mathrm{P}_\epsilon(\gamma)$, for example, using a sampling theorem. Minimization of (3.8) constitutes a strongly nonlinear optimization problem and, in general, iterative numerical solution is necessary. Initialization of such an iterative procedure is critical for successful convergence to a global optimum. The choice of the interpolation points, γ_j, determines convergence properties of the sum of exponentials (Prony) approximation, i.e., behavior of the approximation error in the limit, $\lim_{p\to\infty} \bar{e}_p$. A test on uniform convergence is known as the Weierstrass M-test [55, Sec. 9.6]. According to the Weierstrass test, since $|\tilde{A}_i \, \mathrm{e}^{-\tilde{a}_i \gamma^q}| \leq |\tilde{A}_i|$ for $\tilde{a}_i > 0$ and $\gamma \geq 0$, provided that the sequence, $\{\tilde{A}_i\}_i$, has absolute convergence (i.e., $\{|\tilde{A}_i|\}_i$ is convergent), then the sum of exponentials has uniform convergence.

3.3.1 Prony Approximation of the Conditional Bit-Error Probabilities for M-ary Modulations

We employ numerical search to find the parameters, $\tilde{A}_i$, and, $\tilde{a}_i$, of the Prony approximation (3.6) for the conditional bit-error probabilities of M-ary QAM and M-ary PSK over a AWGN channel. We assume that the values of $\mathrm{P}_\epsilon(\gamma)$ can be computed either analytically, or using a computer simulation. In the first step, we find the initial values for the coefficients, $\tilde{A}_i$, and, $\tilde{a}_i$. In the second step, the initial values are iteratively improved until the required accuracy (i.e., the value of the approximation error) is reached. In general, we have to solve a set of $n \geq 2p$ equations, $\sum_{i=1}^{p} \tilde{A}_i \, \mathrm{e}^{-\tilde{a}_i \gamma_j} = \mathrm{P}_\epsilon(\gamma_j)$, $j = 1, 2, \cdots, n$, of $2p$ unknowns to minimize the error (3.8). Hence, we proceed in the following two steps.

1) Let $p \geq 1$, $\tilde{\gamma}_{\min} < 0\,\mathrm{dB}$, $\tilde{\gamma}_{\max} \gg 0\,\mathrm{dB}$, and initially, the $n = 2p$ SNR points are chosen, such that, $\gamma_j = \tilde{\gamma}_{\min} + (\tilde{\gamma}_{\max} - \tilde{\gamma}_{\min})(j-1)/(n-1)$, $j = 1, 2, \cdots, n$ (assuming all SNR values are in dB). Let the coefficients, $\tilde{A}_i$, and, $\tilde{a}_i$, are randomly chosen from the uniform distribution on

the interval $(0,1)$, and $\tilde{a}_i \neq \tilde{a}_{i'}$, for $i \neq i'$. The initial set of $n = 2p$ equations is solved numerically assuming the objective function (3.8) to improve the estimates of the coefficients, $\tilde{A}_i$, and, $\tilde{a}_i$.

2) Let $n \gg 2p$, and $\gamma_j = \tilde{\gamma}_{\min} + (\tilde{\gamma}_{\max} - \tilde{\gamma}_{\min})(j-1)/(n-1)$ (assuming all SNR values are in dB). We employ a gradient descent algorithm [56] to obtain the final estimates of the coefficients, $\tilde{A}_i$, and, $\tilde{a}_i$. In particular, we search the space of feasible solutions, $\{\tilde{A}_i > 0, \tilde{a}_i \geq 0; i = 1, 2, \cdots, p\}$, using a sliding-hypercube, $\{|\tilde{A}_i - \tilde{A}'_i| < \Delta_A, |\tilde{a}_i - \tilde{a}'_i| < \Delta_a; i = 1, 2, \cdots, p\}$ where $\Delta_A > 0$, $\Delta_a > 0$, $\{\tilde{A}'_1, \cdots, \tilde{A}'_p, \tilde{a}'_1, \cdots, \tilde{a}'_p\}$ is the center of the hypercube that corresponds to the minimum approximation error found, and $\{\tilde{A}_1, \cdots, \tilde{A}_p, \tilde{a}_1, \cdots, \tilde{a}_p\}$ is a point inside the hypercube. If a new point having the smaller approximation error is found inside the hypercube, this point becomes the new center of the hypercube, and the search is repeated.

Note that quantization of the coefficients, $\tilde{A}_i$, and, $\tilde{a}_i$, is used during the search. In general, quantization step and the parameters, Δ_A, and, Δ_a, are initially large in order to slide the hypercube to the region of a global minimum faster, and these parameters are gradually decreased to achieve the desired approximation accuracy. We now consider several examples to illustrate the numerical procedure of finding the coefficients of the Prony approximation. In particular, assume Gray mapping of $m = \log_2 M$ information bits to M-ary symbols, and let the SNR per M-ary symbol, γ_S, be constant for all M, then the probability of bit-error for M-ary square-QAM is [57],

$$\mathrm{P}_\epsilon(\gamma_b) = \frac{1}{m2^{m/2-2}} \sum_{i=0}^{2^{m/2}-2} \tilde{n}_i \, Q\left(\sqrt{3\frac{(2i+1)^2}{2^m - 1}\gamma_b}\right) \tag{3.9a}$$

where $\gamma_b = \gamma_S/m$ is the SNR per bit, and $\tilde{n}_0 = 1$, for $M = 4$, $\tilde{n}_i \in \{3, 2, -1\}$, for $M = 16$, and $\tilde{n}_i \in \{7, 6, -1, 0, 1, 0, -1\}$, for $M = 64$. Note also that $\mathrm{P}_\epsilon(\gamma_b) = Q\big(\sqrt{2\gamma_b}\big)$, for $M = 2$. The probability of bit-error for 8-PSK assuming Gray-mapping of bits to symbols is [58],

$$\mathrm{P}_\epsilon(\gamma_b) = \frac{2}{3}\left(1 - Q_{\mathrm{c}}\left(\sqrt{2\gamma_b \sin^2(\pi/8)}\right) Q_{\mathrm{c}}\left(\sqrt{2\gamma_b \sin^2(3\pi/8)}\right)\right) \tag{3.9b}$$

where $Q_{\mathrm{c}}(x) = 1 - Q(x)$. Interestingly, note that $\sin(\pi/2^k) = \sqrt{\frac{1}{2} - \frac{1}{4}a_k}$, and, $\sin(3\pi/2^k) = \sqrt{\frac{1}{2} + \frac{3}{4}a_k - \frac{1}{4}a_k^3}$, where $a_k = \sqrt{2 + a_{k-1}}$, and, $a_1 = -2$, for $k = 1, 2, \cdots$.

Consider the Prony approximation of the Q-function, and the following lemma from reference [59].

Lemma 3.1 *The infinite sum of exponentials representation of the Q-function is,*

$$Q(x) = \lim_{N\to\infty} \frac{1}{N} \sum_{i=1}^{N} \frac{1}{2} \mathrm{e}^{-\tilde{a}_i x^2} \tag{3.10a}$$

where $\tilde{a}_i = \frac{1}{2} \sin^{-2}\left(\frac{\pi(i-1)}{2(N-1)}\right)$.

Importantly, Lemma 3.1 shows that there exist a sequence of coefficients, $\tilde{A}_i$, and, $\tilde{a}_i$, so that the Prony approximation of $Q(x)$ becomes exact in the limit. Note that the limit in (3.10a) is from above, i.e., $Q(x) \leq \frac{1}{N} \sum_{i=1}^{N} \frac{1}{2} \mathrm{e}^{-\tilde{a}_i x^2}$, $\forall N < \infty$, and, for $N = 1$, the expression (3.10a) becomes the Chernoff bound. In order to reduce the number of terms in (3.10a), the following approximation is suggested in [59],

$$Q(x) \approx \frac{1}{12} \mathrm{e}^{-x^2/2} + \frac{1}{4} \mathrm{e}^{-2x^2/3}. \tag{3.10b}$$

The Prony approximation of $Q\left(\sqrt{\gamma_b}\right)$ obtained for $q = 2$, $q_1 = 1$, $n = 21$, $\tilde{w}_j = 1/Q\left(\sqrt{\gamma_j}\right)$, i.e., the relative approximation error, $e_p(\gamma_b) = Q\left(\sqrt{\gamma_b}\right) / \left(\sum_{i=1}^{p} \tilde{A}_i \, \mathrm{e}^{-\tilde{a}_i \gamma_b}\right) - 1$, $\tilde{\gamma}_{\min} = -5\,\mathrm{dB}$, $\tilde{\gamma}_{\max} = 15\,\mathrm{dB}$, quantization of the coefficients, $\tilde{A}_i$, and, $\tilde{a}_i$, to 3 fractional digits, and having, $p = 2$, terms is,

$$Q(x) \approx 0.208\,\mathrm{e}^{-0.971x^2} + 0.147\,\mathrm{e}^{-0.525x^2} \tag{3.10c}$$

and having, $p = 3$, terms is,

$$Q(x) \approx 0.168\,\mathrm{e}^{-0.876x^2} + 0.144\,\mathrm{e}^{-0.525x^2} + 0.002\,\mathrm{e}^{-0.603x^2}. \tag{3.10d}$$

Note also that the approximation, [60, eq. (13)]

$$Q(x) \approx \sqrt{\frac{8}{\pi}} \frac{\mathrm{e}^{-x^2/2}}{3x + \sqrt{x^2 + 8}} \tag{3.10e}$$

is more accurate than the approximations (3.10a)–(3.10d); however, the approximation (3.10e) appears to be less useful for algebraic manipulations, and thus, it is not considered in this chapter.

The approximations (3.10a)–(3.10d) are compared in Fig. 3.2. We observe from Fig. 3.2 that the Prony approximation using only 2 terms has comparable accuracy as the approximation (3.10a) shown in Fig. 3.2 for $N = 50$ terms (the solid upper curve), and also shown with a negative sign (the solid lower curve). The relative error of the Prony approximation (3.10c) used in the conditional probability of bit-error (3.9a) and (3.9b) is shown in Fig. 3.3. In order to reduce the

approximation error, and also, to express the probability of bit-error in a unified way, we can find the Prony approximations for (3.9a) and (3.9b) directly. Thus, the Prony approximations of (3.9a) and (3.9b) optimized to 3 fractional digits are,

$$\begin{aligned}
\text{2-QAM:}\quad & \mathrm{P}_\epsilon(\gamma_b) \approx 0.204\,\mathrm{e}^{-1.504\gamma_b} + 0.105\,\mathrm{e}^{-1.024\gamma_b} \\
\text{4-QAM:}\quad & \mathrm{P}_\epsilon(\gamma_b) \approx 0.208\,\mathrm{e}^{-0.971\gamma_b} + 0.147\,\mathrm{e}^{-0.525\gamma_b} \\
\text{16-QAM:}\quad & \mathrm{P}_\epsilon(\gamma_b) \approx 0.243\,\mathrm{e}^{-0.382\gamma_b} + 0.145\,\mathrm{e}^{-0.109\gamma_b} \\
\text{64-QAM:}\quad & \mathrm{P}_\epsilon(\gamma_b) \approx 0.254\,\mathrm{e}^{-0.251\gamma_b} + 0.169\,\mathrm{e}^{-0.030\gamma_b} \\
\text{8-PSK:}\quad & \mathrm{P}_\epsilon(\gamma_b) \approx 0.239\,\mathrm{e}^{-0.442\gamma_b} + 0.112\,\mathrm{e}^{-0.156\gamma_b}.
\end{aligned} \tag{3.11}$$

The relative error of the optimized approximations (3.11) is shown in Fig. 3.4. Hence, comparing Fig. 3.3 and Fig. 3.4, we observe that the approximation error is reduced for the optimized Prony approximations of the higher-order M-ary QAM modulations.

Finally, note that if X is a zero-mean unit variance Gaussian random variable, then

$$\begin{aligned}
Q(x) &= \int_0^\infty \tfrac{1}{\sqrt{2\pi}}\,\mathrm{e}^{-(x+X)^2}\mathrm{d}X \\
&= \tfrac{1}{2}\,\mathrm{e}^{-x^2/2}\int_0^\infty \sqrt{\tfrac{2}{\pi}}\,\mathrm{e}^{-X^2/2}\,\mathrm{e}^{-Xx}\,\mathrm{d}X = \tfrac{1}{2}\,\mathrm{e}^{-x^2/2}\Phi_{|X|}(-x)
\end{aligned}$$

where $\Phi_{|X|}(x)$ is the MGF of the one-sided Gaussian random variable, $|X|$. Note also that we can use the exponential functions to find simple approximations of the function, $I_0(x)$. In particular, $I_0(x) \leq \mathrm{e}^x I_0(b)/\exp(b)$, for $x \geq b > 0$, [61, eq. (6)]. We suggest the following approximation,

$$I_0(x) \approx \frac{1}{4}\exp\left(\frac{14}{15}x\right) + \frac{3}{4}.$$

3.3.2 Average Error Rate Evaluation

It was already observed in [40, eq. (10-8-2)] that if the conditional probability of error has the form, $\mathrm{P}_\epsilon(\gamma_b) = \tilde{A}\,\mathrm{e}^{-\tilde{a}\gamma_b}$, $\tilde{A}, \tilde{a} > 0$, then knowledge of the fading power MGF, $\Phi_{g^2}(g^2)$, can be used to obtain the average probability of error; hence, $\bar{\mathrm{P}}_\epsilon(\gamma_b) = \tilde{A}\int_0^\infty \mathrm{e}^{-\tilde{a}g^2\gamma_b} f_{g^2}(g^2)\mathrm{d}g^2 = \tilde{A}\Phi_{g^2}(-\tilde{a}\gamma_b)$. This evaluation of the average probability of error is known as the MGF method [48]. More generally, consider the Prony approximation (3.6), and evaluation of the average probability of error (3.4). One has that,

$$\bar{\mathrm{P}}_\epsilon(\gamma_b) \approx \int_0^\infty \sum_{i=1}^{p} \tilde{A}_i\,\mathrm{e}^{-\tilde{a}_i g^2\gamma_b} f_{g^2}(g^2)\mathrm{d}g^2 = \sum_{i=1}^{p} \tilde{A}_i\,\Phi_{g^2}(-\tilde{a}_i\gamma_b) \tag{3.12}$$

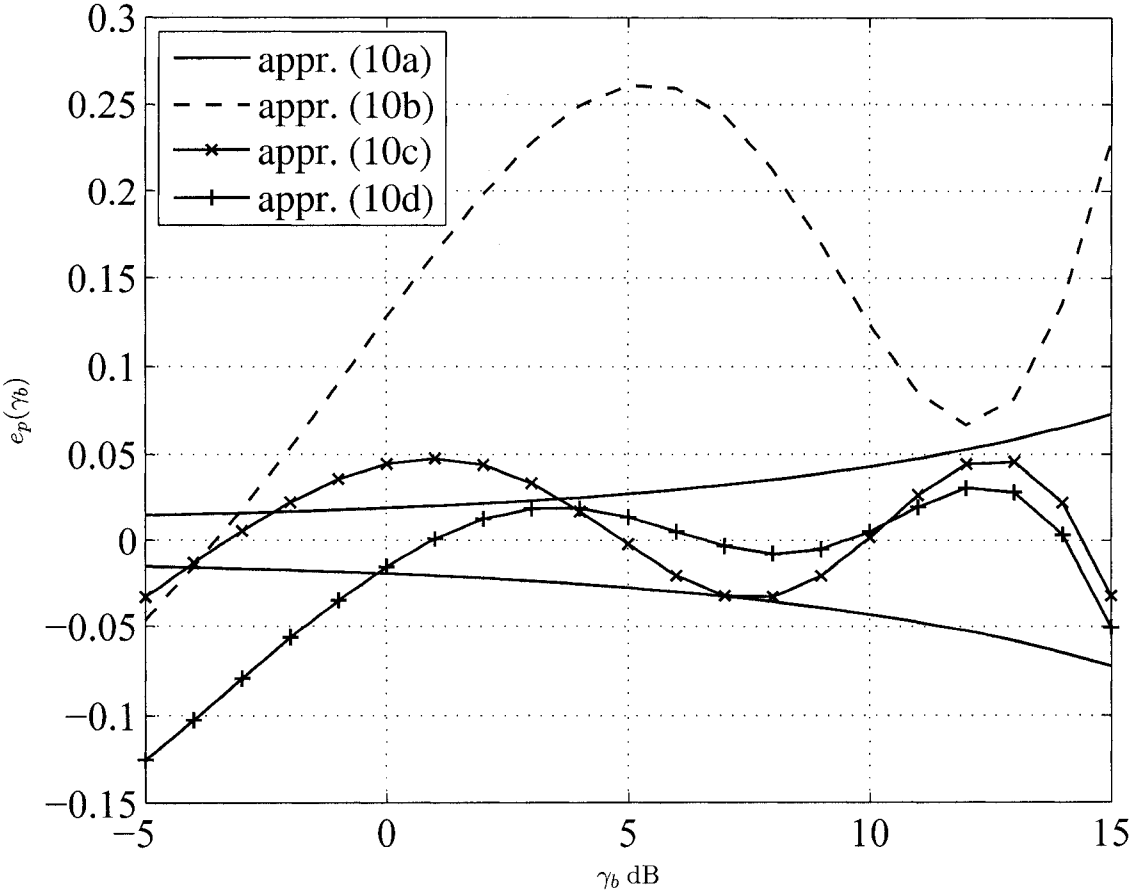

Figure 3.2: The relative approximation error for approximations (3.10a)–(3.10d) of the function, $Q(\sqrt{\gamma_b})$.

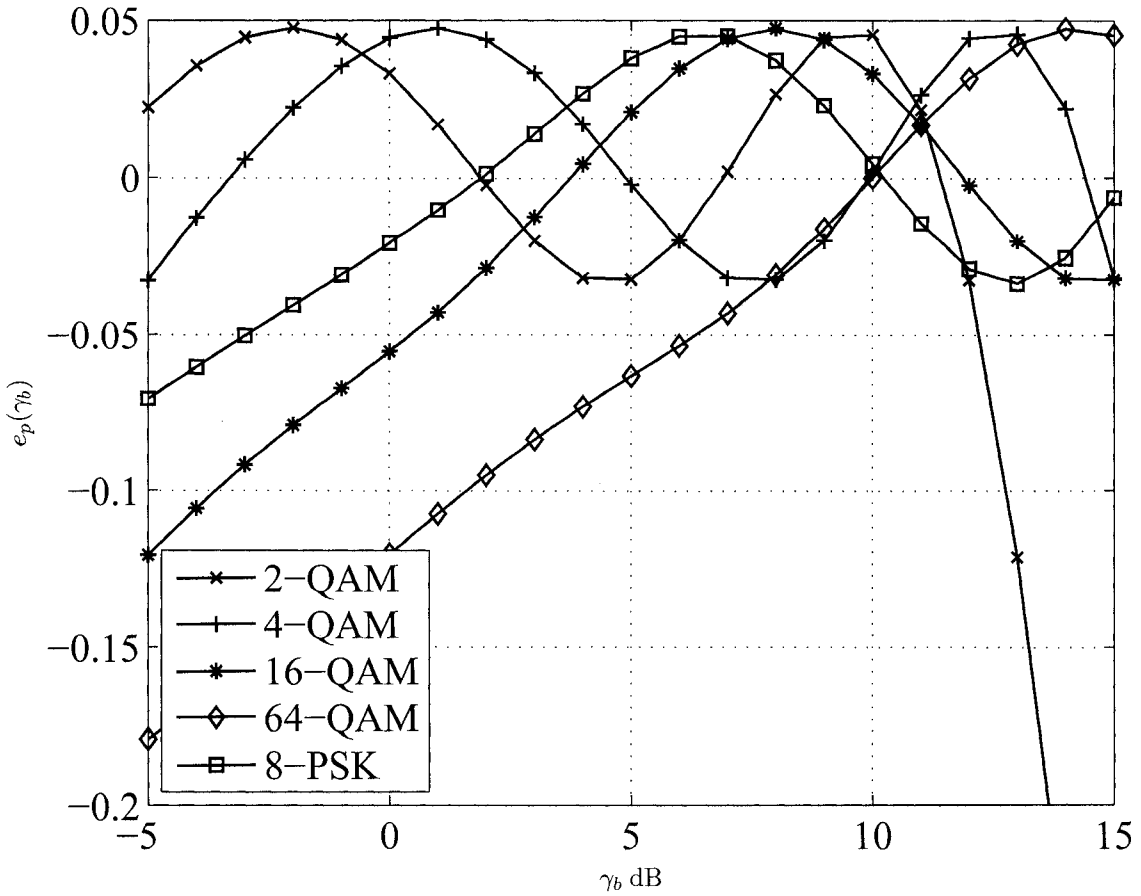

Figure 3.3: The relative approximation error of the Prony approximation (3.10c) for M-ary modulations over a AWGN channel.

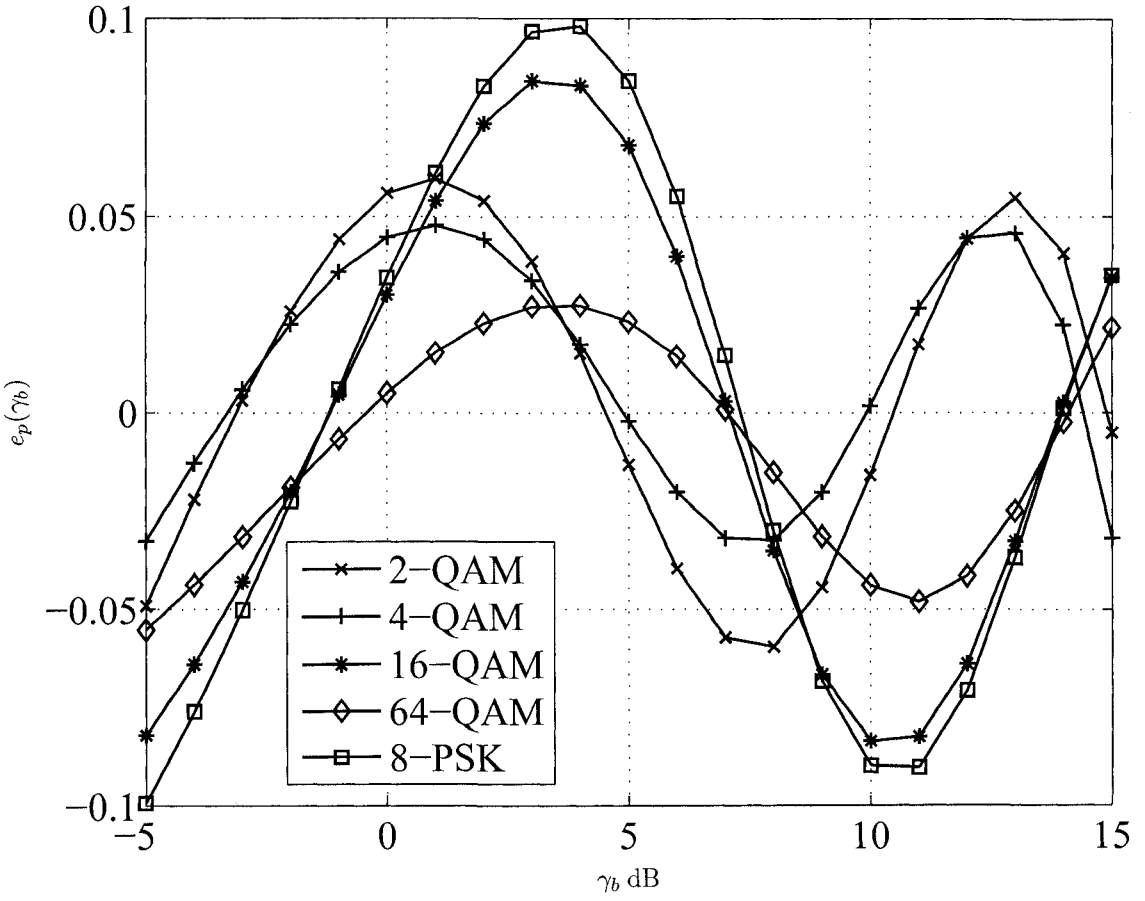

Figure 3.4: The relative approximation error of the optimized Prony approximations (3.11) for M-ary modulations over a AWGN channel.

i.e., we can interchange integration and summation. Note that in the limit, when p goes to infinity, we require that the convergence of the Prony approximation is uniform in order the term-wise integration in (3.12) to be convergent. Since $|\tilde{A}_i \, \mathrm{e}^{-\tilde{a}_i g^2 \gamma_b}| \leq |\tilde{A}_i|$, for $\gamma_b, \tilde{a}_i > 0$, according to the Weierstrass test [55, Sec. 9.6], provided that the sequence, $\tilde{A}_i$, has absolute convergence (i.e., $|\tilde{A}_i|$ is convergent), then the Prony approximation, $\mathrm{P}_\epsilon(\gamma_b) = \lim_{p\to\infty} \sum_{i=1}^{p} \tilde{A}_i \, \mathrm{e}^{-\tilde{a}_i g^2 \gamma_b}$, has uniform convergence, and we can interchange the summation and integration in (3.12), and evaluation of (3.12) converges to the expected value (3.4). Hence, for $p > 1$, the expression (3.12) can be considered as an extension of the classical MGF method [48, Sec. 1.1.3]. Furthermore, for $p = 1$, we can use the Chernoff bound [21] to show that there exists, $\tilde{A}_1$, and, $\tilde{a}_1$, such that $\bar{\mathrm{P}}_\epsilon(\gamma_b) \leq \tilde{A}_1 \Phi_{g^2}(-\tilde{a}_1 \gamma_b)$.

3.4 Polynomial Approximation

We efficiently evaluate the average probability of error (3.4) using a piecewise polynomial approximation of the conditional probability, $\mathrm{P}_\epsilon(\gamma)$. Hence, the domain of γ in (3.4) must be truncated first to the interval, $\gamma \in D = (\tilde{\gamma}_{\min}, \tilde{\gamma}_{\max})$. The truncated domain, D, is then divided into N non-overlapping sub-intervals, $D_i = (\tilde{\gamma}_{i-1}, \tilde{\gamma}_i)$, $i = 1, 2, \cdots, N$, where $0 \leq \tilde{\gamma}_0 = \tilde{\gamma}_{\min}$, $\tilde{\gamma}_N = \tilde{\gamma}_{\max} < \infty$, and, $\tilde{\gamma}_{i-1} < \tilde{\gamma}_i$. In each sub-interval, let $\mathrm{P}_\epsilon(\gamma)$ be approximated by a polynomial, $\sum_{j=0}^{p_i} \tilde{a}_{ij} \gamma^j$, of degree, p_i. Hence, the average probability of error (3.4) is evaluated as,

$$\begin{aligned} \bar{\mathrm{P}}_\epsilon(\gamma_b) &\approx \int_{\tilde{\gamma}_{\min}}^{\tilde{\gamma}_{\max}} \mathrm{P}_\epsilon\big(g^2\gamma_b\big) \, f_{g^2}(g^2) \mathrm{d}g^2 \\ &\approx \sum_{i=1}^{N} \int_{\tilde{\gamma}_{i-1}/\gamma_b}^{\tilde{\gamma}_i/\gamma_b} \sum_{j=0}^{p_i} \tilde{a}_{ij} (g^2\gamma_b)^j f_{g^2}(g^2) \mathrm{d}g^2 \\ &= \sum_{i=1}^{N} \sum_{j=0}^{p_i} \tilde{a}_{ij} \gamma_b^j \int_{\tilde{\gamma}_{i-1}/\gamma_b}^{\tilde{\gamma}_i/\gamma_b} (g^2)^j f_{g^2}(g^2) \mathrm{d}g^2. \end{aligned} \tag{3.13}$$

Note that using a substitution, $\gamma = g^2\gamma_b$, in (3.13), the approximation interval, $(\tilde{\gamma}_{i-1}, \tilde{\gamma}_i)$, of the i-th interval, D_i, becomes, $(\tilde{\gamma}_{i-1}/\gamma_b, \tilde{\gamma}_i/\gamma_b)$. Note that if $\tilde{a}_i = i\,\tilde{a}$, in the Prony approximation (3.6), i.e., $\mathrm{P}_\epsilon(\gamma) \approx \sum_{i=1}^{p} \tilde{A}_i \left(\mathrm{e}^{-\tilde{a}\gamma^q}\right)^i = \sum_{i=1}^{p} \tilde{A}_i \eta^i$, where $\eta = \mathrm{e}^{-\tilde{a}\gamma^q}$, then the Prony approximation (3.6) is equivalent to the polynomial approximation (3.13). Also, note that if $\tilde{a} < 0$, then, $\eta > 1$, and, if $\tilde{a} > 0$, then, $0 \leq \eta < 1$.

Denote $\Upsilon_{g^2 j}(\tilde{\gamma}) = \int_0^{\tilde{\gamma}} (g^2)^j f_{g^2}(g^2) \mathrm{d}g^2$ to be the j-th partial (truncated) general moment of g^2, and thus, the average probability of error,

$$\bar{\mathrm{P}}_\epsilon(\gamma_b) = \sum_{i=1}^{N} \sum_{j=0}^{p_i} \tilde{a}_{ij} \gamma_b^j \big(\Upsilon_{g^2 j}(\tilde{\gamma}_i/\gamma_b) - \Upsilon_{g^2 j}(\tilde{\gamma}_{i-1}/\gamma_b)\big).$$

Using the infinite sum representation of the Bessel function in (C-1b), we obtain the partial general moments of the MRC output squared channel amplitude,

$$\Upsilon_{g_{;j}^2}(\tilde{\gamma}) \overset{\text{(MRC)}}{=} \begin{cases} \frac{(2\sigma^2)^j}{\Gamma(n/2)}\left(\Gamma\left(\frac{n}{2}+j\right)-\Gamma\left(\frac{n}{2}+j,\tilde{\gamma}/2\sigma^2\right)\right) & s=0 \\ \mathrm{e}^{-s^2/2\sigma^2}\sum_{k=0}^{\infty}\frac{(2\sigma^2)^j(s^2/2\sigma^2)^k}{k!\,\Gamma(n/2+k)}\left(\Gamma\left(\frac{n}{2}+k+j\right)-\Gamma\left(\frac{n}{2}+k+j,\tilde{\gamma}/2\sigma^2\right)\right) & s>0. \end{cases} \tag{3.14}$$

Note that the $(j=0)$-th partial moment corresponds to the CDF, i.e., $\Upsilon_{g_{;0}^2}(\tilde{\gamma}) = F_{g^2}(\tilde{\gamma}) = 1 - Q_{n/2}\big(s/\sigma, \sqrt{\tilde{\gamma}}/\sigma\big)$, where $Q_{n/2}(\cdot,\cdot)$ is the Marcum Q-function of order $n/2$, [21]. The partial moments of the EGC output squared channel amplitude can be obtained as,

$$\Upsilon_{g_{;j}^2}(\tilde{\gamma}) \overset{\text{(EGC)}}{=} \frac{\sqrt{K}}{2\pi}\int_{-1}^{1}\prod_{i=1}^{K}\Phi_{g_i}\left(c+\mathrm{j}\frac{c\sqrt{1-x^2}}{x}\right)\xi(c\sqrt{K}(1+\mathrm{j}\frac{\sqrt{1-x^2}}{x}),\tilde{\gamma})\frac{c\,\mathrm{d}x}{x^2\sqrt{1-x^2}}$$

where $\xi(\alpha,\tilde{\gamma}) = \alpha^{-1-n}(\Gamma(1+n)-\Gamma(1+n,\alpha\tilde{\gamma}))$. Applying the GCQ rule, we have the computationally efficient form,

$$\Upsilon_{g_{;j}^2}(\tilde{\gamma}) \overset{\text{(EGC)}}{=} \frac{c\sqrt{K}}{2\nu}\sum_{l=1}^{\nu}\xi(c\sqrt{K}(1+\mathrm{j}\tau_l),\tilde{\gamma})(1+\tau_l^2)\prod_{i=1}^{K}\Phi_{g_i}(c(1+\mathrm{j}\tau_l)).$$

The partial moments of the SC output squared channel amplitude are computed numerically, i.e., using (3.2), one has,

$$\Upsilon_{g_{;j}^2}(\tilde{\gamma}) \overset{\text{(SC)}}{=} \sum_{i=1}^{K}\int_0^{\tilde{\gamma}}(g^2)^j f_{g_i^2}(g^2)\prod_{\substack{j=1\\ j\neq i}}^{K}F_{g_j^2}(g^2)\,\mathrm{d}g^2.$$

For simplicity, assume that $p_i = p, \forall i$. For each approximation interval, D_i, the values of $\mathrm{P}_\epsilon(\gamma)$, are known at (N_1+1) equidistant points, $\tilde{\gamma}'_{ik} = \tilde{\gamma}_{i-1}+(\tilde{\gamma}_i-\tilde{\gamma}_{i-1})(k/N_1)$, $k=0,1,\cdots,N_1$. Hence, for each interval, D_i, we solve the set of (N_1+1) polynomial equations of $(p+1)$ unknowns, i.e.,

$$\begin{bmatrix} (\tilde{\gamma}'_{i0})^p & (\tilde{\gamma}'_{i0})^{p-1} & \cdots & (\tilde{\gamma}'_{i0})^0 \\ (\tilde{\gamma}'_{i1})^p & (\tilde{\gamma}'_{i1})^{p-1} & \cdots & (\tilde{\gamma}'_{i1})^0 \\ \vdots & \vdots & & \vdots \\ (\tilde{\gamma}'_{iN_1})^p & (\tilde{\gamma}'_{iN_1})^{p-1} & \cdots & (\tilde{\gamma}'_{iN_1})^0 \end{bmatrix}\begin{bmatrix} \tilde{a}_{ip} \\ \tilde{a}_{i(p-1)} \\ \vdots \\ \tilde{a}_{i0} \end{bmatrix} = \begin{bmatrix} \mathrm{P}_\epsilon(\tilde{\gamma}'_{i0}) \\ \mathrm{P}_\epsilon(\tilde{\gamma}'_{i1}) \\ \vdots \\ \mathrm{P}_\epsilon(\tilde{\gamma}'_{iN_1}) \end{bmatrix}. \tag{3.15}$$

Importantly, for $N_1 = p$, we can use the matrix inversion to solve (3.15); note, however, that, for small values of $\mathrm{P}_\epsilon(\gamma'_{ik})$, the solution is ill-conditioned. If $N_1 = p = 1$, i.e., we have a piecewise

linear approximation of $\mathrm{P}_\epsilon(\gamma)$, the approximation coefficients,

$$\begin{bmatrix} \tilde{a}_{i1} \\ \tilde{a}_{i0} \end{bmatrix} = \frac{1}{\tilde{\gamma}_i - \tilde{\gamma}_{i-1}} \begin{bmatrix} \mathrm{P}_\epsilon(\tilde{\gamma}_i) - \mathrm{P}_\epsilon(\tilde{\gamma}_{i-1}) \\ -\tilde{\gamma}_{i-1}\mathrm{P}_\epsilon(\tilde{\gamma}_i) + \tilde{\gamma}_i \mathrm{P}_\epsilon(\tilde{\gamma}_{i-1}) \end{bmatrix}.$$

There are two sources of the approximation error in (3.13). In particular, the truncation error in (3.13) can be upper-bounded as,

$$\begin{aligned} \int_0^{\tilde{\gamma}_{\min}} \mathrm{P}_\epsilon(g^2\gamma_b)\, f_{g^2}(g^2)\mathrm{d}g^2 &\leq \mathrm{P}_\epsilon(\alpha)\, F_{g^2}(\tilde{\gamma}_{\min}) \\ \int_{\tilde{\gamma}_{\max}}^{\infty} \mathrm{P}_\epsilon(g^2\gamma_b)\, f_{g^2}(g^2)\mathrm{d}g^2 &\leq \mathrm{P}_\epsilon(\tilde{\gamma}_{\max})\,(1 - F_{g^2}(\tilde{\gamma}_{\max})) \end{aligned}$$

where $F_{g^2}(\gamma) = \int_0^\gamma f_{g^2}(g^2)\mathrm{d}g^2$ denotes the CDF, $0 \leq \alpha \ll \tilde{\gamma}_{\min}\gamma_b$, and $\mathrm{P}_\epsilon(\alpha) \leq \frac{1}{2}$. The truncation interval, D, is chosen to make the truncation error negligible. Thus, choice of $\tilde{\gamma}_{\max}$ ($\tilde{\gamma}_{\min}$) influences the values of the average probability of error at large (small) SNR, and if $\tilde{\gamma}_{\max}$ is too small (or, $\tilde{\gamma}_{\min}$ too large), the computed average probability of error will tend to be smaller than the exact value. For the i-th interval, D_i, we define the approximation error,

$$e_{p_i}(i) = \sum_{k=0}^{N_1} \tilde{w}_{ik} \left| \sum_{j=0}^{p_i} \tilde{a}_{ij} \tilde{\gamma}_{ik}^j - \mathrm{P}_\epsilon(\tilde{\gamma}_{ik}) \right|^{q_1}$$

where $q_1 > 0$, and the weights are chosen, for example, as, $\tilde{w}_{ik} = 1/\mathrm{P}_\epsilon(\tilde{\gamma}_{ik})$. Note that partitioning of D into sub-intervals, D_i, is chosen so that the maximum approximation error, $\max_i e_{p_i}(i)$, is limited. Our numerical experiments indicate that, in general, shorter intervals, D_i, should be chosen in the regions of smaller values of $\mathrm{P}_\epsilon(\gamma)$.

As an example, we investigate the accuracy of the polynomial approximations for the BER of the 2-QAM and 16-QAM modulations over a AWGN channel. In particular, we assume piecewise linear ($p = 1$), quadratic ($p = 2$), and cubic ($p = 3$) polynomial approximations (3.13) of the conditional BER, $\mathrm{P}_\epsilon(\gamma_b)$, for $-5\,\mathrm{dB} \leq \gamma_b \leq 20\,\mathrm{dB}$; thus, $p_i = p$, and, $N_1 = p$, for all sub-intervals, $i = 1, 2, \cdots, N$. Recall that, for $N_1 = p$, the polynomial approximation is exact at the approximation intervals boundary points, $\tilde{\gamma}_i$. Thus, the relative approximation error, $e_p(\gamma_b)$, has oscillatory behavior, and the envelope of the relative approximation error, $\hat{e}_p(\gamma_b)$, can be defined using the maximum values of $e_p(\gamma_b)$ for every approximation interval, $D_i = (\tilde{\gamma}_{i-1}, \tilde{\gamma}_i)$. The envelopes of the relative error, $\hat{e}_p(\gamma_b)$, versus the SNR, γ_b, are shown in Fig. 3.5 and Fig. 3.6, for $N = 15, 25$ and 35 sub-intervals. We observe from Fig. 3.5 and Fig. 3.6 that the values of the

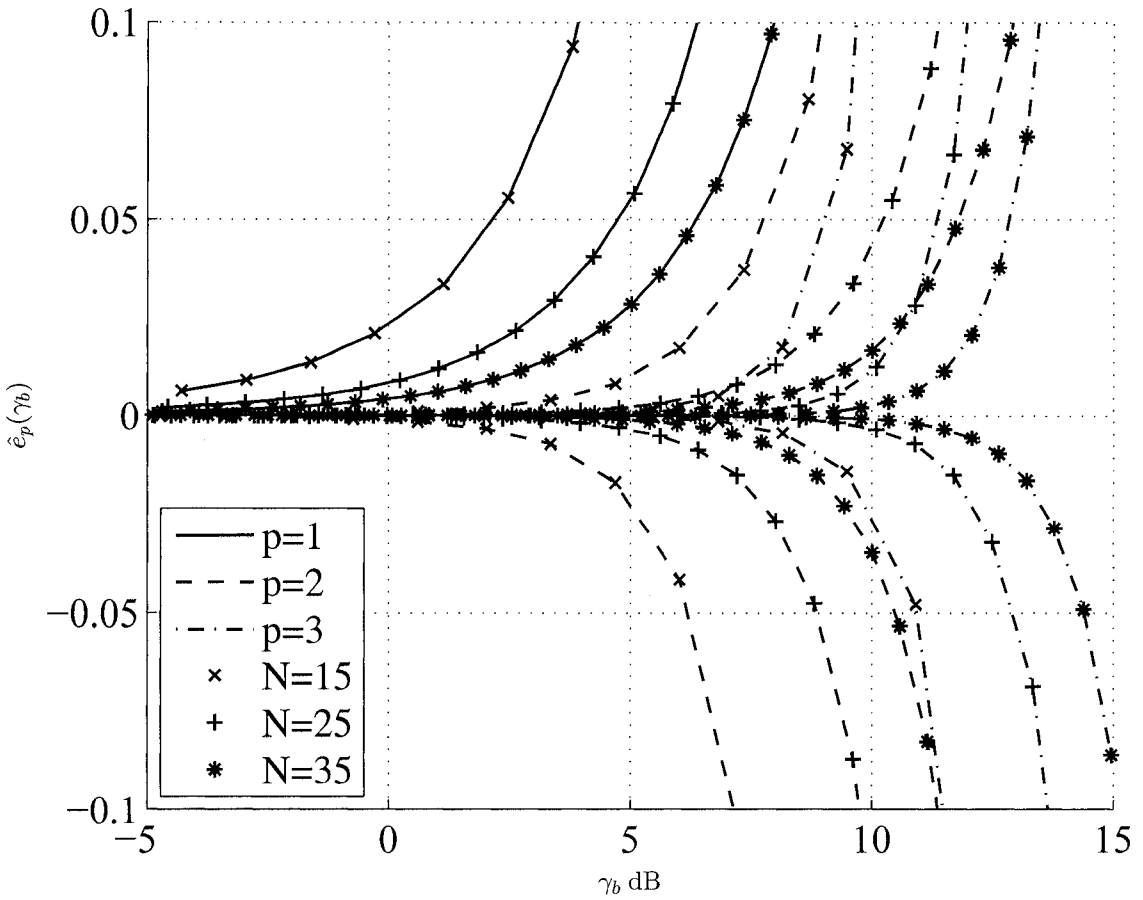

Figure 3.5: The envelopes of relative approximation error for the polynomial approximations of 2-QAM over a AWGN channel.

approximation error increases to infinity with the SNR. Hence, the order, p, of the approximating polynomials, and the number of sub-intervals, N, are determined for the maximum value, γ_b, of the approximating interval, D. In particular, larger values of p and N improves the polynomial approximation towards the larger values of γ_b. Also, for larger values of p (N), we can use smaller values of N (p) to achieve the same approximation error. Furthermore, comparing Fig. 3.5 and Fig. 3.6, we observe that the polynomial approximations are much more accurate for those conditional BER's, $\mathrm{P}_\epsilon(\gamma_b)$, that decrease less steeply with SNR. Finally, we can conclude that the values of the product, $pN \gg 10$, should be used for practical evaluations of the average probability of error using polynomial approximations.

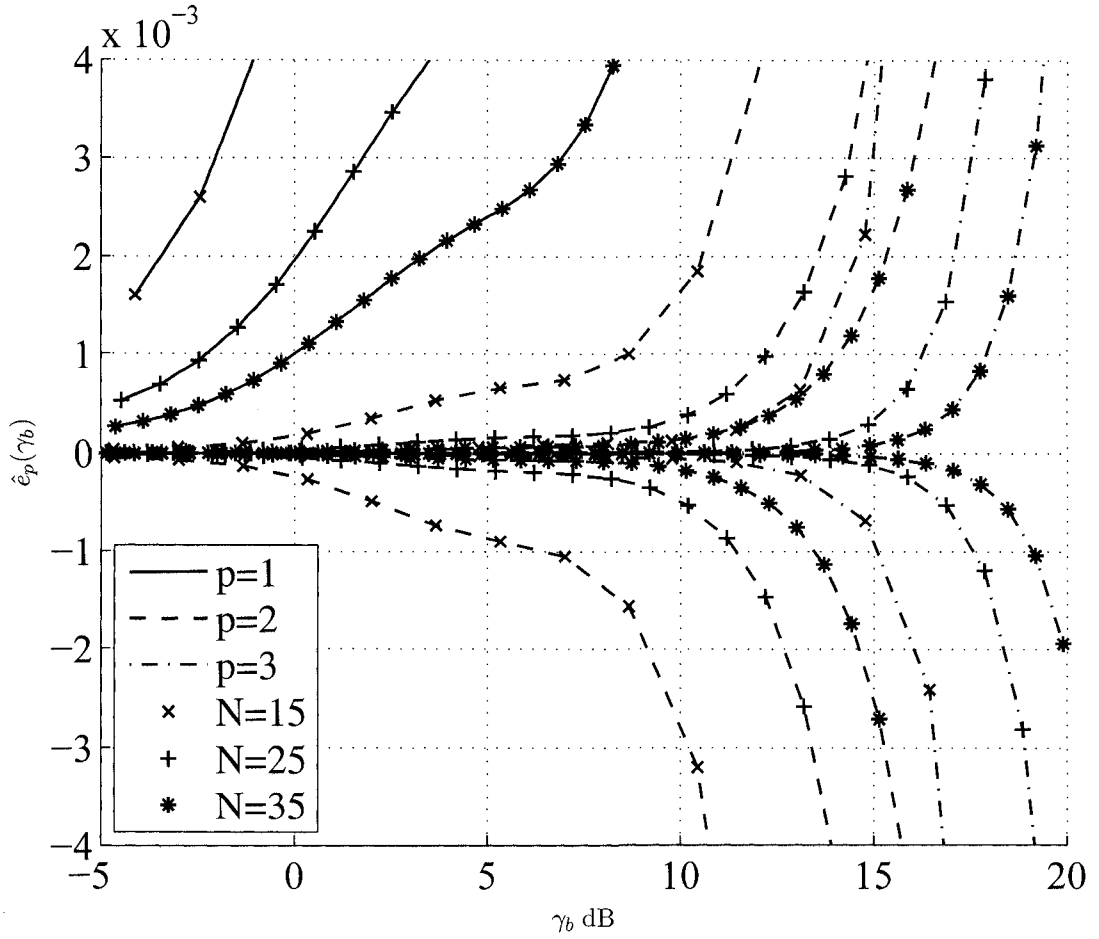

Figure 3.6: The envelopes of relative approximation error for the polynomial approximations of 16-QAM over a AWGN channel.

3.5 Numerical Examples

We use theoretical analysis and numerical integration to obtain the average probability of bit-error (3.4) (corresponding to the BER in all cases considered) for single channel and multi-channel post-combining receivers. We then employ Prony and polynomial approximations to compute these average probabilities, and to evaluate accuracy of the proposed semi-analytical methods.

3.5.1 Single Channel Reception

Assume a single channel coherent reception, and let the conditional BER, $\mathrm{P}_\epsilon(\gamma) = Q\big(\sqrt{\gamma}\big)$, where $\gamma = g^2\gamma_b$, and g is generalized Rayleigh or Ricean distributed [21], i.e., g^2 is central or non-central chi-square distributed with variance, σ^2, per dimension, n degrees of freedom, and non-centrality parameter, $s \geq 0$; see (C-1b). We evaluate the average probability of error (3.4). Hence, for $s > 0$, g^2 is non-central chi-square distributed, and using the infinite series representation of the $I_n(x)$ function, one has that,

$$\begin{aligned}\int_0^\infty Q\Big(\sqrt{g^2\gamma_b}\Big)\, \mathrm{e}^{-g^2/2\sigma^2}(g^2)^{\frac{n}{2}-1+k}\, \mathrm{d}g^2 = 2^{\frac{n}{2}+k-1}\sigma^{2k+n}\times \\ \times\Big(\Gamma\left(\tfrac{n}{2}+k\right) - \tfrac{1}{\sqrt{\pi}}\mathrm{Im}\big\{\beta_{-\gamma_b\sigma^2}\left(\tfrac{1}{2}, -\tfrac{n}{2}-k+\tfrac{1}{2}\right)\big\}\,\Gamma\left(\tfrac{n}{2}+k+\tfrac{1}{2}\right)\Big)\end{aligned}$$

where $\mathrm{Im}\{\cdot\}$ denotes the imaginary part of a complex number, and $\beta_z(a,b)$ is the incomplete beta function; see (A-7). Hence, the average BER over a generalized Ricean fading,

$$\begin{aligned}\bar{\mathrm{P}}_\epsilon(\gamma_b) = \tfrac{1}{2} - \tfrac{1}{2\sqrt{\pi}}\,\mathrm{e}^{-\frac{s^2}{2\sigma^2}}\times \\ \times\textstyle\sum_{k=0}^{\infty}\frac{(s^2/2\sigma^2)^k}{k!}\mathrm{Im}\big\{\beta_{-\gamma_b\sigma^2}\left(\frac{1}{2}, -\frac{n}{2}-k+\frac{1}{2}\right)\big\}\,\frac{\Gamma\left(\frac{n}{2}+k+\frac{1}{2}\right)}{\Gamma\left(\frac{n}{2}+k\right)}.\end{aligned} \tag{3.16}$$

If $s = 0$, i.e., g^2 is central chi-square distributed, we substitute $Q\big(\sqrt{\gamma}\big) = \frac{1}{2} - \frac{1}{2\sqrt{\pi}}\int_0^{\gamma/2}\frac{\mathrm{e}^{-u}}{\sqrt{u}}\mathrm{d}u$ [62], and eq. (C-1b) into (3.4). Using the definition of the gamma function [62, 8.310], the integral, $\int_0^\infty x^{\nu-1}\,\mathrm{e}^{-\mu x}\,\mathrm{d}x = \mu^{-\nu}\Gamma(\nu)$, $\mu, \nu > 0$, [62, 3.381.4], and the definition of the hypergeometric function (A-8b), we obtain the average BER over a generalized Rayleigh fading [63],

$$\bar{\mathrm{P}}_\epsilon(\gamma_b) = \frac{1}{2} - \sqrt{\frac{\gamma_b\sigma^2}{\pi}}\,\frac{\Gamma\left(\frac{n}{2}+\frac{1}{2}\right)}{\Gamma\left(\frac{n}{2}\right)}\,{}_2F_1\Big(\frac{n}{2}+\frac{1}{2}, \frac{1}{2}; \frac{3}{2}, -\gamma_b\sigma^2\Big). \tag{3.17}$$

As an example, consider the average BER for the 2-QAM and 16-QAM modulations over a generalized Ricean fading channel. The exact BER can be computed assuming the conditional BER (3.9a) and using (3.16). Note that the infinite summation in (3.16) converges quickly (say, $k <= 40$)

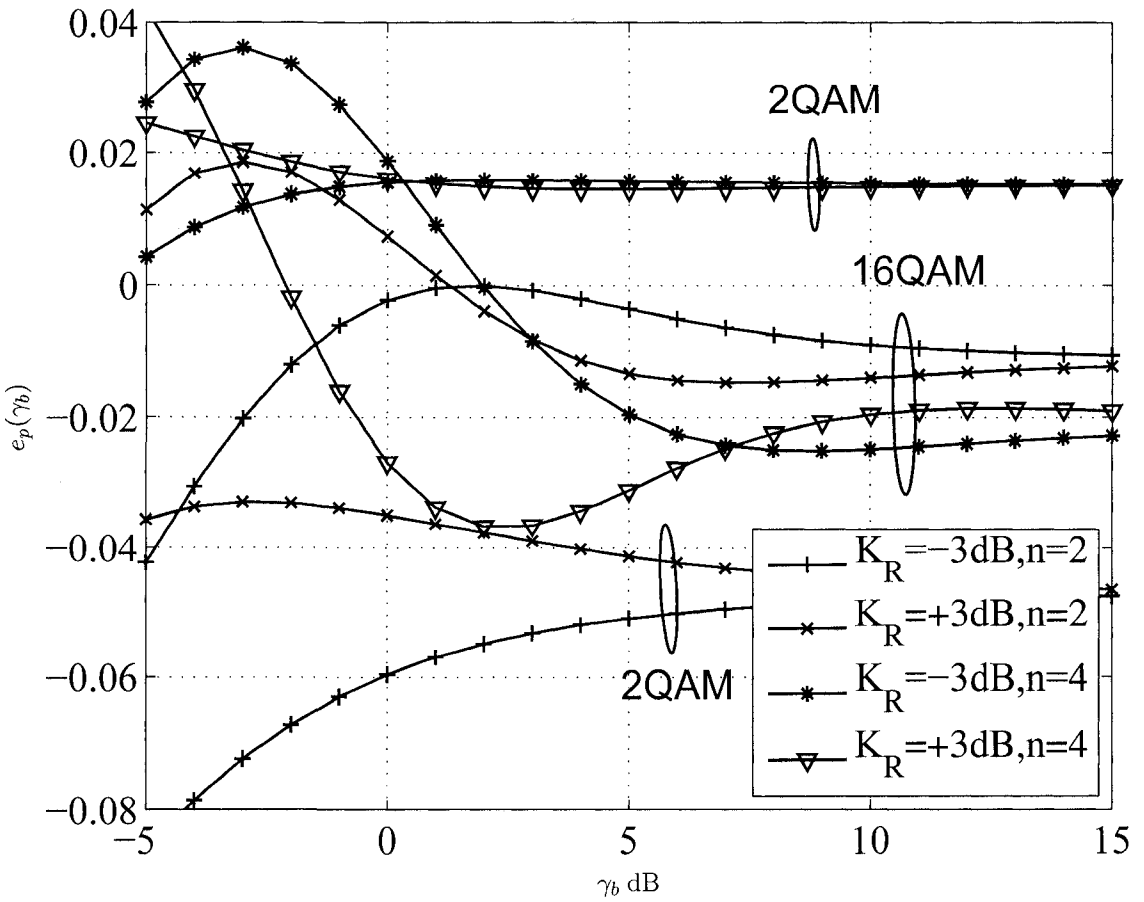

Figure 3.7: The relative approximation error of the Prony approximation for 2-QAM and 16-QAM modulations over a generalized Ricean fading channel.

due to the factorial term in the denominator. The average BER is also obtained assuming the Prony approximation (3.11) of the conditional BER's for QAM modulations, and substituting the MGF of the non-central chi-square variable (C-4b) into (3.12). The exact average BER is used as a reference to evaluate the accuracy of the Prony approximation. In particular, the relative approximation error, $e_p(\gamma_b)$, versus the SNR, γ_b, for the Ricean factor, $K_{\rm R} = -3\,{\rm dB}$ and $3\,{\rm dB}$, and $n = 2$ and 4 degrees of freedom is shown in Fig. 3.7. Importantly, we observe from Fig. 3.7 that the approximation error is finite for all values of SNR considered. Note also that the Prony approximation method is strictly a lower bound (i.e., $e_p(\gamma_b) < 0$, $\forall \gamma_b$), for $n = 2$, and strictly an upper bound (i.e., $e_p(\gamma_b) > 0$, $\forall \gamma_b$), for $n = 4$, of the exact average BER.

As another example, we employ the polynomial approximation to evaluate the average BER for the 2-QAM and 16-QAM modulations over a generalized Ricean fading channel with the parame-

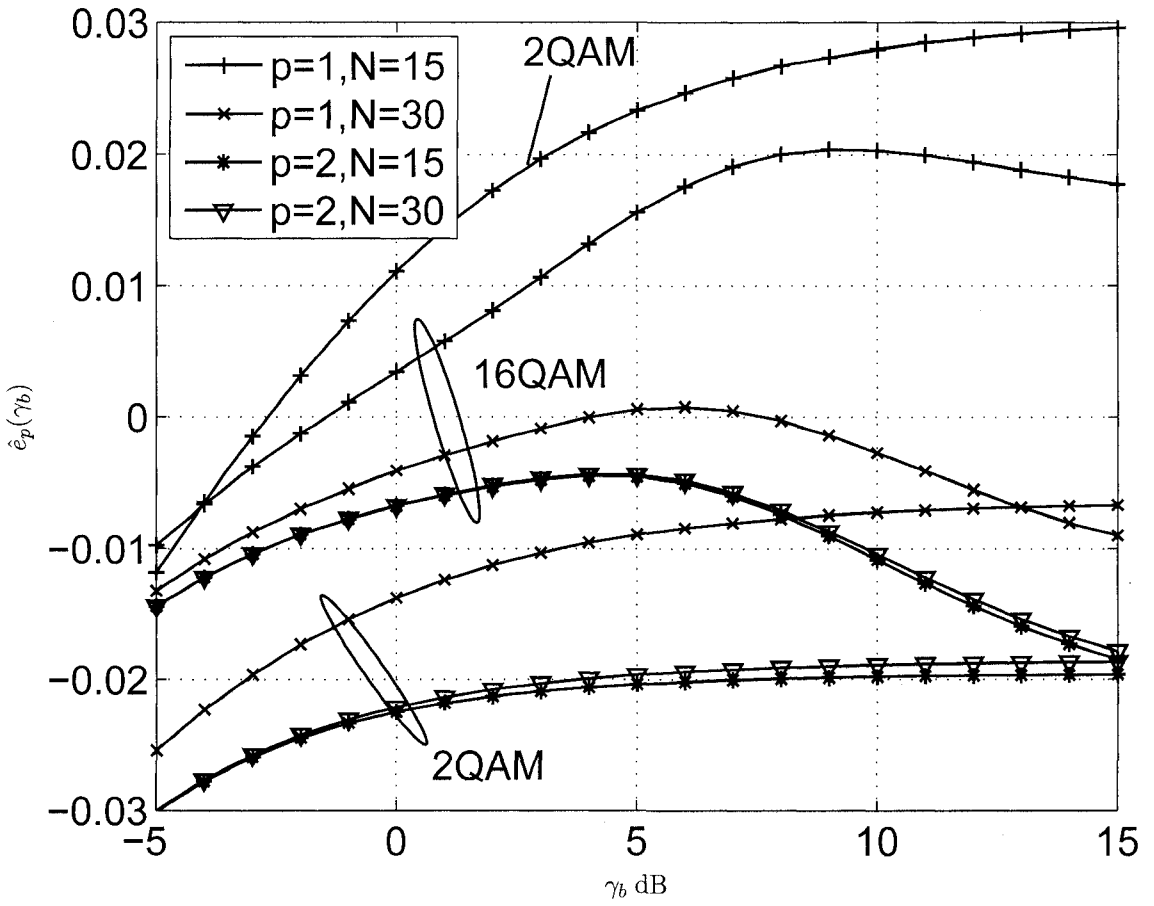

Figure 3.8: The relative approximation error of the polynomial approximations of 2-QAM and 16-QAM modulations over a generalized Ricean fading channel, for $K_{\mathrm{R}} = -3\,\mathrm{dB}$, and, $n = 2$.

ters, $K_{\mathrm{R}} = -3\,\mathrm{dB}$, and, $n = 2$. We assume the approximation interval, $-5\,\mathrm{dB} < \gamma_b < 20\,\mathrm{dB}$, and $N = 15$ and 30 approximation sub-intervals. The relative approximation error, $\hat{e}_p(\gamma_b)$, versus the SNR, γ_b, is shown in Fig. 3.8. We observe from Fig. 3.8 that the approximation error is smaller for 16-QAM than for 2-QAM, as expected; cf. Fig. 3.6. Furthermore, the smallest approximation error occurs for the case of linear approximation (i.e., $p = 1$) and $N = 30$ approximation sub-intervals.

Finally, we use the GCQ rule [46] obtained in Appendix B to evaluate the average probability of error for the scenarios in Fig. 3.7 and Fig. 3.8. The relative approximation error, $\hat{e}_p(\gamma_b)$, versus the SNR, γ_b, is shown in Fig. 3.9. The results in Fig. 3.9 have been obtained for $c = 0$ and $\nu = 5$; see Appendix B. Thus, provided that the region of convergence of the MGF is known, we can select the value of c and ν to obtain the average probability of error for single channel reception with smaller approximation error than the polynomial approximation method.

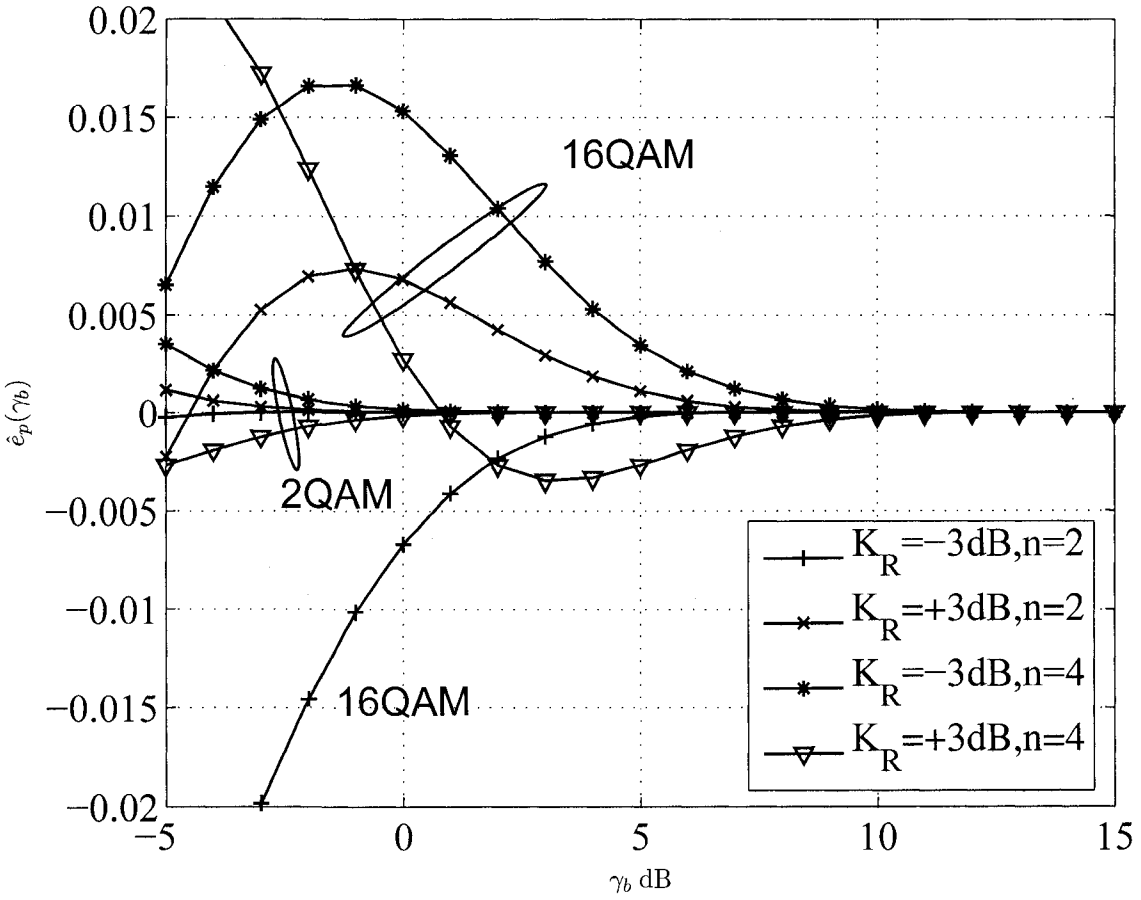

Figure 3.9: The relative approximation error of the GCQ rule for $c = 0$ and $\nu = 5$, and for 2-QAM and 16-QAM modulations over a generalized Ricean fading channel.

3.5.2 Multi-Channel Reception

Consider multi-channel postcombining receivers for K slowly flat fading channels. Assuming knowledge of the fading amplitudes and phases at the receiver, the decision variable is the output of MRC. When only either amplitudes or phases are known at the receiver, the decision variable corresponds to the SC or EGC, respectively.

Assume K correlated generalized Rayleigh slow fading channels with variance, σ^2, per dimension, n degrees of freedom, and MRC receiver. Let the normalized correlation coefficient between branches, i, and, j, be defined as, [64]

$$\rho_{i,j} = \frac{\mathrm{E}\left[g_i^2 g_j^2\right] - 1}{\sqrt{\left(\mathrm{E}\left[g_i^4\right] - 1\right)\left(\mathrm{E}\left[g_j^4\right] - 1\right)}}.$$

The MGF of the combiner output SNR is, [64, eq. (29), (30)]

$$\Phi_{g^2}(t) = \sum_{k=1}^{K} \sum_{i=1}^{n} \tilde{A}_{k,i}(1 - t\sigma^2\lambda_k)^{-i} \tag{3.18}$$

where

$$\tilde{A}_{k,i} = \frac{1}{\sigma^2\lambda_k(n-i)!} \frac{\mathrm{d}^{(n-i)}}{\mathrm{d}t^{(n-i)}} \left\{\Phi_{g^2}(t)(1 - t\sigma^2\lambda_k)^n\right\}\Big|_{t=(\sigma^2\lambda_k)^{-1}}$$

and λ_k are the K eigenvalues of the correlation matrix with elements, $\rho_{i,j}$. Hence, we can invert (3.18) to obtain the PDF of the MRC output SNR,

$$f_{g^2}(g^2) \overset{\text{(MRC)}}{=} \sum_{k=1}^{K} \sum_{i=1}^{n} \tilde{A}_{k,i} \frac{g^{2(i-1)}\, \mathrm{e}^{-g^2/(\sigma^2\lambda_k)}}{\Gamma(i)\,(\sigma^2\lambda_k)^i}. \tag{3.19}$$

The average BER for QAM modulations over a generalized Rayleigh fading channel can be evaluated exactly using (3.19) and the expression (3.17), and approximately, using the Prony approximation (3.11) and the MGF (3.18) in (3.12). A numerical example verifying high accuracy of the Prony approximation for the average BER evaluation for the 8-PSK modulation over generalized Rayleigh fading channels and MRC is given in [63, Fig. 5].

For the EGC postcombining receiver, we assume that the K branches are independent. Let the

conditional BER, $\mathrm{P}_\epsilon(\gamma) = Q\big(\sqrt{\gamma}\big)$. Hence, we derive the Laplace transform of the Q-function,

$$\int_0^\infty Q(g\sqrt{\gamma_b})\ \mathrm{e}^{-tg}\mathrm{d}g = \frac{1}{2t} - \frac{\mathrm{e}^{\frac{t^2}{2\gamma_b}} Q\big(t/\sqrt{\gamma_b}\big)}{t} \tag{3.20}$$

where the region of convergence, $\mathrm{Re}\{t\} > 0$, and $\mathrm{Re}\{\cdot\}$ denotes the real part of a complex number. Using (3.20) and the PDF (3.1), we obtain the exact average BER for the EGC postcombining receiver, i.e.,

$$\begin{aligned}\bar{\mathrm{P}}_\epsilon(\gamma_b) &\overset{\text{(EGC)}}{=} \int_0^\infty Q(g\sqrt{\gamma_b})\, f_g(g)\mathrm{d}g = \\ &= \frac{1}{2\pi}\int_{-\infty}^{\infty} \frac{\prod_{i=1}^K \Phi_{g_i}(c+\mathrm{j}\omega)}{(c+\mathrm{j}\omega)\sqrt{K}} \left(\frac{1}{2} - \mathrm{e}^{\frac{(c+\mathrm{j}\omega)^2 K}{2\gamma_b}} Q\left(\frac{(c+\mathrm{j}\omega)\sqrt{K}}{\sqrt{\gamma_b}}\right)\right)\mathrm{d}\omega. \end{aligned} \tag{3.21}$$

The BER (3.21) can be evaluated using the GCQ rule, i.e.,

$$\bar{\mathrm{P}}_\epsilon(\gamma_b) \overset{\text{(EGC)}}{=} \frac{1}{2\nu}\sum_{l=1}^{\nu} \frac{\prod_{i=1}^K \Phi_{g_i}(c(1+\mathrm{j}\tau_l))}{\sqrt{K}} \left(\frac{1}{2} - \mathrm{e}^{\frac{(1+\mathrm{j}\tau_l)^2 c^2 K}{2\gamma_b}} Q\left(\frac{(1+\mathrm{j}\tau_l)c\sqrt{K}}{\sqrt{\gamma_b}}\right)\right)\frac{(1+\tau_l^2)}{(1+\mathrm{j}\tau_l)}$$

and $c > 0$. We use the Prony approximation (3.6), for $q = 1$, to evaluate the average BER for EGC. In particular, since,

$$\int_0^\infty \mathrm{e}^{-\tilde{a}g^2 - tg}\mathrm{d}g = \sqrt{\frac{\pi}{\tilde{a}}}\,\mathrm{e}^{\frac{t^2}{4\tilde{a}}} Q\left(\frac{t}{\sqrt{\tilde{a}}}\right)$$

for $\tilde{a} > 0$, and, $\mathrm{Re}\{t\} > 0$, the average BER for EGC is,

$$\begin{aligned}\bar{\mathrm{P}}_\epsilon(\gamma_b) &\overset{\text{(EGC)}}{\approx} \int_0^\infty \sum_{j=1}^p \tilde{A}_j\, \mathrm{e}^{-\tilde{a}_j g^2\gamma_b} f_g(g)\mathrm{d}g \\ &= \sqrt{\frac{K}{4\pi\gamma_b}} \sum_{j=1}^p \frac{\tilde{A}_j}{\sqrt{\tilde{a}_j}} \int_{-\infty}^{\infty} \left(\prod_{i=1}^K \Phi_{g_i}(c+\mathrm{j}\omega)\right) \mathrm{e}^{\frac{(c+\mathrm{j}\omega)^2 K}{4\tilde{a}_j\gamma_b}} Q\left(\frac{(c+\mathrm{j}\omega)\sqrt{K}}{\sqrt{\tilde{a}_j\gamma_b}}\right)\mathrm{d}\omega. \end{aligned}$$

Using the GCQ rule, one has that, for $c > 0$,

$$\bar{\mathrm{P}}_\epsilon(\gamma_b) \overset{\text{(EGC)}}{\approx} \frac{1}{2\nu}\sqrt{\frac{K\pi}{\gamma_b}} \sum_{j=1}^p \frac{\tilde{A}_j}{\sqrt{\tilde{a}_j}} \sum_{l=1}^{\nu} \left(\prod_{i=1}^K \Phi_{g_i}(c(1+\mathrm{j}\tau_l))\right) \mathrm{e}^{\frac{c^2(1+\mathrm{j}\tau_l)^2 K}{4\tilde{a}_j\gamma_b}} Q\left(\frac{c(1+\mathrm{j}\tau_l)\sqrt{K}}{\sqrt{\tilde{a}_j\gamma_b}}\right)(1+\tau_l^2).$$

As an example, we use the Prony approximation (3.11) for the 2-QAM and 16-QAM modulations to obtain the relative approximation error of the average BER over $K = 2$ and 4 independent generalized Ricean distributed branches having $n = 2$, the Ricean factor $K_\mathrm{R} = -3\,\mathrm{dB}$, and $3\,\mathrm{dB}$,

and using EGC; assuming, $\nu = 256$, and, $c = 0.3$, the results are shown in Fig. 3.10. We observe from Fig. 3.10 that the approximation error, $|e_p(\gamma_b)| < 0.05$, for $\gamma_b > -5\,\mathrm{dB}$.

For SC, we use numerical integration to obtain the average BER (3.4) using the exact conditional probability of error (3.9a) and using the Prony approximations (3.11). As an example, assume $K = 2$ and 4 independent generalized Ricean distributed branches having $n = 2$, the Ricean factor, $K_\mathrm{R} = -3\,\mathrm{dB}$, and $3\,\mathrm{dB}$, and SC. Fig. 3.11 shows the relative approximation error of the Prony approximation for the average BER of the 2-QAM and 16-QAM modulations. We observe from Fig. 3.11 that the approximation error, $|e_p(\gamma_b)| < 0.06$, for $\gamma_b > -5\,\mathrm{dB}$.

3.6 Summary

We proposed a novel semi-analytical technique to evaluate the average probability of error for digital communication systems operating over slowly fading channels. This technique is based on the Prony (sum of the exponentials) approximation of the conditional probability of error; thus, knowledge of the MGF of the instantaneous SNR is required to obtain the average probability of error. We also considered the Chernoff bound to obtain the Prony approximation. Many examples of the Prony approximation of the conditional probability of error over a AWGN channel for M-ary QAM and 8-PSK modulations were presented. We observed that the sum of only two exponentials can approximate the conditional probability of error with a high accuracy; the relative approximation error was less than 10% for most cases considered. The overall approximation error of the exact average probability of error over fading channels was less than 6% for most cases considered. Furthermore, we also investigated a piecewise polynomial approximation of the conditional probability of error as an alternative to the Prony approximation. Knowledge of the partial moments of the SNR is required to obtain the average probability of error using the polynomial approximation. Our numerical examples indicate that the polynomial approximation requires that the product of the polynomial degree and the number of sub-intervals should be much larger than, 10. Since the parameters of the polynomial approximation must be obtained for every sub-interval, and the number of sub-intervals can be large, the Prony approximation is, in general, significantly less complex, and thus, is preferred to the polynomial approximation. In conclusion, the piecewise semi-numerical evaluation of the average probability of error is more complex than the Prony approximation and the GCQ methods. However, the piecewise polynomial approximation of the conditional probability of error is less complex than the ordinary piecewise polynomial integration. The accuracy of the

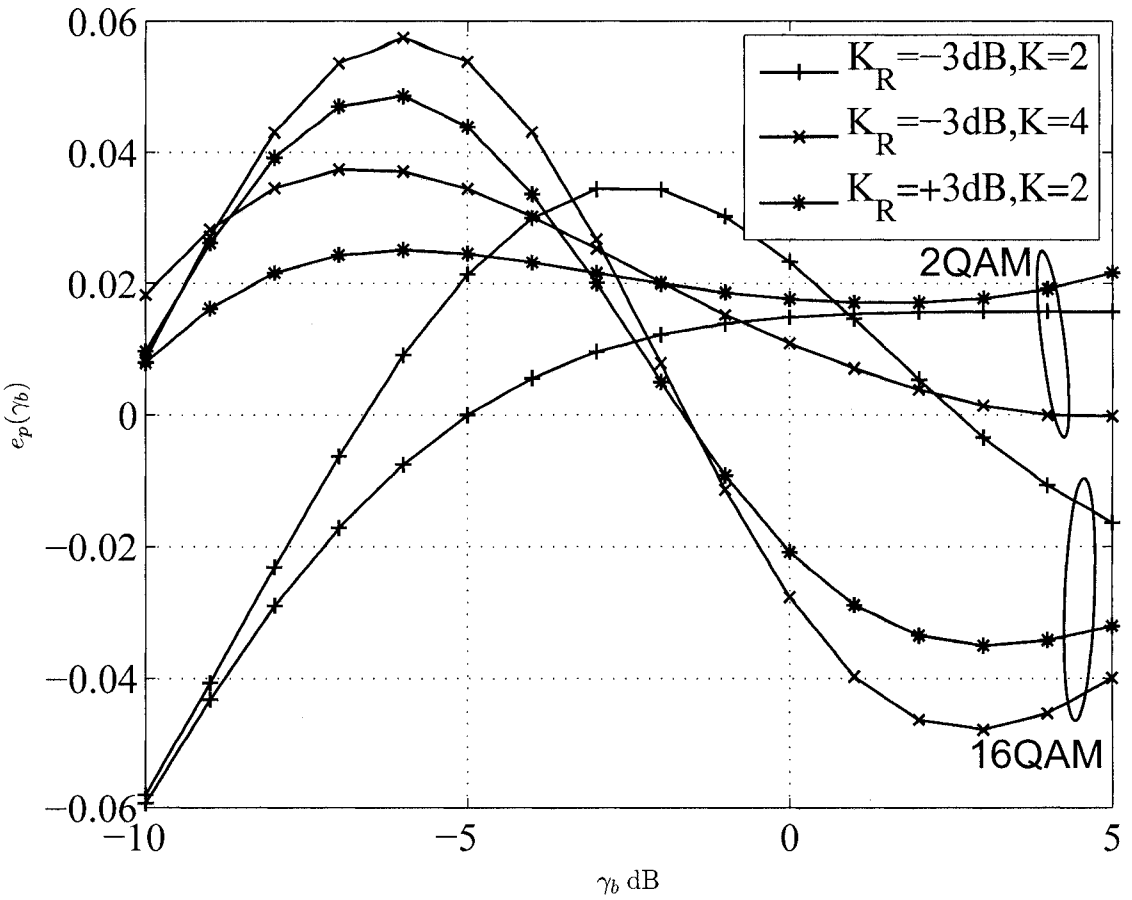

Figure 3.10: The relative approximation error of the Prony approximation for 2-QAM and 16-QAM modulations, and EGC over $K = 2$ and $K = 4$ IID generalized Ricean fading channels.

piecewise semi-numerical evaluation method could be improved if the samples of the conditional probability of error are not taken uniformly.

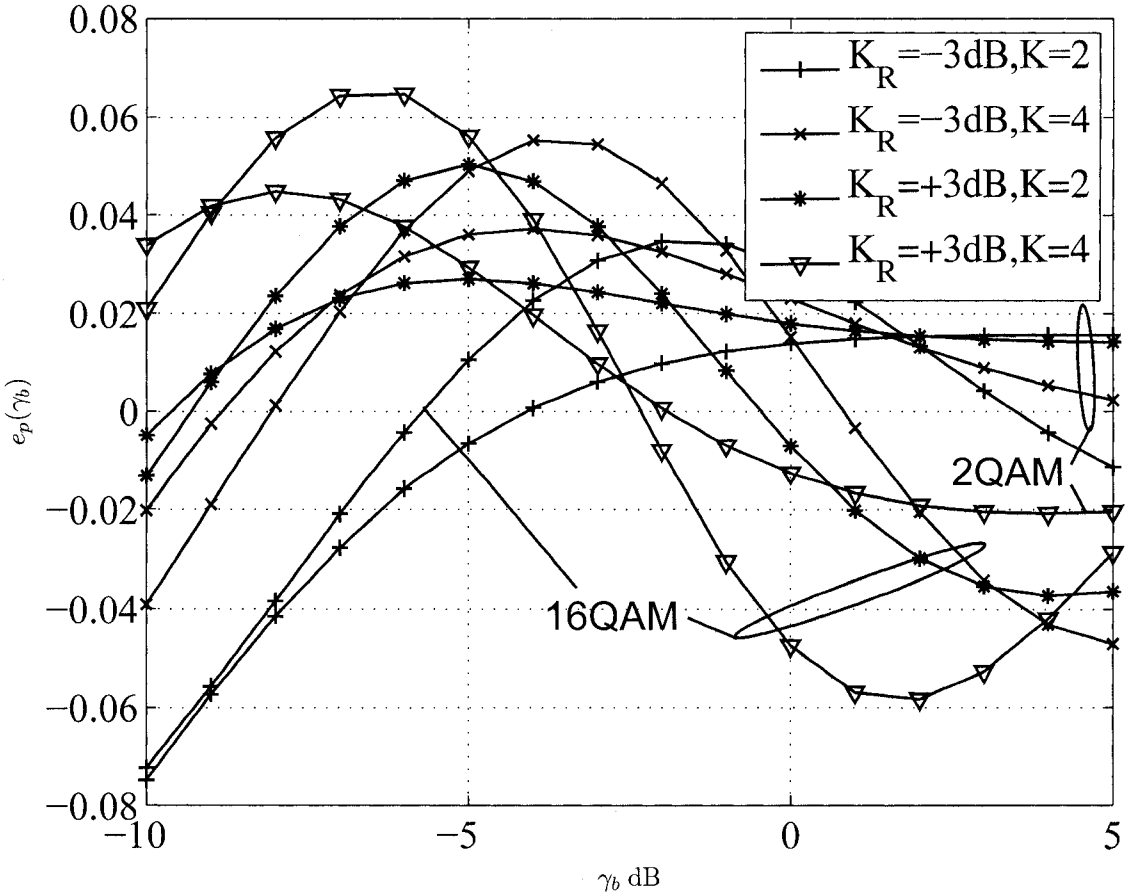

Figure 3.11: The relative approximation error of the Prony approximation for 2-QAM and 16-QAM modulations, and SC over $K = 2$ and $K = 4$ IID generalized Ricean fading channels.

Chapter 4

Efficient Channel Modeling

In this chapter, we simplify the performance analysis of one-stage and two-stage DCS's operating over correlated fading channels by considering two efficient channel models. We also consider decorrelation and orthogonalization of the branches prior to employing the diversity combining.

4.1 Background

Diversity reception is an important fading countermeasure. Realistic channel models having correlated branches are, in general, difficult to analyze [65], [66]. Hence, it is desirable to investigate channel models having the well-defined branch correlations, and importantly, that allow less complex performance analysis. In this chapter, we consider a linear correlations channel model where the branch channel coefficients are linear combinations of mutually independent input random processes. In this model, the channel coefficients are described using several parameters, and therefore, a good fit to realistic propagation conditions can be achieved. While we specify the distribution of the input independent processes, the distribution of the output processes corresponding to the correlated channel coefficients does not have to be specified. This model is useful for analyzing the performance of HS/MRC schemes. In particular, we investigate decorrelation [67] and orthogonalization [68] of the diversity branches prior to employing HS/MRC. For a linear correlations channel model, if the branches have equal variances, decorrelation transforms the problem of correlated order statistics into a much simpler problem of independent order statistics, [53], [69]. Also, we propose a fading amplitude channel model assuming vector norm superposition of the plane waves envelope amplitudes. This channel model is shown to be useful for analysis of MRC and EGC schemes over correlated fading channels. Furthermore, assuming knowledge of the MGF of the

HS/MRC diversity output SNR, the Prony approximation method [70] can be used to significantly simplify the analysis of HS/MRC diversity schemes, and importantly, to analyze the performance for cases that cannot be solved exactly.

Exact error rates for specific cases of MRC and EGC diversity were obtained in [71]. The SNR maximization for a general case of correlated branches is considered in [72, p. 33]. A general framework for analysis of SC diversity over correlated fading channels is established in [73]. Optimum decorrelation of Gaussian branches and MRC is investigated in [67]. A virtual branch technique for performance analysis of HS/MRC was proposed in [74]. The BER of HS/MRC for specific branch correlation structures were evaluated, for example, in [75] and [76]. Two-stage DCS's used to reduce the complexity of the combining are studied in [77] and [78]. The MGF of the HS/MRC diversity output SNR for independent branches was obtained, for example, in [79] and [80], using a method of recursive substitutions.

This chapter is organized as follows. The system and channel models for correlated branches are introduced in Section 4.2. Decorrelation and orthogonalization of the diversity branches prior to combining is investigated. Performance analysis of one-stage and two-stage DCS's is considered in Section 4.3. Numerical examples and verification of analytical results by computer simulation are presented in Section 4.4. The chapter is summarized in Section 4.5.

4.2 Diversity Combining In Correlated Fading

Consider transmission of uncoded modulation symbols over flat slowly fading correlated channels. The signals are represented using equivalent complex envelopes in the baseband and using one sample per symbol. Assuming multiple receiver antennas, the received signals are combined in one or two stages as shown in Fig. 4.1. Thus, the $\sum_{i=1}^{K} L_i$ received signals are combined in K groups of L_i antennas to obtain a decision variable at the detector input. In particular, employing EGC or SC at the first stage requires knowledge of the channel phases and amplitudes, respectively. At the second stage, either channel amplitudes or phases are estimated as required, so that MRC should be used to exploit the full channel knowledge. Note that channel estimation at the second stage can benefit from the increased SNR after the first combining stage. For one stage combining, we consider HS/MRC diversity where L out of K received signals having the largest SNR are selected and combined using MRC. If $L = K$, HS/MRC corresponds to MRC, and, if $L = 1$, HS/MRC corresponds to SC. We also consider one stage EGC diversity.

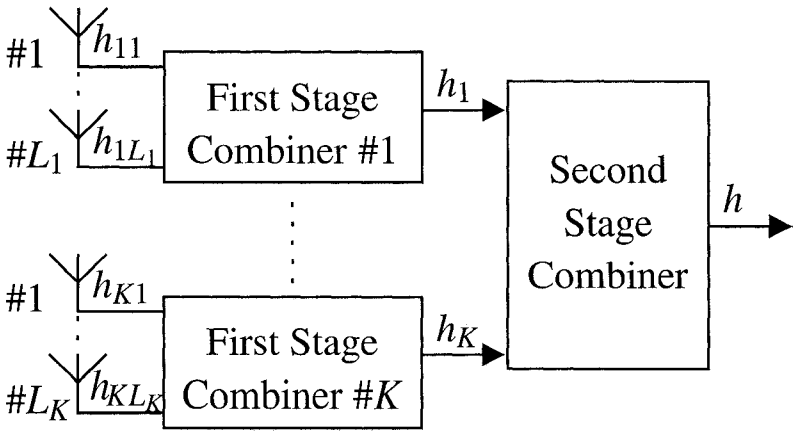

Figure 4.1: A generic two-stage diversity combining scheme.

The K baseband received signals, $\mathbf{y} \in \mathbb{C}^K$, are written as,

$$\mathbf{y} = \mathbf{h}\, x + \mathbf{w} \tag{4.1}$$

where $\mathbf{h} \in \mathbb{C}^K$ is a column vector of the channel coefficients, $x \in \mathbb{C}$ is a transmitted data symbol, and $\mathbf{w} \in \mathbb{C}^K$ is a column vector of zero-mean mutually uncorrelated additive noises. Let the i-th channel coefficient be, $h_i = g_i\, \mathrm{e}^{\mathrm{j}\theta_i}$, where g_i is the channel fading amplitude, θ_i is the channel fading phase, and $i = 1, 2, \cdots, K$. The additive noises, $\mathbf{w}$, have the covariance matrix, $\mathrm{E}\big[\mathbf{w}\mathbf{w}^H\big] = \sigma_w^2 \mathbf{I}_{(K)}$, where σ_w^2 is the variance, $(\cdot)^H$ is the vector transpose conjugate, and $\mathbf{I}_{(K)}$ is the $K \times K$ identity matrix. The channel coefficients and the additive noises are mutually uncorrelated, i.e., $\mathrm{E}\big[\mathbf{w}(\mathbf{h} - \mathrm{E}[\mathbf{h}])^H\big] = \mathrm{E}\big[\mathbf{w}\mathbf{h}^H\big] = \mathbf{0}_{(K)}$, where $\mathbf{0}_{(K)}$ is the $K \times K$ all-zero matrix. If the transmitted symbol, x, is complex-valued, then the variance, $\sigma_w^2 = N_0$, otherwise, if $x \in \mathbb{R}$, then $\sigma_w^2 = N_0/2$, where N_0 denotes the one-sided noise power spectral density. The transmitted symbols, x, are normalized, so that the average energy per symbol, $E_s = \mathrm{E}\big[|x|^2\big] = 1$. For the i-th received signal in (4.1), we define the (instantaneous) SNR as, $\gamma_i = g_i^2 \gamma_b$, where $\gamma_b = E_b/N_0$ is the SNR per transmitted bit, and $E_b = E_s/\log_2 M$, for M-ary modulation symbols, x. Assuming coherent combining, the received signals (4.1) can be equivalently written as,

$$\mathbf{y} = |\mathbf{h}|\, x + \mathbf{w} = \mathbf{g}\, x + \mathbf{w} \tag{4.2}$$

where $|\mathbf{h}| = (|h_1|, \cdots, |h_K|)^T$, and $\mathbf{g} = |\mathbf{h}| = (g_1, \cdots, g_K)^T$ are the column vectors of the channel fading amplitudes, $|\cdot|$ is the absolute value of a complex number, $(\cdot)^T$ is the vector transpose,

$x \in \mathbb{C}$, $\mathbf{w} \in \mathbb{C}^K$, $\mathrm{E}[\mathbf{w}\mathbf{w}^H] = \sigma_w^2 \mathbf{I}_{(K)}$, and $\mathrm{E}[\mathbf{w}(\mathbf{g} - \mathrm{E}[\mathbf{g}])^H] = \mathrm{E}[\mathbf{w}\mathbf{g}^H] = \mathbf{0}_{(K)}$. Furthermore, we assume perfect channel estimation at the receiver.

4.2.1 HS/MRC Diversity Combining

Consider the received signals (4.1). Note that for symbol-by-symbol detection at the receiver to be optimal requires that the additive noises are white (i.e., uncorrelated from symbol to symbol). The diversity branches are ordered according to their instantaneous SNR's, $\gamma_i = g_i^2 \gamma_b$, $i = 1, 2, \cdots, K$. The L branches, $1 \leq L \leq K$, having the largest instantaneous SNR's are combined using MRC. Note that knowledge of all K channel amplitudes, g_i, is required to select the L branches, and, for the selected branches, knowledge of the channel phases, θ_i, is required to perform coherent combining. Note also that, in fact, ordering of branches is sufficient knowledge for the branch selection. In the case of joint estimation of the channel amplitudes and phases, for example, using pilot symbol assisted modulation, MRC without any branch selection can be used. Hence, using (4.1), the decision variable at the combiner output is,

$$y = \mathbf{c}^H \mathbf{A}_\mathbf{g} \mathbf{y} = \mathbf{c}^H \mathbf{A}_\mathbf{g} \mathbf{h}\, x + \mathbf{c}^H \mathbf{A}_\mathbf{g} \mathbf{w}$$

where $\mathbf{c} = (c_1, c_2, \cdots, c_K)^T \in \mathbb{C}^K$ is a vector of linear combining weights. The elements of diagonal matrix, $\mathbf{A}_\mathbf{g} \in \{0, 1\}^{K \times K}$, are equal to 1 if the corresponding branch is selected, and 0, otherwise. The subscript, $\mathbf{g}$, indicates that $\mathbf{A}_\mathbf{g}$ is a function of the fading amplitudes, $\mathbf{g}$; thus, $\mathbf{A}_\mathbf{g}$ will be referred to as the selection matrix. Note that, $\mathbf{A}_\mathbf{g} = \mathbf{A}_\mathbf{g}^T$, and, $\mathbf{A}_\mathbf{g}\mathbf{A}_\mathbf{g} = \mathbf{A}_\mathbf{g}$. The combiner weights, $\mathbf{c}$, are computed in order to maximize the combiner output instantaneous SNR subject to (s.t.) combining exactly L branches, i.e.,

$$\begin{aligned} &\max_{(\mathbf{c}^H \mathbf{A}_\mathbf{g}) \in \mathbb{C}^L} \frac{\mathbf{c}^H \mathbf{A}_\mathbf{g} \mathbf{h}\, \mathbf{h}^H \mathbf{A}_\mathbf{g} \mathbf{c}}{\mathrm{E}[\mathbf{c}^H \mathbf{A}_\mathbf{g} \mathbf{w}\mathbf{w}^H \mathbf{A}_\mathbf{g} \mathbf{c}]} \\ &\text{s.t. } \operatorname{rank} \mathbf{A}_\mathbf{g} = L. \end{aligned} \tag{4.3}$$

Using the Schwartz inequality [40], one can show that (4.3) is maximized if $\mathbf{c} = \mathbf{g}$, for any value of L. Then, for $\mathbf{c} = \mathbf{g}$, the selection matrix, $\mathbf{A}_\mathbf{g}$, maximizing (4.3) corresponds to the L branches having the largest fading amplitudes, g_i. Correspondingly, the signal at the output of HS/MRC is,

$$y \overset{\text{(HS/MRC)}}{=} \mathbf{h}^H \mathbf{A}_\mathbf{g} \mathbf{h}\, x + \mathbf{h}^H \mathbf{A}_\mathbf{g} \mathbf{w}. \tag{4.4}$$

Assume that the channel coefficients, h_i, are correlated having the covariance matrix, $\mathbf{C_h} = \mathrm{E}\big[\mathbf{h}\mathbf{h}^H\big] - \mathrm{E}[\mathbf{h}]\,\mathrm{E}[\mathbf{h}]^H$. The selected channel coefficients, $\mathbf{A_g h}$, correspond to the order statistics of $\mathbf{h}$, and have the covariance matrix, $\mathbf{C_{A_g h}} = \mathrm{E}\big[\mathbf{A_g h h}^H\mathbf{A_g}\big] - \mathrm{E}[\mathbf{A_g h}]\,\mathrm{E}[\mathbf{A_g h}]^H$. Intuitively, the selected branches can be decorrelated before employing MRC [67]. Hence, denote the singular value decomposition (SVD) of the covariance matrix, $\mathbf{C_{A_g h}} = \mathrm{E}\big[\mathbf{A_g h h}^H\mathbf{A_g}\big] - \mathrm{E}[\mathbf{A_g h}]\,\mathrm{E}[\mathbf{A_g h}]^H$, as, $\mathbf{C_{A_g h}} = \mathbf{U}\boldsymbol{\Lambda}\mathbf{V}^H$, where $\mathbf{U}$ and $\mathbf{V}$ are unitary matrices and $\boldsymbol{\Lambda}$ is a diagonal matrix of eigenvalues. We can show that, for regular processes, $\mathbf{h}$, the matrix, $\mathbf{C_{A_g h}}$, is Hermitian and positive semi-definite, i.e., $\mathbf{U} = \mathbf{V}$, and the eigenvalues are real and non-negative [81]. Furthermore, assume that $\mathbf{w}$ are mutually uncorrelated zero-mean AWGN's of equal variances. We can use the matrix, $\mathbf{U}$, to decorrelate the selected branches as follows. Denote a complementary diagonal matrix, $\bar{\mathbf{A}}_\mathbf{g}$, such that, $\mathbf{A_g} + \bar{\mathbf{A}}_\mathbf{g} = \mathbf{I}_{(K)}$, i.e., the matrix, $\bar{\mathbf{A}}_\mathbf{g}$, corresponds to the $(K - L)$ branches having the smallest fading amplitudes, g_i. Let $\mathbf{w}'$ be a complex-valued random vector of mutually uncorrelated zero-mean AWGN's having the variances, σ_w^2. The AWGN's, $\mathbf{w}$, and, $\mathbf{w}'$, are uncorrelated, i.e., $\mathrm{E}\big[\mathbf{w}'\mathbf{w}^H\big] = \mathbf{0}_{(K)}$. Then, the auxiliary signals, $\mathbf{y}' = \mathbf{A_g y} + \bar{\mathbf{A}}_\mathbf{g}\mathbf{w}'$, are decorrelated using the matrix, $\mathbf{U}^H$, i.e., $\mathbf{U}^H\mathbf{y}' = \mathbf{U}^H\mathbf{A_g h}\,x + \hat{\mathbf{w}} = \hat{\mathbf{h}}\,x + \hat{\mathbf{w}}$, where the AWGN's, $\hat{\mathbf{w}} = \mathbf{U}^H(\mathbf{A_g w} + \bar{\mathbf{A}}_\mathbf{g}\mathbf{w}')$, have zero-mean, and the covariance matrix, $\mathrm{E}\big[\hat{\mathbf{w}}\hat{\mathbf{w}}^H\big] = \mathrm{E}\big[\mathbf{w}\mathbf{w}^H\big]$. Hence, the decorrelated channel coefficients, $\hat{\mathbf{h}} = \mathbf{U}^H\mathbf{A_g h}$, have the covariance matrix, $\mathbf{C}_{\hat{\mathbf{h}}} = \boldsymbol{\Lambda}$. It is straightforward to show that, after decorrelation, the HS/MRC output is, $\hat{y} = \hat{\mathbf{h}}^H\mathbf{U}^H\mathbf{y}' = \mathbf{h}^H\mathbf{A_g}\mathbf{y}' = \mathbf{h}^H\mathbf{A_g y}$, since $\mathbf{A_g}\bar{\mathbf{A}}_\mathbf{g} = \mathbf{0}$. Thus, decorrelating the selected branches does not change the HS/MRC output statistics, for any distribution of $\mathbf{h}$ that is uncorrelated with the AWGN's. Note that decorrelating the auxiliary signals, $\mathbf{y}'$, rather than the received signals, $\mathbf{y}$, is necessary, in order that, after decorrelation, the additive noises remain white.

In general, although the channel coefficients, $\mathbf{h}$, can be decorrelated, they will not become independent, and thus, their order statistics are difficult to obtain. In order to facilitate the performance analysis of the HS/MRC schemes, we have to transform the case of correlated order statistics into the case of independent order statistics. Hence, assume that the channel coefficients can be written as,

$$\mathbf{h} = \sqrt{\mathbf{P_h}}\mathbf{U_z}\mathbf{z} + \bar{\mathbf{h}} \tag{4.5}$$

where $\mathbf{z} \in \mathbb{C}^n$ is a column vector of mutually *independent* (i.e., uncorrelated) zero-mean RV's, z_j, $j = 1, \cdots, n$, and $\mathrm{E}\big[\mathbf{z}\mathbf{z}^H\big] = \boldsymbol{\Sigma}_\mathbf{z}$ is a diagonal matrix of the variances, $\sigma_{z_j}^2$. The matrix, $\mathbf{U_z} \in \mathbb{C}^{K\times n}$, is semi-unitary, i.e., $\mathbf{U}_\mathbf{z}^H\mathbf{U_z} = \mathbf{I}_{(n)}$, and $\sqrt{\mathbf{P_h}} = \mathrm{diag}\big(\sqrt{P_{h_1}}, \cdots, \sqrt{P_{h_K}}\big)$ is a

diagonal matrix of the branch powers, P_{h_i}, $i = 1, \cdots, K$, and $\bar{\mathbf{h}} = \mathrm{E}[\mathbf{h}]$. Then, the covariance matrix of $\mathbf{h}$ is, $\mathbf{C_h} = \sqrt{\mathbf{P_h}}\mathbf{C_z}\sqrt{\mathbf{P_h}}$, where $\mathbf{C_z} = \mathbf{U_z}\mathbf{\Sigma_z}\mathbf{U_z}^H$. Provided that the vector, $\mathbf{z}$, is jointly Gaussian, the channel coefficients, $\mathbf{h}$, are jointly Gaussian. Also, if $\mathbf{\Sigma_z} = \sigma_z^2\mathbf{I}_{(n)}$ and $\mathbf{U_z}$ is unitary, then $\mathbf{C_h} = \sigma_z^2\mathbf{P_h}$, i.e., the channel coefficients, $\mathbf{h}$, are uncorrelated, but not independent. Note that, for any row and column, $\mathbf{u}$, of the unitary matrix, $\mathbf{U} \in \mathbb{C}^{K\times K}$, the vector norm, $\|\mathbf{u}\|_2 = \sqrt{|u_1|^2 + \cdots + |u_K|^2} = 1$, and, $\|(1, \cdots, 1)\mathbf{U}\|_2 = \left\|(1, \cdots, 1)\mathbf{U}^H\right\|_2 = \sqrt{K}$. Correspondingly, provided that the branch powers are equal, i.e., $P_{h_i} = P_h \; \forall i = 1, \cdots, K$, we can decorrelate the channel coefficients (4.5) using the matrix, $\mathbf{U}^H$. Hence, the channel coefficients, $\hat{\mathbf{h}} = \mathbf{U}^H\mathbf{h} = \sqrt{P}\,\mathbf{z} + \mathbf{U}^H\bar{\mathbf{h}}$, are independent and have the covariance matrix, $\mathbf{C}_{\hat{\mathbf{h}}} = P\,\mathbf{\Sigma_z}$.

Furthermore, provided that the fading is fast and cannot be estimated at the receiver, and to avoid frequent antenna switching, it is useful to investigate a linear DCS having time-invariant (i.e., fixed) combining weights. Hence, using (4.1), the decision variable at the combiner output is, $y = \mathbf{c}^H\mathbf{h}\,x + \mathbf{c}^H\mathbf{w}$. The combining weights, $\mathbf{c}$, are computed in order to maximize the *average* SNR at the combiner output, i.e.,

$$\max_{\mathbf{c}\in\mathbb{C}^K} \frac{\mathrm{E}\left[\mathbf{c}^H\mathbf{h}\mathbf{h}^H\mathbf{c}\right]}{\mathrm{E}[\mathbf{c}^H\mathbf{w}\mathbf{w}^H\mathbf{c}]} = \max_{\mathbf{c}\in\mathbb{C}^K} \frac{1}{\sigma_w^2}\frac{\mathbf{c}^H}{\|\mathbf{c}\|_2}\mathbf{R_h}\frac{\mathbf{c}}{\|\mathbf{c}\|_2} \tag{4.6}$$

where the correlation matrix, $\mathbf{R_h} = \mathrm{E}\left[\mathbf{h}\mathbf{h}^H\right]$. We have the following lemma.

Lemma 4.1 *The time-invariant linear combining weights maximizing the output combiner average SNR are the components of the eigenvector corresponding to the largest eigenvalue of the channel amplitudes correlation matrix.*

Proof: Optimization of (4.6) is achieved using the SVD, $\mathbf{R_h} = \mathbf{U}\mathbf{\Lambda}\mathbf{U}^H$. Since $\mathbf{U}$ is unitary, the row vector, $\mathbf{c}' = \frac{\mathbf{c}^H}{\|\mathbf{c}\|_2}\mathbf{U}$, lies on the sphere of unit radius. Hence, maximization of (4.6) is equivalent to, $\max_{\mathbf{c}'\in\mathbb{C}^K:\|\mathbf{c}'\|_2=1} \mathbf{c}'\mathbf{\Lambda}\mathbf{c}'^H$. Using the method of Lagrange multipliers, we can show that the maximum occurs for the components, $|c'_{i^*}| = 1$, and, $|c'_i| = 0$, $i \neq i^*$, where i^* is the index of the largest eigenvalue of $\mathbf{R_h}$. Thus, $\frac{\mathbf{c}^H}{\|\mathbf{c}\|_2} = \mathbf{c}'\mathbf{U}^H$, and the optimum weights are a column vector of the matrix, $\mathbf{U}$, (i.e., the eigenvector) corresponding to the largest eigenvector. ■

Hence, the branches are orthogonalized (decorrelated, if the channel coefficients have zero mean), and the one having the largest average SNR is selected. Importantly, Lemma 4.1 can be extended to consider the L eigenvectors corresponding to the L largest eigenvalues. The L orthogonalized branches are then combined using MRC. Such a DCS has been proposed in [68, Lemma 1] and is referred to as principal components combining (PCC). However, note that, while the derivation

in [68] assumes a semi-unitary preprocessing matrix, the proof of Lemma 4.1 in this chapter does not require any such assumption.

In general, let $\mathbf{Z}$ be a unitary matrix, and $\mathbf{w}$ be a vector of mutually uncorrelated zero-mean AWGN's having equal variances. Then, for any vector, $\mathbf{h}$, we have that, $\|\mathbf{Zh}\|_2^2 = (\mathbf{Zh})^H(\mathbf{Zh}) = \mathbf{h}^H\mathbf{h} = \|\mathbf{h}\|_2^2$, and $\mathbf{Zw}$ is a vector of mutually uncorrelated zero-mean AWGN's having the covariance matrix, $\mathrm{E}\big[(\mathbf{Zw})(\mathbf{Zw})^H\big] = \mathrm{E}\big[\mathbf{w}\mathbf{w}^H\big]$. Hence, for $L = K$, the MRC outputs for the received signals, $\mathbf{y} = \mathbf{h}\,x + \mathbf{w}$, and, $\hat{\mathbf{y}} = \mathbf{Z}^H\mathbf{y}$, are identical. Provided that $\mathbf{Z} = \mathbf{U}^H$, where the SVD, $\mathbf{C_h} = \mathbf{U}\mathbf{\Lambda}\mathbf{U}^H$, the signals, $\hat{\mathbf{y}}$, are uncorrelated. Furthermore, if the signals, $\mathbf{y}$, are jointly Gaussian, i.e., the vectors, $\mathbf{h}$, and, $\mathbf{w}$, are jointly Gaussian and mutually uncorrelated (thus, independent), the signals, $\hat{\mathbf{y}}$, are independent [67]. However, in general, if $L < K$, the selected branches are not Gaussian. On the other hand, it is well-known that the branch correlations decrease the available diversity order [66]. Hence, one can expect that decorrelation and orthogonalization of the diversity branches prior to branch selection and combining (i.e., prior to HS/MRC) can be used to restore some of the diversity lost due to the correlations between branches. Hence, we have the following four HS/MRC DCS's for correlated diversity branches. In traditional HS/MRC, the L branches having the largest SNR are selected and combined using MRC, i.e., the combiner output signal is,

$$\begin{aligned} y_1^{(\mathrm{HS/MRC})} &= (\mathbf{h}^H\mathbf{A_g})\mathbf{A_g}\mathbf{y} \\ &= \mathbf{h}^H\mathbf{A_g}\mathbf{h}\,x + \mathbf{h}^H\mathbf{A_g}\mathbf{w}. \end{aligned} \tag{4.7}$$

Using the SVD, $\mathbf{C_h} = \mathbf{U}\mathbf{\Lambda}\mathbf{U}^H$, the received signals can be decorrelated, and then combined using HS/MRC. In this case, the combiner output signal is,

$$\begin{aligned} y_2^{(\mathrm{HS/MRC})} &= (\mathbf{h}^H\mathbf{U}\mathbf{A_g})\mathbf{A_g}\mathbf{U}^H\mathbf{y} \\ &= \mathbf{h}^H\mathbf{U}\mathbf{A_g}\mathbf{U}^H\mathbf{h}\,x + \mathbf{h}^H\mathbf{U}\mathbf{A_g}\mathbf{U}^H\mathbf{w}. \end{aligned} \tag{4.8}$$

Motivated by Lemma 4.1, the received signals can also be orthogonalized, and then combined using HS/MRC. Thus, the combiner output signal is,

$$\begin{aligned} y_3^{(\mathrm{HS/MRC})} &= (\mathbf{h}^H\mathbf{U}\mathbf{A_g})\mathbf{A_g}\mathbf{U}^H\mathbf{y} \\ &= \mathbf{h}^H\mathbf{U}\mathbf{A_g}\mathbf{U}^H\mathbf{h}\,x + \mathbf{h}^H\mathbf{U}\mathbf{A_g}\mathbf{U}^H\mathbf{w} \end{aligned} \tag{4.9}$$

where the orthogonalization matrix, $\mathbf{U}^H$, corresponds to the SVD, $\mathbf{R_h} = \mathbf{U}\mathbf{\Lambda}\mathbf{U}^H = \mathbf{C_h} + \mathrm{E}[\mathbf{h}]\,\mathrm{E}\big[\mathbf{h}^H\big]$. Finally, the received signals can be combined using PCC. Thus, the received sig-

nals are orthogonalized and combined using HS/MRC having the time-invariant selection matrix, $\mathbf{A_g} = \mathbf{A}$, of L non-zero diagonal elements. The corresponding combiner output signal is,

$$\begin{aligned} y_4^{(\mathrm{HS/MRC})} &= (\mathbf{h}^H\mathbf{V})\mathbf{y} \\ &= \mathbf{h}^H\mathbf{V}\mathbf{h}\,x + \mathbf{h}^H\mathbf{V}\mathbf{w} \end{aligned} \tag{4.10}$$

where the time-invariant matrix, $\mathbf{V} = \mathbf{U}\mathbf{A}\mathbf{U}^H$. We can show that the matrix, $\mathbf{V}$, is Hermitian and positive semi-definite, and $\mathbf{V}\mathbf{V} = \mathbf{V}$. Finally, note that, if $L = K$ (i.e., no branch selection is employed), then, for any realization of the vectors, $\mathbf{h}$, and, $\mathbf{w}$, the combiner output signals (4.7)–(4.10) are identical.

4.2.2 MRC and EGC Diversity Combining

In order to facilitate the performance analysis of MRC and EGC DCS's over correlated fading channels, we adopt a fading amplitude model based on the plane waves vector norm superposition. We assume that there are n plane waves arriving at the receiver antennas; see Fig. 4.2. Denote by G_j the instantaneous envelope amplitude of the j-th plane wave, $G_j \geq 0$, and $j = 1, 2, \cdots, n$. Recall the vector norm (A-10), and let the channel fading coefficient corresponding to the i-th receiver antenna be,

$$h_i = \|\mathbf{g}_i\|_\alpha \, \mathrm{e}^{\mathrm{j}\theta_i} = g_i \, \mathrm{e}^{\mathrm{j}\theta_i} \tag{4.11}$$

where g_i is the channel fading amplitude, and θ_i is the channel fading phase. For example, provided that the envelope amplitudes, G_j, are independent and one-sided Gaussian distributed, i.e., having the PDF, $f_{G_j}(G_j) = \frac{\mathrm{e}^{-(G_j - m_j)^2/2\sigma^2}}{Q(m_j/\sigma)\sqrt{2\pi\sigma^2}}$, where σ^2 is the variance and m_j is the mean value of the underlying Gaussian distribution, then the channel fading amplitudes, g_i, are generalized Ricean distributed.

Similarly to (4.5), in eq. (4.11), we assume that the vector, $\mathbf{g}_i = (d_{i1}G_1, d_{i2}G_2, \cdots, d_{in}G_n)$, where the coefficients, $d_{ij} \geq 0$, are related to the angles-of-arrival of impinging plane waves, and thus, they influence correlations between the branch fading amplitudes, g_i. In this chapter, we consider the plane waves vector norm amplitude and squared-amplitude (i.e., power) superpositions corresponding to $\alpha = 1$ and $\alpha = 2$, respectively. Thus, for $i = 1, 2, \cdots, K$, we have that,

$$g_i \overset{(\alpha=1)}{=} d_{i1}G_1 + d_{i2}G_2 + \cdots + d_{in}G_n \tag{4.12a}$$

$$g_i^2 \overset{(\alpha=2)}{=} d_{i1}^2G_1^2 + d_{i2}^2G_2^2 + \cdots + d_{in}^2G_n^2 \tag{4.12b}$$

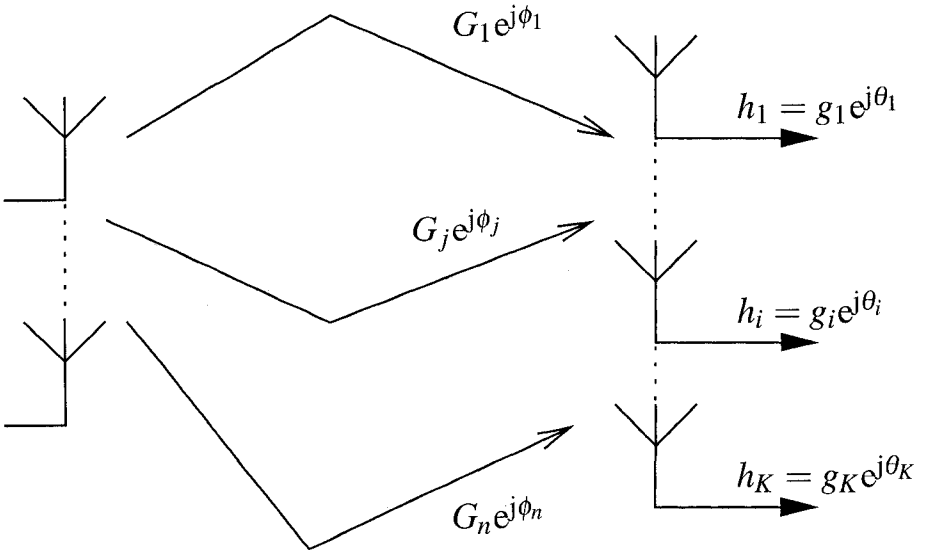

Figure 4.2: Amplitudes, G_i, and phases, ϕ_i, of n plane waves arriving at the K receiver antennas.

where we assume that the plane waves envelope amplitudes, G_j, are mutually independent. Denote the matrix, $\mathbf{D}$, having the rows, $\mathbf{d}_i = (d_{i1}, \cdots, d_{in})$, the matrix, $\mathbf{D}^2$, having the rows, $\mathbf{d}_i^2 = (d_{i1}^2, \cdots, d_{in}^2)$, and the column vectors, $\mathbf{G} = (G_1, \cdots, G_n)^T$, and, $\mathbf{G}^2 = (G_1^2, \cdots, G_n^2)^T$. Then, $\mathbf{g} = \mathbf{DG}$, and, $\mathbf{g}^2 = \mathbf{D}^2\mathbf{G}^2$, and the correlation coefficients of the fading amplitudes and squared amplitudes, respectively, are, $\rho_g(i,i') = \mathrm{E}[g_i g_{i'}] - \mathrm{E}[g_i]\,\mathrm{E}[g_{i'}] = \mathbf{d}_i\,\mathbf{C}_G\,\mathbf{d}_{i'}^T$, and, $\rho_{g^2}(i,i') = \mathrm{E}\big[g_i^2 g_{i'}^2\big] - \mathrm{E}\big[g_i^2\big]\,\mathrm{E}\big[g_{i'}^2\big] = \mathbf{d}_i^{2^T}\,\mathbf{C}_{G^2}\,\mathbf{d}_{i'}^{2^T}$. Since the envelope amplitudes, G_j, are assumed to be independent (thus, uncorrelated), the covariance matrices, $\mathbf{C}_G$ of $\mathbf{G}$, and, $\mathbf{C}_{G^2}$ of $\mathbf{G}^2$, are diagonal. Hence, the covariance matrices of the channel amplitudes and squared amplitudes, respectively, are,

$$\begin{aligned}
\mathbf{C}_{\mathbf{g}} &\overset{(4.12a)}{=} \mathrm{E}\big[\mathbf{g}\mathbf{g}^T\big] - \mathrm{E}[\mathbf{g}]\,\mathrm{E}[\mathbf{g}]^T = \mathbf{D}\mathbf{C}_G\mathbf{D}^T \\
\mathbf{C}_{\mathbf{g}^2} &\overset{(4.12b)}{=} \mathrm{E}\Big[\mathbf{g}^2\mathbf{g}^{2T}\Big] - \mathrm{E}\big[\mathbf{g}^2\big]\,\mathrm{E}\big[\mathbf{g}^2\big]^T = \mathbf{D}\mathbf{C}_{G^2}\mathbf{D}^T.
\end{aligned}$$

If the envelope amplitudes, G_j, are generalized Ricean distributed [21] having uncorrelated underlying Gaussian distributed components, then, the envelope amplitudes, G_j, are independent. Then, for $d_{ij}^2 = d_i^2$, $i = 1, \cdots, K$, and $j = 1, \cdots, n$, the squared fading amplitudes, g_i^2, are non-central chi-square distributed having the Rice factor, $K_{\mathrm{R}} = s^2/(n\sigma^2)$, where the non-centrality parameter, $s^2 = \sum_{j=1}^{n} m_j^2$. The correlation coefficient, $\rho_{g^2}(i,i') = \mu\, d_i^2 d_{i'}^2$ where $\mu = 2n\sigma^4 + 4\sigma^2 s^2$ [21, (2-1-125)], and the covariance matrix, $\mathbf{C}_{\mathbf{g}^2} = \mathrm{E}\Big[\mathbf{g}^2\mathbf{g}^{2T}\Big] - \mathrm{E}\big[\mathbf{g}^2\big]\,\mathrm{E}\Big[\mathbf{g}^{2T}\Big] = \mu\,\mathbf{d}^2\mathbf{d}^{2T}$, where the column vector, $\mathbf{d}^2 = (d_1^2, \cdots, d_K^2)^T$. In general, assuming that g is generalized Ricean

distributed, and thus, g^2 is non-central chi-square distributed, the expressions for the PDF, $f_g(g)$, and, $f_{g^2}(g^2)$, the CDF, $F_g(g)$, and, $F_{g^2}(g^2)$, the MGF, $\Phi_g(t) = \mathrm{E}\left[\mathrm{e}^{gt}\right]$, and, $\Phi_{g^2}(t) = \mathrm{E}\left[\mathrm{e}^{g^2 t}\right]$, where a dummy variable, $t = c + \mathrm{j}\omega$, and $c, \omega \in \mathbb{R}$, and the upper incomplete MGF, $\phi_g(t,u) = \int_u^\infty \mathrm{e}^{gt} f_g(g)\mathrm{d}g$, and, $\phi_{g^2}(t,u) = \int_u^\infty \mathrm{e}^{g^2 t} f_{g^2}(g^2)\mathrm{d}g^2$, are summarized in Appendix C.

To illustrate further, consider the fading model (4.12a), and assume that the number of impinging plane waves, n, is equal to the number of receiver antennas, K, and that the matrix, $\mathbf{D}$, is invertible. Then, the joint PDF of the channel amplitudes, $\mathbf{g}$, is, [53]

$$f_{\mathbf{g}}(\mathbf{g}) = \left|\det(\mathbf{D}^{-1})\right| f_{\mathbf{G}}(\mathbf{D}^{-1}\mathbf{g}) \tag{4.13}$$

where $f_{\mathbf{G}}(\mathbf{G})$ is the joint PDF of the envelope amplitudes, $\mathbf{G}$, the operator, $\det(\cdot)$, denotes the matrix determinant, and $(\cdot)^{-1}$ is the matrix inverse.

Finally, recall that the EGC output fading amplitude, $g = \frac{1}{\sqrt{K}} \sum_{i=1}^{K} g_i$, [16]. Assuming the fading model (4.12a), we have that, $g = \tilde{\mathbf{d}}\mathbf{G} = \sum_{j=1}^{n} \tilde{d}_j G_j$, where $\tilde{\mathbf{d}} = (\tilde{d}_1, \cdots, \tilde{d}_n)$, and the components, $\tilde{d}_j = \frac{1}{\sqrt{K}} \sum_{i=1}^{K} d_{ij}$. Similarly, the MRC squared output fading amplitude is, $g^2 = \sum_{i=1}^{K} g_i^2$. Assuming the fading model (4.12b), we have that, $g^2 = \tilde{\mathbf{d}}^2\mathbf{G}^2 = \sum_{j=1}^{n} \tilde{d}_j^2 G_j^2$, where $\tilde{\mathbf{d}}^2 = (\tilde{d}_1^2, \cdots, \tilde{d}_n^2)$, and the components, $\tilde{d}_j^2 = \sum_{i=1}^{K} d_{ij}^2$. Correspondingly, the combiners output signals are written as,

$$y^{(\mathrm{EGC})} = \left(\sum_{j=1}^{n} \tilde{d}_j G_j\right) x + w \tag{4.14}$$

$$y^{(\mathrm{MRC})} = \left(\sqrt{\sum_{j=1}^{n} \tilde{d}_j^2 G_j^2}\right) x + w \tag{4.15}$$

where $\tilde{d}_j > 0$, and the envelope amplitudes, G_j, are mutually independent. Hence, using channel models (4.12a) and (4.12b) for MRC and EGC schemes, we convert the branch correlations into a sum of unbalanced and independent RV's. This, in turn, greatly simplifies the performance analysis of MRC and EGC schemes over correlated fading branches.

4.2.3 MGF of Sum of Order Statistics

The analysis in the sequel requires the MGF of a sum of the L largest out of K RV's. In general, denote the ordered RV's, x_i, as, $x_{(1)} \geq x_{(2)} \geq \cdots \geq x_{(K)}$. Define the vector of the RV's, $\mathbf{x} = (x_1, x_2, \cdots, x_K)$, and denote by $\mathbf{x}_i$ the i-th component of the vector, $\mathbf{x}$. Let $\mathbf{\Pi}_{K,L}(\mathbf{x})$ denote all

possible permutations of the RV's, x_i, divided into three subsets of $(L-1)$, 1, and $(K-L)$ unordered RV's. Thus, the cardinality, $|\mathbf{\Pi}_{K,L}(\mathbf{x})| = \frac{K!}{(L-1)!1!(K-L)!}$. In order to simplify the indices, we assume that, for $\forall \mathbf{x} \in \mathbf{\Pi}_{K,L}(\mathbf{x})$, the RV's, $\mathbf{x}_i \geq \mathbf{x}_L$, $i = 1, \cdots, L-1$, are unordered, and the RV's, $\mathbf{x}_i \leq \mathbf{x}_L$, $i = L+1, \cdots, K$, are also unordered. Then, the PDF of the (L)-th order statistic, $x_{(L)}$, can be written as [53],

$$f_{x_{(L)}}(u) = \sum_{\mathbf{\Pi}_{K,L}(\mathbf{x})} f_{\mathbf{x}_L}(u) \left(\prod_{i=1}^{L-1} (1 - F_{\mathbf{x}_i}(u)) \right) \left(\prod_{i=L+1}^{K} F_{\mathbf{x}_i}(u) \right). \tag{4.16}$$

Correspondingly, using the result in [79] and [80], we have that the MGF of an auxiliary RV, $z = \sum_{i=i_0}^{i_0+L-1} x_{(i)}$, can be computed as,

$$\Phi_z(t) = \begin{cases} \sum_{\mathbf{\Pi}_{K,L}(\mathbf{x})} \int_{-\infty}^{\infty} f_{\mathbf{x}_{1+L}}(u) \times \\ \times \left(\prod_{i=1}^{L} \phi_{\mathbf{x}_i}(t,u) \right) \left(\prod_{i=L+2}^{K} F_{\mathbf{x}_i}(u) \right) \mathrm{d}u \\ \qquad \text{for } i_0 = 1, \text{ and, } 1 \leq L < K \\ \int_{-\infty}^{\infty} \mathrm{e}^{ut} f_{x_{(i_0)}}(u) \mathrm{d}u \\ \qquad \text{for } 1 \leq i_0 \leq K, \text{ and, } L = 1 \\ \prod_{i=1}^{K} \Phi_{x_i}(t) \\ \qquad \text{for } i_0 = 1, \text{ and, } L = K. \end{cases} \tag{4.17}$$

Furthermore, if the branches are IID, then the MGF expression (4.17) can be simplified giving [79], [80],

$$\Phi_z(t) = \frac{K!}{L!(K-L-1)!} \int_{-\infty}^{\infty} f_{x_{1+L}}(u) \phi_{x_i}(t,u)^L F_{x_i}(u)^{K-L-1} \mathrm{d}u$$

for $i_0 = 1$, and, $1 \leq L < K$.

4.3 Performance Analysis

We evaluate the average BER for one-stage and two-stage DCS's operating over correlated fading branches. We assume that the additive noises are zero-mean, white and Gaussian and have equal variances. Thus, denote the decision variable as, $y = g\,x + w$, where g is the channel fading amplitude at the combiner output, w is a zero-mean additive noise, and the SNR, $\gamma = g^2\gamma_b$. Assuming knowledge of the MGF of the squared fading amplitude, g^2, the average BER is efficiently evaluated using the Prony approximation method [70]. Let $\mathrm{P}_\epsilon(\gamma)$ be the conditional BER corresponding to

the uncoded transmission over an AWGN channel (i.e., for $g = 1$). Denote the Prony approximation of $\mathrm{P}_\epsilon(\gamma)$ as, $\mathrm{P}_\epsilon(\gamma) \approx \sum_{i=1}^{q} \tilde{A}_i \, \mathrm{e}^{-\tilde{a}_i \gamma}$, where the coefficients, $\tilde{A}_i, \tilde{a}_i > 0 \; \forall i$, are modulation and bits-to-symbol mapping dependent. If the MGF, $\Phi_{g^2}(t)$, of g^2 is known, the average BER is evaluated as [70],

$$\begin{aligned} \bar{\mathrm{P}}_\epsilon(\gamma_b) &= \int_0^\infty \mathrm{P}_\epsilon(g^2\gamma_b) \, f_{g^2}(g^2) \mathrm{d}g^2 \\ &\approx \int_0^\infty \sum_{i=1}^{q} \tilde{A}_i \, \mathrm{e}^{-\tilde{a}_i g^2 \gamma_b} f_{g^2}(g^2) \mathrm{d}g^2 \\ &= \sum_{i=1}^{q} \tilde{A}_i \Phi_{g^2}(-\tilde{a}_i \gamma_b). \end{aligned} \tag{4.18a}$$

On the other hand, if the MGF, $\Phi_g(t)$, of g is known, then the MGF, $\Phi_{g^2}(t)$, of g^2 can be obtained using a single integration as shown in Appendix D. In this case, the average BER is evaluated as,

$$\begin{aligned} \bar{\mathrm{P}}_\epsilon(\gamma_b) &= \int_0^\infty \mathrm{P}_\epsilon(g^2\gamma_b) \, f_g(g) \mathrm{d}g \\ &\approx \int_0^\infty \sum_{i=1}^{q} \tilde{A}_i \, \mathrm{e}^{-\tilde{a}_i g^2 \gamma_b} f_g(g) \mathrm{d}g \\ &= \sum_{i=1}^{q} \frac{\tilde{A}_i}{\sqrt{\pi}\,\mathrm{j}} \int_{c-\mathrm{j}\infty}^{c+\mathrm{j}\infty} \Phi_g(2\sqrt{\tilde{a}_i \gamma_b} t) \, \mathrm{e}^{t^2} Q\Big(\sqrt{2t}\Big) \mathrm{d}t. \end{aligned} \tag{4.18b}$$

The integral in (4.18b) can be evaluated using, for example, the GCQ rule as detailed in Appendix B. We assume the following branch correlation models, i.e.,

$$\rho(i, i') = r_0^{1-\delta_{ij}} \tag{4.19a}$$

$$\rho(i, i') = r_0^{|i-j|} \tag{4.19b}$$

where the Kronecker delta, $\delta_{ij} = 1$, if $i = j$, and 0, otherwise, and $0 \leq r_0 \leq 1$. The model (4.19a) corresponds to equi-correlated branches. For $r_0 = \mathrm{e}^{-r_1}$, where $r_1 > 0$ is the normalized antenna separation, the model (4.19b) corresponds to exponentially correlated branches.

In general, using the law of total probability and the method of Lagrange multipliers, we can show that the average BER can be upper bounded as,

$$\bar{\mathrm{P}}_\epsilon(\gamma_b) = \sum_{\mathbf{A}} \Pr(\mathbf{A}) \, \bar{\mathrm{P}}_\epsilon(\gamma_b | \mathbf{A}) \leq \max_{\mathbf{A}} \bar{\mathrm{P}}_\epsilon(\gamma_b | \mathbf{A})$$

where the probability of selecting the branches, $\mathbf{A}$, can be computed as, $\Pr(\mathbf{A}) = \Pr(a_1, \cdots, a_L) = \sum_{i=1}^{L} \Pr(a_i | a_{i-1}, \cdots, a_1)$, and a_i, $i = 1, \cdots, L$, are the indices of the selected branches. Hence, the average BER is dominated by selection of the worst L branch channels combination. Note that, if the branches are identically distributed and equi-correlated, i.e., the normalized covariance matrix, $\mathbf{C_h}$, has the elements given by eq. (4.19a), then, the probability, $\Pr(\mathbf{A}) = \frac{L!(K-L)!}{K!}$. Such a case is referred to as exchangeable branches in [75], and the average BER is then independent of the particular branch selection, $\mathbf{A}$, i.e., $\bar{\mathrm{P}}_\epsilon(\gamma_b) = \bar{\mathrm{P}}_\epsilon(\gamma_b | \mathbf{A})$. Furthermore, if the branches are exchangeable, then the sum over all combinations, $\mathbf{\Pi}_{K,L}(\mathbf{x})$, in (4.17) is eliminated.

4.3.1 HS/MRC Diversity Combining

Recall that we have four HS/MRC output signals (4.7)–(4.10). Although, in some cases, the average BER of HS/MRC can be evaluated exactly (see, e.g., [75]), the Prony approximation method [70] can be used to significantly simplify the analysis in these cases, as well as to treat cases that cannot be solved exactly. In particular, for the case of independent branches, the HS/MRC output signal is given by eq. (4.7), and we can use the MGF (4.17) and the Prony approximation method (4.18a). If the channel coefficients, $\mathbf{h}$, are Gaussian, or, if the channel coefficients (4.5) have equal variances, then, for an arbitrary covariance matrix, $\mathbf{C_h}$, the decorrelated branches become independent. In this case, the average BER can be evaluated using the MGF (4.17) and the Prony approximation method (4.18a). Hence, consider the HS/MRC output signal (4.8), and let the decorrelated received signals be written as, $\hat{\mathbf{y}} = \mathbf{U}^H \mathbf{y} = \hat{\mathbf{h}}\, x + \hat{\mathbf{w}}$, where the SVD, $\mathbf{C_h} = \mathbf{U} \mathbf{\Lambda} \mathbf{U}^H$. The decorrelated channel coefficients, $\hat{\mathbf{h}} = \mathbf{U}^H \mathbf{h}$, where $\mathrm{E}\left[\hat{\mathbf{h}}\right] = \mathbf{U}^H \mathrm{E}[\mathbf{h}]$, have a diagonal covariance matrix, i.e., $\mathbf{C}_{\hat{\mathbf{h}}} = \mathrm{E}\left[\hat{\mathbf{h}} \hat{\mathbf{h}}^H\right] - \mathrm{E}\left[\hat{\mathbf{h}}\right] \mathrm{E}\left[\hat{\mathbf{h}}^H\right] = \mathbf{\Lambda}$, and the additive noises, $\hat{\mathbf{w}} = \mathbf{U}^H \mathbf{w}$. Thus, decorrelation translates the branch correlations into unbalanced branch powers [67]. For example, assume that the normalized covariance matrix, $\mathbf{C_h}$, is equi-correlated, i.e., its elements are given by eq. (4.19a). The eigenvalues of an equi-correlated matrix can be obtained by solving the matrix characteristic function [81]; then, the eigenvalues, $\lambda_1 = 1 + r_0(K-1)$, and $\lambda_i = 1 - r_0$, for $i = 2, \cdots, K$, are equal if and only if the branches are uncorrelated, i.e., $r_0 = 0$. For PCC and the HS/MRC output signal (4.10), it is straightforward to show that the SNR at the combiner output is, $\gamma = \mathbf{h}^H \mathbf{V} \mathbf{h}\, \gamma_b$. If the channel coefficients, $\mathbf{h}$, are Gaussian and have an arbitrary covariance matrix, $\mathbf{C_h}$, then the MGF of $g^2 = \mathbf{h}^H \mathbf{V} \mathbf{h}$ is [82, eq. (15)],

$$\Phi_{g^2}(t) = \mathrm{E}\left[\exp\left(\mathbf{h}^H \mathbf{V} \mathbf{h}\, t\right)\right] = \frac{\mathrm{e}^{\mathrm{E}[\mathbf{h}^H] \mathbf{V} (\mathbf{I} - t\, \mathbf{C_h} \mathbf{V})^{-1} \mathrm{E}[\mathbf{h}]}}{\det(\mathbf{I} - t\, \mathbf{C_h} \mathbf{V})}$$

and the average BER can be evaluated using the Prony approximation method (4.18a).

Finally, consider the fading model (4.5) for $\mathbf{P_h} = \mathbf{I}$, i.e., the channel coefficients, $\mathbf{h} = \mathbf{U_z z} + \bar{\mathbf{h}}$, and the components of $\mathbf{z}$ are assumed to be independent. Then, the decorrelated received signals, $\hat{\mathbf{y}} = \mathbf{U}^H\mathbf{y} = (\mathbf{z} + \mathbf{U}^H\bar{\mathbf{h}})\,x + \mathbf{U}^H\mathbf{w} = \hat{\mathbf{h}}\,x + \hat{\mathbf{w}}$, are independent provided that $\mathbf{w}$ are AWGN's. Hence, for the fading model (4.5) and any PDF, $f_{\mathbf{z}}(\mathbf{z}) = \prod_{i=1}^{n} f_{z_i}(z_i)$, of the vector, $\mathbf{z} = (z_1, \cdots, z_n)^T$, the average BER of HS/MRC that decorrelates the branches prior to selection and MRC can be evaluated using the MGF (4.17) and the Prony approximation method (4.18a).

4.3.2 MRC, EGC and SC Diversity Combining

We evaluate the average BER of MRC, EGC and SC diversity schemes assuming the fading amplitude channel models (4.12a) and (4.12b). In particular, for MRC, the decision variable is given by eq. (4.15), i.e., $g^2 = \sum_{j=1}^{n} \tilde{d}_j^2 G_j^2$, and the MGF of g^2 is, $\Phi_{g^2}(t) = \prod_{j=1}^{n} \Phi_{G_j^2}(\tilde{d}_j^2\, t)$. The average BER of MRC is then computed using the Prony approximation (4.18a).

For EGC, the decision variable is given by eq. (4.14), i.e., $g = \sum_{j=1}^{n} \tilde{d}_j G_j$. Thus, the MGF of g is, $\Phi_g(t) = \prod_{j=1}^{n} \Phi_{G_j}(\tilde{d}_j\, t)$, where $\Phi_{G_j}(t)$ is the MGF of G_j, and $\tilde{d}_j > 0$. The average BER of EGC is then computed using the Prony approximation method (4.18b).

For SC, the decision variable, $y = (\max_{i=1,\cdots,K} g_i)\,x + w$. Assume that $K = n$, $\mathbf{D}^2$ is invertible, and denote $z = \max_{i=1,\cdots,K} g_i^2$. The MGF of z can be obtained for the case of exponentially distributed squared envelope amplitudes, G_j^2, i.e., the envelope amplitudes, G_j, are Rayleigh distributed [69]. Hence, the PDF of G_j^2 is, $f_{G_j^2}(G_j^2) = \frac{1}{2\sigma_j^2}\,\mathrm{e}^{-G_j^2/2\sigma_j^2}$, where $\mathrm{E}\left[G_j^2\right] = 2\sigma_j^2$. Using (4.13), one has that, $f_{\mathbf{g}^2}(\mathbf{g}^2) = \frac{1}{|\det \mathbf{D}^2|} \prod_{j=1}^{K} \frac{1}{2\sigma_j^2}\,\mathrm{e}^{-g_j^2 d'_j/2\sigma_j^2}$, where $d'_j = \sum_{i=1}^{K} d_{[-1]ij}^2$, and $d_{[-1]ij}^2$ are the elements of the inverse matrix, $(\mathbf{D}^2)^{-1}$. The CDF of z is, $F_z(z) = F_{g^2}(z, \cdots, z)$, and taking the derivative, the PDF of z becomes, [53]

$$f_z(z) = \frac{\mathrm{d}}{\mathrm{d}z} F_z(z) = \frac{1}{|\det \mathbf{D}^2|} \sum_{j=1}^{K} \frac{\mathrm{e}^{-\frac{d'_j z}{2\sigma_j^2}}}{2\sigma_j^2} \prod_{\substack{i=1 \\ i\neq j}}^{K} \frac{1 - \mathrm{e}^{-\frac{d'_i z}{2\sigma_i^2}}}{d'_i}.$$

For a specific value of K, we can obtain a closed-form expression for the MGF, $\Phi_z(t) = \mathrm{E}\left[\mathrm{e}^{z\,t}\right]$. For example, let $K = n = 2$. Then, the MGF of $z = \max(g_1^2, g_2^2)$ is,

$$\Phi_z(t) = \frac{1}{|d_{11}^2 d_{22}^2 - d_{12}^2 d_{21}^2|} \frac{1}{(-2t\sigma_1^2\sigma_2^2 + d'_1\sigma_2^2 + d'_2\sigma_1^2)} \left(\frac{\sigma_1^2}{-2t\sigma_1^2 + d'_1} + \frac{\sigma_2^2}{-2t\sigma_2^2 + d'_2} \right)$$

where $d'_j = d^2_{[-1]1j} + d^2_{[-1]2j}$, d^2_{ij} are the elements of the matrix, $\mathbf{D}^2$, and $j = 1, 2$. Realizing that $g^2 = z$, the average BER of SC is computed using the Prony approximation method (4.18a).

4.3.3 Two-Stage EGC-MRC and SC-MRC Diversity Combining

We evaluate the average BER for two-stage EGC-MRC and SC-MRC DCS's. The two-stage DCS's can sometimes be used to reduce the complexity of the combining schemes for a large number of diversity branches. The received signals, $y_{ij} = h_{ij}\, x + w_{ij}$, are divided into K groups of L_i signals per group where $i = 1, \cdots, K$, and $j = 1, \cdots, L_i$; see Fig. 4.1. Denote by g_i the channel fading amplitudes after the first combining stage, so that, $g_i = \frac{1}{\sqrt{L_i}} \sum_{j=1}^{L_i} g_{ij}$, for EGC, and, $g_i = \max_{j=1,\cdots,L_i} g_{ij}$, for SC. Since after the first combining stage, the channel amplitudes, g_i, are known, the K signals, $y_i = g_i\, x + w_i$, are combined using MRC, and the decision variable is written as, $y = (\sqrt{\sum_{i=1}^{K} g_i^2})\, x + w$.

Assume that there are n plane waves arriving at the receiver antennas. We can show that the EGC-MRC combiner output can be written as, $y = (\sqrt{\mathbf{G}^T(\sum_{i=1}^{K} \tilde{\mathbf{d}}_i^T \tilde{\mathbf{d}}_i)\mathbf{G}})\, x + w$, where $\tilde{\mathbf{d}}_i = (\tilde{d}_{i1}, \cdots, \tilde{d}_{in})$, and the output channel amplitude of the i-th EGC combiner is, $g_i = \sum_{j=1}^{n} \tilde{d}_{ij} G_j$. On the other hand, assuming that the groups of antennas are sufficiently separated, then the channels are correlated within the groups of antennas and independent between the groups. In this case, the MGF of the MRC output squared channel amplitude, g^2, is, $\Phi_{g^2}(t) = \prod_{i=1}^{K} \Phi_{g_i^2}(t)$, where the MGF's, $\Phi_{g_i^2}(t)$, for EGC and SC diversity combining were obtained in the previous subsections. Again, the average BER is computed using the Prony approximation method (4.18a).

4.4 Numerical Examples

Without loss of generality, we assume BPSK modulation having the conditional BER, $\mathrm{P}_\epsilon(\gamma) = Q(\sqrt{2\gamma}) \approx 0.204\,\mathrm{e}^{-1.504\gamma} + 0.105\,\mathrm{e}^{-1.024\gamma}$. For higher order modulations, the conditional BER can be also expressed with a high accuracy using a sum of only two exponentials [70].

Consider the four HS/MRC schemes corresponding to the output signals (4.7)–(4.10). The branches can be decorrelated (DEC) or orthogonalized (ORT) prior to the SNR selection (SEL) or fixed (pre-determined) selection (FSEL), and the selected branches then combined using MRC. We assume the channel model (4.5), i.e., $\mathbf{h} = \sqrt{\mathbf{P_h}}\mathbf{U_z}\mathbf{z} + \bar{\mathbf{h}}$, and let $\mathbf{z}$ be a Gaussian random vector. Then, the branch average SNR is, $\mathrm{E}[\gamma] = \mathrm{E}[g_i^2]\, \gamma_b$, where $\mathrm{E}[g_i^2] = P_{h_i}(\sum_{j=1}^{n} \lambda_{z_j}) + \bar{h}_i^2$. The normalized covariance matrix of the vector, $\mathbf{U_z z}$, is, $\mathbf{C_z} = \mathbf{U_z \Sigma_z U_z^H}$, where $\mathbf{\Sigma_z} =$

$\text{diag}(\lambda_{z_1}, \cdots, \lambda_{z_n})$, and the eigenvalues, λ_{z_j}, correspond to the variances of the components of the vector, $\mathbf{z}$. We also assume that $K = n$, and that the branches are equi-correlated; see (4.19a). Note also that, $\sum_{j=1}^{n} \lambda_{z_j} = K$, and the channel powers are normalized, so that $\sum_{i=1}^{K} P_{h_i} = 1$. The average BER's of four HS/MRC schemes (4.7)–(4.10) are compared in Fig. 4.3–Fig. 4.7. We assume $K = 8$ receiver antennas, $L = 1$ and 4 selected branches, the Rice factor, $K_{\text{R}} = -3\,\text{dB}$ and $+3\,\text{dB}$, the correlation coefficient in (4.19a), $r_0 = 0.1$ and 0.6, and the branch powers are either uniformly distributed, i.e., $P_{h_i} = 1/K$, or unbalanced, e.g., let $P_{h_i}/P_{h_{i+1}} = 2$. The average BER for MRC in Fig. 4.3–Fig. 4.7 is shown as a reference. Although, in some cases, the average BER can be computed analytically, we use computer simulations to obtain the performance of HS/MRC schemes; thus, the same received signal is processed by all four HS/MRC schemes. We have the following observations from Fig. 4.3–Fig. 4.7. For a given value of the average BER, the SNR differences decrease with the number of selected branches, L. For $L = K$, we can show that the average BER of all four HS/MRC schemes is identical. In general, orthogonalization of the branches prior to HS/MRC outperforms decorrelation, especially for small values of L, large values of K_{R}, and for less correlated branches. Orthogonalization and decorrelation of the received signals always outperform the traditional HS/MRC scheme; as shown in Fig. 4.3, the SNR improvement can be as large as 2 dB, if $L = 1$. Also, orthogonalization and the fixed branch selection can outperform the traditional HS/MRC scheme, for small to medium values of SNR, larger values of K_{R}, and $L = 1$.

Consider the fading amplitude models (4.12a) and (4.12b), and let the plane waves envelope amplitudes, G_j, be mutually independent and generalized Ricean distributed having n_1 degrees-of-freedom, non-centrality parameter, s^2, and variance, σ^2, per degree-of-freedom. Hence, let $n_1 = 2$, $\sigma^2 = 1$, $K_{\text{R}} = -3\,\text{dB}$ and $+3\,\text{dB}$, and the number of plane waves, $n = 2$ and 1. The average BER is evaluated analytically using (4.18a), in the case of MRC, and (4.18b), in the case of EGC; see Fig. 4.8 and Fig. 4.9. The markers in Fig. 4.8 and Fig. 4.9 are the average BER values obtained using computer simulations. We observe that the average BER is minimized, if the correlation coefficients, $\tilde{d}_j$ are all equal; this can be shown using the method of Lagrange multipliers.

Finally, consider two-stage EGC-MRC and SC-MRC DCS's. We assume the complex valued Gaussian distributed branches (4.5) having equal powers. Then, the decorrelated branches become independent, and the channel amplitudes, $|h_{ij}|$, are generalized Ricean distributed where $n = 2$, $\sigma^2 = 1$, $K_{\text{R}} = 3\,\text{dB}$, and $K = 4$ and 8 receiver antennas. For EGC-MRC, the MGF is evaluated using the GCQ rule, for $c = 0.1$ and $\nu = 256$; see Appendix B. We use the notation, MRC K, and EGC K, for one-stage combining schemes, and EGC-MRC $L \times K$, for two-stage combining

schemes. The circles in Fig. 4.10 are the simulation results corresponding to 2×2 and 4×2 EGC-MRC diversity. The average BER's are also compared in Fig. 4.11 for $(1/L) \times K$ SC-MRC schemes and L/K HS/MRC schemes; the circles are the simulation results corresponding to $(1/4) \times 2$ and $(1/2) \times 4$ SC-MRC diversity. As expected, HS/MRC outperforms SC-MRC, however, the SNR difference is less than $0.5\,\mathrm{dB}$ for all schemes considered.

4.5 Summary

One-stage and two-stage DCS's over correlated fading channels were studied. For a linear correlation channel model, decorrelation and orthogonalization of the branches prior to employing diversity combining was investigated. In particular, decorrelation of branches having equal variances makes the branches independent, and, in turn, facilitates the performance analysis. For time-invariant combining weights, orthogonalization of the branches maximizes the average SNR. Furthermore, a fading amplitude channel model was proposed assuming vector norm superposition of the plane waves envelope amplitudes. Such a channel model can significantly simplify the performance analysis of MRC and EGC schemes operating over correlated fading channels. Finally, the average BER of several DCS's was analyzed. It was found that decorrelation and orthogonalization of the correlated non-zero mean Gaussian branches improves the performance of HS/MRC schemes, especially when there is a strong line-of-sight component, and for small numbers of selected branches. This can be explained by the fact that decorrelation and orthogonalization of the Gaussian branches prior to employing diversity combining restores some of the diversity lost due to the branch correlations.

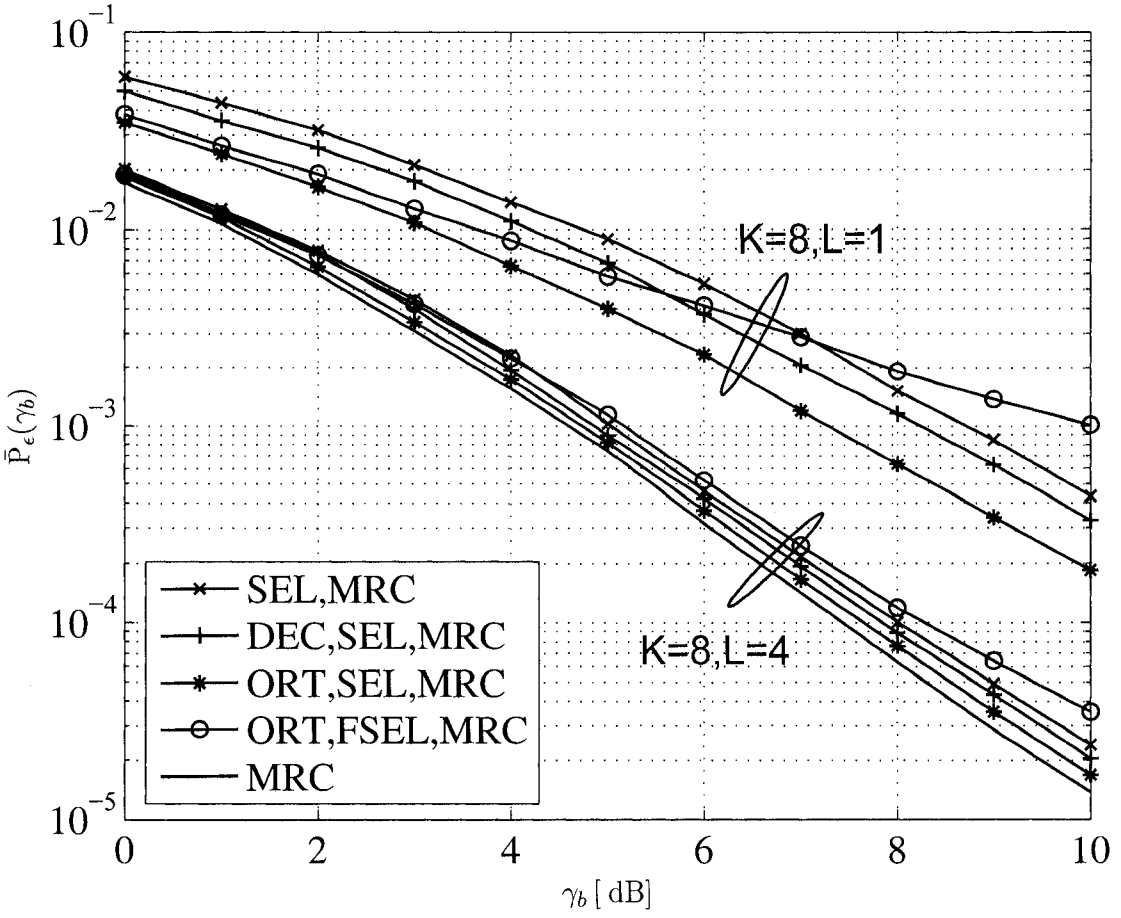

Figure 4.3: The average BER of four HS/MRC diversity schemes for BPSK with unbalanced branch powers, $K_{\mathrm{R}} = +3\,\mathrm{dB}$, and $r_0 = 0.1$.

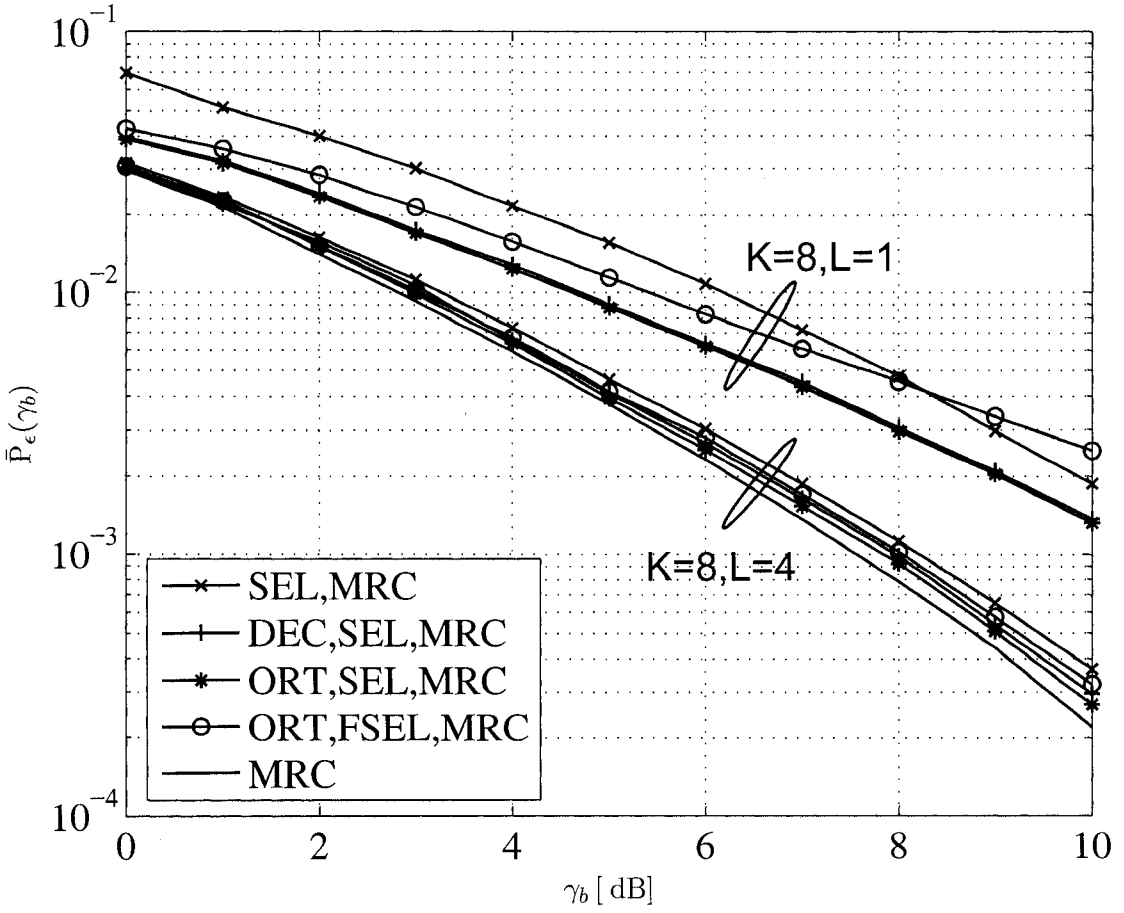

Figure 4.4: The average BER of four HS/MRC diversity schemes for BPSK with unbalanced branch powers, $K_{\mathrm{R}} = +3\,\mathrm{dB}$, and $r_0 = 0.6$.

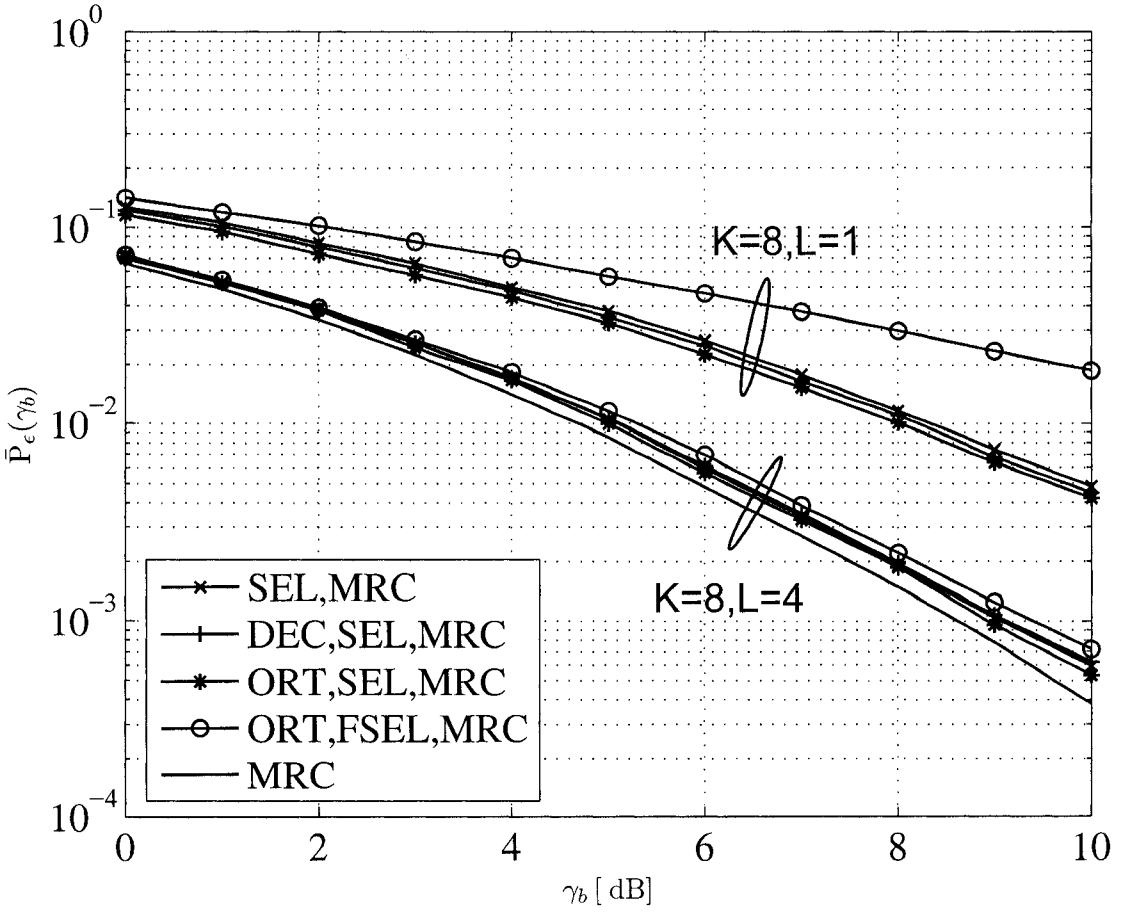

Figure 4.5: The average BER of four HS/MRC diversity schemes for BPSK with unbalanced branch powers, $K_{\mathrm{R}} = -3\,\mathrm{dB}$, and $r_0 = 0.1$.

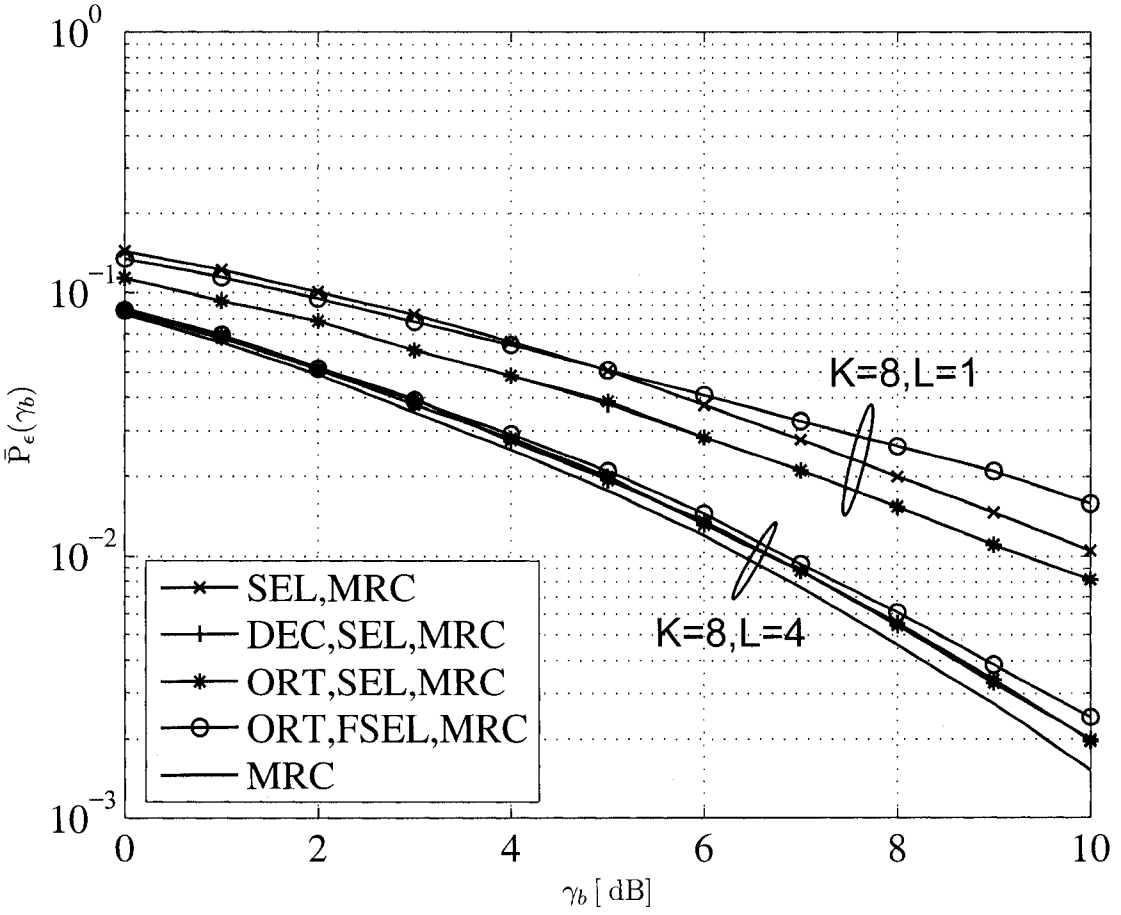

Figure 4.6: The average BER of four HS/MRC diversity schemes for BPSK with unbalanced branch powers, $K_{\mathrm{R}} = -3\,\mathrm{dB}$, and $r_0 = 0.6$.

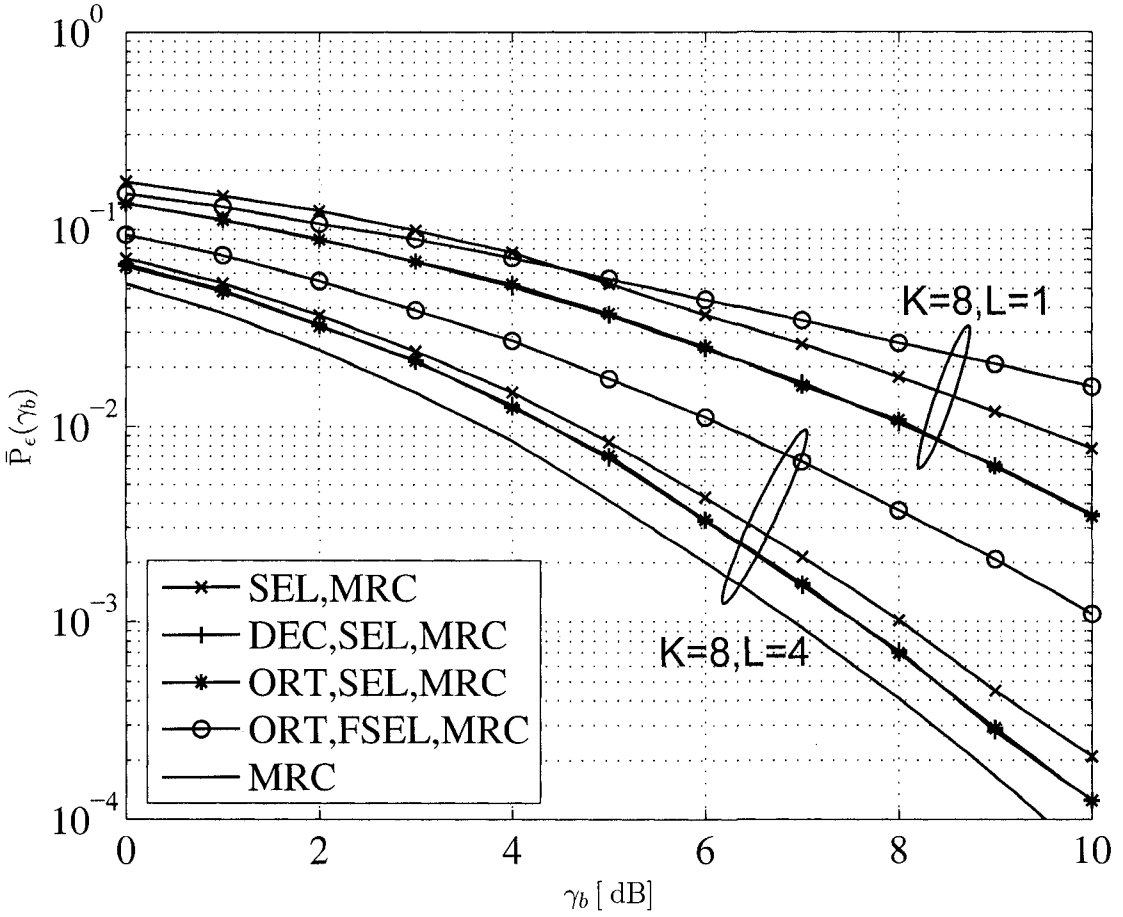

Figure 4.7: The average BER of four HS/MRC diversity schemes for BPSK with uniform branch powers, $K_{\mathrm{R}} = -3\,\mathrm{dB}$, and $r_0 = 0.1$.

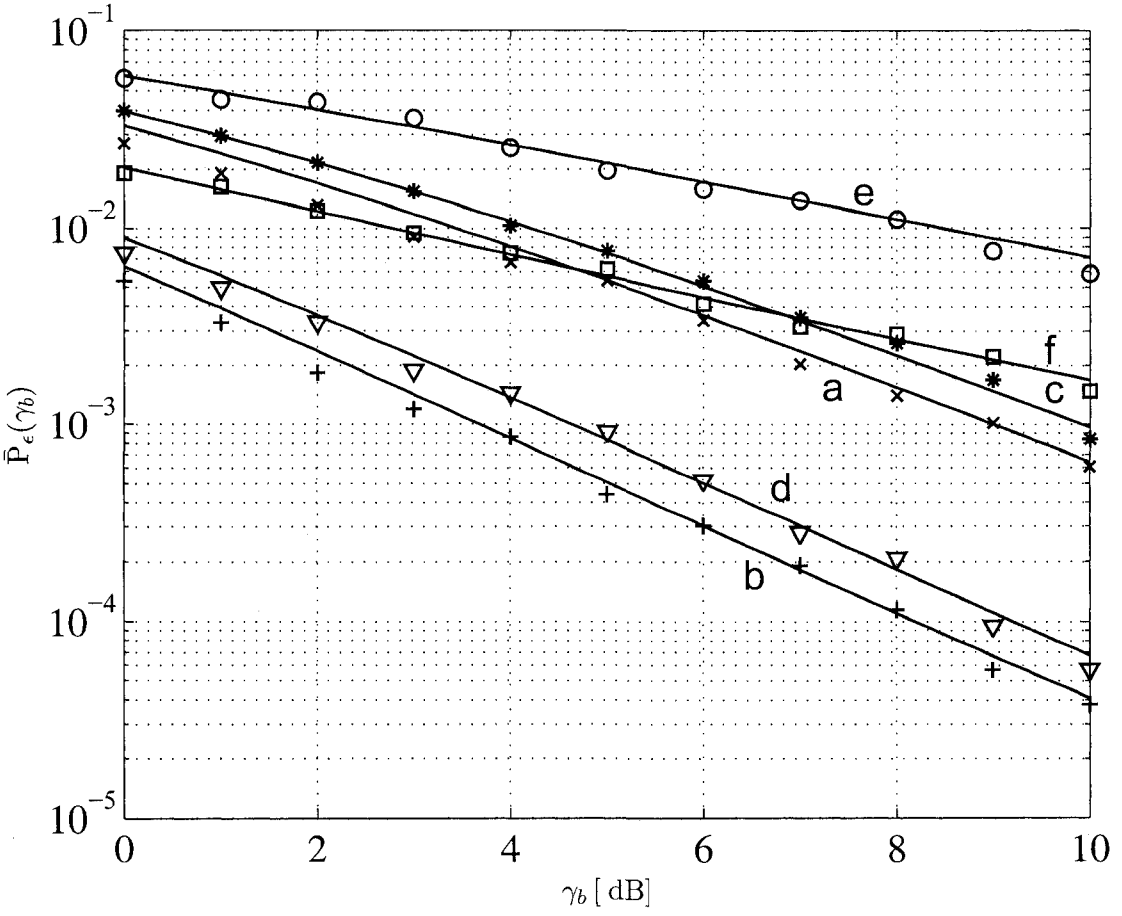

Figure 4.8: The average BER of MRC diversity scheme for BPSK and $K_{\mathrm{R}} = -3\,\mathrm{dB}$ (curves 'a','c','e') and $+3\,\mathrm{dB}$ (curves 'b','d','f'), $n = 2$ (curves 'a','b','c','d') and 1 (curves 'e','f'), $\tilde{d}_j \in \{0.5, 0.5\}$ (curves 'a','b'), $\tilde{d}_j \in \{0.8, 0.2\}$ (curves 'c','d'), and $\tilde{d}_1 = 1$ (curves 'e','f').

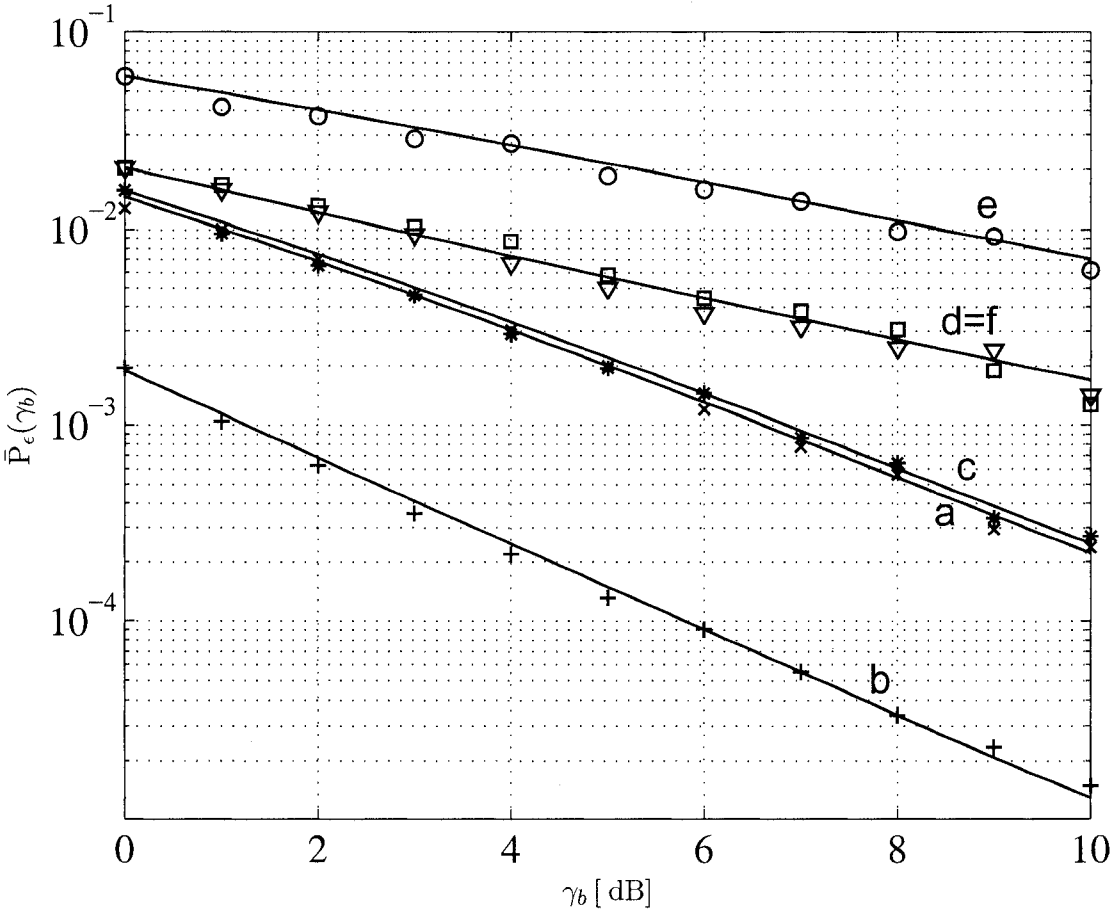

Figure 4.9: The average BER of EGC diversity scheme for BPSK and $K_{\mathrm{R}} = -3\,\mathrm{dB}$ (curves 'a','c','e') and $+3\,\mathrm{dB}$ (curves 'b','d','f'), $n = 2$ (curves 'a','b','c','d') and 1 (curves 'e','f'), $\tilde{d}_j \in \{1/\sqrt{2}, 1/\sqrt{2}\}$ (curves 'a','b'), $\tilde{d}_j \in \{2/\sqrt{5}, 1/\sqrt{5}\}$ (curves 'c','d'), and $\tilde{d}_1 = 1$ (curves 'e','f').

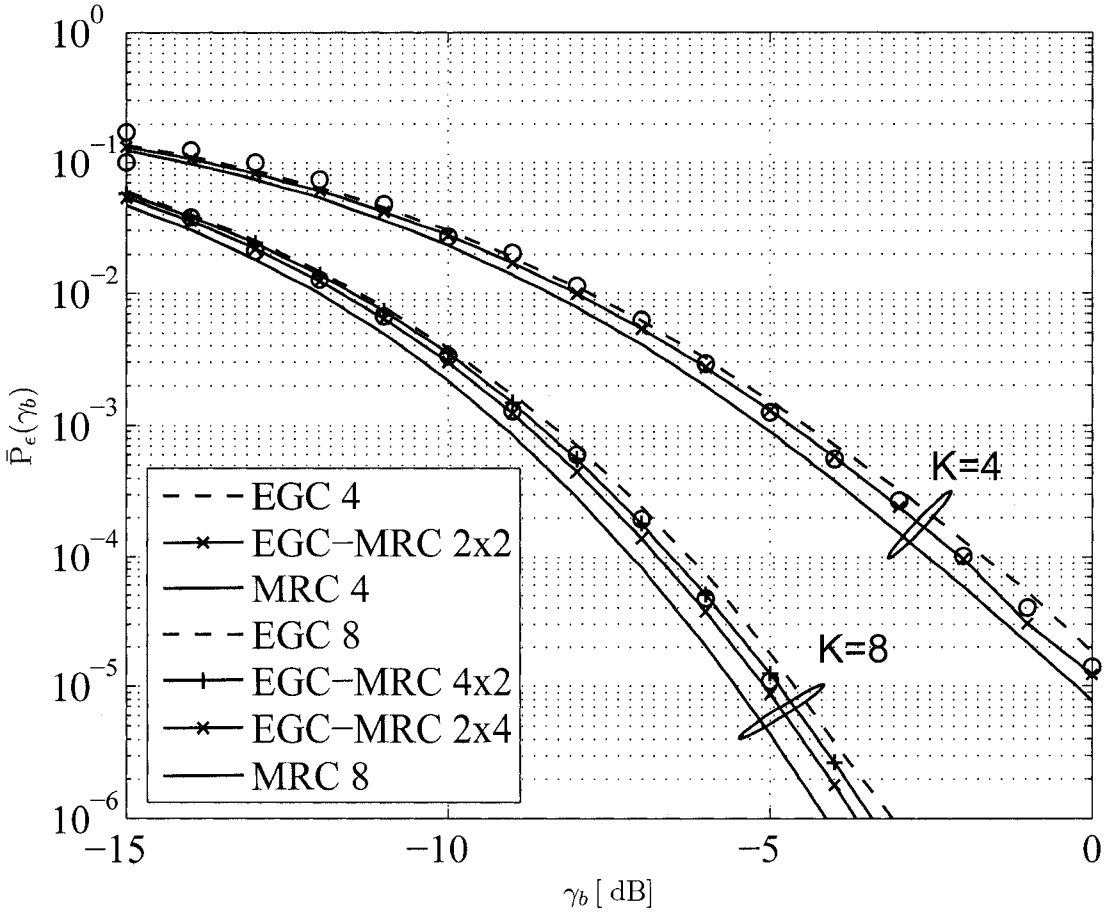

Figure 4.10: The average BER of MRC, EGC and two-stage EGC-MRC diversity schemes with BPSK over decorrelated Ricean branches.

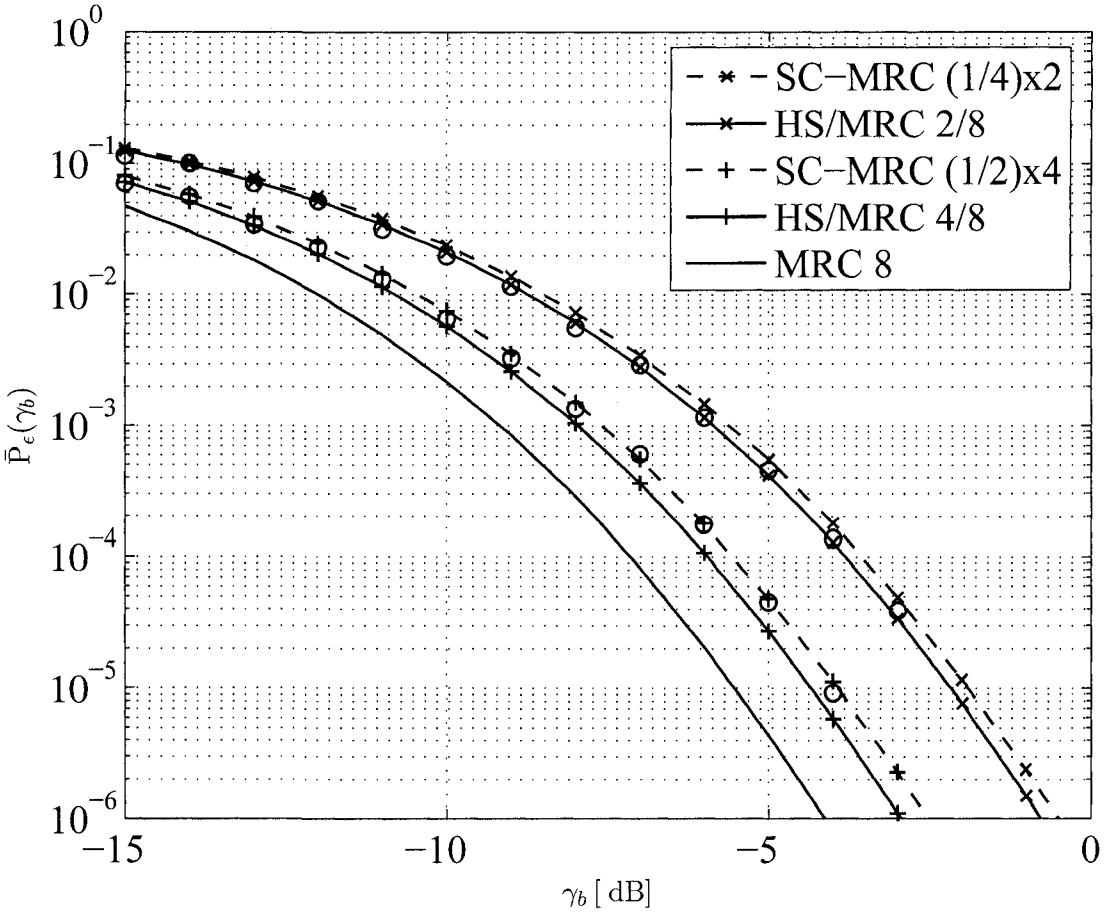

Figure 4.11: The average BER of MRC, SC-MRC and HS/MRC diversity schemes with BPSK over decorrelated Ricean branches.

Chapter 5

Performance Analysis of Coded MIMO-OFDM Systems Over Arbitrary Correlated Generalized Ricean Channels

Efficient performance evaluation techniques developed in Chapters 2–4 are used in Chapters 5–8 to either analyze more realistic system models, or to obtain novel design guidelines. In Chapter 5, coded MIMO-OFDM systems over arbitrary correlated generalized Ricean fading channels are analyzed. The results for correlated Rayleigh fading channels can be then obtained as a special case when the mean values of the fading processes are set to zero. In particular, we evaluate a UB of the BER and the probability of outage, and we also derive the maximum achievable diversity gain and coding gain.

5.1 Background

Combination of MIMO and OFDM and forward error correction coding (FEC) to extract spatial, frequency and temporal diversity creates multi-fold trade-offs between performance and complexity [83]– [88]. The MIMO-OFDM systems are well-suited for broadband fixed wireless access [89]. Furthermore, a recent approval of the IEEE 802.16 Standard [89] limits possibilities for further amendments, and thus, performance analysis of the approved standard in various propagation environments is now important. The IEEE 802.16 Standard employs bit-interleaved coded modulation (BICM) [90] and transmitter diversity OFDM techniques [85]. Interestingly, no spreading is spec-

ified in [89] in order to improve spectral efficiency and reduce multiple access interference in the system.

Literature on space-time-frequency coded systems in correlated Rayleigh and Ricean fading channels is plentiful. For example, references [91] and [84]– [88] apply the Chernoff bound of the PEP, and then use the MGF to obtain design rules for maximum achievable diversity and coding gain. The exact PEP for STBC's in Rayleigh and Ricean fading channels was obtained in references [82], [83] and [92]. The exact symbol-error probability of orthogonal STBC's is derived in [93]. However, literature on combined FEC and space-time-frequency coded MIMO-OFDM systems in correlated Ricean fading channels is scarce. For example, BICM for MIMO-OFDM system is investigated in [94] using an expurgated union bound and assuming ideal interleaving and symmetry of the bit-subchannels [90], [95]. Simulation results for turbo product coded MIMO-OFDM systems are presented in [96]. The performance of BICM for coded MIMO-OFDM systems over independent Rayleigh fading channels is analyzed in [97] and [98].

In this chapter, we establish a framework to analyze the performance of turbo product coded MIMO-OFDM system over arbitrary correlated generalized Ricean fading channels. We assume correlated transmitter and receiver antennas as well as correlated multipath frequency selective channels. We derive the MGF of the SNR at the input of the channel decoder for orthogonal space-time coding and SNR maximizing beamforming transmitter diversity OFDM schemes. The MGF is used to compute the probability of outage, the PEP, the BER and diversity and coding gains of MIMO-OFDM systems. We also prove that exactly the same rank and determinant design criteria [91] for space-time-frequency coding as obtained for the Chernoff bound of the PEP can be also obtained for the exact PEP.

This chapter is organized as follows. An equivalent system model in the frequency domain for OFDM systems using orthogonal STBC's and using transmitter beamforming to maximize the SNR at a receiver antenna is developed in Section 5.2. Bit-interleaved and iteratively decoded turbo product code and Gray encoded M-ary QAM are studied. In Section 5.3, the MGF is derived and the probability of outage, the PEP, the BER and the diversity order and coding gain of MIMO-OFDM systems are analyzed. Numerical results are presented in Section 5.4. The chapter is summarized in Section 5.5.

5.2 System Model

Consider a coded MIMO-OFDM system where the users in the uplink and downlink are separated using OFDM multiple access (OFDMA) [89]. These systems typically operate in line-of-sight to non-line-of-sight channels for fixed broadband wireless access. Thus, multipath channel models having Ricean distributed fading envelopes best describe the propagation conditions of these broadband wireless systems [86]. Note that the L propagation paths are, in general, correlated [99] violating the widely employed assumption of uncorrelated scattering [100]. Furthermore, the paths can have different Ricean factors and Doppler spreads [101]; however, the path delays are usually equal for all transmitter-receiver antenna pairs [86]. Lack of scatterers in the vicinity of high positioned antennas causes the signals departing from the N_t transmitter antennas and arriving at the N_r receiver antennas to be correlated [86]. Note that the base station (BS) usually has more antennas than the subscriber station (SS) to minimize the number of radio frequency interfaces in the network. In general, we assume perfect time and frequency synchronization and perfect channel estimation (knowledge of amplitudes and phases) at the receiver. The intercarrier-interference (ICI) of OFDM systems due to Doppler spread can be neglected in low mobility (fixed access) networks, or, for a large number of subcarriers, the ICI can be approximated as a equivalent AWGN [102].

5.2.1 Generalized Ricean Fading

Assume a discrete time complex baseband multipath channel model between the i-th transmitter and the j-th receiver [84], [100],

$$\mathbf{h}_{ij}(o,\tau) = \sum_{l=0}^{L-1} \mathbf{h}_{ij}(o,l)\,\delta_{\tau\tau_l}$$

where $i = 1, 2, \cdots, N_t$, $j = 1, 2, \cdots, N_r$, the symbol o denotes the discrete time, and τ and $\tau_0 = 0 < \tau_1 < \cdots < \tau_{L-1}$ are the discrete delay times obtained using a sampling period, T_s, $\delta_{\tau\tau_l} = 1$, if $\tau = \tau_l$, and 0, if $\tau \neq \tau_l$, notation $\mathbf{h}_{ij}$ is used to denote the i-th row and the j-th column element of the matrix, $\mathbf{h}$, and the complex valued matrix, $\mathbf{h}(o,\tau) \in \mathbb{C}^{N_r \times N_t}$. The magnitude of $\mathbf{h}_{ij}(o,l)$ is assumed to be generalized Ricean distributed with $2m$ degrees of freedom and noncentrality parameter, s_{ij}^2. Then, one has that [100, eq. (2-1-143)],

$$|\mathbf{h}_{ij}(o,l)| = \sqrt{\sum_{u=1}^{2m} \mathbf{z}_{ij}(o,u,l)^2} \quad \forall i,j,o,l$$

where $s_{ij}^2 = \sum_{u=1}^{2m} \mathrm{E}\big[\mathbf{z}_{ij}(o,u,l)^2\big]$, and $\mathbf{z}(o,u,l) \in \mathbb{R}^{N_r \times N_t}$, for $\forall o,u,l$, are real-valued jointly Gaussian matrices independent in the dimension variable, u; see Fig. 5.1. Thus, the correlations, $\mathrm{E}\big[\mathbf{z}(o_1,u_1,l_1)\mathbf{z}(o_2,u_2,l_2)^T\big] = \mathbf{0}_{(N_r \times N_r)}$, and, $\mathrm{E}\big[\mathbf{z}(o_1,u_1,l_1)^T\mathbf{z}(o_2,u_2,l_2)\big] = \mathbf{0}_{(N_t \times N_t)}$, for $u_1 \neq u_2$, where $\mathbf{0}$ denotes the all-zero matrix, and $(\cdot)^T$ is the matrix transpose. Let the time $o = 0, 1, \cdots, S_u - 1$, and define,

$$\mathbf{z}(o,u,l) = \sqrt{G(l)}\left(\frac{\mathbf{R}_{\mathrm{Rx}}^{1/2}\mathbf{z}_0(o,u,l)\mathbf{R}_{\mathrm{Tx}}^{1/2}}{\sqrt{2m}\,\|\mathbf{R}_{\mathrm{Rx}} \otimes \mathbf{R}_{\mathrm{Tx}}\|} + \bar{\mathbf{z}}(l)\,\delta_{u1}\right)$$

where $\mathbf{z}_0(o,u,l) \in \mathbb{R}^{N_r \times N_t}$ are zero-mean real-valued jointly Gaussian matrices having uncorrelated elements of equal variance, $\sigma_{\mathbf{z}}^2$, $\mathrm{E}[\mathbf{z}(o,u,l)] = \bar{\mathbf{z}}(l)\,\delta_{u1}$, $\mathbf{R}_{\mathrm{Rx}}^{T/2}\mathbf{R}_{\mathrm{Rx}}^{1/2} = \mathbf{R}_{\mathrm{Rx}}$ and $\mathbf{R}_{\mathrm{Tx}}^{1/2}\mathbf{R}_{\mathrm{Tx}}^{T/2} = \mathbf{R}_{\mathrm{Tx}}$ are the transmitter and receiver antenna correlation matrices (assuming that they can be separated [86]), respectively, $\|\cdot\|$ is the Frobenius norm of the matrix, the operator, $\otimes$, denotes the Kronecker matrix product [81], and $G(l)$ is the power of the l-th path. Then, the correlations are given as,

$$\begin{aligned}\mathrm{E}[\mathbf{z}_{i_1 j_1}(o_1,u_1,l_1)\mathbf{z}_{i_2 j_2}(o_2,u_2,l_2)] &= \tfrac{\delta_{u_1 u_2}}{2m}\sqrt{G(l_1)G(l_2)}\times \\ \times R_{\mathrm{x}}(i_1,j_1,i_2,j_2)R_{\mathrm{tl}}(o_1-o_2,l_1,l_2) &+ \bar{\mathbf{z}}_{i_1 j_1}\bar{\mathbf{z}}_{i_2 j_2}\delta_{u_1 1}\delta_{u_2 1}\end{aligned}$$

where we assume that, $R_{\mathrm{tl}}(\Delta o,l_1,l_2) = R_{\mathrm{t}}(\Delta o,l_1)R_{\mathrm{t}}(\Delta o,l_2)R_{\mathrm{l}}(l_1,l_2)$, and $R_{\mathrm{t}}(\Delta o,l)$ is the wide-sense stationary (WSS) time correlation function of the l-th path, and $R_{\mathrm{l}}(l_1,l_2)$ is the correlation function between path l_1 and l_2, and the correlation between the transmitter and receiver antenna pairs, (i_1,j_1), and, (i_2,j_2), is,

$$R_{\mathrm{x}}(i_1,j_1,i_2,j_2) = \frac{\mathrm{row}\Big(\mathbf{R}_{\mathrm{Rx}}^{1/2}\Big)_{j_1}\mathrm{row}\Big(\mathbf{R}_{\mathrm{Rx}}^{1/2}\Big)_{j_2}^T\mathrm{col}\Big(\mathbf{R}_{\mathrm{Tx}}^{1/2}\Big)_{i_1}^T\mathrm{col}\Big(\mathbf{R}_{\mathrm{Tx}}^{1/2}\Big)_{i_2}}{\|\mathbf{R}_{\mathrm{Rx}} \otimes \mathbf{R}_{\mathrm{Tx}}\|^2}. \tag{5.1}$$

In (5.1), $\mathrm{col}(\mathbf{A})_i$ and $\mathrm{row}(\mathbf{A})_j$ denote the i-th column and the j-th row of the matrix, $\mathbf{A}$, respectively. The correlation functions are normalized, so that the diagonal elements of $\mathbf{R}_{\mathrm{Rx}}$ and $\mathbf{R}_{\mathrm{Tx}}$ are unity, and $R_{\mathrm{tl}}(0,l,l) = 1$, for $\forall l$. The total power, $P(l)$, of the l-th path is,

$$P(l) = \sum_{i=1}^{N_t}\sum_{j=1}^{N_r}\mathrm{E}\big[\mathbf{h}_{ij}(o,l)^2\big] = G(l)(r_{\mathrm{x}}\sigma_{\mathbf{z}}^2 + \|\bar{\mathbf{z}}(l)\|^2)$$

where $r_{\mathrm{x}} = \sum_{i=1}^{N_t}\sum_{j=1}^{N_r} R_{\mathrm{x}}(i,i,j,j)$. Let $\sigma_{\mathbf{z}}^2 = 1/r_{\mathrm{x}}$, then $G(l) = P(l)/(1 + K_r(l))$ where $K_r(l) = \|\bar{\mathbf{z}}(l)\|^2$ is the Ricean factor of the l-th path, and thus, let $\bar{\mathbf{z}}_{ij}(l) = \sqrt{K_r(l)/(N_t N_r)}$ (cf. [101]).

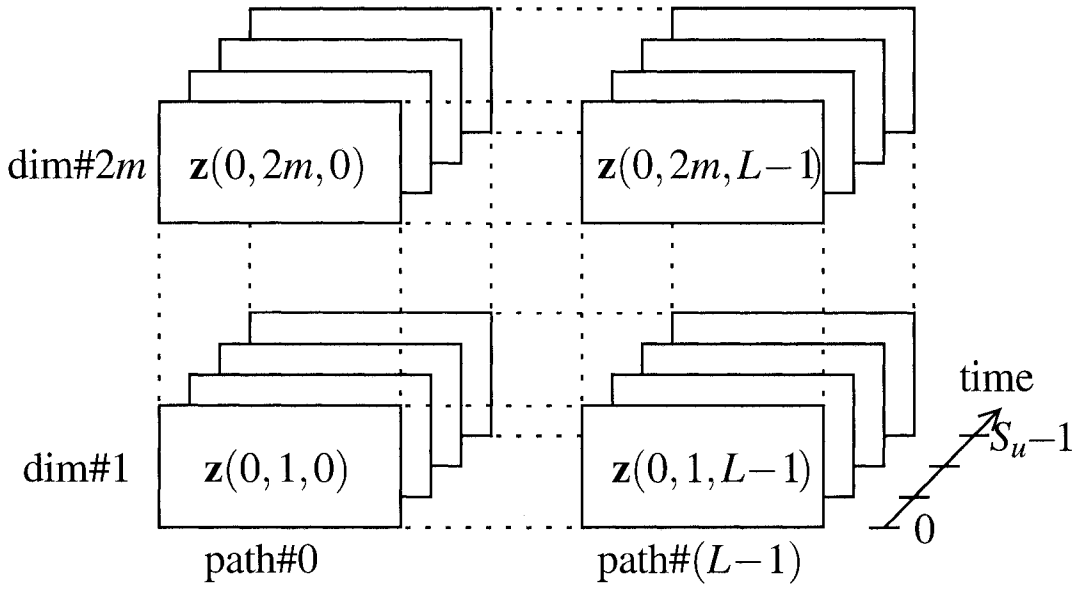

Figure 5.1: The underlying Gaussian matrices in the time domain.

5.2.2 Equivalent System Model

It is useful to obtain an equivalent system model of MIMO-OFDM systems in the frequency domain. Define the discrete Fourier transform of the matrices, $\mathbf{z}(o,u,l)$, as,

$$\mathbf{Z}_{ij}(o,u,n) = \sum_{l=0}^{L-1} \mathbf{z}_{ij}(o,u,l)\, \mathrm{e}^{-\mathrm{j}\frac{2\pi}{N_{\mathrm{fft}}}\tilde{n}(n)\tau_l}$$

where N_{fft} is the number of subcarriers, $\tilde{n}(n)$ is the mapping from the logical channel, n, to the subcarrier, $\tilde{n}$, where $n = 0, 1, \cdots, N_u - 1$, and usually, $N_u \ll N_{\mathrm{fft}}$. Then, the subcarrier spacing, $\Delta f = 1/(T_s N_{\mathrm{fft}})$. The elements, $\mathbf{Z}_{ij}(o,u,n)$, are complex-valued non-zero mean jointly Gaussian random variables having even symmetry in the magnitude and odd symmetry in the phase in the frequency variable, n. The magnitude of the channel in the frequency domain, i.e.,

$$|\mathbf{H}_{ij}(o,n)| = \sqrt{\sum_{u=1}^{2m} |\mathbf{Z}_{ij}(o,u,n)|^2} \tag{5.2}$$

is exactly generalized Ricean distributed. Note that we do not specify the phase of the complex channel coefficients, $\mathbf{H}_{ij}(o,n)$. The frequency correlation function of $\mathbf{Z}_{ij}(o_1,u,n_1)$ and $\mathbf{Z}_{ij}(o_2,u,n_2)$

can be written as,

$$B_{\mathbf{Z}}(\Delta o, n_1, n_2) = \sum_{l_1=0}^{L-1} \sum_{l_2=0}^{L-1} \sqrt{G(l_1)G(l_2)} \times \\ \times R_{\mathrm{tl}}(\Delta o, l_1, l_2)\, \mathrm{e}^{-\mathrm{j}\frac{2\pi}{N_{\mathrm{fft}}}(\tilde{n}(n_1)\tau_{l_1} - \tilde{n}(n_2)\tau_{l_2})} \tag{5.3}$$

where $\Delta o = o_1 - o_2$. The power correlation function in the frequency domain can be obtained using the result derived in Appendix E, i.e.,

$$\begin{aligned} &\rho_{\mathbf{H} i_1 i_2 j_1 j_2}(o_1 - o_2, n_1, n_2) = \\ &= \mathrm{E}\big[|\mathbf{H}_{i_1 j_1}(o_1, n_1)|^2 |\mathbf{H}_{i_2 j_2}(o_2, n_2)|^2\big] = 4m|M_{11}|^2 \\ &\quad + 4\bar{V}_1 \bar{V}_2^* M_{11} + (2m\,\sigma_{V_1}^2 + |\bar{V}_1|^2)(2m\,\sigma_{V_2}^2 + |\bar{V}_2|^2) \end{aligned} \tag{5.4}$$

where

$$\begin{aligned} \bar{V}_1 &= \mathrm{E}[\mathbf{Z}_{i_1 j_1}(o_1, u_1, n_1)] = \bar{\mathbf{Z}}_{i_1 j_1}(n_1)\delta_{u_1 1} \\ \sigma_{V_1}^2 &= \mathrm{E}\big[|\mathbf{Z}_{i_1 j_1}(o_1, u_1, n_1)|^2\big] - |\mathrm{E}[\mathbf{Z}_{i_1 j_1}(o_1, u_1, n_1)]\,|^2 \\ &= \tfrac{1}{2m} R_{\mathrm{x}}(i_1, i_1, j_1, j_1) c B_{\mathbf{Z}}(0, n_1, n_1) \\ M_{11} &= \mathrm{E}[\mathbf{Z}_{i_1 j_1}(o_1, u_1, n_1)\mathbf{Z}_{i_2 j_2}(o_2, u_2, n_2)^*] \\ &\quad - \mathrm{E}[\mathbf{Z}_{i_1 j_1}(o_1, u_1, n_1)]\,\mathrm{E}[\mathbf{Z}_{i_2 j_2}(o_2, u_2, n_2)^*] \\ &= \delta_{u_1 u_2} \tfrac{1}{2m} R_{\mathrm{x}}(i_1, i_2, j_1, j_2) B_{\mathbf{Z}}(o_1 - o_2, n_1, n_2) \end{aligned} \tag{5.5}$$

and $(\cdot)^*$ denotes the complex conjugate.

5.2.3 Diversity Techniques

We consider two transmit diversity techniques for MIMO-OFDM system depicted in Fig. 5.2, [85], [89]. In particular, System I assumes orthogonal STBC, so that the space-time codeword, $\mathbf{X}$, has the property, $\mathbf{X}\mathbf{X}^H = \|\mathbf{X}\|^2 \mathbf{I}$, where $(\cdot)^H$ denotes the matrix transpose conjugate, and $\mathbf{I}$ is the identity matrix. Thus, the channel coefficient of System I at time, o, and subcarrier, n, after space-time combining at the receiver, is written as,

$$\mathbf{H}^{\mathrm{I}}(o, n) = \sqrt{\sum_{i=1}^{N_t} \sum_{j=1}^{N_r} |\mathbf{H}_{ij}(o, n)|^2}. \tag{5.6}$$

System II assumes perfect knowledge of the channel phases at the transmitter and one receiver antenna. Then, transmitter beamforming is used to maximize the SNR at the receiver antenna (equivalently, one can assume one transmitter antenna and equal gain combining at the receiver).

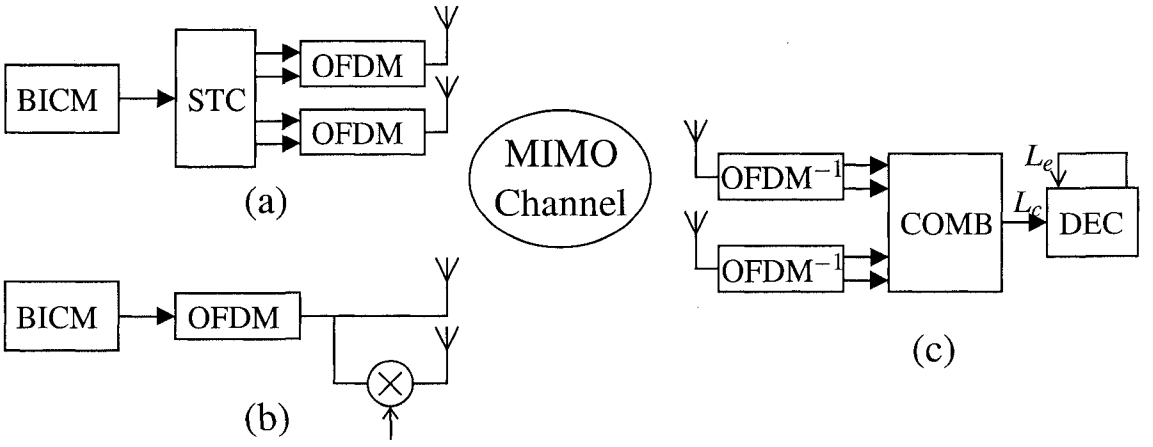

Figure 5.2: Bit-interleaved coded modulation system with (a) space-time coding, (b) beamforming, and (c) the subcarrier combining and iterative decoding at the receiver.

For $N_r = 1$, the channel coefficient of System II at time, o, and subcarrier, n, is written as,

$$\mathbf{H}^{\mathrm{II}}(o,n) = \sum_{i=1}^{N_t} |\mathbf{H}_{i1}(o,n)|. \tag{5.7}$$

In general, the distribution or the MGF of the sum of correlated generalized Ricean distributed variables is not known. Therefore and importantly, in order to simplify the analysis of System II, we rewrite (5.7) as,

$$\begin{aligned} \mathbf{H}^{\mathrm{II}}(o,n)^2 &= \mathbf{H}^{\mathrm{I}}(o,n)^2 + \sum_{i_1=1}^{N_t} \sum_{\substack{i_2=1 \\ i_2 \neq i_1}}^{N_t} \sqrt{|\mathbf{H}_{i_1 1}(o,n)|^2 |\mathbf{H}_{i_2 1}(o,n)|^2} \\ &= \mathbf{H}^{\mathrm{I}}(o,n)^2 + \eta(o,n). \end{aligned} \tag{5.8}$$

Recall the Jensen inequality, i.e., for any random variable, $Z \geq 0$, inequality, $\mathrm{E}\left[\sqrt{Z}\right] \leq \sqrt{\mathrm{E}[Z]}$, holds. Assuming small Doppler spread in low mobility scenarios, we approximate the sum in (5.8) by an upper-bound of its mean-value, i.e.,

$$\mathrm{E}[\eta(o,n)] \leq \bar{\eta}(n) = \sum_{i_1=1}^{N_t} \sum_{\substack{i_2=1 \\ i_2 \neq i_1}}^{N_t} \sqrt{\mathrm{E}[|\mathbf{H}_{i_1 1}(o,n)|^2 |\mathbf{H}_{i_2 1}(o,n)|^2]}.$$

Then, we can write that,

$$\mathbf{H}^{\mathrm{II}}(o,n)^2 \approx \mathbf{H}^{\mathrm{I}}(o,n)^2 + \bar{\eta}(n) \tag{5.9}$$

and we substitute the power correlation values from (5.4) into $\bar{\eta}(n)$. Comparing eqs. (5.6) and (5.9), we observe that the performance of System II can be analyzed assuming the channel coefficients (5.9); then, letting, $\bar{\eta}(n) = 0$, one obtains the performance analysis for System I. For example, the amount of fading for System II is computed as [103],

$$\begin{aligned} \mathrm{AF}(n) &= \frac{\mathrm{E}\left[\mathbf{H}^{\mathrm{II}}(o,n)^4\right] - \mathrm{E}\left[\mathbf{H}^{\mathrm{II}}(o,n)^2\right]^2}{\mathrm{E}[\mathbf{H}^{\mathrm{II}}(o,n)^2]^2} \\ &= \frac{\sum_{i_1=1}^{N_t}\sum_{i_2=1}^{N_t}\rho_{\mathbf{H}i_1i_211}(0,n,n) - (r_{\mathrm{x}}B_{\mathbf{Z}}(0,n,n) + \left\|\bar{\mathbf{Z}}(n)\right\|^2)^2}{(r_{\mathrm{x}}B_{\mathbf{Z}}(0,n,n) + \left\|\bar{\mathbf{Z}}(n)\right\|^2 + \bar{\eta}(n))^2} \end{aligned}$$

where we again substitute the power correlation values from (5.4). The amount of fading for System I is obtained by substituting, $\bar{\eta}(n) = 0$. The Ricean factor for System II is computed as [48],

$$K(n) = \frac{\left\|\bar{\mathbf{Z}}(n)\right\|^2 + \bar{\eta}(n)}{r_{\mathrm{x}}B_{\mathbf{Z}}(0,n,n)}$$

and we substitute, $\bar{\eta}(n) = 0$, for System I.

5.2.4 Encoding and Decoding

In general, denote by $C = (n, k, d_{\min})$ a binary block code of block length, n, dimension, k, and minimum Hamming distance, $d_{\min}$. The transmitter employs BICM described in [89]. Hence, the $K_c = k_x k_y$ input information bits, $\mathbf{u} \in \{0,1\}^{k_x \times k_y}$, are encoded using a binary block turbo product code, $C = C_x \times C_y = (n_x, k_x, d_x) \times (n_y, k_y, d_y) = (N_c, K_c, d_{\min})$, having minimum Hamming distance, $d_{\min} = d_x\, d_y$, block length, $N_c = n_x n_y$, and code rate, $R_c = K_c/N_c$. Assuming ($M = 2^{\tilde{m}}$)-ary modulation, the codewords, $\mathbf{c}$, are bit-interleaved, and the interleaved codewords, $\pi(\mathbf{c}) \in \{0,1\}^{\tilde{m}\times N_c/\tilde{m}}$, are mapped to the codewords, $\mathbf{X}$, of $(N_c/\tilde{m})$ M-ary modulation symbols. In this chapter we assume Gray bits-to-symbol mapping and M-ary square-QAM constellation symbols, $(2i+1-\sqrt{M})+\mathrm{j}(2j+1-\sqrt{M})$, where $\mathrm{j} = \sqrt{-1}$ is the imaginary unit, and $i, j = 0, 1, \cdots, (\sqrt{M}-1)$. Gray mapping from the interleaved coded bits, $\pi(\mathbf{c})$, to QAM symbols can be written as,

$$\mathbf{X} = 2\begin{bmatrix} \mathbf{b} \\ \mathrm{j}\,\mathbf{b} \end{bmatrix}^T \left(\begin{bmatrix} \mathbf{a} & \mathbf{0} \\ \mathbf{0} & \mathbf{a} \end{bmatrix} \pi(\mathbf{c}) + \begin{bmatrix} \tilde{\mathbf{a}} \\ \tilde{\mathbf{a}} \end{bmatrix} \right)_2 - (\tilde{b} + \mathrm{j}\tilde{b}) \tag{5.10}$$

where $\mathbf{b} = (2^{\tilde{m}/2-1}, \cdots, 2^1, 2^0)^T$, the square matrix, $\mathbf{a} \in \{0,1\}^{\tilde{m}/2\times\tilde{m}/2}$, has the elements, $\mathbf{a}_{ij} = 1$ if $j \le i$ and 0, otherwise, $\tilde{\mathbf{a}} = (1,0,1,0,\cdots)^T \in \{0,1\}^{\tilde{m}/2\times 1}$, $\tilde{b} = 2^{\tilde{m}/2}$, and $(\cdot)_2$ denotes the

modulo 2 operation. The M-ary codewords, $\tilde{c}\,\mathbf{X}$, are mapped to N_u subcarriers over S_u consecutive OFDMA symbols where $N_c/\tilde{m} = S_u N_u$. The scaling constant, $\tilde{c} = \sqrt{3/(2^{\tilde{m}+1}-2)}$, sets the average energy per M-ary modulated symbol to unity, and the constant, $\tilde{c} = (2^{(\tilde{m}+1)/2} - 2^{1/2})^{-1}$, preserves the constant peak power of QAM symbols, for all $\tilde{m}$. The received symbol at time, o, and subcarrier, n, before decoding can be written as,

$$Y(o,n) = \tilde{\mathbf{H}}(o,n)\,\tilde{c}X(o,n) + W(o,n) \tag{5.11}$$

where $X(o,n) \in \mathbf{X}$, and $Y(o,n) \in \mathbf{Y}$ where $\mathbf{Y}$ is the received M-ary codeword. The channel coefficients are given as,

$$\tilde{\mathbf{H}}(o,n) = \begin{cases} \mathbf{H}^{\mathrm{I}}(o,n) & \text{for System I} \\ \mathbf{H}^{\mathrm{II}}(o,n) & \text{for System II.} \end{cases}$$

The zero-mean AWGN samples, $W(o,n)$, have variance, $\sigma_W^2 = \mathrm{E}\big[|W(o,n)|^2\big] = N_0/2$, per real dimension where N_0 denotes the one-sided noise power spectral density. Denote by E_b the energy per uncoded bit per subcarrier per transmitter antenna, so that the total transmitter energy is, $E_{\mathrm{tot}} = N_t N_u \tilde{m} E_b$. Then, the SNR is defined as, $\gamma_b = E_b/N_0$.

We employ iterative soft-input bit decoding of the received M-ary codewords, $\mathbf{Y}$; see Fig. 5.2. Such decoding well approximates the ML decoding at larger values of SNR when error propagation in decoding iterations can be neglected [97]. Particularly, the QAM demodulator produces the channel LLR values for all bits in the received M-ary sequence. After deinterleaving, the channel LLR values are used as soft-inputs to decode the channel code. Importantly, note that, although the iterative channel decoder produces soft-output values, these values are not fed back to the QAM demodulator as a priori values of bits in the received QAM symbols. In general, it is shown in [90] that Gray mapping of bits to modulation symbols in BICM is asymptotically optimum, and the feedback of the channel decoder output values to the QAM demodulator provides negligible performance improvement. On the other hand, for other bits-to-symbol mappings, the feedback from the channel decoder to the QAM demodulator can increase the coding gain of BICM [95]; however, this case is not considered in this chapter.

Hence, assuming perfect knowledge of the channel coefficients, $\tilde{\mathbf{H}}(o,n)$, at the receiver, the

channel LLR values at the output of the QAM demodulator are given as [104],

$$L_c(\mathbf{c}_{ij}|\mathbf{Y}) = \log \frac{p(\mathbf{Y}|\mathbf{c}_{ij}=1)}{p(\mathbf{Y}|\mathbf{c}_{ij}=0)}$$

where $\mathbf{c}_{ij}$ is the (i,j)-th transmitted bit of the codeword, $\mathbf{c}$, for $i = 1, 2, \cdots, n_x$, and, $j = 1, 2, \cdots, n_y$, where the a posteriori PDF is,

$$p(\mathbf{Y}|\mathbf{c}_{ij}) = \sum_{X(o,n):\mathbf{c}_{ij}} \frac{1}{2\sigma_W\sqrt{\pi}} \exp\left(\frac{-|Y(o,n) - \tilde{\mathbf{H}}(o,n)\,\tilde{c}X(o,n)|^2}{4\sigma_W^2}\right).$$

For high rate codes, the extrinsic information, L_e, is efficiently computed using the dual codes, $C_x^{\perp}$, and, $C_y^{\perp}$, respectively, i.e., [105, eq. (89)],

$$\begin{aligned} L_e^{(q+1)}(\mathbf{c}_{ij};x) &= \log \frac{\sum_{\mathbf{c}_x \in C_x^{\perp}} \left(\prod_{k=1,k\neq i}^{n_x} f_{kj}^{(q)}(x)\right)}{\sum_{\mathbf{c}_x \in C_x^{\perp}} \left((-1)^{[\mathbf{c}_x]_k} \prod_{k=1,k\neq i}^{n_x} f_{kj}^{(q)}(x)\right)} \\ L_e^{(q+1)}(\mathbf{c}_{ij};y) &= \log \frac{\sum_{\mathbf{c}_y \in C_y^{\perp}} \left(\prod_{k=1,k\neq i}^{n_y} f_{kj}^{(q)}(y)\right)}{\sum_{\mathbf{c}_x \in C_y^{\perp}} \left((-1)^{[\mathbf{c}_y]_k} \prod_{k=1,k\neq i}^{n_y} f_{kj}^{(q)}(y)\right)} \end{aligned}$$

where

$$\begin{aligned} f_{kj}^{(q)}(x) &= \tanh((L_c(\mathbf{c}_{kj}|\mathbf{Y}) + L_e^{(q)}(\mathbf{c}_{kj};y))/2))^{[\mathbf{c}_x]_k} \\ f_{kj}^{(q)}(y) &= \tanh((L_c(\mathbf{c}_{kj}|\mathbf{Y}) + L_e^{(q)}(\mathbf{c}_{kj};x))/2))^{[\mathbf{c}_y]_k} \end{aligned}$$

and $[\mathbf{c}]_k$ is the k-th bit of the codeword, $\mathbf{c}$, and $q = 1, 2, \cdots, q_{\max}$, is the iteration number. The final decision of the bit, $\mathbf{c}_{ij}$, is given by the sign of the LLR,

$$L_c(\mathbf{c}_{ij}|\mathbf{Y}) + L_e^{(q+1)}(\mathbf{c}_{ij};x) + L_e^{(q)}(\mathbf{c}_{ij};y).$$

5.3 Performance Analysis

The performance analysis of System I and System II can be obtained at the symbol level [97], [98], or at the bit level [90], [95]. Particularly, the list of codewords for computing a union bound of the BER is different for the symbol level analysis from the bit level analysis. However, in general, the symbol level analysis is mathematically less complex, and thus, is preferred in this chapter. Recall also that we do not consider iterative updating of the channel LLR values, and thus, the iterative

decoding approaches the ML decoding at large values of SNR [97].

Let $\mathbf{X}$ and $\hat{\mathbf{X}}$ be two distinct codewords, and denote, $\Delta(o,n) = \tilde{c}(\mathbf{X}(o,n) - \hat{\mathbf{X}}(o,n))$. Performance analysis of System I requires knowledge of the MGF of the random variable,

$$\{\xi^{\mathrm{I}}|\mathbf{X},\hat{\mathbf{X}}\} = \sum_{o=0}^{S_u-1}\sum_{n=0}^{N_u-1} \mathbf{H}^{\mathrm{I}}(o,n)^2|\Delta(o,n)|^2 = \sum_{u=1}^{2m}\{\xi_u^{\mathrm{I}}|\mathbf{X},\hat{\mathbf{X}}\}$$

conditioned on codewords, $\mathbf{X}$, and, $\hat{\mathbf{X}}$. The random variables,

$$\{\xi_u^{\mathrm{I}}|\mathbf{X},\hat{\mathbf{X}}\} = \sum_{o=0}^{S_u-1}\sum_{n=0}^{N_u-1}\sum_{i=1}^{N_t}\sum_{j=1}^{N_r} |\Delta(o,n)\,\mathbf{Z}_{ij}(o,u,n)|^2$$

for $u = 1,\cdots,2m$, are independent. Note that, conditioned on channel realization, $\mathbf{H}^{\mathrm{I}}$, the variable, $\{\xi^{\mathrm{I}}|\mathbf{X},\hat{\mathbf{X}},\mathbf{H}^{\mathrm{I}}\}$, corresponds to the squared Euclidean distance between the codewords, $\mathbf{X}$, and, $\hat{\mathbf{X}}$, at the receiver. Correspondingly, the MGF of $\{\xi^{\mathrm{I}}|\mathbf{X},\hat{\mathbf{X}}\}$ can be written as,

$$\Phi_{\{\xi^{\mathrm{I}}|\mathbf{X},\hat{\mathbf{X}}\}}(s) = \mathrm{E}\Big[\,\mathrm{e}^{s\{\xi^{\mathrm{I}}|\mathbf{X},\hat{\mathbf{X}}\}}\Big] = \prod_{u=1}^{2m}\Phi_{\{\xi_u^{\mathrm{I}}|\mathbf{X},\hat{\mathbf{X}}\}}(s)$$

where $\Phi_{\{\xi_u^{\mathrm{I}}|\mathbf{X},\hat{\mathbf{X}}\}}(s) = \mathrm{E}\Big[\,\mathrm{e}^{s\{\xi_u^{\mathrm{I}}|\mathbf{X},\hat{\mathbf{X}}\}}\Big]$. We obtain the MGF, $\Phi_{\{\xi_u^{\mathrm{I}}|\mathbf{X},\hat{\mathbf{X}}\}}(s)$, using the statistics of the underlying, $N_tN_rS_uN_u$, correlated jointly Gaussian random variables, $\mathbf{Z}_{ij}(o,u,n)$. Hence, define the $(N_tN_rS_uN_u \times 1)$ jointly Gaussian column random vector, $\hat{\mathbf{Z}}_u$, having the elements, $\Delta(o,n)\,\mathbf{Z}_{ij}(o,u,n)$. Denote the mean vector, $\mathbf{m}_u = \mathrm{E}\Big[\hat{\mathbf{Z}}_u\Big]$, and the covariance matrix, $\mathbf{M}_u = \mathrm{E}\Big[(\hat{\mathbf{Z}}_u - \mathbf{m}_u)(\hat{\mathbf{Z}}_u - \mathbf{m}_u)^H\Big]$. Then, $\{\xi_u^{\mathrm{I}}|\mathbf{X},\hat{\mathbf{X}}\} = \Big\|\hat{\mathbf{Z}}_u\Big\|^2 = \hat{\mathbf{Z}}_u^H\hat{\mathbf{Z}}_u$, and note that, $\mathbf{m}_u = \mathbf{0}$, for $u = 2,\cdots,2m$. Using the derivation in Appendix F, the MGF of $\{\xi^{\mathrm{I}}|\mathbf{X},\hat{\mathbf{X}}\}$ is given as,

$$\Phi_{\{\xi^{\mathrm{I}}|\mathbf{X},\hat{\mathbf{X}}\}}(s) = \frac{\exp(s\,\mathbf{m}_1^H(\mathbf{I} - 2s\mathbf{M}_1)^{-1}\mathbf{m}_1)}{\prod_{u=1}^{2m}\det(\mathbf{I} - 2s\mathbf{M}_u)} \tag{5.12}$$

where $\det(\cdot)$ denotes the matrix determinant, and $(\cdot)^{-1}$ is the matrix inverse. The covariance matrix, $\mathbf{M}_u$, and the mean vector, $\mathbf{m}_u$, can be expressed as,

$$\begin{aligned}\mathbf{M}_u &= (\mathbf{B}\odot\mathbf{d}\mathbf{d}^T)\otimes(\mathbf{R}_{\mathrm{X}}/2m)\\ \mathbf{m}_u &= (\mathbf{d}\otimes\mathbf{1}_{(N_tN_r,1)})\odot(\bar{\mathbf{Z}}_0\otimes\mathbf{1}_{(S_u,1)})\end{aligned}$$

where the operator, $\odot$, denotes the Hadamard matrix product [81]. The $(S_uN_u \times S_uN_u)$ ma-

trix, $\mathbf{B}$, has the elements, $B_{\mathbf{Z}}(|\Delta o|, n_1, n_2)$, the $(N_t N_r \times N_t N_r)$ matrix, $\mathbf{R}_{\mathrm{x}}$, has the elements, $R_{\mathrm{x}}(i_1, j_1, i_2, j_2)$, the $(S_u N_u \times 1)$ column vector, $\mathbf{d}$, has the components, $\Delta(o, n)$, the $(N_t N_r N_u, 1)$ column vector, $\bar{\mathbf{Z}}_0$, has the components, $\bar{\mathbf{Z}}_{ij}(n)$, and $\mathbf{1}$ is the all-one vector; see eq. (5.5). Furthermore, provided that, $B_{\mathbf{Z}}(|\Delta o|, n_1, n_2) = B^*_{\mathbf{Z}}(|\Delta o|, n_2, n_1)$, the matrix, $\mathbf{M}_u$, is Hermitian, and one has that the SVD of the matrix, $\mathbf{M}_u$, is, $\mathbf{M}_u = \mathbf{U}_u \mathbf{\Sigma}_u \mathbf{U}_u^H$, where $\mathbf{U}_u$ is a unitary matrix, $\mathbf{\Sigma}_u = \mathrm{diag}(\lambda_{u1}, \lambda_{u2}, \cdots, \lambda_{ur_u}, 0, \cdots, 0)$ is the diagonal matrix of r_u non-zero eigenvalues, and r_u denotes the rank of $\mathbf{M}_u$, and $r_u \leq N_t N_r S_u N_u$. Then, the MGF (5.12) can be written as,

$$\Phi_{\{\xi^{\mathrm{I}}|\mathbf{X},\hat{\mathbf{X}}\}}(s) = \frac{\prod_{q=1}^{r_1} \exp\left(s \frac{|\hat{m}|_{1q}^2}{1-2s\lambda_{1q}}\right)}{\prod_{u=1}^{2m} \prod_{q=1}^{r_u} (1 - 2s\lambda_{uq})} \tag{5.13}$$

where $\hat{m}_{1q}$ is the q-th component of the vector, $\mathbf{m}_1^H \mathbf{U}_1$.

For System II, we have the random variable,

$$\begin{aligned} \{\xi^{\mathrm{II}}|\mathbf{X}, \hat{\mathbf{X}}\} &= \{\xi^{\mathrm{I}}|\mathbf{X}, \hat{\mathbf{X}}\} + \sum_o \sum_n \bar{\eta}(n) \Delta(o, n)^2 \\ &= \{\xi^{\mathrm{I}}|\mathbf{X}, \hat{\mathbf{X}}\} + \{\tilde{\eta}|\mathbf{X}, \hat{\mathbf{X}}\}. \end{aligned}$$

Thus, the MGF of $\{\xi^{\mathrm{II}}|\mathbf{X}, \hat{\mathbf{X}}\}$ can be computed using knowledge of the MGF of $\{\xi^{\mathrm{I}}|\mathbf{X}, \hat{\mathbf{X}}\}$, i.e.,

$$\Phi_{\{\xi^{\mathrm{II}}|\mathbf{X},\hat{\mathbf{X}}\}}(s) = \mathrm{E}\left[\mathrm{e}^{s\{\xi^{\mathrm{II}}|\mathbf{X},\hat{\mathbf{X}}\}}\right] = \mathrm{e}^{s\{\tilde{\eta}|\mathbf{X},\hat{\mathbf{X}}\}}\, \Phi_{\{\xi^{\mathrm{I}}|\mathbf{X},\hat{\mathbf{X}}\}}(s). \tag{5.14}$$

In the sequel, we evaluate the probability of outage, the PEP, the BER, and the achievable diversity order and coding gain of MIMO-OFDM systems I and II using the MGF's, $\Phi_{\{\xi^{\mathrm{I}}|\mathbf{X},\hat{\mathbf{X}}\}}(s)$, and, $\Phi_{\{\xi^{\mathrm{II}}|\mathbf{X},\hat{\mathbf{X}}\}}(s)$, respectively.

5.3.1 Probability of Outage

We define the probability of outage, $\mathrm{P}_{\mathrm{out}}$, as the probability that the total instantaneous received power is below a given threshold [48]. Hence, denote by $\mu_{\mathrm{th}}^{\mathrm{I}}$ the threshold for System I, so that the probability of outage is,

$$\begin{aligned} \mathrm{P}_{\mathrm{out}}^{I} &= \Pr\left(\sum_{o,n} \mathbf{H}^{\mathrm{I}}(o, n)^2 < \mu_{\mathrm{th}}^{\mathrm{I}}\right) \\ &= \frac{1}{2\pi \mathrm{j}} \int_{v-\mathrm{j}\infty}^{v+\mathrm{j}\infty} \frac{\Phi_{\{\xi^{\mathrm{I}}|1,0\}}(s)\, \mathrm{e}^{-s\mu_{\mathrm{th}}^{\mathrm{I}}}}{s} \mathrm{d}s \end{aligned} \tag{5.15}$$

where $\Pr(\cdot)$ denotes the probability, and $\upsilon \in \mathbb{R}$ is chosen in the region of convergence. The integral (5.15) can be efficiently computed using the Gauss-Chebyshev quadrature rule [82].

For System II, we substitute, $\Phi_{\{\xi^{\mathrm{II}}|\mathbf{1},\mathbf{0}\}}(s)$, and, $\mu_{\mathrm{th}}^{\mathrm{II}} = \mu_{\mathrm{th}}^{\mathrm{I}} + S_u \sum_n \bar{\eta}(n)$, in eq. (5.15).

5.3.2 Pairwise Error Probability

The PEP for the M-ary codewords, $\mathbf{X}$, and, $\hat{\mathbf{X}}$, is evaluated as [82, eq. (12)],

$$\mathrm{P}(\mathbf{X} \mapsto \hat{\mathbf{X}}) = \mathrm{E}\Big[Q\Big(\sqrt{\gamma_b \, \{\xi^{\mathrm{I}}|\mathbf{X}, \hat{\mathbf{X}}\}}\Big)\Big]. \tag{5.16}$$

For System II, we substitute, $\{\xi^{\mathrm{II}}|\mathbf{X}, \hat{\mathbf{X}}\}$, in eq. (5.16). Several methods have been proposed to compute the PEP in (5.16). In particular, one has that,

$$\begin{aligned}
Q(\sqrt{x}) &= \frac{1}{\pi}\int_0^{\pi/2} \exp\Big(-\frac{x}{2\sin^2\theta}\Big)\,\mathrm{d}\theta && \text{(5.17a)}\\
Q(\sqrt{x}) &\leq \frac{1}{2}\,\mathrm{e}^{x/2} && \text{(5.17b)}\\
Q(\sqrt{x}) &\approx \sum_{i=1}^{p} \tilde{A}_i\,\mathrm{e}^{-\tilde{a}_i x} && \text{(5.17c)}
\end{aligned}$$

where eq. (5.17a) is Craig's formula [48], eq. (5.17b) is the Chernoff upper-bound [83], and eq. (5.17c) is the Prony approximation proposed in [70] where $p \geq 1$; thus, with a high accuracy, $Q(\sqrt{x}) \approx 0.208\,\mathrm{e}^{-0.971x} + 0.147\,\mathrm{e}^{-0.525x}$. Then, substituting expressions (5.17a)–(5.17c) into (5.16), and recognizing a definition of the MGF, the PEP can be evaluated as,

$$\begin{aligned}
\mathrm{P}(\mathbf{X} \mapsto \hat{\mathbf{X}}) &= \frac{1}{\pi}\int_0^{\pi/2} \Phi_{\{\xi^{\mathrm{I}}|\mathbf{X},\hat{\mathbf{X}}\}}\Big(-\frac{\gamma_b}{2\sin^2\theta}\Big)\,\mathrm{d}\theta && \text{(5.18a)}\\
\mathrm{P}(\mathbf{X} \mapsto \hat{\mathbf{X}}) &\leq \frac{1}{2}\,\Phi_{\{\xi^{\mathrm{I}}|\mathbf{X},\hat{\mathbf{X}}\}}\Big(-\frac{\gamma_b}{2}\Big) && \text{(5.18b)}\\
\mathrm{P}(\mathbf{X} \mapsto \hat{\mathbf{X}}) &\approx \sum_{i=1}^{p} \tilde{A}_i\,\Phi_{\{\xi^{\mathrm{I}}|\mathbf{X},\hat{\mathbf{X}}\}}(-\tilde{a}_i\gamma_b). && \text{(5.18c)}
\end{aligned}$$

For System II, we substitute the MGF (5.14) into expressions (5.18a)–(5.18c).

5.3.3 Bit Error Rate

In general, the BER is computed as, $\mathrm{P}_b = \mathrm{E}_{\mathbf{H},\mathbf{X},\hat{\mathbf{X}}}\Big[e(\mathbf{X},\hat{\mathbf{X}})/K_c\Big]$, where $e(\mathbf{X},\hat{\mathbf{X}})$ is the number of information bit errors between the transmitted codeword, $\mathbf{X}$, and the decoded codeword, $\hat{\mathbf{X}}$. Then,

the MC estimator for J simulation trials is,

$$\hat{\mathrm{P}}_b^{\mathrm{MC}} = \frac{1}{J}\sum_{j=1}^{J} \frac{e(\mathbf{X}^{(j)}, \hat{\mathbf{X}}^{(j)})}{K_c} \tag{5.19}$$

and this estimator is unbiased. However, we can use a biased and more efficient semi-analytical BER estimator based on the union bound, i.e., [100],

$$\hat{\mathrm{P}}_b^{\mathrm{UB}} = \frac{1}{J}\sum_{j=1}^{J} \sum_{\hat{\mathbf{X}} \in \mathcal{L}_{\mathbf{X}^{(j)}}} \frac{e(\mathbf{X}^{(j)}, \hat{\mathbf{X}})}{K_c} \mathrm{P}(\mathbf{X}^{(j)} \mapsto \hat{\mathbf{X}}) \tag{5.20}$$

where $\mathcal{L}_{\mathbf{X}^{(j)}}$ denotes the list of M-ary codewords corresponding to the randomly generated transmitted codeword, $\mathbf{X}^{(j)}$. In general, the list of codewords should consist of the most likely pairwise error events, so that, $\mathcal{L}_{\mathbf{X}^{(j)}} = \{\hat{\mathbf{X}} : \mathrm{P}(\mathbf{X}^{(j)} \mapsto \hat{\mathbf{X}}) \geq \epsilon P_j\}$, where $P_j = \max_{\hat{\mathbf{X}}} \mathrm{P}(\mathbf{X}^{(j)} \mapsto \hat{\mathbf{X}})$, and the constant, $0 \leq \epsilon < 1$, controls the size of the list. Hence, the list is constructed for a particular interleaving, bits-to-symbol mapping, and mapping of symbols to subcarriers and antennas. In this chapter, we assume that the list consists of the most likely pairwise codewords in the smallest Euclidean distance from the transmitted codeword, $\mathbf{X}^{(j)}$, i.e., let $\mathcal{L}_{\mathbf{X}^{(j)}} = \cup_{o,n} \mathcal{L}_{\mathbf{X}^{(j)}}(o,n)$, where $\mathcal{L}_{\mathbf{X}^{(j)}}(o,n) = \{\hat{\mathbf{X}} : e(\mathbf{X}^{(j)}(o_1,n_1), \hat{\mathbf{X}}(o_1,n_1)) > 0$, if and only if, $o_1 = o, n_1 = n\}$. Such a list construction is in agreement with the design guidelines suggested in [98], i.e., consecutive coded bits should be mapped to different symbols on different subcarriers and different antennas. Importantly, note also that, in this chapter, the list is constructed for the symbol level analysis, i.e., for the pairwise error events, $\mathbf{X} \mapsto \hat{\mathbf{X}}$. On the other hand, for the bit level analysis, the list is constructed for the pairwise error events, $\mathbf{c} \mapsto \hat{\mathbf{c}}$, of binary codewords, $\mathbf{c}$, and, $\hat{\mathbf{c}}$, and assuming the corresponding PEP's, $\mathrm{P}(\mathbf{c} \mapsto \hat{\mathbf{c}})$; see [98].

Furthermore, note that interleaving and Gray mapping (5.10) of codewords, $\mathbf{c}$, to M-ary codewords, $\mathbf{X}$, violates the uniform error property [48], and thus, the BER should be averaged over all possible transmitted codewords. On the other hand, since, $(c_1 + c_2)_2 = |c_1 - c_2|$, for $c_1, c_2 \in \{0, 1\}$, we can use the bound,

$$|\Delta(o,n)| \leq 2\tilde{c} \begin{bmatrix} \mathbf{b} \\ \mathrm{j}\,\mathbf{b} \end{bmatrix}^T \left(\begin{bmatrix} \mathbf{a} & \mathbf{0} \\ \mathbf{0} & \mathbf{a} \end{bmatrix} \pi(\mathbf{c} + \hat{\mathbf{c}}) \right)_2 \tag{5.21}$$

to compute the PEP (5.16) assuming that the all-zero codeword, $\mathbf{c} = \mathbf{0}$, was transmitted. However,

the bound (5.21) will bias the estimators (5.19) and (5.20).

5.3.4 Diversity Order and Coding Gain

Assuming eq. (5.17a), one can obtain an infinite sum representation of the Q-function, i.e., [59],

$$Q\left(\sqrt{x}\right) = \lim_{p\to\infty} \frac{1}{p} \sum_{i=1}^{p} \frac{1}{2} \mathrm{e}^{-\frac{x}{2}\sin^{-2}\left(\frac{\pi(i-1)}{2(p-1)}\right)}.$$

Note that, in this case, it is required that, $p \gg 1$, say, $p = 50$, while a high accuracy is achieved by Prony approximation (5.17c) even for $p = 2$. Hence, let $\tilde{A}_i = \frac{1}{2p}$, and $\tilde{a}_i = \frac{1}{2}\sin^{-2}\left(\frac{\pi(i-1)}{2(p-1)}\right)$. Then, substituting the MGF (5.13) into eq. (5.18c), one has that the exact PEP is,

$$\mathrm{P}(\mathbf{X} \mapsto \hat{\mathbf{X}}) = \lim_{p\to\infty} \sum_{i=1}^{p} \tilde{A}_i \frac{\prod_{q=1}^{r_1} \exp\left(-\frac{\tilde{a}_i\gamma_b|\hat{m}|_{1q}^2}{1+2\tilde{a}_i\gamma_b\lambda_{1q}}\right)}{\prod_{u=1}^{2m}\prod_{q=1}^{r_u}(1+2\tilde{a}_i\gamma_b\lambda_{uq})}. \tag{5.22}$$

Asymptotically, for large values of SNR, γ_b, the PEP (5.22) can be rewritten as,

$$\mathrm{P}(\mathbf{X} \mapsto \hat{\mathbf{X}}) \approx \lim_{p\to\infty} \sum_{i=1}^{p} \tilde{A}_i' \gamma_b^{-\sum_{u=1}^{2m} r_u} = \left(A^{-1/D_{\max}}\gamma_b\right)^{-D_{\max}}$$

where $D_{\max} = \sum_{u=1}^{2m} r_u$ is the maximum achievable diversity order of MIMO-OFDM systems operating over correlated generalized Ricean fading channels, and the constants,

$$\begin{aligned} \tilde{A}_i' &= \tilde{A}_i \frac{\prod_{q=1}^{r_1} \exp(-\frac{|\hat{m}|_{1q}^2}{2\lambda_{1q}})}{\prod_{u=1}^{2m}\prod_{q=1}^{r_u}\tilde{a}_i\lambda_{uq}} \\ A &= \lim_{p\to\infty} \sum_{i=1}^{p} \tilde{A}_i' \end{aligned}$$

are independent of γ_b. Thus, MIMO-OFDM systems achieve the coding gain, $A^{-1/D_{\max}}$.

Importantly, note that the design criteria for mapping of symbols to antennas and subcarriers (sometimes referred to as the space-time-frequency coding) to minimize the PEP are usually obtained using the Chernoff upper-bound (5.17b). In particular, the rank criterion maximizes the diversity gain, and the determinant criterion maximizes the coding gain [91]. However, we can prove that exactly the same design criteria (formulated without assumption of asymptotically large SNR) as obtained for the Chernoff upper-bound of the PEP [91] can be also obtained for the exact PEP. Hence, we have the following lemma.

Lemma 5.1 *The rank and determinant criteria to maximize the diversity gain and the coding gain, respectively, of the space-time-frequency codes for MIMO-OFDM systems operating over correlated generalized Ricean fading channels are valid for the* exact *PEP,* $\mathrm{P}(\mathbf{X} \mapsto \hat{\mathbf{X}})$*, of the codewords,* $\mathbf{X}$*, and,* $\hat{\mathbf{X}}$*.*

Proof: Using (5.22), the exact PEP is computed as, $\mathrm{P}(\mathbf{X} \mapsto \hat{\mathbf{X}}) = \lim_{p\to\infty} \sum_{i=1}^{p} \mathrm{P}_i(\mathbf{X} \mapsto \hat{\mathbf{X}})$. The rank and determinant criteria of [91] are obtained by minimizing the particular PEP, $\mathrm{P}_i(\mathbf{X} \mapsto \hat{\mathbf{X}})$. Since such rank and determinant criteria are independent of i, they also minimize the exact PEP, $\mathrm{P}(\mathbf{X} \mapsto \hat{\mathbf{X}})$. ■

Recall that the rank, r_u, in each dimension, u, is constrained by the number of antennas, N_t, and, N_r, and the number of M-ary symbols, $S_u N_u$, in one codeword. The maximum diversity order of a single-input single-output frequency selective channel is equal to the number of multipath, L, provided that the paths are independent and $N_u \geq L$ [97], [98]. In this chapter, the paths are correlated, and thus, $r_u \leq N_t N_r S_u L$; in low mobility scenarios, the diversity order in the time domain, S_u, is reduced further. Also, assuming the PEP, $\mathrm{P}(\mathbf{c} \mapsto \hat{\mathbf{c}})$, of the binary codewords, $\mathbf{c}$, and, $\hat{\mathbf{c}}$, it can be shown that the BICM employing M-ary modulation can increase the achievable diversity order to $MD_{\min}$, and it is required that the minimum Hamming distance of the channel code, $d_{\min} \geq S_u L$, [98].

5.4 Numerical Results

We study the performance of an OFDMA system with transmitter diversity described in [89, 8.4.8]. In the downlink, we have $N_{\text{fft}} = 2048$, subcarriers having the frequency spacing, $\Delta f = 11.161$ kHz. The transmitter has $N_t = 4$ antennas, and the receiver has $N_r = 1$ antenna. The $K_c = 128$ information bits are encoded using the single parity code, $C_x = (6, 5, 2)$, and the shortened Hamming code, $C_y = (32, 26, 4)$, so that the overall code rate, $R_c = 2/3$, [89, 8.4.9.2.2]. The $N_c = 192$ encoded bits are block-interleaved [89, 8.4.9.3], and row-by-row Gray mapped to 16-QAM symbols [89, Fig. 263]. The codewords, $\mathbf{X}$, are periodically mapped to $S_u = 3$ consecutive OFDMA symbols and $N_u = 16$ subcarriers. We assume the subcarrier mapping (permutation), $\bar{n}(n) = n_{\text{offset}} + n \cdot n_{\text{step}}$, where $n_{\text{offset}} = n_{\text{step}} = 128$.

The Stanford University Interim (SUI) channel models have been approved for evaluation of fixed broadband wireless access systems having tens of MHz bandwidth, and operating in frequency bands between 1 and 4 GHz [101]. As an example, we consider the SUI-5 channel model for 30°

antenna radiation pattern and 50% cell coverage (i.e., guaranteed Ricean factor). The 3 taps have delays 0, 4 and 10 μs, power levels 0, -5 and -10 dB, and Doppler spreads 2, 1.5 and 2.5 Hz, respectively. The first path has non-zero Ricean factor, $K_r(1) = 8.45$ dB. A guard interval of $N_g = 256$ samples is used to completely cancel the interference from the multipath propagation. The RMS delay spread of 1.276 μs corresponds to a coherence bandwidth of about 70 subcarriers (note that $N_{\text{fft}}/70 \doteq 29$). The coherence time of thousands of OFDMA symbols makes the channel virtually constant over the transmission of one codeword and does not provide any time diversity. Hence, interleaving provides gain in spatial and frequency domains only. We assume constant correlations between transmitter antennas having the correlation factor, 0.9, and constant correlations between the paths having the correlation factor, 0.1. The fading autocorrelation given in [101, p. 9] is well approximated for small Doppler spreads by a constant correlation model having the correlation factor, 0.5837. In the simulation, we use filtering to obtain the desired correlations [101, p. 29]; the filters are normalized using lemma (L5) in Appendix G. Assuming that the number of degrees of freedom, $m = 2$, the amount of fading and Ricean factor is -15 and 11.6 dB, for System I, and -27 and 17.8 dB for System II.

Fig. 5.3 and Fig. 5.4 compare the probability of outage (5.15) for System I and System II, respectively. The simulation results are in excellent agreement with the analytical expression for System I; however, approximation (5.9) underestimates the probability of outage of System II by almost 2 dB. The Monte Carlo and union bound BER estimators (5.19) and (5.20) are compared in Fig. 5.5 and Fig. 5.6 assuming $q_{\max} = 10$ iterations. We observe that assuming the all-zero codeword was transmitted biases the BER estimator as expected. The truncated union bound (5.20) can predict well the decoded BER for larger values of SNR for System I; however, it underestimates the BER performance of System II by 2 dB for larger values of SNR. Importantly, note that while the Chernoff bound is loose for both systems and all values of SNR considered, the Prony approximation is in excellent agreement with the exact PEP computed using (5.18a) for all SNR values considered.

In general, the Chernoff upper bound is often used to assess the performances of communication systems. Although performance analysis using the Chernoff bound is simple, and can provide some limited design guidelines, such analysis is often inaccurate and can be biased as shown in Fig. 5.5 and Fig. 5.6. On the other hand, it is seen that the Prony approximation, which being a sum of exponentials approximation requires no more information than the Chernoff bound, is also simple to use, but has excellent accuracy. Since the MGF is often known even for cases of correlated channels, the Prony approximation method is very useful for obtaining a highly accurate performance analysis,

and in turn, design guidelines for communication systems operating over correlated fading channels with AWGN.

5.5 Summary

In this chapter, a framework to study the performance of bit-interleaved turbo product coded M-ary QAM MIMO-OFDM systems over arbitrary correlated generalized Ricean fading channels was investigated. A frequency domain equivalent system model assuming correlations between the transmitter and receiver antennas and between the paths of a frequency selective channel was developed. Orthogonal STBC and transmitter beamforming to maximize the SNR at a receiver antenna for OFDM signaling were considered. The MGF of the SNR at the input of the channel decoder was derived. The MGF was used to obtain the probability of outage, the PEP, and the BER for the two transmitter diversity OFDM schemes. Diversity gain and coding gain of MIMO-OFDM systems were derived. It was proved that the rank and determinant design criteria for space-time-frequency block coding are valid not only for the Chernoff bound of the PEP, but also for the exact PEP. Numerical examples indicate that approximate analysis of the system with transmitter beamforming using (5.9) underestimates the performance by 2 dB. Also, the assumption that the all-zero codeword was transmitted overestimates the performance by more than 1 dB. Finally, the computationally efficient Prony approximation method was found to be in excellent agreement with the exact PEP values for all values of SNR considered.

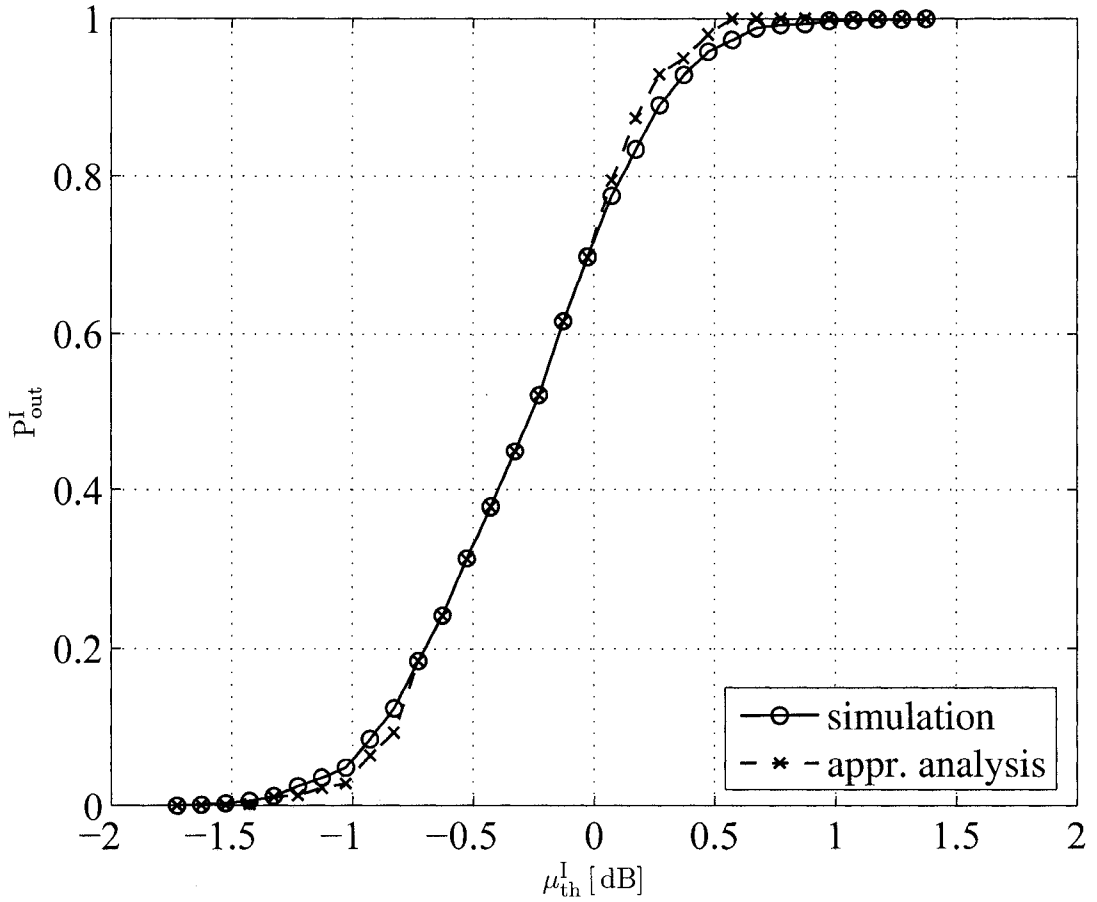

Figure 5.3: Probability of outage versus threshold, $\mu^{\mathrm{I}}_{\mathrm{th}}$ for System I.

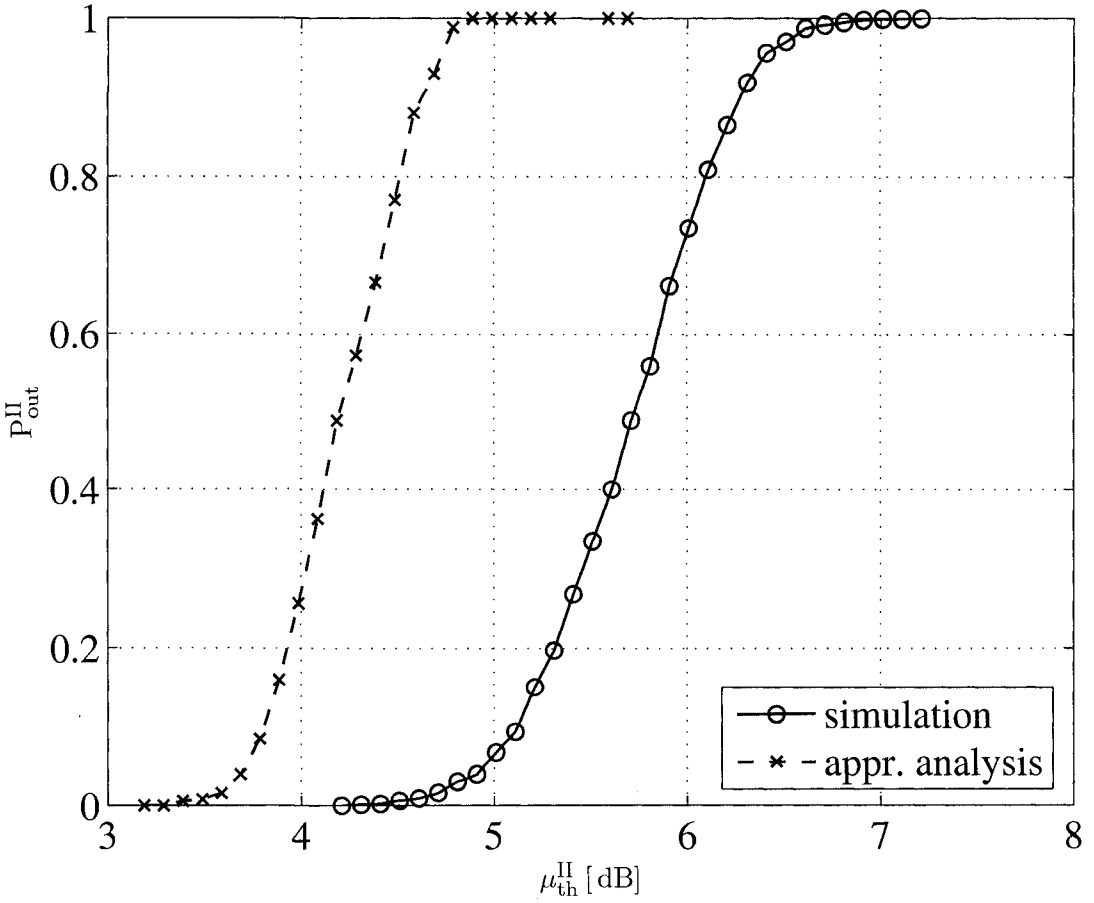

Figure 5.4: Probability of outage versus threshold, $\mu_{\text{th}}^{\text{II}}$ for System II.

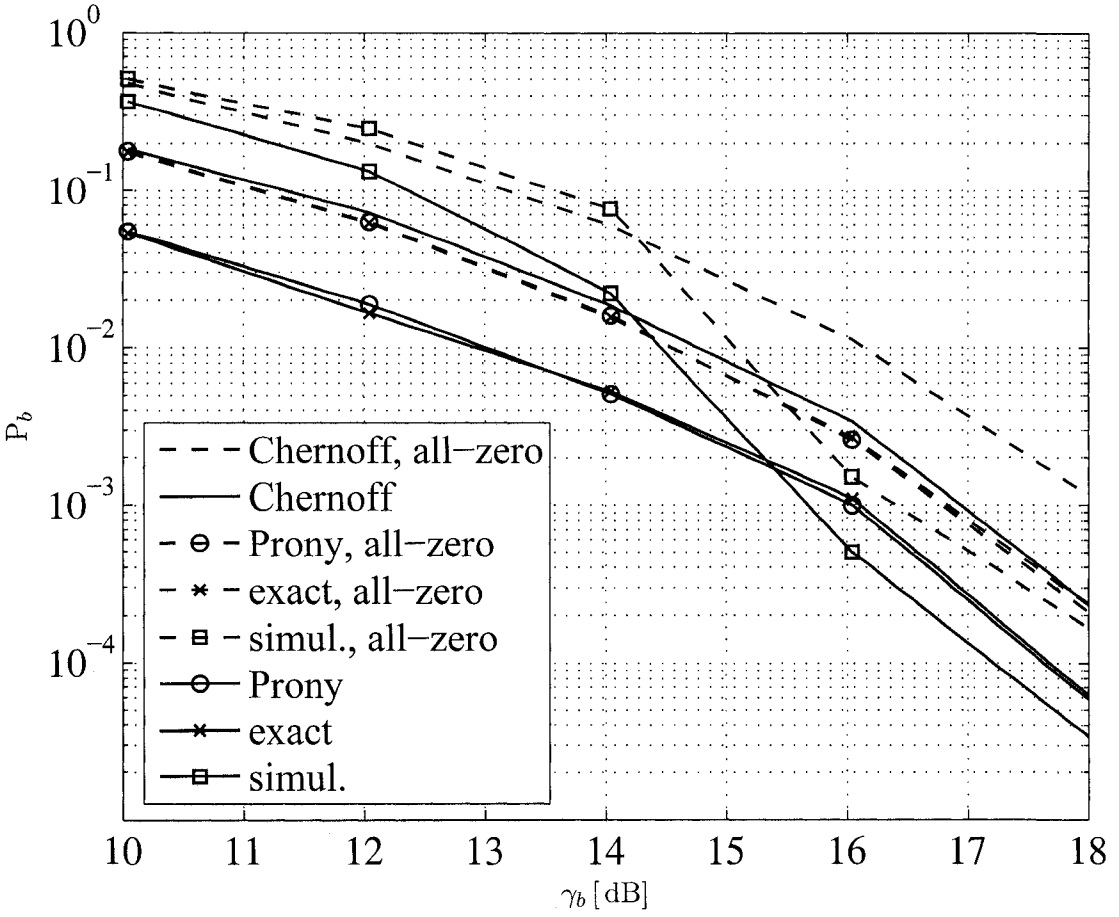

Figure 5.5: The BER union bounds and simulation results for System I.

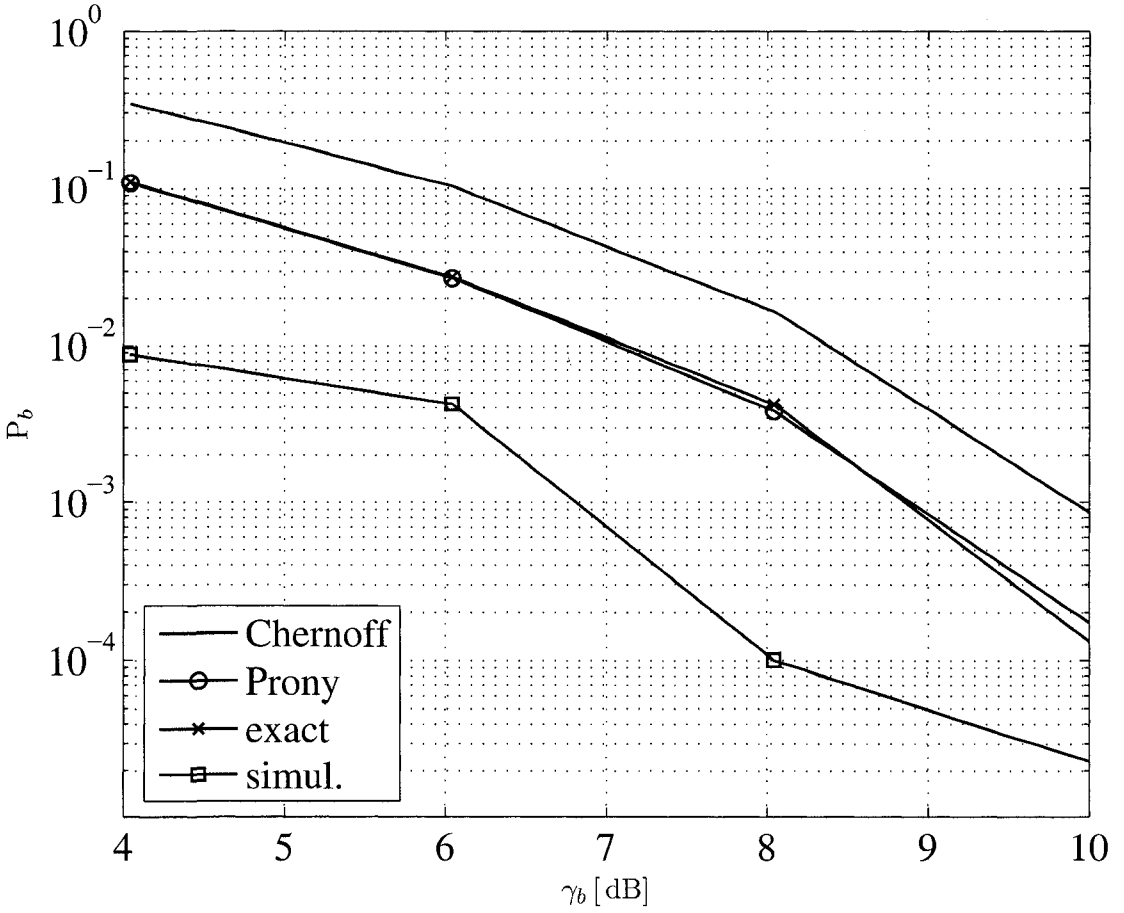

Figure 5.6: The BER union bounds and simulation results for System II.

Chapter 6

BER Analysis of Binary Hamming Codes

In this chapter, we show that binary Hamming codes can be constructed recursively. The recursive structure is then used to enumerate the input-output weights, and to compute the exact BER.

6.1 Background

Binary Hamming codes are the first known error correcting codes [106]. Nowadays, Hamming codes are used, for example, as forward-error correcting codes in the Bluetooth standard [107], and to protect data stored in semiconductor memories [108]. Hamming codes are well-suited for low-cost, low-power applications [109], and when used as component codes of a turbo product code and decoded iteratively, they can approach the capacity of an AWGN channel [110]. The Hamming codes are termed perfect codes (the equal-radius spheres around the codewords perfectly fill the entire vector space), and they meet the Hamming bound [111, p. 76].

We make an important observation that binary Hamming codes can be constructed recursively from binary block repetition codes with a parity bit. The recursive construction can be exploited to compute the input-output weight enumerator (IOWE) for any block-length whereas brute-force enumeration can only be used for short block-lengths. Although the IOWE function has been obtained recently in [112], the recursive evaluation of the IOWE presented in this chapter appears to be more computationally efficient. The IOWE can be used to implement encoding and decoding, and to evaluate the exact probability of decoded bit error for binary antipodal signaling and hard-decision demodulation over an AWGN channel. The numerically computed coding gain of the hard-decision

ML word-decoder (i.e., the decoder that maximizes the likelihood of the hard-decoded codewords) is shown not to be monotonic in the probability of bit error, but rather exhibits a minimum for a particular small value of the SNR. This contradicts statements found in the literature. Importantly, note that the probability of bit error curve of binary Hamming codes is monotonically increasing with SNR, and thus, there is a one-to-one mapping between the probability of bit error and SNR. Hence, monotonicity of the coding gain can be equivalently expressed in terms of SNR.

This chapter is organized as follows. In Section 6.2, we present a recursive construction of binary Hamming codes. The IOWE of binary Hamming codes is obtained in Section 6.3, and in Section 6.4, we use the IOWE to evaluate the exact BER. Extended binary Hamming codes are discussed in Section 6.5. The chapter is summarized in Section 6.6.

6.2 Code Construction

The binary Hamming code is denoted as $\mathscr{H}_m = (n, k, d_{\min})$ where $n = 2^m - 1$ is the codeword length, $k = 2^m - 1 - m$ is the code dimensionality (length of input information vector), $m = n - k \geq 2$ is the number of parity bits, and $d_{\min} = 3$ is the minimum Hamming distance between any two codewords [18]. In a systematic form, $\mathbf{G}_m = [\mathbf{I}_{(k)} \vdots \mathbf{P}_{(k,m)}] \in \mathbb{Z}_2^{(k,n)}$ is the generator matrix where $\mathbb{Z}_2 = \{0, 1\}$, $\mathbf{P}_{(k,m)} \in \mathbb{Z}_2^{(k,m)}$ is the parity matrix, $\mathbf{I}_{(k)} \in \mathbb{Z}_2^{(k,k)}$ is the identity matrix, and the corresponding parity check matrix is $\mathbf{H}_m = [\mathbf{P}_{(k,m)}^T \vdots \mathbf{I}_{(m)}]^T \in \mathbb{Z}_2^{(n,m)}$. The Hamming codes are single-error correcting and two-errors detecting perfect codes. Hence, the parity check matrix is composed of all non-zero m-tuples and can be readily rearranged into a systematic form. Denote the all-ones matrix as $\mathbf{1}$, and $\mathscr{H}_m = (n_1, k_1, 3)$, then $\mathscr{H}_{m+1} = (n_2, k_2, 3)$ has the generator matrix,

$$\mathbf{G}_{m+1} = \underbrace{\begin{bmatrix} \mathbf{I}_{(k_1)} & \mathbf{0}_{(k_1,m)} & \mathbf{0}_{(k_1,k_1)} \\ \mathbf{0}_{(m,k_1)} & \mathbf{I}_{(m)} & \mathbf{0}_{(m,k_1)} \\ \mathbf{0}_{(k_1,k_1)} & \mathbf{0}_{(k_1,m)} & \mathbf{I}_{(k_1)} \end{bmatrix}}_{\mathbf{I}_{(k_2)}} \underbrace{\begin{bmatrix} \mathbf{0}_{(k_1,1)} & \mathbf{P}_{(k_1,m)} \\ \mathbf{1}_{(m,1)} & \mathbf{I}_{(m)} \\ \mathbf{1}_{(k_1,1)} & \mathbf{P}_{(k_1,m)} \end{bmatrix}}_{\mathbf{P}_{(k_2,m+1)}}$$

and the parity check matrix,

$$\mathbf{H}_{m+1} = \underbrace{\begin{bmatrix} \mathbf{0}_{(1,k_1)} & \mathbf{1}_{(1,m)} & \mathbf{1}_{(1,k_1)} \\ \mathbf{P}_{(k_1,m)}^T & \mathbf{I}_{(m)} & \mathbf{P}_{(k_1,m)}^T \end{bmatrix}}_{\mathbf{P}_{(k_2,m+1)}^T} \underbrace{\begin{bmatrix} 1 & \mathbf{0}_{(1,m)} \\ \mathbf{0}_{(m,1)} & \mathbf{I}_{(m)} \end{bmatrix}^T}_{\mathbf{I}_{(m+1)}}$$

where

$$\begin{aligned} n_2 &= 2m + 2k_1 + 1 &= 2^{m+1} - 1 \\ k_2 &= 2^{m+1} - m - 2 &= n_1 + k_1. \end{aligned}$$

Based on the structure of the generator matrix, $\mathbf{G}_{m+1}$, we can show that the codewords of the $\mathscr{H}_{m+1}$ code can be constructed as a modulo 2 sum of the zero-padded codewords of the $\mathscr{H}_m$ code, and the block repetition code of rate $1/2$, $\mathscr{R}_2^k = (\mathbb{Z}_2^k, \mathbb{Z}_2^k) = (2k, k, 2)$ (i.e., the block of k information bits and its copy are concatenated), and appending a parity bit. This is proved in the following theorem.

Theorem 6.1 *The Hamming code* $\mathscr{H}_{m+1} = (\mathscr{H}_m \circ \mathbb{Z}_2^{(2^m-1)}, \pi) = \{(\mathbf{x} \circ \mathbf{y}, \pi(\mathbf{y})), \mathbf{x} \in \mathscr{H}_m, \mathbf{y} \in \mathbb{Z}_2^{(2^m-1)}\}$ *where the operator,* $\circ$*, combines the codewords as,*

$$\begin{aligned} \mathbf{x} \circ \mathbf{y} &= (x_0, x_1, \cdots, x_{n_1-1}) \circ (y_0, y_1, \cdots, y_{n_1-1}) \\ &= (y_0, \cdots, y_{n_1-1}, x_0 + y_0, \cdots, x_{n_1-1} + y_{n_1-1}) \\ &= (\mathbf{y}, \mathbf{x} + \mathbf{y}) \end{aligned}$$

and $n_1 = 2^m - 1$, $\pi(\mathbf{y}) = \sum_{i=0}^{n_1-1} y_i$ *is the even-parity bit, and all additions are modulo* 2.

Proof: Let the input information vector, $\mathbf{u}$, of the $\mathscr{H}_{m+1}$ code having dimensionality, $\dim(\mathbf{u}) = k_2$, be partitioned as $\mathbf{u} = (\mathbf{u}_1, \mathbf{u}_2, \mathbf{u}_3)$ where $\dim(\mathbf{u}_1) = \dim(\mathbf{u}_3) = k_1$ and $\dim(\mathbf{u}_2) = m$. Then, the codeword $\mathbf{u}\mathbf{G}_{m+1} = (\mathbf{u}_1 + \mathbf{u}_3 + \mathbf{u}_3, \mathbf{u}_2, \mathbf{u}_3 \vdots \pi(\mathbf{u}_2) + \pi(\mathbf{u}_3), \mathbf{u}_1\mathbf{P}_{(k_1,m)} + \mathbf{u}_2 + \mathbf{u}_3\mathbf{P}_{(k_1,m)})$. Hence, $\mathbf{x} = (\mathbf{u}_1 + \mathbf{u}_3, \mathbf{u}_1\mathbf{P}_{(k_1,m)} + \mathbf{u}_3\mathbf{P}_{(k_1,m)})$ is a codeword of the $\mathscr{H}_m$ code, and $(\mathbf{y}, \mathbf{y}) = (\mathbf{u}_3, \mathbf{u}_2, \mathbf{u}_3, \mathbf{u}_2)$ is the block repetition code $\mathscr{R}_2^{n_1}$ with the parity bit $\pi = \pi(\mathbf{y}) = \pi(\mathbf{u}_3) + \pi(\mathbf{u}_2)$. Finally, applying the operator, $\circ$, concludes the proof. ■

The construction using the operator, $\circ$, was introduced in [113, p. 447], and later used independently in [114, p. 717], and generalized in [115]. Similar to the construction of Theorem 6.1, Vasil'ev [116, p. 77] applies a strictly nonlinear mapping as the parity bit to construct perfect single-error correcting codes which are not equivalent to any linear code. However, the Vasil'ev construction using a linear mapping to generate binary Hamming codes is not considered in [116, p. 77]. The construction of Theorem 6.1 can be used for the encoding and decoding of Hamming codes as follows.

Proposition 6.2 *The Hamming code* $\mathscr{H}_{m+1}$ *can be encoded (decoded) using the encoder (decoder) for the code* $\mathscr{H}_m$.

Proof: Encoding proceeds directly according to Theorem 6.1. Assume a binary symmetric channel. We will show that one bit error in a $\mathscr{H}_{m+1}$ codeword can be corrected using the decoder for

the $\mathscr{H}_m$ code. Let $(\mathbf{x}, \mathbf{y}, \pi)$ be the transmitted binary codeword of the $\mathscr{H}_{m+1}$ code. In a systematic form, according to Theorem 6.1, let $\dim(\mathbf{x}) = \dim(\mathbf{y}) = 2^m - 1$ and $\dim(\pi) = 1$. Then, let $(\mathbf{x}', \mathbf{y}', \pi')$ be the corresponding received vector. If an error is within $(\mathbf{x}', \pi')$ bits, the even-parity of $(\mathbf{x}', \pi')$ is 1, and the nonzero syndrome $(\mathbf{x}' + \mathbf{y}')\mathbf{H}_m$ corresponds to the position of the error within $\mathbf{x}'$. Otherwise, the zero syndrome $(\mathbf{x}' + \mathbf{y}')\mathbf{H}_m$ indicates π' is in error. If an error is within $\mathbf{y}'$, the even-parity of $(\mathbf{x}', \pi')$ is zero, and the syndrome $(\mathbf{x}' + \mathbf{y}')\mathbf{H}_m$ corresponds to the position of the error within $\mathbf{y}'$. ■

Therefore, the encoding (decoding) of the Hamming code $\mathscr{H}_{m+1}$ can be done using the less complex encoder (decoder) for the Hamming code $\mathscr{H}_m$.

6.3 Input-Output Weight Enumerator

For convenience, we represent the IOWE [17, p. 513] of the code $(n, k, d_{\min})$ as the matrix $\mathbf{A}_{(\text{iowe})}$ having the o-th row and w-th column element, $[\mathbf{A}_{(\text{iowe})}]_{o,w}$, equal to the number of codewords of input information vector weight o and the total (output) weight w where $o = 0, 1, \cdots, k$ and $w = 0, 1, \cdots, n$. Note that $[\mathbf{A}_{(\text{owe})}]_w = [\mathbf{1}_{(1,k+1)}\mathbf{A}_{(\text{iowe})}]_w$ is the output weight enumerator which is well-known [18, p. 81]. The IOWE can be related to the input-redundancy weight enumerator (IRWE) [117] as $[\mathbf{A}_{(\text{irwe})}]_{o,p} = [\mathbf{A}_{(\text{iowe})}]_{o,o+p}$ where $p = (w - o) \in 0, 1, \cdots, m$ is the weight of parity check bits. Note also that contrary to the output weight enumerator, in general, even for a systematic representation, the code IOWE is not unique but depends on the form of the generator matrix. However, in the particular case of Hamming codes, the IOWE is unique.

The IOWE of the binary Hamming code $\mathscr{H}_m$ can be obtained by a brute-force method, say, for $m \leq 5$. For larger values of m (i.e., $m > 5$), recursive evaluation of the IOWE exploiting the recursive structure of binary Hamming codes is computationally efficient. The derivation is performed in the Appendix H using the following claims.

Claim 6.3 *The IOWE matrix of serially concatenated codes $\mathscr{C}_1$ and $\mathscr{C}_2$ having the IOWE matrices $\mathbf{A}^{\mathscr{C}_1}_{(\text{iowe})}$ and $\mathbf{A}^{\mathscr{C}_2}_{(\text{iowe})}$, respectively, is given by 2-dimensional (2D) convolution, i.e.,*

$$\mathbf{A}^{(\mathscr{C}_1,\mathscr{C}_2)}_{(\text{iowe})} = \mathbf{A}^{\mathscr{C}_1}_{(\text{iowe})} \otimes \mathbf{A}^{\mathscr{C}_2}_{(\text{iowe})}.$$

Proof: Let $\mathbf{x} \in \mathscr{C}_1$ have input and output weights o_1 and w_1, respectively. Similarly, $\mathbf{y} \in \mathscr{C}_2$ has weights o_2 and w_2. The serially concatenated codeword $(\mathbf{x}, \mathbf{y}) \in (\mathscr{C}_1, \mathscr{C}_2)$ has weights $o =$

$o_1 + o_2$ and $w = w_1 + w_2$. For every pair o and w, we sum over all permissible codewords $\mathbf{x}$ and $\mathbf{y}$, i.e.,

$$[\mathbf{A}_{(\text{iowe})}^{(\mathscr{C}_1,\mathscr{C}_2)}]_{o,w} = \sum_u \sum_v [\mathbf{A}_{(\text{iowe})}^{\mathscr{C}_1}]_{u,v} [\mathbf{A}_{(\text{iowe})}^{\mathscr{C}_2}]_{o-u,w-v}.$$

■

Claim 6.4 *If the all-ones vector is a codeword of a linear binary block code, then the IOWE matrix of the code is symmetric, i.e.,* $[\mathbf{A}_{(\text{iowe})}]_{o,w} = [\mathbf{A}_{(\text{iowe})}]_{k-o,n-w}$.

Proof: The code is linear, and hence, for every codeword, $\mathbf{c} \in \mathscr{C}$, there exists exactly one complementary codeword, $\bar{\mathbf{c}} \in \mathscr{C}$. ■

Corollary 6.5 $[\mathbf{A}_{(\text{iowe})}]_{0,0} = [\mathbf{A}_{(\text{iowe})}]_{k,n} = 1$.

Hence, the IOWE matrix, $\mathbf{A}_{(\text{iowe})}^{\mathscr{H}_{m+1}}$, of the $\mathscr{H}_{m+1} = (n_2, k_2, 3)$ code is constructed from the IOWE matrix, $\mathbf{A}_{(\text{iowe})}^{\mathscr{H}_m}$, of the $\mathscr{H}_m = (n_1, k_1, 3)$ code as,

$$\left[\mathbf{A}_{(\text{iowe})}^{\mathscr{H}_{m+1}}\right]_{o,w} = \begin{cases} 1 & \text{for } w=0, o=0 \text{ and } w=n_2, o=k_2 \\ \mathscr{A}(o, w, I_1', \mathbf{A}_{(\text{iowe})}^{\mathscr{H}_m}) + & \\ \quad + \mathscr{A}(o, w-1, I_1'', \mathbf{A}_{(\text{iowe})}^{\mathscr{H}_m}) & \\ \qquad \text{for} \quad w=3,4,\cdots,n_1 & \\ \qquad\quad o=\max(1, w-m-1), \cdots, w & \\ \left[\mathbf{A}_{(\text{iowe})}^{\mathscr{H}_{m+1}}\right]_{k_2-o,n_2-w} & \\ \qquad \text{for} \quad w = n_1+1, \cdots, n_2-3 & \\ \qquad\quad o = 0, 1, \cdots, k_2 & \\ 0 & \text{otherwise} \end{cases} \tag{6.1}$$

where

$$\mathscr{A}(o, w, I_1'', \mathbf{A}_{(\text{iowe})}^{\mathscr{H}_m}) =$$
$$= \sum_{x=\max(w-2m, o-m, 0)}^{\min(w, 2k_1, o)} \left\{ \binom{k_1}{x/2} \binom{m}{o-x} I_1'' + \binom{m}{o-x-\frac{w-x-m}{2}} 2^{k_1-1} I_2 + \right.$$
$$\left. + \sum_{v=3}^{n_1-3} \sum_{u=\max(1, v-m)}^{\min(v, k_1-1)} [\mathbf{A}_{(\text{iowe})}^{\mathscr{H}_m}]_{u,v} \, 2^{u-1} \binom{k_1-u}{\frac{x-u}{2}} \binom{m-v+u}{\frac{w-x-v+u}{2}} \binom{v-u}{o-x-\frac{w-x-v+u}{2}} I_3 \right\}$$

$$
\begin{aligned}
I_1' &= \delta_{o-x-\frac{w-x}{2}} \bmod_2(x+1) \times \\
&\quad \times \Big(\delta_{\bmod_4(x)} \bmod_2(o+1) + \delta_{\bmod_4(x-2)} \bmod_2(o) \Big) \\
I_1'' &= \delta_{o-x-\frac{w-x}{2}} \bmod_2(x+1) \times \\
&\quad \times \Big(\delta_{\bmod_4(x)} \bmod_2(o) + \delta_{\bmod_4(x-2)} \bmod_2(o+1) \Big) \\
I_2 &= \bmod_2(-x-1+k_1) \bmod_2(w-n_1-1) \times \\
&\quad \times \delta_{x-k_1} \delta_{w-x-m} \\
I_3 &= \bmod_2(-x-1+u) \bmod_2(w-v-1).
\end{aligned}
$$

Definitions of δ_a, $\bmod_b(a)$, and $\binom{a}{b}$ are given by (A-11)–(A-13), respectively, in Appendix A.

6.4 Probability of Decoded Bit-Error and Coding Gain

Assume binary antipodal signaling, an AWGN channel, hard-decision demodulation and complete (standard array) decoding. Then, for equally probable codewords, assuming the all-zeros codeword was transmitted (i.e., the code is linear), the average probability of decoded bit error is [116, p. 20], [17, p. 513], [111, p. 244], [3, p. 804],

$$
\mathrm{P}_b(e) = \frac{1}{k} \sum_{j=d_{\min}}^{n} B_j \Pr(j) \tag{6.2}
$$

where $B_j = \sum_{i=0}^{k} i \, [\mathbf{A}_{(\text{iowe})}]_{i,j}$ is the total weight of information bits in all codewords of weight j, and $\Pr(j)$ is the probability of decoding the codeword of Hamming weight j. The expression (6.2) implicitly assumes that the probability of decoding a particular codeword depends only on its Hamming weight. Thus, the expression (6.2) is also valid for binary antipodal signaling and perfectly quantized soft-decisions (the Euclidean distance is directly proportional to the Hamming distance). Note that $\sum_{j=d_{\min}}^{n} B_j = k\, 2^{k-1}$. In general, the expression (6.2) is difficult to evaluate. However, for the class of perfect codes, $\Pr(j)$ equals the probability that the codeword of weight j is the closest to the received word. In particular, $\Pr(j) = \sum_{d=0}^{\lfloor (d_{\min}-1)/2 \rfloor} \mathrm{P}_d^j$ where P_d^j is the probability that the received word is at Hamming distance d from a codeword of weight j. Assuming i out of j-ones bits and $(d-i)$ out of $(n-j)$-zeros bits are inverted giving the word at Hamming distance d from the original weight j word, then $\mathrm{P}_d^j = \sum_{i=0}^{d} p^{j+d-2i} q^{n-j+2i-d} \binom{j}{i} \binom{n-j}{d-i}$ where $p = \mathrm{Q}\left(\sqrt{2\frac{k}{n}\gamma_b} \right)$ is the probability of a bit error, $q = 1-p$, and γ_b is the SNR per uncoded antipodal

symbol [111, p. 244], [118]. For cyclic codes, the coefficients, B_j, can be also computed from the output weights using [119, eq. (13)] which can be used to obtain the exact probability of decoded bit-error [118], [120]. A tight upper-bound for the probability of decoded bit-error for binary perfect codes is given in [121].

The coding gain is defined as the decrease in the required average energy per transmitted bit for the coded systems to maintain a given average probability of decoded bit error as compared to an uncoded modulation scheme having the same data rate [17, p. 456], [111, p. 11]. The coding gains of selected Hamming codes are shown in Fig. 6.2 and Fig. 6.4. We observe that the coding gain attains a minimum at a particular small value of SNR for $m > 5$, and that the minimum coding gain is always negative. Interestingly, if R_m denotes the rate of the Hamming code $\mathscr{H}_m$, then the asymptotic coding gain at low SNR is approximately computed as $g_0 \doteq R_{m-1}$ for $m \geq 3$. The asymptotic coding gain at large values of SNR is known to be [17, eq. (10.89)],

$$g_\gamma \doteq R_m \left(d_{\min} - \frac{n \ln 2}{\gamma} \right) \text{ for } \gamma \gg 0.$$

It is commonly believed (or perhaps loosely stated) that coding gain monotonically increases with the probability of bit error. For example, Jacobs [122] expects the coding gain to increase with SNR (in the context of positive values of coding gain). Benedetto and Biglieri [17, p. 457] state explicitly that:

> *The coding gain increases with the signal-to-noise ratio, and tends (for SNR$\rightarrow$ 0 and hence for* $\mathrm{P}_b(e) \rightarrow 0$*) to an asymptotic value.*

Jovanović [123] conjectured that the coding gain might not be monotonic in SNR, however, only a trivial example of repetition coding is given where the coding gain monotonically decreases with increasing SNR. Fig. 6.4 provides counterexamples proving that coding gain is not necessarily a monotonically increasing function of the probability of bit error, although the gain is monotonically increasing with the probability of bit error in regions of positive coding gain. Note that Jovanović [123] also plots the coding gain versus SNR for Hamming codes $\mathscr{H}_3$ and $\mathscr{H}_4$, but for these codes and the SNR region chosen the minima cannot be observed.

6.5 Extended Hamming Codes

The extended Hamming code, $\mathscr{H}_m^{\mathrm{e}} = (2^{m-1}, 2^{m-1} - m, 4)$, is created from the Hamming code, $\mathscr{H}_{m-1}$, by appending an overall parity bit. Thus, the minimum Hamming distance, $d_{\min} = 4$, is

achieved if all columns of the parity check matrix are different and non-zero, and as well modulo 2 sums of all the parity check matrix column pairs and triplets are non-zero [111]. The extended Hamming codes are no longer perfect; for example, we can use the standard array [18] to show that some but not all double errors can be corrected. Therefore, the probabilities, $\Pr(j)$, are not easy to obtain, and thus, computation of the exact probability, $\mathrm{P}_b(e)$, using (6.2) is cumbersome. We prove the following theorem.

Theorem 6.6 *Extended binary Hamming codes attain the Hamming bound.*

Proof: Let $A(n, d_{\min})$ be the maximum number of codewords in a binary linear or nonlinear code for given length n and minimum distance $d_{\min}$. According to [124, Theorem 1], $A(n-1, 2\delta-1) = A(n, 2\delta)$, and hence, the Hamming bound from [111, p. 76] [18, p. 83] can be restated as

$$A(n, d_{\min}) \leq \begin{cases} 2^n V_2^{-1}(n, t) & d_{\min} - \text{odd} \\ 2^{n-1} V_2^{-1}(n-1, t) & d_{\min} - \text{even} \end{cases}$$

where $V_2(n, t) = \sum_{i=0}^{t} \binom{n}{i}$ is volume of the n-dimensional hypersphere of radius, $t = \lfloor \frac{d_{\min}-1}{2} \rfloor$. Thus, for extended binary Hamming codes, $A(n, d_{\min}) = 2^{n-1} V_2^{-1}(n-1, t) = 2^k$ where k is the length of input information vector. ■

The IOWE matrix, $\mathbf{A}^{\mathscr{H}_m^{\mathrm{e}}}$, $m > 3$, of extended Hamming code, $\mathscr{H}_m^{\mathrm{e}} = (n, k, 4)$, can be computed conditioned on knowledge of the IOWE matrix of the corresponding Hamming code, $\mathscr{H}_{m-1}$, i.e.,

$$\left[\mathbf{A}^{\mathscr{H}_m^{\mathrm{e}}}\right]_{o,w} = \left[\mathbf{A}^{\mathscr{H}_{m-1}}\right]_{o,\min(w,n-1)} + \left[\mathbf{A}^{\mathscr{H}_{m-1}}\right]_{o,\max(0,w-1)} (1 - \delta_{\mathrm{mod}_n(w)})$$

for $w = 0, 2, 4, \cdots, n$, and $o = 0, 1, 2, \cdots, k$. This can be rearranged into a more computationally efficient form,

$$\left[\mathbf{A}^{\mathscr{H}_m^{\mathrm{e}}}\right]_{o,w} = \begin{cases} 1 & \text{for } w = 0, o = 0 \text{ and } w = n, o = k \\ \left[\mathbf{A}^{\mathscr{H}_{m-1}}\right]_{o,w-1} + \left[\mathbf{A}^{\mathscr{H}_{m-1}}\right]_{o,w} & \text{for } \begin{matrix} w = 4, 6, \cdots, \frac{n}{2} \\ o = 1, 2, \cdots, k-1 \end{matrix} \\ \left[\mathbf{A}^{\mathscr{H}_m^{\mathrm{e}}}\right]_{k-o,n-w} & \text{for } \begin{matrix} w = \frac{n+2}{2}, \cdots, n-4 \\ o = 1, 2, \cdots, k-1 \end{matrix} \\ 0 & \text{for otherwise.} \end{cases}$$

6.6 Summary

The IOWE of binary Hamming codes was shown to be efficiently obtained using their recursive structure, and the fact that the IOWE of serially concatenated codes is given by $2D$-convolution. Knowledge of the IOWE can be used to compute the exact probability of decoded bit error of binary Hamming codes over AWGN channels using hard-decision demodulation. The numerically computed coding gains of Hamming codes using the hard-decisions and the ML word-decoder revealed a surprising fact that the coding gain is minimum for a particular value of the probability of bit error corresponding to a small value of SNR, and the minimum coding gain is always negative. Whether the coding gain is not monotonic in SNR for other types of decoders (e.g., the soft-decision decoding, and the ML bit-decoding) remains an open problem. Finally, it was proved that extended binary Hamming codes attain the Hamming bound.

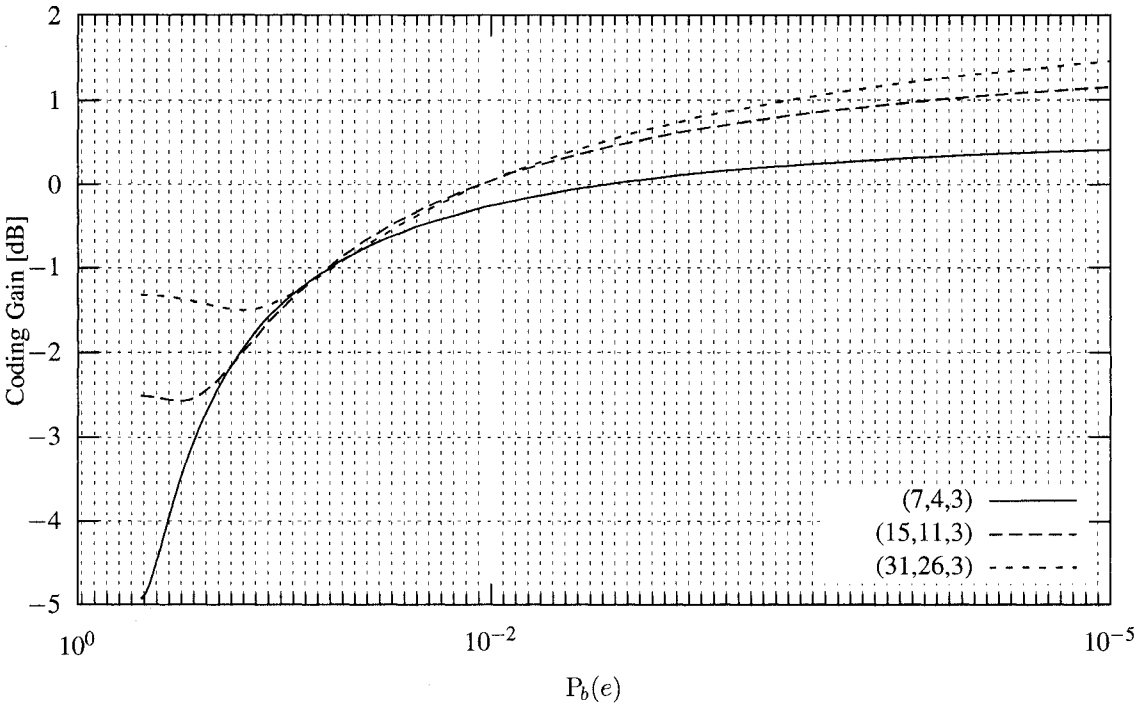

Figure 6.1: Coding gain of Hamming codes versus the probability of bit error, $P_b(e)$.

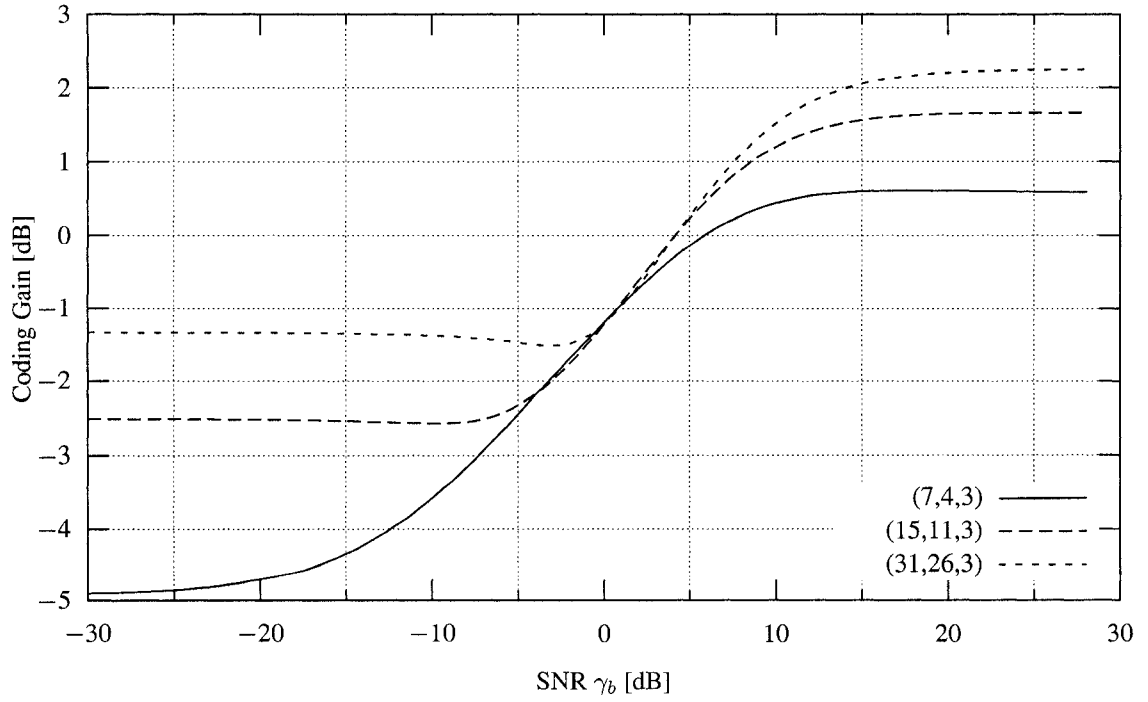

Figure 6.2: Coding gain of Hamming codes versus SNR per uncoded bit, γ_b.

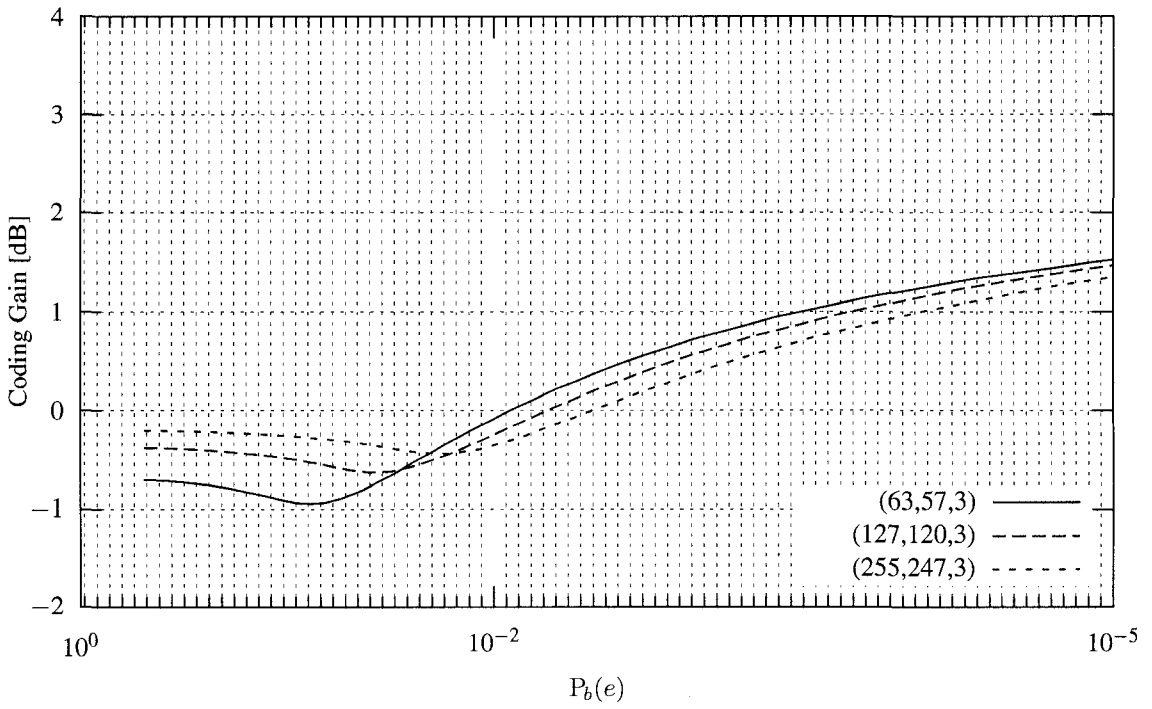

Figure 6.3: Coding gain of Hamming codes versus the probability of bit error, $P_b(e)$.

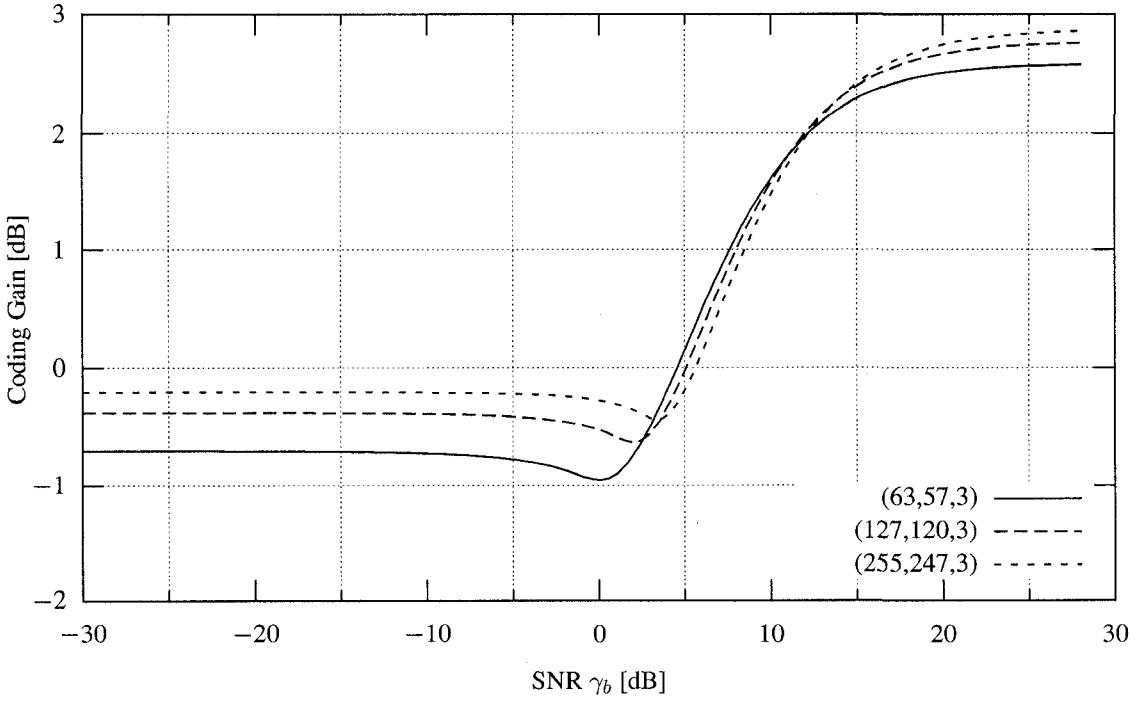

Figure 6.4: Coding gain of Hamming codes versus SNR per uncoded bit, γ_b.

Chapter 7

Improved Binary Repetition Codes

Improved binary repetition codes (IBRC's) are proposed in this chapter as an example of how the performance analysis can be used to obtain design guidelines. In particular, it was shown in Chapter 6 that binary Hamming codes can be constructed recursively. Furthermore, assuming the generator matrix, $\mathbf{G} = [\mathbf{I}|\mathbf{P}]$, of a systematic binary Hamming code, we can show that the parity matrix, $\mathbf{P}$, can be rearranged, so that its columns are the cyclic shifts of the generating column vector. Hence, in general, one can construct binary block codes assuming recursive (modulo 2) additions of the cyclic shifts of the input information vector.

In the first part of this chapter, we introduce a family of multidimensional binary block codes referred to as IBRC's. We study their properties, and consider some of their applications. In the second part of this chapter, we investigate a coded protocol employing IBRC's and SPC codes for uplink and downlink transmission in a network of cooperating nodes.

7.1 Multidimensional Improved Binary Repetition Codes, Properties and Applications

7.1.1 Background

Symbol repetitions are used when the cost and complexity of the encoding and decoding is a primary concern. Repetition coding is robust against impulsive noise [125], and is well suited for error control over fading channels [126]. The Hamming distance [126], [17] is well known to be a good design criterion for achieving diversity in fading channels. For BPSK signaling, the Euclidean distance is proportional to the Hamming distance, and we can expect good performance in fading

channels as well as AWGN channels [17, p. 720]. The minimum Hamming distance of block repetition codes can be increased using cyclic shifts of the input information vectors [127]. Such codes are sometimes referred to as IBRC's [128]. The generator matrix of these codes has a circulant structure. Binary cyclic matrices have many useful properties, and thus, they have been used to design forward error correction codes since the 60's. In particular, quasi-cyclic block codes maximize the minimum Hamming distance for a given block length [129], [116]. The tail-biting convolutional codes (CC's) avoid the rate loss of trellis termination by forcing the initial and ending states to be equal [130]. Computer search is usually employed to design quasi-cyclic and tail-biting codes exploiting their trellis structure [131], [132]. The tail-biting CC's for the product codes are considered in [133]. Low density parity check codes (LDPC's) based on circulant matrices were proposed in [134]– [136]. The quasi-cyclic LDPC codes and the repeat accumulate codes [137], [138] are designed to optimize iterative soft-decision decoding and to approach channel capacity. On the other hand, the IBRC's trade-off complexity of the encoding and decoding with the desired minimum Hamming distance using sequences of cyclic shifts of the variable-length input information vectors. Also, product codes in multiple dimensions [139] are used to increase the minimum Hamming distance at the cost of bandwidth expansion. The transmission bandwidth is not increased if one exploits multidimensional set partitioning and multilevel modulation schemes [140]. On the other hand, the multidimensional IBRC's preserve bandwidth while increasing the minimum Hamming distance by employing cyclic shifts in multiple dimensions.

In this section, we extend the IBRC's introduced in [128] to multiple dimensions, and then, investigate applications of such multidimensional IBRC's. We introduce two optimization criteria to design IBRC's in multiple dimensions. We show that the description of IBRC's using the cyclic shifts of the input information vectors simplifies searching for good codes. We present an efficient algorithm to design one (1D), two (2D) and three (3D) dimensional IBRC's. The proposed IBRC's are shown to support numerous applications. In particular, we employ the 1D IBRC's for adaptive coding, turbo product coding, retransmission schemes and multihop routing, and block differential encoding. We also apply the 2D and 3D IBRC's as the inner codes to concatenate the 1D codewords improving the overall minimum Hamming distance, and importantly, without increasing the transmission bandwidth. Finally, we use a truncated union bound of the BER after decoding to optimize distribution of the transmission energy over the codewords to improve the BER of IBRC's over AWGN as well as fading channels.

This section is organized as follows. Properties of binary cyclic matrices are discussed in Sec-

tion 7.1.2. Binary repetition codes in multiple dimensions are defined in Section 7.1.3. Examples of IBRC's are presented in Section 7.1.4. Applications of IBRC's are considered in Section 7.1.5. The transmission energy optimization is investigated in Section 7.1.6.

7.1.2 Binary Cyclic Matrices

We investigate the properties of binary cyclic matrices. All operations are assumed over a binary Galois field, GF(2). Hence, define the $(k \times k)$ permutation matrix,

$$\mathbf{J}_{(k)} = \begin{bmatrix} \mathbf{0}^T_{(1,k-1)} & \mathbf{I}_{(k-1)} \\ 1 & \mathbf{0}_{(1,k-1)} \end{bmatrix} \in \mathbb{Z}_2^{k \times k}$$

where $\mathbb{Z}_Q = \{0, 1, \cdots, Q-1\}$, $\mathbf{0}_{(1,k-1)} \in \mathbb{Z}_2^{1\times(k-1)}$ is the all-zero row vector, $\mathbf{I}_{(k-1)} \in \mathbb{Z}_2^{k\times k}$ is the identity matrix, and $\mathbf{J}^T_{(k)}\mathbf{J}_{(k)} = \mathbf{J}_{(k)}\mathbf{J}^T_{(k)} = \mathbf{I}_{(k)}$ where T denotes the vector transpose. Then, the a-th cyclic shift, $a = 0, 1, 2, \cdots$, of the vector, $\mathbf{u} = (u_0, u_1, \cdots, u_{k-1})$, can be written as the product, $\mathbf{u}\,\mathbf{J}^a_{(k)} = (u_{k-\mathrm{mod}_k(a)}, \cdots, u_{k-1}, u_0, \cdots, u_{k-\mathrm{mod}_k(a)-1})$, where $\mathrm{mod}_k(a) = a - \left\lfloor \frac{a}{k} \right\rfloor k$, and $\lfloor \cdot \rfloor$ is the floor function. We have the following definition.

Definition 7.1 *The $k \times k$ binary cyclic matrix, $\mathbf{A} \in \mathbb{Z}_2^{k\times k}$, generated by the vector of cyclic shifts, $\mathbf{a} = (a_0, \cdots, a_{K-1})$, where $0 \le a_0 < a_1 < \cdots < a_{K-1}$, can be written as, $\mathbf{A} = \sum_{i=0}^{K-1} \mathbf{J}^{a_i}_{(k)}$.*

Note that the cyclic shifts, a_i, are considered modulo k. Thus, the generating vector, $\mathbf{a}$, can be normalized, so that, $a_0 = 0$. For example, let the generating vector, $\mathbf{a}' = (a + a_0, a + a_1, \cdots, a + a_{K-1})$, $a \ge 0$, correspond to the cyclic matrix, $\mathbf{A}' = \mathbf{J}^a_{(k)} \sum_{i=0}^{K-1} \mathbf{J}^{a_i}_{(k)} = \mathbf{J}^a_{(k)}\mathbf{A}$; then the value, $a = k - a_0$, normalizes the vector, $\mathbf{a}'$. Note also that the permutation matrix, $\mathbf{J}_{(k)}$, is cyclic having the generating vector, $\mathbf{a} = (1)$, and the identity matrix $\mathbf{I}_{(k)}$, is cyclic having the generating vector, $\mathbf{a} = (k)$, i.e, $\mathbf{I}_{(k)} = \mathbf{J}^k_{(k)}$.

Let $\mathbf{u} \in \mathbb{Z}_2^k$ and $\mathbf{v} \in \mathbb{Z}_2^k$ be binary row vectors. Let $\mathbf{A}_1 \in \mathbb{Z}_2^{k\times k}$ and $\mathbf{A}_2 \in \mathbb{Z}_2^{k\times k}$ be binary cyclic matrices. In general, we denote by $\mathbf{u}_i$ the i-th component of a vector, $\mathbf{u}$, and we omit the dimension index, k, in denoting the matrices, $\mathbf{I}_{(k)}$, and, $\mathbf{J}_{(k)}$. We have the following properties.

Property 7.2 *The product, $\mathbf{v} = \mathbf{u}\mathbf{A}$, corresponds to a cyclic convolution, $\mathbf{v}_i = \sum_{j=0}^{k-1} \mathbf{u}_j [\mathbf{A}]_{0,\mathrm{mod}_k(i-j)}$, of the polynomials, $u(Z) = \sum_{i=0}^{k-1} u_i Z^i$, and, $A(Z) = \sum_{i=0}^{K-1} Z^{a_i}$, where Z is a dummy variable. Hence, the vector, $\mathbf{v}$, is a sum of K vectors, $\mathbf{u}$, cyclically shifted by a_i bits, i.e., $\mathbf{v} = \sum_{i=0}^{K-1} \mathbf{u}\mathbf{J}^{a_i}$.*

Property 7.3 *The sum,* $\mathbf{A} = \mathbf{A}_1 \oplus \mathbf{A}_2$*, and the product,* $\mathbf{A} = \mathbf{A}_1\mathbf{A}_2$*, are cyclic matrices. Also, if* $\mathbf{A} = \mathbf{A}_1 \oplus \mathbf{A}_2$*, or* $\mathbf{A} = \mathbf{A}_1\mathbf{A}_2$*, and* $\mathbf{A}$ *and* $\mathbf{A}_1$ *are cyclic, then* $\mathbf{A}_2$ *is cyclic.*

Property 7.3 can be obtained using the cyclic convolution Property 7.2.

Property 7.4 *If there exists a matrix,* $\mathbf{A}^\dagger$*, such that* $\mathbf{A}^\dagger\mathbf{A} = \mathbf{A}\mathbf{A}^\dagger = \mathbf{I}$*, and* $\mathbf{A}$ *is cyclic, then* $\mathbf{A}^\dagger$ *is cyclic.*

Property 7.4 follows using Property 7.3 and the fact that $\mathbf{I}$ is a cyclic matrix. Consequently, $\mathbf{A}_2 = \mathbf{A}_1^\dagger\mathbf{A}$ is a cyclic deconvolution of $\mathbf{A} = \mathbf{A}_1\mathbf{A}_2$.

Property 7.5 *If the determinant,* $\det(\mathbf{A}) \neq 0$*, and thus, (algebraic) matrix inverse,* $\mathbf{A}^{-1}$*, exists, then, in some cases,* $\mathbf{A}^\dagger$ *can be efficiently computed as,* $\mathbf{A}^\dagger = \mathrm{mod}_2\big(\lfloor \mathbf{A}^{-1}\det(\mathbf{A}) \rceil\big)$*, where* $\lfloor\cdot\rceil$ *denotes the rounding function.*

Note that, if $\mathrm{mod}_2\big(\lfloor \mathbf{A}^{-1}\det(\mathbf{A}) \rceil\big) = \mathbf{1}$ (the all-ones matrix), then it indicates that the inversion using Property 7.5 has failed. It is not known whether the inversion, $\mathrm{mod}_2\big(\lfloor \mathbf{A}^{-1}\det(\mathbf{A}) \rceil\big)$, fails for every matrix, $\mathbf{A}$, that is not invertible over $\mathbb{Z}_2^{k\times k}$.

Property 7.6 *If* $\mathbf{A}^\dagger$ *exists, then* $\mathbf{v} = \mathbf{u}\mathbf{A}$ *is a one-to-one mapping referred to as the permutation.*

Finally, the following three parameters are useful for characterizing cyclic matrices.

Definition 7.7 *Let the cyclic matrix,* $\mathbf{A} \in \mathbb{Z}_2^{k\times k}$*, be generated by the vector,* $\mathbf{a} = (a_0, \cdots, a_{K-1})$*, of length,* K*, where* $0 \leq a_0 < \cdots < a_{K-1} < k$*, i.e.,* $a_i = \mathrm{mod}_k(a_i)$*. Then, we can define the following three parameters to describe the cyclic matrix,* $\mathbf{A}$*, i.e.,*

$$\begin{aligned} &\textit{constraint weight:} && K_{\mathbf{a}} &&= K \\ &\textit{constraint length:} && \nu_{\mathbf{a}} &&= a_{K-1} - a_0 \\ &\textit{span:} && \mu_{\mathbf{a}} &&= \nu_{\mathbf{a}} + 1. \end{aligned}$$

The parameters given in Definition 7.7 are directly related to the complexity of encoding and decoding, provided that the matrix, $\mathbf{A}$, or, equivalently, the vector of the cyclic shifts, $\mathbf{a}$, are used to generate the codewords. The properties of binary cyclic matrices are used to define multidimensional IBRC's and their properties.

7.1.3 Multidimensional IBRC's

We define IBRC's in multiple dimensions and their design criteria. Let $C = (n, k, d_{\min})$ denote a linear binary block code of dimension, k, block length, n, code rate, $R = k/n$, and minimum Hamming distance, $d_{\min}$. Let $\mathbf{u} \in \mathbb{Z}_2^k$ denote the input information vector, and let $\mathbf{c} \in \mathbb{Z}_2^n$ be the corresponding codeword. We consider D-dimensional linear codes defined over a D-dimensional binary Galois field, GF(2). In particular, let the D-dimensional matrix of the input information bits be written as, $\mathbf{u} = (\mathbf{u}_1, \mathbf{u}_2, \cdots, \mathbf{u}_M)$, where $\mathbf{u}_i \in \mathbb{Z}_2^{k_1 \times k_2 \times \cdots \times k_D}$, $i = 1, 2 \cdots, M$, $M \geq 1$, and thus, the overall code dimension is, $k = M \prod_{i=1}^{D} k_i$. The codewords of the D-dimensional code, $\mathscr{C}^{(D)} = (n, k, d_{\min})$, are written as, $\mathbf{c} = (\mathbf{c}_1, \mathbf{c}_2, \cdots, \mathbf{c}_{L+1})$, where $\mathbf{c}_i \in \mathbb{Z}_2^{n_1 \times n_2 \times \cdots n_D}$, $i = 1, 2, \cdots, (L+1)$, $L \geq 1$, and the overall code block length is, $n = (L+1) \prod_{i=1}^{D} n_i$. The D-dimensional mapping, $\mathscr{C}^{(D)} : \mathbf{u} \mapsto \mathbf{c}$, from input information bits to codewords is assumed to be linear, and is given by a set of D mappings, $\mathscr{C}_d$, corresponding to D dimensions, $d = 1, 2, \cdots, D$, i.e., $\mathscr{C}^{(D)} = \mathscr{C}_1 \circ \cdots \circ \mathscr{C}_D$. Hence, the mappings, $\mathscr{C}_d$, are linear binary codes, for all dimensions, d. Correspondingly, we define the D-dimensional codes considered in this chapter as follows.

Definition 7.8 *Let $\mathscr{C}^{(D)}$ be a linear D-dimensional code, such that, $\mathscr{C}^{(D)} = \mathscr{C}_1 \circ \cdots \circ \mathscr{C}_D$, where $\mathscr{C}_1 = ((L+1)n_1, M\,k_1, d_{\min 1})$ is a linear binary code of rate, $R_1 = (M/(L+1))k_1/n_1$, corresponding to dimension, $d = 1$, and $\mathscr{C}_d = (n_d, k_d, d_{\min d})$ are linear binary codes of rate, $R_d = k_d/n_d$, corresponding to dimensions, $d \geq 2$. Then, $\mathscr{C}^{(D)}$ is a linear D-dimensional product code of rate, $R^{(D)}$, and the minimum Hamming distance, $d_{\min}^{(D)}$, given as [139],*

$$\begin{aligned} R^{(D)} &= \frac{M}{L+1} \prod_{d=1}^{D} \frac{k_d}{n_d} \\ d_{\min}^{(D)} &= \prod_{d=1}^{D} d_{\min d}. \end{aligned}$$

Multidimensional IBRC's are then defined assuming Definition 7.8 and the following constraints.

Definition 7.9 *A multidimensional IBRC, $\mathscr{C}^{(D)-\text{IBRC}}$, is constructed using a 1D IBRC, $\mathscr{C}_1^{\text{IBRC}} = ((L+1)k, Mk, d_{\min 1})$, of rate, $R_1 = M/(L+1)$, and using $(D-2)$ permutations, $\mathscr{C}_d = (k, k, 1)$, for dimensions, $d \geq 2$. The code, $\mathscr{C}^{(D)-IBRC}$, has rate, $R^{(D)-\text{IBRC}}$, and the minimum Hamming distance, $d_{\min}^{(D)-\text{IBRC}}$, given as,*

$$R^{(D)-\text{IBRC}} = \prod_{d=1}^{D} R_d = R_1 = \frac{M}{L+1}$$

$$d_{\min 1} \leq d_{\min}^{(D)-\mathrm{IBRC}} \leq \prod_{d=1}^{D} d_{\min d}.$$

Importantly, comparing Definition 7.8 and Definition 7.9, we observe that the D-dimensional product codes achieve a large minimum Hamming distance at the cost of bandwidth expansion. On the other hand, we can show that, for sufficiently large dimensions, k_d, $d = 1, \cdots, D$, the D-dimensional IBRC's can achieve the same minimum Hamming distance as the D-dimensional binary product codes, however, the bandwidth of the D-dimensional IBRC's depends only on the rate of the coding scheme employed in the first dimension, i.e., for $d = 1$. Hence, although the D-dimensional IBRC's can be used to obtain the same minimum Hamming distance as the product codes, i.e., $d_{\min}^{(D)} = \prod_{d=1}^{D} d_{\min d}$, and without bandwidth expansion, it is often sufficient to design D-dimensional IBRC's having the minimum Hamming distance, such that, $d_{\min 1} \ll d_{\min}^{(D)-\mathrm{IBRC}}$, and, $d_{\min}^{(D)-\mathrm{IBRC}} < d_{\min}^{(D)}$.

The generator matrix of the code, $\mathscr{C}_1^{\mathrm{IBRC}}$, in the first dimension, i.e., for $d = 1$, is constructed using several cyclic matrices [128]. On the other hand, the generator matrices of the codes, $\mathscr{C}_d$, for dimensions, $d \geq 2$, are cyclic matrices. Thus, after the first encoding in dimension, $d = 1$, the encoded bits are only permuted across dimensions, $d = 2, \cdots, D$, in order to increase the minimum Hamming distance of the code. Furthermore, since permutation of bits across dimensions, $d = 2, \cdots, D$, does not produce any additional parity bits, the bandwidth of the code is not increased by encoding, $\mathscr{C}_d$, in dimensions, $d \geq 2$; see Property 7.6. Also, we can show that the minimum Hamming distance of the D-dimensional IBRC's is upper-bounded as,

$$d_{\min}^{(D)} \leq 1 + \prod_{d=1}^{D} K_d$$

where K_d are the constraint weights of the binary cyclic matrices, $\mathbf{A}_d$, that are used for encoding and permutation of bits across dimensions, d. More generally, the code, $\mathscr{C}_1$, corresponding to the first dimension, i.e., for $d = 1$, can be any 1D binary block code. Then, we have the following important application of Definition 7.9.

Definition 7.10 *The set of $\prod_{j=2}^{D} k_d$ 1D codewords of equal block length, n_1, generated by a code, $\mathscr{C}_1 = (n_1, k_1, d_{\min 1})$, can be compounded using permutations of these codewords across dimensions, $d = 2, \cdots, D$.*

Note that the construction of the D-dimensional block code given in Definition 7.10 increases the overall minimum Hamming distance of compounded $1D$ codewords without increasing the transmission bandwidth. Hence, assuming the properties of binary cyclic matrices and using Definition 7.1–Definition 7.10, we can define the design criteria of multidimensional IBRC's.

Design Criteria for Multidimensional IBRC's

In general, the codes based on circulant matrices can be formally described using a regular trellis, or using a quasi-cyclic parity check matrix. Design criteria of these codes are chosen for a specific application at hand. Hence, we extend definitions of the parameters in Definition 7.7, for the case of D-dimensional IBRC's, so that,

$$\begin{array}{lrcl} \text{constraint weight:} & K^{(D)-\text{IBRC}} & = & \sum_{d=1}^{D} K_d \\ \text{constraint length:} & \nu^{(D)-\text{IBRC}} & = & \sum_{d=1}^{D} \nu_d \\ \text{span:} & \mu^{(D)-\text{IBRC}} & = & \sum_{d=1}^{D} \mu_d = \nu^{(D)-\text{IBRC}} + K. \end{array}$$

Provided that more than one cyclic matrix is used for permutation of bits in a particular dimension, d, then the constraint weight, K_d is given by a maximum constraint weight used in dimension, d. Similarly, the constraint length, ν_d, in dimension, d, is given by a maximum value of constraint length employed in dimension, d.

Consider a cyclic matrix, $\mathbf{A}$, generated by the vector, $\mathbf{a} = (a_0 = 0, a_1, \cdots, a_{K-1})$. Such a matrix has the constraint length, $\nu = a_{K-1}$. Since multiplication of a cyclic matrix and a vector corresponds to cyclic convolution, we can use a trellis having 2^{ν} states to describe encoding and decoding of D-dimensional IBRC's. Note that the last a_{K-1} rows of the matrix, $\mathbf{A}$, correspond to the input information bits that return the encoder either to its initial state (cf. the tail-biting codes [130]), or to the all-zero state (cf. trellis termination). Correspondingly, for D-dimensional IBRC's, the complexity of the encoding and optimum (maximum-likelihood sequence) decoding using the trellis representation is given by the total constraint length, i.e., $\nu^{(D)-\text{IBRC}} = \sum_{d=1}^{D} \nu_d$. In this case, the design criterion of D-dimensional IBRC's is written as,

$$\begin{aligned} & \max_{\{\mathbf{A}_d\}_d} d_{\min}^{(D)-\text{IBRC}} \\ \text{s.t.} \quad & d_{\min}^{(D)-\text{IBRC}} \geq d_{\min}^{*} \\ & \nu^{(D)-\text{IBRC}} \leq \nu_{\max} \\ & \mathbf{k} \in \mathbf{\Omega}_{\mathbf{k}}. \end{aligned} \tag{7.1}$$

Hence, the minimum Hamming distance, $d_{\min}^{(D)-\text{IBRC}}$, is maximized over the set of cyclic matrices, $\mathbf{A}_d \in \mathbb{Z}_2^{k_d \times k_d}$, that are used to generate the codewords of a D-dimensional IBRC subject to (s.t.) the lower-bound on the desired minimum Hamming distance, $d_{\min}^*$, the upper-bound on the constraint length, $\nu_{\max}$ (corresponding to the maximum complexity of the encoding and decoding), and the vector of input dimensions, $\mathbf{k} = (k_1, \cdots, k_D)$, to be in the set of feasible dimensions, $\mathbf{\Omega_k}$, so that $d_{\min}^{(D)-\text{IBRC}} \geq d_{\min}^*$ is achievable. We can approximate the set, $\mathbf{\Omega_k}$, using the component-wise inequalities, i.e., let $\mathbf{\Omega_k} = \{\mathbf{k} : \mathbf{k} \geq \mathbf{k}_0\} = \{\mathbf{k} : k_1 \geq k_{01}, k_2 \geq k_{02}, \cdots, k_D \geq k_{0D}\}$. Note that, for a suboptimum multistage decoding (i.e., the independent decoding of all dimensions), the optimization (7.1) is subject to a complexity constraint, $\max_d \nu_d \leq \nu_{\max}$.

Also, one can consider multidimensional IBRC's to be modulo 2 sums of the cyclically shifted input information vectors. In this case, the complexity of the encoding and decoding is given by the constraint weight, $K^{(D)-\text{IBRC}} = \sum_{d=1}^{D} K_d$, and the design criterion is,

$$\begin{aligned} &\max_{\{\mathbf{A}_d\}_d} d_{\min}^{(D)-\text{IBRC}} \\ \text{s.t.} \quad &d_{\min}^{(D)-\text{IBRC}} \geq d_{\min}^* \\ &K^{(D)-\text{IBRC}} \leq K_{\max} \\ &\mathbf{k} \in \mathbf{\Omega_k}. \end{aligned} \tag{7.2}$$

Hence, the minimum Hamming distance, $d_{\min}^{(D)-\text{IBRC}}$, is maximized subject to the upper-bound on the constraint weight, $K_{\max}$. Again, for a suboptimum multistage decoding, optimization (7.2) is subject to the complexity constraint, $\max_d K_d \leq K_{\max}$. Importantly, since typically, $K_d \ll \nu_d$, the design of multidimensional IBRC's using optimization (7.2) leads to less complex cyclic shifts based encoding and decoding than when using optimization (7.1) and the trellis based encoding and decoding; hence, in this chapter, we consider the design (7.2). Furthermore, optimization (7.2) trades-off $d_{\min}^{(D)-\text{IBRC}}$ with the complexity of the encoding and decoding.

It is useful to consider a universal design for obtaining the desired minimum Hamming distance, $d_{\min}^{(D)-\text{IBRC}}$, by lengthening and shortening of the generating vectors, $\mathbf{a}_d = (a_{d0}, a_{d1}, \cdots, a_{d(K_d-1)})$, corresponding to the cyclic matrices, $\mathbf{A}_d$. In particular, while lengthening of the vector, $\mathbf{a}_d$, appends a component, $a_{dK_d} > a_{d(K_d-1)}$, to $\mathbf{a}_d$, shortening of the vector, $\mathbf{a}_d$, removes the component, $a_{d(K_d-1)}$, from $\mathbf{a}_d$. In general, lengthening of the vector, $\mathbf{a}_d$, increases $d_{\min}^{(D)-\text{IBRC}}$, and shortening of the vector, $\mathbf{a}_d$, decreases $d_{\min}^{(D)-\text{IBRC}}$, and also, the complexity of the encoding and decoding. It is desirable that lengthening and shortening of the vectors, $\mathbf{a}_d$, is mutually independent between

dimensions, d. We can use the following procedure to obtain the generating vectors, $\mathbf{a}_d$.

Algorithm 7.11

1. *initialize* $\mathbf{a}_d = (a_{d0})$ *where* $a_{d0} \geq 0$, $K_d = 1$, *and* $d_{\min}^{(D)-\mathrm{IBRC}} = 1$
2. *for* $\Delta > 0$, *select the dimension,* $\hat{d}$, *and find,* $a_{\hat{d}K_{\hat{d}}}$, *such that,* $(a_{\hat{d}K_{\hat{d}}} - a_{\hat{d}(K_{\hat{d}}-1)}) \leq \Delta$, *and* $d_{\min}^{(D)-\mathrm{IBRC}}$ *is increased; then let* $\mathbf{a}_{\hat{d}} := (\mathbf{a}_{\hat{d}}, a_{\hat{d}K_{\hat{d}}})$, *and* $K_{\hat{d}} := K_{\hat{d}} + 1$
3. *when no such* $a_{\hat{d}K_{\hat{d}}}$ *exists for a given,* Δ, *either use another* $a_{\hat{d}(K_{\hat{d}}-1)}$ *of* $\mathbf{a}_{\hat{d}}$, *or select another dimension,* $\hat{d}$, *or increase the dimensions,* $\mathbf{k}$, *or increase* Δ
4. *repeat the search in step* 2 *until the code of* $d_{\min}^{(D)-\mathrm{IBRC}} \geq d_{\min}^{*}$ *is found*

Thus, the components are added to the vectors, $\mathbf{a}_d$, recursively until the desired minimum Hamming distance, $d_{\min}^{*}$, is reached. Note that, for every candidate set of generating sequences, $\{\mathbf{a}_d\}_d$, we have to evaluate the corresponding minimum Hamming distance, $d_{\min}^{(D)-\mathrm{IBRC}}$. The efficient evaluation of $d_{\min}^{(D)-\mathrm{IBRC}}$ enumerates small weights input information vectors [128], [129]. Hence, it is useful to systematically generate binary vectors of given weight. In particular, let the input information vector of dimension, k, and weight, o, corresponding to the l-th ordered combination of o out of k elements, for $l = 1, \cdots, \binom{k}{o}$, have the "1" bits in the positions, $\mathbf{b} = (b_0, b_1, \cdots, b_{o-1}) \in \mathbb{Z}_k^o$. We can show that the combination number, l, can be computed from the "1" bits positions, $\mathbf{b}$, as,

$$\begin{aligned} l \;=\; & \sum_{i=1}^{b_0} \binom{k-i}{o-1} + \sum_{i=1}^{b_1-b_0-1} \binom{k-1-b_0-i}{o-2} + \cdots \\ & + \sum_{i=1}^{b_{o-2}-b_{o-3}-1} \binom{k-1-b_{o-3}-i}{1} + b_{o-1} - b_{o-2}. \end{aligned}$$

On the other hand, the vector of "1" bits positions, $\mathbf{b}$, can be obtained from the combination number, l, using the following algorithm.

Algorithm 7.12 ***Input:*** k, o, l ***Output:*** $\mathbf{b}$

! *find the* l*-th combination* o *out of* k

$s := 0$

for $i = 0:(o-2)$

  $b_i := s$

  for $j = 0:(k-o+i-s-1)$

    if $l > \binom{k-s-1-j}{o-i-1}$ *then*

      $b_i := b_i + 1$

      $l := l - \binom{k-s-1-j}{o-i-1}$

    else

      break

    end if

  end for

  $s := b_i + 1$

end for

$b_{o-1} := b_{o-2} + l$

For example, the simplest algorithm to estimate $d_{\min}^{(D)-\mathrm{IBRC}}$ of systematic binary block codes enumerates all codewords corresponding to the input information vectors of weight, $o = 1, 2, \cdots, O_1$, where $O_1 < d_{\min}^{(D)-\mathrm{IBRC}}$. If the number of such codewords, i.e., $\sum_{o=1}^{O_1} \binom{k}{o}$, is large, then, using Algorithm 7.12, we can generate randomly additional codewords of input information weight, $o = O_1 + 1, \cdots, O_2$, where $O_1 < O_2 < d_{\min}^{(D)-\mathrm{IBRC}}$.

Recall that we search for sequences of cyclic shifts of the input information bits. These sequences are then shortened in order to obtain the desired minimum Hamming distance, $d_{\min}^*$, while minimizing the constraint weight, $K^{(D)-\mathrm{IBRC}}$, and the complexity of the encoding and decoding; see the design (7.2). Note also that, for particular vectors of cyclic shifts, $\mathbf{a}_d$, we have to specify minimum dimensions, $\mathbf{k}_0 = (k_{01}, \cdots, k_{0D})$, that guarantee the minimum Hamming distance, $d_{\min}^*$. We have the following theorem.

Theorem 7.13 *For any vectors of cyclic shifts,* $\mathbf{a}_d$*, that are used to generate a* D*-dimensional IBRC,* $\mathscr{C}^{(D)-\mathrm{IBRC}} = (n, k, d_{\min}^{(D)-\mathrm{IBRC}})$*, there exist minimum dimensions,* $\mathbf{k}_0$*, such that, for all dimensions,* $\mathbf{k} \geq \mathbf{k}_0$*, the minimum Hamming distance,* $d_{\min}^{(D)-\mathrm{IBRC}}$*, is independent of* $\mathbf{k}$*.*

Proof: For a particular dimension, d, we can use Theorem 1 in [128] to prove that there exists minimum dimension, k_{0d}, such that, for $\forall k_d \geq k_{0d}$, the minimum Hamming distance, $d_{\min}^{(D)-\text{IBRC}}$, is independent of $\mathbf{k}$. In turn, we can show that, for sufficiently large dimensions, $\mathbf{k}$, the dimensions become independent and can be arbitrarily increased without changing the value of $d_{\min}^{(D)-\text{IBRC}}$. ■

Corollary 7.14 *If d_0 is the minimum Hamming distance of a D-dimensional IBRC of dimensions, $\mathbf{k}$, then the vectors of cyclic shifts, $\mathbf{a}_d$, can be arbitrarily shortened to obtain a D-dimensional IBRC of dimensions, $\mathbf{k}$, and the minimum Hamming distance, $2 \leq d_{\min}^{(D)-\text{IBRC}} \leq d_0$.*

7.1.4 Examples of IBRC's

We consider examples of 1D, 2D and 3D IBRC's. We assume IBRC's given in Definition 7.9, for $M = L$ and $M = 1$. We investigate non-systematic codes having systematic codes as a special case. In general, non-systematic codes have typically much larger minimum Hamming distances than systematic codes. Hence, we present sequences of cyclic shifts that can be arbitrarily shortened to obtain the desired minimum Hamming distance, $d_{\min}$. For particular vectors of cyclic shifts, $\mathbf{a}_d$, we also provide the values of minimum dimensions, $\mathbf{k}_0$, as indicated by Theorem 7.13.

1D IBRC's

Let $M = L$ in Definition 7.9. Assume the generator matrix of the rate, $L/(L+1)$, IBRC, i.e.,

$$\mathbf{G} = \left[\begin{array}{ccc|c} \mathbf{A}_1 & & & \mathbf{A}_1^T\mathbf{A}_{11} \\ & \ddots & & \vdots \\ & & \mathbf{A}_1 & \mathbf{A}_1^T\mathbf{A}_{1L} \end{array}\right] \tag{7.3}$$

where $\mathbf{A}_1$ and $\mathbf{A}_{11}, \cdots, \mathbf{A}_{1L}$ are $k_1 \times k_1$ cyclic matrices having the generating vectors, $\mathbf{a}_1$ and $\mathbf{a}_{11}, \cdots, \mathbf{a}_{1L}$, respectively. Using Algorithm 7.11, we obtain the following sequences of cyclic shifts for a IBRC of rate $R = 4/5$, i.e., for $L = 4$,

$\mathbf{a}_{11}$ =(0, 1, 2, 4, 5, 7, 9, 12, 15, 21, 24, 25, 29, 32, 38, 41, 46, 49, 50, 51, 55, 57, 62, 63)
$\mathbf{a}_{12}$ =(0, 1, 5, 8, 10, 14, 16, 18, 20, 25, 27, 31, 32, 38, 42, 43, 50, 51, 53, 56, 58, 61, 64, 67)
$\mathbf{a}_{13}$ =(0, 2, 3, 11, 13, 18, 22, 23, 28, 31, 33, 34, 35, 39, 44, 47, 48, 52, 54, 59, 60, 64, 68, 69)
$\mathbf{a}_{14}$ =(0, 3, 5, 12, 15, 19, 24, 25, 29, 33, 34, 36, 37, 42, 45, 49, 51, 54, 55, 61, 63, 66, 71, 72)
$\mathbf{a}_1$ = (0, 2, 5, 7, 8, 9, 10, 12, 14, 15, 18, 19, 22, 23, 27, 29, 30, 31, 34, 35, 36, 37, 39, 41).

Assuming shortening of the sequences, $\mathbf{a}_{11}, \mathbf{a}_{12}, \mathbf{a}_{13}$ and $\mathbf{a}_{14}$ to K_{1i} components, and $\mathbf{a}_1$ to K_1 components, Table 7.1 gives $d_{\min}$ for dimension, k_1, and the maximum achievable $d_{\min}$ for dimension, $k_1 \gg 1$. We can obtain other 1D IBRC's using an arbitrary subset of L sequences, $\mathbf{a}_{11}, \mathbf{a}_{12}, \mathbf{a}_{13}$ and $\mathbf{a}_{14}$, for $L = 1, 2$ and 3. Note also that, in general, a search for the low rate IBRC's is easier than for the high rate IBRC's; thus, codes having the generator matrix (7.3) are rarely reported in the literature, for $L > 2$, [132].

Let $M = 1$ in Definition 7.9. Consider the generator matrix of the rate, $R = 1/(L+1)$, systematic 1D IBRC, i.e.,

$$\mathbf{G} = [\mathbf{I}|\ \mathbf{A}_{11} \cdots \mathbf{A}_{1L}]\,.$$

Assuming $L = 4$, we obtain the following generating sequences, i.e.,

$$\begin{aligned}
\mathbf{a}_{11} &= (0,1,2,4,5,7,9,12,15,21,24,25,29,32,38,41,46,49,50,51,55,57,62,63)\\
\mathbf{a}_{12} &= (0,1,3,5,7,10,11,14,16,19,22,27,31,33,34,37,39,40,42,44,46,48,52,53)\\
\mathbf{a}_{13} &= (0,1,2,5,6,9,11,12,13,14,16,18,19,22,23,26,27,28,30,32,33,34,35,37)\\
\mathbf{a}_{14} &= (0,1,3,5,7,11,13,14,15,16,17,19,20,21,22,25,26,29,31,33,34,35,37,38).
\end{aligned}$$

Note that we can again use an arbitrary subset of L sequences, $\mathbf{a}_{11}$, $\mathbf{a}_{12}$, $\mathbf{a}_{13}$, and $\mathbf{a}_{14}$ to obtain IBRC's of rate, $R = 1/(L+1)$, for $L = 1, 2$ and 3.

2D IBRC's

We assume two types of 2D IBRC's of rate, $1/2$. In particular, the codewords can be written as, $\mathbf{c} = (\mathbf{u}\mathbf{A}_0, \mathbf{A}_2^T\mathbf{u}\mathbf{A}_1)$, where the information matrix, $\mathbf{u} \in \mathbb{Z}_2^{k_2 \times k_1}$, and the cyclic matrices, $\mathbf{A}_0 \in \mathbb{Z}_2^{k_1 \times k_1}$, $\mathbf{A}_1 \in \mathbb{Z}_2^{k_1 \times k_1}$, and, $\mathbf{A}_2 \in \mathbb{Z}_2^{k_2 \times k_2}$, are generated by the vectors, $\mathbf{a}_0$, $\mathbf{a}_1$, and, $\mathbf{a}_2$, respectively. Note that $\mathbf{A}_2^T\mathbf{u}$ corresponds to the vertical parity bits, and $\mathbf{u}\mathbf{A}_1$ corresponds to the horizontal parity bits of a binary product code. Furthermore, we propose a class of 2D IBRC's of rate, $1/2$, having the codewords, $\mathbf{c} = (\mathbf{u}\mathbf{A}_0, \mathbf{A}_2^T\mathbf{u} \oplus \mathbf{u}\mathbf{A}_1)$; note that, in this case, the vertical encoding does not increase the transmission bandwidth. Then, using Algorithm 7.11, we obtain the following generating sequences, i.e.,

$$\begin{aligned}
\mathbf{a}_0 &= (0,2,3,6,8)\\
\mathbf{a}_1 &= (0,1,2,4,5,7,9,12,13,15,17,20,22,23,25)\\
\mathbf{a}_2 &= (1,2,4,6,7).
\end{aligned}$$

Table 7.2 shows $d_{\min}$ and the minimum input dimensions, $\mathbf{k}_0$, for the 2D IBRC's assuming that the generating sequences, $\mathbf{a}_0$, $\mathbf{a}_1$, and, $\mathbf{a}_2$, are shortened to K_0, K_1, and K_2 components, respectively.

3D IBRC's

Assume a 2D IBRC of rate, $1/2$, having the codewords, $\mathbf{c} = (\mathbf{u}, \mathbf{A}_2^T \mathbf{u} \mathbf{A}_1)$, and denote $\mathbf{A}_3$ to be the cyclic matrix used for permutation of bits across the 2D codewords. Using Algorithm 7.11, we obtain the following generating sequences, i.e.,

$$\begin{aligned}
\mathbf{a}_1 &= (0, 1, 2, 4, 5, 7) \\
\mathbf{a}_2 &= (1, 2, 4, 6, 7) \\
\mathbf{a}_3 &= (0, 1, 3, 5, 6).
\end{aligned}$$

Examples of the 3D IBRC's are given in Table 7.3 assuming that the generating sequences, $\mathbf{a}_1$, $\mathbf{a}_2$, and, $\mathbf{a}_3$, are shortened to K_1, K_2, and K_3 components, respectively.

Furthermore, consider the design of 3D IBRC's for concatenation of 1D codewords. In particular, Table 7.4 shows $d_{\min}$ and $\mathbf{k}_0$ of the 3D IBRC's assuming the generating sequences,

$$\begin{aligned}
\mathbf{a}_2 &= (1, 2, 4, 6, 7) \\
\mathbf{a}_3 &= (0, 1, 3, 5, 6)
\end{aligned}$$

for permutation of bits in dimensions, $d = 2$, and, $d = 3$, and shortened to K_2 and K_3 components, respectively. The 1D codes in dimension, $d = 1$, in Table 7.4 are the Hamming $(15, 11, 3)$ and $(7, 4, 3)$ codes, the Golay perfect code, $(23, 12, 7)$, and the SPC code, $(12, 11, 2)$.

Table 7.1: Examples of 1D IBRC's of rate $R = 4/5$.

$d_{\min}$(max)	$K_{1i} =$						
k_1	1	4	8	12	16	20	24
$K_1 = 1$	2(2)	5(5)	9(9)	13(13)	17(17)	21(21)	25(25)
	≥ 1	≥ 18	≥ 32	≥ 46	≥ 56	≥ 75	≥ 91
2	X	8(8)	10(12)	16(16)	X	X	X
		≥ 17	≥ 25	≥ 45			
3	6(6)	9(9)	14(16)	19(19)	26(26)	34(34)	X
	≥ 11	≥ 15	≥ 32	≥ 43	≥ 63	≥ 80	
4	8(8)	14(14)	16(18)	X	28(30)	X	X
	≥ 11	≥ 25	≥ 32		≥ 65		
5	10(10)	X	16(16)	24(24)	32(32)	X	42(42)
	≥ 15		≥ 31	≥ 53	≥ 76		≥ 95
6	12(12)	18(18)	18(18)	26(26)	32(34)	36(36)	42(42)
	≥ 20	≥ 31	≥ 31	≥ 46	≥ 65	≥ 82	≥ 87
7	14(14)	20(20)	20(21)	27(27)	33(33)	36(40)	44(46)
	≥ 19	≥ 32	≥ 34	≥ 53	≥ 70	≥ 71	≥ 90
8	16(16)	20(20)	22(24)	30(32)	34(38)	40(42)	X
	≥ 20	≥ 37	≥ 37	≥ 53	≥ 65	≥ 75	
9	18(18)	24(24)	22(22)	32(33)	37(37)	42(43)	48(51)
	≥ 34	≥ 41	≥ 43	≥ 54	≥ 74	≥ 81	≥ 91
10	20(20)	26(26)	24(28)	34(34)	38(38)	X	X
	≥ 25	≥ 41	≥ 42	≥ 65	≥ 79		
11	22(22)	28(30)	26(35)	36(40)	40(49)	44(44)	50(54)
	≥ 40	≥ 41	≥ 39	≥ 60	≥ 72	≥ 100	≥ 97
12	24(24)	30(32)	28(36)	36(38)	42(48)	X	52(58)
	≥ 31	≥ 45	≥ 39	≥ 74	≥ 75		≥ 93
13	26(26)	32(37)	30(40)	38(45)	44(52)	56(57)	54(60)
	≥ 33	≥ 47	≥ 52	≥ 65	≥ 73	≥ 100	≥ 105
14	28(28)	34(38)	32(40)	38(44)	44(48)	X	56(64)
	≥ 44	≥ 57	≥ 56	≥ 68	≥ 92		≥ 101
15	30(30)	36(40)	34(44)	40(54)	48(58)	58(66)	58(72)
	≥ 50	≥ 57	≥ 56	≥ 67	≥ 88	≥ 100	≥ 104
16	32(32)	38(44)	36(52)	44(56)	50(62)	60(68)	66(68)
	≥ 41	≥ 55	≥ 55	≥ 69	≥ 83	≥ 105	≥ 128
17	34(34)	40(47)	40(50)	50(57)	54(66)	62(69)	66(68)
	≥ 44	≥ 60	≥ 67	≥ 80	≥ 92	≥ 101	≥ 115
18	36(36)	42(50)	42(52)	50(60)	54(66)	62(68)	66(76)
	≥ 56	≥ 56	≥ 73	≥ 79	≥ 87	≥ 109	≥ 116
19	38(38)	44(48)	44(55)	52(64)	58(62)	64(73)	68(81)
	≥ 49	≥ 72	≥ 67	≥ 83	≥ 99	≥ 107	≥ 119
20	40(40)	46(50)	46(56)	54(62)	60(70)	66(70)	68(80)
	≥ 53	≥ 68	≥ 75	≥ 90	≥ 96	≥ 117	≥ 128
21	42(42)	48(56)	48(58)	58(64)	64(68)	66(74)	71(81)
	≥ 56	≥ 67	≥ 72	≥ 93	≥ 102	≥ 112	≥ 118
22	44(44)	50(60)	50(60)	60(64)	66(74)	70(74)	68(80)
	≥ 67	≥ 74	≥ 72	≥ 92	≥ 113	≥ 118	≥ 115
23	46(46)	52(57)	52(62)	64(71)	66(77)	70(72)	70(87)
	≥ 56	≥ 75	≥ 79	≥ 102	≥ 105	≥ 135	≥ 125
24	48(48)	54(60)	54(68)	64(76)	68(74)	72(78)	80(90)
	≥ 71	≥ 80	≥ 76	≥ 100	≥ 125	≥ 130	≥ 134

Table 7.2: Examples of 2D-IBRC's.

	$(\mathbf{u}\mathbf{A}_0, \mathbf{A}_2^T\mathbf{u} \oplus \mathbf{u}\mathbf{A}_1)$				$(\mathbf{u}\mathbf{A}_0, \mathbf{A}_2^T\mathbf{u}\mathbf{A}_1)$			
	$K_2=1, K_0=5$		$K_2=5, K_0=1$		$K_2=1, K_0=5$		$K_2=5, K_0=1$	
K_1	$d_{\min}$	$\mathbf{k} \geq \mathbf{k}_0$	$d_{\min}$	$\mathbf{k} \geq \mathbf{k}_0$	$d_{\min}$	$\mathbf{k} \geq \mathbf{k}_0$	$d_{\min}$	$\mathbf{k} \geq \mathbf{k}_0$
1	7	(2, 10, 10)	7	(15, 1, 1)	6	(1, 10, 10)	6	(13, 1, 1)
2	8	(2, 9, 9)	8	(9, 2, 2)	7	(2, 13, 13)	9	(12, 13, 13)
3	9	(2, 9, 9)	9	(9, 3, 3)	8	(2, 12, 12)	10	(9, 6, 6)
4	10	(2, 9, 9)	10	(8, 5, 5)	9	(3, 15, 15)	12	(9, 8, 8)
5	11	(2, 13, 13)	11	(9, 6, 6)	10	(2, 17, 17)	14	(9, 10, 10)
6	12	(2, 13, 13)	12	(8, 8, 8)	11	(4, 22, 22)	12	(9, 8, 8)
7	13	(2, 15, 15)	13	(8, 10, 10)	12	(4, 25, 25)	18	(9, 14, 14)
8	14	(2, 16, 16)	14	(8, 13, 13)	13	(5, 19, 19)	14	(9, 14, 14)
9	15	(2, 20, 20)	15	(8, 14, 14)	14	(5, 24, 24)	18	(9, 14, 14)
10	16	(2, 22, 22)	16	(8, 16, 16)	15	(5, 25, 25)	22	(9, 16, 16)
11	17	(3, 25, 25)	17	(8, 18, 18)	16	(6, 25, 25)	22	(9, 16, 16)
12	18	(3, 25, 25)	18	(8, 22, 22)	17	(6, 28, 28)	22	(9, 16, 16)
13	19	(3, 28, 28)	19	(8, 24, 24)	18	(6, 29, 29)	20	(9, 17, 17)
14	20	(3, 30, 30)	20	(8, 24, 24)	19	(6, 32, 32)	21	(9, 17, 17)
15	21	(3, 32, 32)	21	(8, 27, 27)	20	(6, 33, 33)	22	(9, 17, 17)

Table 7.3: Examples of 3D IBRC's assuming 2D codewords, $\mathbf{c} = (\mathbf{u}, \mathbf{A}_2^T\mathbf{u}\mathbf{A}_1)$.

$\mathbf{a}_2 = (1,2,4,6,7)$ $\mathbf{a}_3 = (0,1,3,5,6)$								
$\mathbf{a}_1 = (0)$			$\mathbf{a}_1 = (0,1,2)$			$\mathbf{a}_1 = (0,1,2,4,5,7)$		
$K_{1,2,3}$	$d_{\min}$	$\mathbf{k} \geq \mathbf{k}_0$	$K_{1,2,3}$	$d_{\min}$	$\mathbf{k} \geq \mathbf{k}_0$	$K_{1,2,3}$	$d_{\min}$	$\mathbf{k} \geq \mathbf{k}_0$
1 1 1	2	(1, 1, 1)	3 1 1	4	(4, 1, 5)	6 1 1	7	(11, 1, 1)
1 2 1	3	(1, 3, 1)	3 2 1	6	(4, 4, 1)	6 2 1	13	(11, 5, 7)
1 3 1	4	(1, 4, 1)	3 3 1	8	(4, 5, 10)	6 3 1	19	(11, 7, 6)
1 4 1	5	(1, 8, 1)	3 4 1	10	(4, 6, 7)	6 4 1	25	(11, 8, 7)
1 5 1	6	(1, 9, 1)	3 5 1	12	(4, 6, 6)	6 5 1	31	(11, 12, 5)
1 1 2	4	(1, 1, 2)	3 1 2	8	(3, 1, 2)	6 1 2	14	(11, 7, 2)
1 2 2	6	(1, 3, 2)	3 2 2	12	(4, 3, 2)	6 2 2	26	(11, 8, 2)
1 3 2	8	(1, 4, 2)	3 3 2	16	(4, 4, 2)	6 3 2	38	(11, 8, 7)
1 4 2	10	(1, 8, 2)	3 4 2	20	(4, 7, 2)	6 4 2	50	(11, 10, 6)
1 5 2	12	(1, 7, 2)	3 5 2	24	(4, 9, 2)	6 5 2	62	(11, 12, 4)
1 1 3	6	(1, 1, 7)	3 1 3	12	(4, 1, 7)	6 1 3	21	(11, 7, 7)
1 2 3	9	(1, 3, 7)	3 2 3	18	(4, 5, 7)	6 2 3	39	(11, 9, 7)
1 3 3	12	(1, 4, 7)	3 3 3	24	(4, 7, 7)	6 3 3	57	(11, 7, 10)
1 4 3	15	(1, 8, 7)	3 4 3	30	(4, 10, 8)	6 4 3	75	(11, 8, 7)
1 5 3	18	(1, 9, 7)	3 5 3	36	(4, 9, 9)	6 5 3	93	(12, 7, 6)
1 1 4	8	(1, 1, 12)	3 1 4	16	(4, 6, 9)	6 1 4	28	(11, 7, 8)
1 2 4	12	(1, 3, 12)	3 2 4	24	(5, 5, 10)	6 2 4	52	(11, 8, 8)
1 3 4	16	(1, 4, 12)	3 3 4	32	(4, 8, 8)	6 3 4	76	(11, 9, 8)
1 4 4	20	(1, 8, 11)	3 4 4	40	(5, 9, 9)	6 4 4	100	(11, 9, 11)
1 5 4	24	(1, 9, 11)	3 5 4	48	(6, 7, 3)	6 5 4	124	(11, 10, 8)

Table 7.4: Examples of 3D IBRC's for concatenated codewords.

$\mathbf{a}_2 = (1,2,4,6,7)$ $\mathbf{a}_3 = (0,1,3,5,6)$											
$C=(15,11,3)$			$C=(7,4,3)$			$C=(23,12,7)$			$C=(12,11,2)$		
$K_{2,3}$	$d_{\min}$	$\mathbf{k}_0$	$K_{2,3}$	$d_{\min}$	$\mathbf{k}_0$	$K_{2,3}$	$d_{\min}$	$\mathbf{k}_0$	$K_{2,3}$	$d_{\min}$	$\mathbf{k}_0$
1 1	3	(1,1)	1 1	3	(1,1)	1 1	7	(1,1)	1 1	2	(1,1)
1 2	6	(1,4)	1 2	6	(1,5)	1 2	14	(1,4)	1 2	4	(1,4)
1 3	9	(1,7)	1 3	9	(1,8)	1 3	21	(1,7)	1 3	6	(1,7)
1 4	12	(1,8)	1 4	12	(1,11)	1 4	28	(1,8)	1 4	8	(1,9)
2 1	4	(4,3)	2 1	4	(4,2)	2 1	12	(5,5)	2 1	2	(2,1)
2 2	8	(4,3)	2 2	8	(4,4)	2 2	24	(5,5)	2 2	4	(2,3)
2 3	12	(4,4)	2 3	12	(4,7)	2 3	36	(5,5)	2 3	6	(2,4)
2 4	16	(4,6)	2 4	16	(4,8)	2 4	48	(5,8)	2 4	8	(2,8)
3 1	5	(4,3)	3 1	5	(4,2)	3 1	13	(5,1)	3 1	2	(4,1)
3 2	10	(4,3)	3 2	10	(4,4)	3 2	26	(5,3)	3 2	4	(4,3)
3 3	15	(4,4)	3 3	15	(4,7)	3 3	39	(5,4)	3 3	6	(4,4)
3 4	20	(4,6)	3 4	20	(4,8)	3 4	52	(5,6)	3 4	8	(4,6)
4 1	6	(6,2)	4 1	6	(6,1)	4 1	22	(6,3)	4 1	2	(6,1)
4 2	12	(6,3)	4 2	12	(6,3)	4 2	44	(6,3)	4 2	4	(6,3)
4 3	18	(6,4)	4 3	18	(6,4)	4 3	66	(6,4)	4 3	6	(6,4)
4 4	24	(6,6)	4 4	24	(6,7)	4 4	88	(6,8)	4 4	8	(6,6)

7.1.5 Applications of IBRC's

We consider applications of IBRC's and analyze their BER performance. In general, assume mapping of codewords, $\mathbf{c} \in \mathbb{Z}_2^n$, to BPSK sequences, $\mathbf{x} = ((-1)^{c_0}, \cdots, (-1)^{c_{n-1}}) \in \{-1, +1\}^n$. The sequence, $\mathbf{x}$, is transmitted over an AWGN channel, $\mathbf{w}$, of variance, $\sigma_w^2 = N_0/2$, per dimension where N_0 is the one-sided noise power spectral density. Then, the received sequence, $\mathbf{y} = \mathbf{x} + \mathbf{w}$. The energy per coded modulated symbol is, $E_b = 1$, and thus, $\sigma_w^2 = (2R\gamma_b)^{-1}$ where R denotes the code rate, and $\gamma_b = E_b/N_0$ is the SNR.

We consider soft-input soft-output (SISO) decoding of IBRC's. The channel soft-output for the j-th bit (in the log-likelihood domain) is, $L_c(j) = 2\mathbf{y}_j/\sigma_w^2$, and $j = 0, 1, \cdots, n-1$ [17]. The SISO decoder outputs the a posteriori values [141], [142],

$$L_a(j) = \frac{\|\mathbf{y} - \mathbf{x}_{0j}\|^2 - \|\mathbf{y} - \mathbf{x}_{1j}\|^2}{2\sigma_w^2} = \frac{1}{\sigma_w^2} \sum_{i=0}^{2k-1} \mathbf{y}_i(\mathbf{x}_{1ji} - \mathbf{x}_{0ji}) \tag{7.4}$$

where $\mathbf{x}_{0j}$ and $\mathbf{x}_{1j}$ are the codewords at the smallest Euclidean distance from the received vector, $\mathbf{y}$, having the j-th bit 0 and 1, respectively. Then, the extrinsic information, $L_e(j) = L_a(j) - L_c(j)$. We adapt the algorithm proposed in [141] to compute a posteriori values (7.4). This algorithm is a sphere-decoder in the input information domain over a basis of the most reliable bits given as,

1. generate the initial estimate of the information vector, $\mathbf{u}_0$
2. search the sphere of radius, d_1, about $\mathbf{u}_0$ to find the codewords, $\mathbf{x}_{0j}$, and, $\mathbf{x}_{1j}$, for $\forall j$.

The sphere search enumerates the $\sum_{i=0}^{d_1} \binom{k}{i}$ codewords. For each codeword, $\mathbf{x}$, we compute the metric, $m(\mathbf{x}) = \mathbf{y}^T\mathbf{x}/(2\sigma_w^2)$, and update the table of the largest metrics for all n bits being 0 and 1. Then, $L_a(j) = m(\mathbf{x}_{1j}) - m(\mathbf{x}_{0j})$, $\forall j$. We can obtain the initial estimate, $\mathbf{u}_0$, using hard-decision decoding, for example, assuming only the information bits of the systematic code. Note that $d_1 = k$ corresponds to the optimum maximum a posteriori (MAP) decoding while reference [141] suggests that $d_1 = \lceil d_{\min}/4 \rceil$ for negligible performance loss where $\lceil \cdot \rceil$ is the ceiling function. Although a simple enumeration of sequences within a given Hamming distance about the initial estimate can be too complex for the real-time implementation of the decoder, this method is well suited for computer simulation evaluation of the performance of block coding schemes.

In general, a union bound of the BER over an AWGN channel can be written as [17], [100],

$$\mathrm{P}_b^{\mathrm{UB}}(\gamma_b) = \sum_{w=d_{\min}}^{n} \frac{A_w}{k} Q\Big(\sqrt{2Rw\gamma_b}\Big) \tag{7.5}$$

where $A_w = \sum_{i=0}^{k} iA(i,w)$ is the number of information bits encoded in all codewords of weight, w, $A(i,w)$ is the number of codewords of input information weight, i, and output weight, w. For cyclic codes, we can use Theorem 2 in [119] to efficiently evaluate the coefficients, $A_w = R\,wA(w)$, where $A(w) = \sum_{i=0}^{k} A(i,w)$; our numerical results indicate that this expression is a good approximation for systematic 1D double circulant codes. Then, we can approximate the union bound of the BER as,

$$\mathrm{P}_b^{\mathrm{UB}}(\gamma_b) \doteq \sum_{w=d_{\min}}^{n} \frac{w}{n} A(w)\, Q\Big(\sqrt{2Rw\gamma_b}\Big).$$

Adaptive Coding

As indicated by Theorem 7.13, for a given minimum Hamming distance, the dimensions of IBRC's can have arbitrary values greater than some minimum dimensions. Also, for given dimensions, the minimum Hamming distance of IBRC's can be chosen up to a certain maximum value; see Corollary 7.14. Correspondingly, IBRC's are well-suited for packet transmission, and particularly, when the channel quality between the source and the destination is known at the transmitter.

As an example, consider the vector of cyclic shifts,

$$\mathbf{a} = (0, 1, 2, 4, 5, 7, 9, 12, 15, 17, 20).$$

This vector can be shortened to $1 \leq K \leq 11$ components to generate a cyclic matrix, $\mathbf{A}$, of minimum dimension, $k_0 = 34$. Then, a systematic 1D IBRC of rate, $1/2$, has the generator matrix, $[\mathbf{I}|\mathbf{A}]$, and minimum Hamming distance, $d_{\min} = 1 + K$.

Turbo Product Coding

Consider a turbo product code (TPC), $C_p = C_x \times C_y = (n_x, k_x, d_x) \times (n_y, k_y, d_y) = (n_p, k_p, d_p)$, of rate $R_p = (k_x k_y)/(n_x n_y)$, and minimum Hamming distance, $d_p = d_x d_y$. The weight enumerator coefficients of TPC, $A_{C_p}(w)$, for $w = 0, 1, \cdots, d_x d_y + \max(d_x\lceil d_y/2\rceil, d_y\lceil d_x/2\rceil)$, can be obtained using Theorem 1 of [143], i.e., $A_{C_p}(w) = \sum_{i|w} A_{C_x}(i)\, A_{C_y}(w/i)$ where $A_{C_x}(w)$ and $A_{C_y}(w)$ are weight enumerators of component codes, and $i|w$ denotes i divides w. We assume that the horizontal

encoding, C_x, is a 1D IBRC, and the vertical encoding, C_y, is a high rate binary code. For high rate codes, the extrinsic information for the j-th bit of the C_y code, $L_e(j; C_y)$, can be efficiently computed using the dual code, $C_y^{\perp}$, i.e. [105, eq. (89)],

$$L_e(j; C_y) = \log \frac{\sum_{\mathbf{c} \in C_y^{\perp}} \left(\prod_{k=1, k \neq i}^{n_y} \tanh(\frac{L_a(j)}{2})^{c_k} \right)}{\sum_{\mathbf{c} \in C_y^{\perp}} \left((-1)^{c_k} \prod_{k=1, k \neq i}^{n_x} \tanh(\frac{L_a(j)}{2})^{c_k} \right)}$$

where the a posteriori values are computed as, $L_a(j) = L_c(j) + L_e(j; C_x)$. The extrinsic values, $L_e(j; C_x)$, corresponding to the horizontal code, C_x, are evaluated using (7.4).

As an example, we evaluate the BER of two TPC's assuming the 1D IBRC, $(48, 24, 9)$, for horizontal encoding, and the single parity check code, $(8, 7, 2)$, and the extended Hamming code, $(8, 4, 4)$, for vertical encoding, respectively. The IBRC, $(48, 24, 9)$, is systematic and has the generator matrix, $\mathbf{G} = [\mathbf{I}|\mathbf{A}]$, where the cyclic matrix, $\mathbf{A} \in \mathbb{Z}_2^{24 \times 24}$, is generated by the vector of cyclic shifts, $\mathbf{a} = (0, 1, 2, 4, 5, 7, 9, 12)$. We assume input sphere decoding of radius, $d_1 = \lceil 9/4 \rceil = 3$, i.e., $\sum_{i=0}^{3} \binom{24}{i} = 2325$ codewords are evaluated to obtain the extrinsic values, $L_e(j, C_x)$, for the horizontal IBRC. The initial estimate for the input sphere decoder is given by hard decision of the systematic bits. Assuming 5 iterations between the horizontal and vertical decoders, the BER approaches the union bound (7.5) as shown in Fig. 7.1.

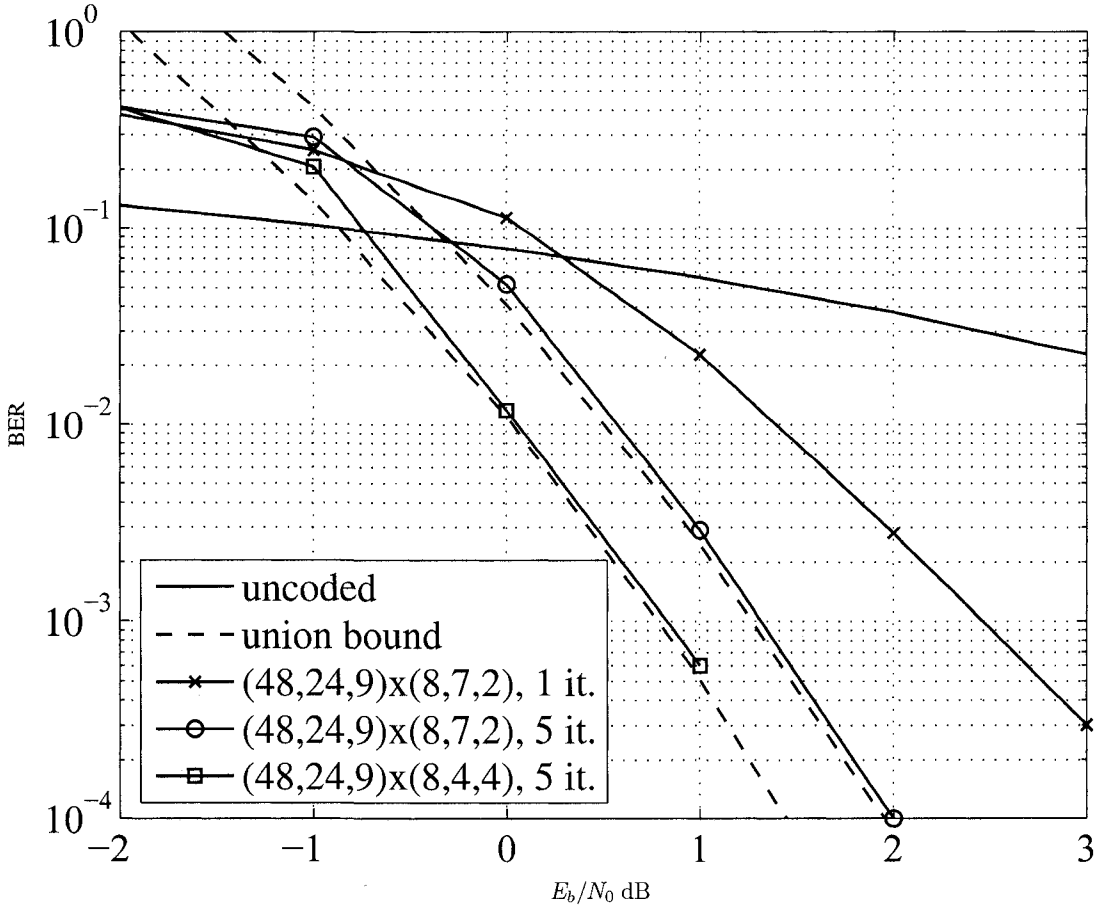

Figure 7.1: The BER of the $(48, 24, 9) \times (8, 7, 2)$ and $(48, 24, 9) \times (8, 4, 4)$ TPC's versus the SNR, E_b/N_0.

Table 7.5: Examples of doubly circulant IBRC's for retransmission schemes.

$\mathbf{a}_1$	$\mathbf{a}_2$	$d_{\min}$	k_0	k_{hb}
0	0, 2	3	5	4
0	0, 1, 2	4	4	4
0	0, 2, 5	4	6	5
0	0, 1, 2, 4	5	8	8
0, 2	0, 1, 2	5	9	8
0, 2	0, 2, 5	5	9	8
0, 1, 2	0, 1, 2, 4	5	8	8
0, 2	0, 1, 2, 4	6	8	8
0, 1, 2	0, 2, 5	6	10	9
0	0, 1, 2, 4, 5	6	10	9
0, 1, 2	0, 1, 2, 4, 5	6	10	9
0, 2	0, 1, 2, 4, 5	7	15	13
0, 2, 5	0, 1, 2, 4	7	16	13
0, 1, 2, 4	0, 1, 2, 4, 5	6	15	10
0, 2, 5	0, 1, 2, 4, 5	8	16	14

Retransmission and Multihop Routing

Consider a sequence of L cyclic matrices, $(\mathbf{A}_1, \mathbf{A}_2, \cdots, \mathbf{A}_L)$, and the input information vector, $\mathbf{u}$. During the i-th transmission from source to destination, we transmit the encoded bits, $\mathbf{u}\mathbf{A}_i$. Hence, at the destination, the compounded codeword, $\mathbf{c}_i = (\mathbf{u}\mathbf{A}_1, \mathbf{u}\mathbf{A}_2, \cdots, \mathbf{u}\mathbf{A}_i)$, corresponds to a IBRC of rate, $R = 1/i$, and the minimum Hamming distance, $d_{\min i}$. This code has generator matrix, $\mathbf{G}_i = [\mathbf{A}_1|\mathbf{A}_2|\cdots|\mathbf{A}_i]$. The design criteria for such a compounded IBRC are that $d_{\min i}$ should be increasing with the transmission number, i.

Table 7.5 shows examples of the vectors of cyclic shifts, $\mathbf{a}_1$, and $\mathbf{a}_2$, used to generate cyclic matrices, $\mathbf{A}_1$, and $\mathbf{A}_2$, respectively. Assuming IBRC's having the double circulant generator matrix, $[\mathbf{A}_1|\mathbf{A}_2]$, Table 7.5 provides the values of corresponding minimum Hamming distance, $d_{\min}$, and minimum dimension, k_0, and k_{hb} denotes the Hamming bound for given $d_{\min}$ and block length, $2k_0$, [116]. Note that combination of the received vectors corresponding to different cyclic matrices, $\mathbf{A}_1$, and, $\mathbf{A}_2$, results in different values of $d_{\min}$; this is useful for multihop routing protocols.

Block Differential Encoding

We consider 1D IBRC's compounded with block differential encoding. Hence, assume a rate, $1/2$, IBRC, $(2k, k, d_{\min})$, having the double circulant generator matrix, $\mathbf{G} = [\mathbf{A}_1|\mathbf{A}_2]$. The codewords,

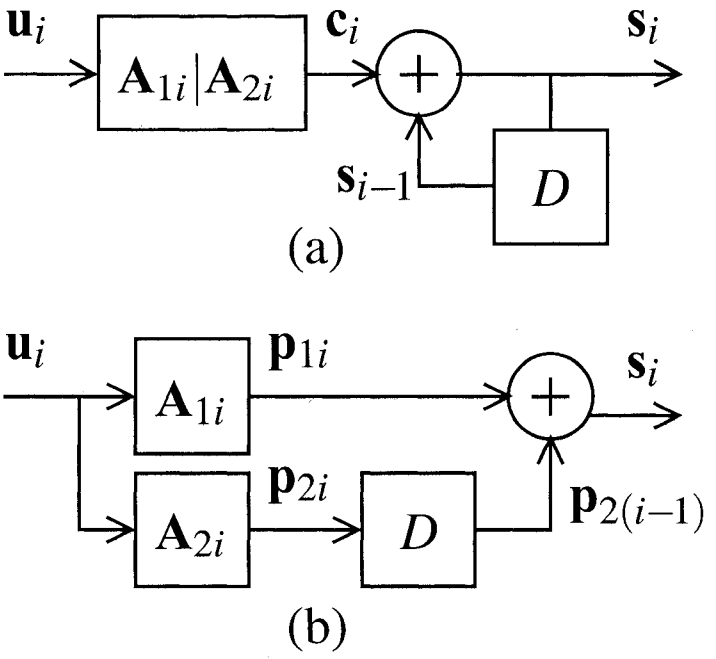

Figure 7.2: Block differential encoders, (a) recursive, and (b) non-recursive.

$\mathbf{c} = (\mathbf{p}_1, \mathbf{p}_2)$, where $\mathbf{p}_1 = \mathbf{u}\mathbf{A}_1$, $\mathbf{p}_2 = \mathbf{u}\mathbf{A}_2$, and $\mathbf{u}$ is the input information vector, are block differentially encoded as shown in Fig. 7.2. If the block differential encoding is recursive, then the differentially encoded codewords are written as, $\mathbf{s}_i = \mathbf{s}_{i-1} \oplus \mathbf{c}_i$, where i is the discrete time index; see Fig. 7.2(a). Hence, for L transmitted codewords, $\mathbf{c}_i$, $i = 1, 2, \cdots, L$, the compounded $(2k \times L)$ codeword, $(\mathbf{s}_1, \mathbf{s}_2, \cdots, \mathbf{s}_L)$, has rate, $1/2$. On the other hand, we propose to use a non-recursive differential encoding shown in Fig. 7.2(b) to improve the code rate. In this case, the differentially encoded codewords are written as, $\mathbf{s}_i = \mathbf{p}_{1i} \oplus \mathbf{p}_{2(i-1)}$. For L transmitted codewords, the non-recursive block differential encoder corresponds to a $((L+1)k, Lk, d_{\min})$ code of rate, $R_L = L/(L+1)$. This code has the generator matrix,

$$\mathbf{G}_L = \begin{bmatrix} \mathbf{A}_1 & \mathbf{A}_2 & & & \\ & \mathbf{A}_1 & \mathbf{A}_2 & & \\ & & \ddots & \ddots & \\ & & & \mathbf{A}_1 & \mathbf{A}_2 \end{bmatrix}$$

and the corresponding compounded codewords are, $(\mathbf{u}_1, \mathbf{u}_2, \cdots, \mathbf{u}_L)\mathbf{G}_L$. Denote by $\mathbf{a}_1$ and $\mathbf{a}_2$ generating vectors of the cyclic matrices, $\mathbf{A}_1$, and, $\mathbf{A}_2$, respectively. Similarly to Theorem 7.13, we can formulate the following theorem.

Theorem 7.15 *For any design,* $\mathbf{a}_1$*, and,* $\mathbf{a}_2$*, of the IBRC,* $((L+1)k, Lk, d_{\min})$*, there exist dimensions,* k_0*, and,* L_0*, such that, for* $\forall k \geq k_0$ *and* $\forall L \geq L_0$*, the minimum Hamming distance,* $d_{\min}$*, does not depend on* k *nor* L*.*

Proof: For a particular value of L, if dimension, k, is increased by one, then we insert L bits into the input information vector, $(\mathbf{u}_1, \cdots, \mathbf{u}_L)$. We can use the argument in the proof of Theorem 1 in [128] to show that, for sufficiently large k, the inserted bits cannot change $d_{\min}$. Also, for a particular value of k, if dimension, L, is increased by one, then the matrices, $\mathbf{A}_1$, and, $\mathbf{A}_2$, are appended to the generator matrix, $\mathbf{G}_L$. We can show that, for sufficiently large L, all input information vectors, $(\mathbf{u}_1, \cdots, \mathbf{u}_L)$, corresponding to codewords of weight, $d_{\min}$, contain at least k consecutive zeros; thus, increasing dimension, L, by one does not change $d_{\min}$. ■

Using Theorem 7.15, we have the following property.

Property 7.16 *Non-recursive block differential encoding in Fig. 7.2(b) of codewords of any doubly circulant binary code guarantees that the overall code rate,* $\lim_{L\to\infty} \frac{L}{L+1} = 1$*, with the number of differentially encoded codewords,* L*, while the minimum Hamming distance,* $d_{\min}$*, is fixed.*

In general, larger values of dimensions, k_0, and, L_0, are required for larger values of $d_{\min}$. Importantly, note that, for convolutional codes, both rate and minimum Hamming distance are independent of block length. Note also that, conditioned on knowledge of $\mathbf{u}_i$, the dimension is reduced to $(L-i)k$; thus, the sequence to be decoded is, $(\mathbf{u}_{i+1}, \cdots, \mathbf{u}_L)$.

For example, assume non-recursive block differential encoding of systematic 1D IBRC's, i.e., the generator matrix, $\mathbf{G} = [\mathbf{I}|\mathbf{A}]$, and let $L_0 = 1$. Table 7.6 gives cyclic shifts, $\mathbf{a}$, corresponding to the cyclic matrix, $\mathbf{A}$, and the values of $d_{\min}$, k_0, and the Hamming bound for block length, $2k_0$.

7.1.6 Transmitter Power Optimization

Consider the problem of how to distribute the transmission energy over the binary codeword to minimize the BER while the average energy per transmitted binary symbol, E_b, is kept constant. The exact BER is approximated using the union bound. We assume ideal interleaving, and thus, the channel fading coefficients are independent for each transmitted binary symbol; this corresponds to the fast fading assumption.

Assume a systematic 1D code, $(n, k, d_{\min})$, of rate, $R = k/n$, having the codewords, $\mathbf{c} = (\mathbf{u}, \mathbf{p})$, where $\mathbf{u}$ is the input information vector of k bits, and $\mathbf{p}$ is the vector of $(n-k)$ parity bits.

Table 7.6: Examples of IBRC's for non-recursive block differential encoding.

$\mathbf{a}$	$d_{\min}$	$k \geq k_0, L_0 = 1$	k_{hb}
0	2	≥ 1	1
$0,1$	3	≥ 5	4
$0,1,2$	4	≥ 7	5
$0,1,2,5$	5	≥ 12	9
$0,1,2,5,6$	6	≥ 13	10
$0,1,2,5,6,8$	7	≥ 17	13
$0,1,2,5,6,8,9$	8	≥ 19	15
$0,1,2,5,6,8,9,11$	9	≥ 23	18
$0,1,2,5,6,8,9,11,13$	10	≥ 30	20

For simplicity, denote by β_u^2 the transmission energy for information bits, and by β_p^2 the transmission energy for parity bits. Thus, the average transmission energy per binary information symbol, i.e.,

$$E_b = R\beta_u^2 + (1-R)\beta_p^2$$

is assumed to be constant. Correspondingly, given E_b, we can optimize the value of β_u^2 or β_p^2; this constitutes a 1D optimization problem in one variable only. We have that, $0 < \beta_u^2 < E_b/R$, and, $0 < \beta_p^2 < E_b/(1-R)$. Thus, if $\beta_p^2 > E_b$, then $\beta_u^2 < E_b$, and vice versa. The case, $\beta_u^2 = \beta_p^2 = E_b$, corresponds to uniform energy distribution over a transmitted codeword. Importantly, note also that, if $\mathbf{p} = \mathbf{uA}$ where $\mathbf{A}$ is a cyclic matrix, then all information and parity bits are equally protected. In this case, using the constant energy, β_u^2, for all information bits, and, β_p^2, for all parity bits, is optimum.

The codewords, $\mathbf{c}$, are interleaved and mapped to BPSK sequences, $\mathbf{x} \in \{-1,+1\}^n$. The sequences, $\mathbf{x}$, are transmitted over a Rayleigh fading channel, and coherently detected at the receiver. Hence, the i-th received binary symbol, $i = 0, 1, \cdots, (n-1)$, after coherent demodulation can be written as,

$$y_i = g_i \beta_i x_i + w_i$$

where g_i is the Rayleigh distributed channel fading amplitude, $\beta_i = \beta_u$, if the transmitted symbol, x_i, corresponds to the information bit, and $\beta_i = \beta_p$, if x_i corresponds to the parity bit, and w_i is a sample of a zero mean AWGN of variance, σ_w^2. The channel fading amplitude is normalized, so that, $\mathrm{E}\left[g_i^2\right] = 1$, and we let $E_b = 1$. Then, the SNR is defined as, $\gamma_i = g_i^2 \gamma_b$, and, $\gamma_b = E_b/N_0$.

The PEP

In order to evaluate a union bound of the average BER, we have to obtain the PEP; cf. eq. (7.5). Hence, consider the PEP that codeword, $\mathbf{c}$, is transmitted, and $\mathbf{c}'$ is decoded. Then, conditioned on perfect knowledge of the channel coefficients, g_i, $i = 0, 1, \cdots, (n-1)$, at the receiver, the PEP is computed as [21], [82],

$$\mathrm{PEP}(\mathbf{c} \mapsto \mathbf{c}' | \{g_i\}_i) = Q\left(\sqrt{\frac{2}{N_0}\left(\sum_{i=0}^{k-1} \beta_u^2 g_i^2 (\mathbf{c}_i \oplus \mathbf{c}'_i) + \sum_{i=k}^{n-1} \beta_p^2 g_i^2 (\mathbf{c}_i \oplus \mathbf{c}'_i)\right)}\right)$$

where $\mathbf{c}_i$ and $\mathbf{c}'_i$ denote the i-th binary symbols of the codewords. We can use a Prony approximation of the Q-function to efficiently evaluate the average PEP, i.e., let

$$Q(\sqrt{x}) \approx \sum_{j=1}^{p} \tilde{A}_j \exp(-\tilde{a}_j x)$$

where, for $p = 2$, $\tilde{A}_1 = 0.208$, $\tilde{A}_2 = 0.147$, $\tilde{a}_1 = 0.971$, and $\tilde{a}_2 = 0.525$, [70]. Then, assuming that the all-zero codeword was transmitted, the PEP can be expressed as,

$$\mathrm{PEP}(\mathbf{0} \mapsto \mathbf{c}' | \{g_i\}_i) = \sum_{j=1}^{2} \tilde{A}_j \prod_{i=0}^{n-1} \mathrm{e}^{-\tilde{a}_j f_i g_i^2} \tag{7.6}$$

where $f_i = 2\beta_{u(p)}^2 \mathbf{c}'_i / N_0$, and g_i^2 are exponentially distributed. Since $\int_0^\infty \mathrm{e}^{-(1+\tilde{a}_j f_i)t} \mathrm{d}t = (1 + \tilde{a}_j f_i)^{-1}$, and the channel coefficients, g_i, are mutually independent (recall the fast fading assumption), we obtain the average PEP as,

$$\overline{\mathrm{PEP}}(\mathbf{0} \mapsto \mathbf{c}') = \sum_{j=1}^{2} \tilde{A}_j \prod_{\substack{i=0 \\ i:\mathbf{c}'_i=1}}^{n-1} \frac{1}{1 + \tilde{a}_j f_i}.$$

Correspondingly, the union bound of the average BER becomes [21],

$$\mathrm{BER} \approx \sum_{\mathbf{c}' \in \mathscr{L}(o_{\max})} \frac{\mathrm{w_H}(\mathbf{c}'_u)}{nR} \overline{\mathrm{PEP}}(\mathbf{0} \mapsto \mathbf{c}') \tag{7.7}$$

where $\mathrm{w_H}(\mathbf{c}'_u)$ denotes the Hamming weight of the input information bits in the codeword, $\mathbf{c}'$, and the list of the codewords, $\mathscr{L}(o_{\max}) = \{\mathbf{c}' : \mathrm{w_H}(\mathbf{c}'_u) = o, o = 1, \cdots, o_{\max}\}$. For codes of large dimension, the list, $\mathscr{L}(o_{\max})$, can be approximated by a MC method, and using Algorithm 7.12.

Also, for transmission over an AWGN channel, the fading coefficients, $g_i = 1$, and we use the PEP (7.6) in the union bound (7.7).

We illustrate optimization of the transmission energy distribution, (β_u^2, β_p^2), using numerical examples. In particular, the union bound of the BER versus the transmission energy for the information bits, β_u^2, for three systematic IBRC's, $(36, 18, 6)$, $(36, 24, 5)$, and $(36, 12, 7)$, generated by cyclic shifts, $(0, 1, 2, 4, 5)$, $(0, 1, 2, 4)$, and $(0, 1, 2, 4, 5, 7)$, respectively, the extended Hamming code, $(16, 11, 4)$, and the extended Golay code, $(24, 12, 8)$, over a AWGN channel, for SNR, $E_b/N_0 = 2$ dB, is shown in Fig. 7.3. Recall also that $\beta_u^2 = 1$ corresponds to the case of uniform energy distribution over a codeword. We observe from Fig. 7.3 that the BER for higher code rates, i.e., $R > 1/2$, exhibits a minimum of the BER for values of $\beta_u^2 < 1$. On the other hand, for code rates, $R \leq 1/2$, the BER curves have local maxima. Thus, in general, less energy should be allocated for information bits, and more energy for parity check bits.

Fig. 7.4 shows the union bound of the BER for the codes from Fig. 7.3 over a Rayleigh fading channel (assuming fast fading and coherent detection), for SNR, $E_b/N_0 = 5$ dB. We can observe from Fig. 7.4 that the optimum energy, $\beta_u^2 < 1$, for code rates, $R \gg 1/3$, while the optimum energy, $\beta_u^2 > 1$, for code rates, $R \leq 1/3$.

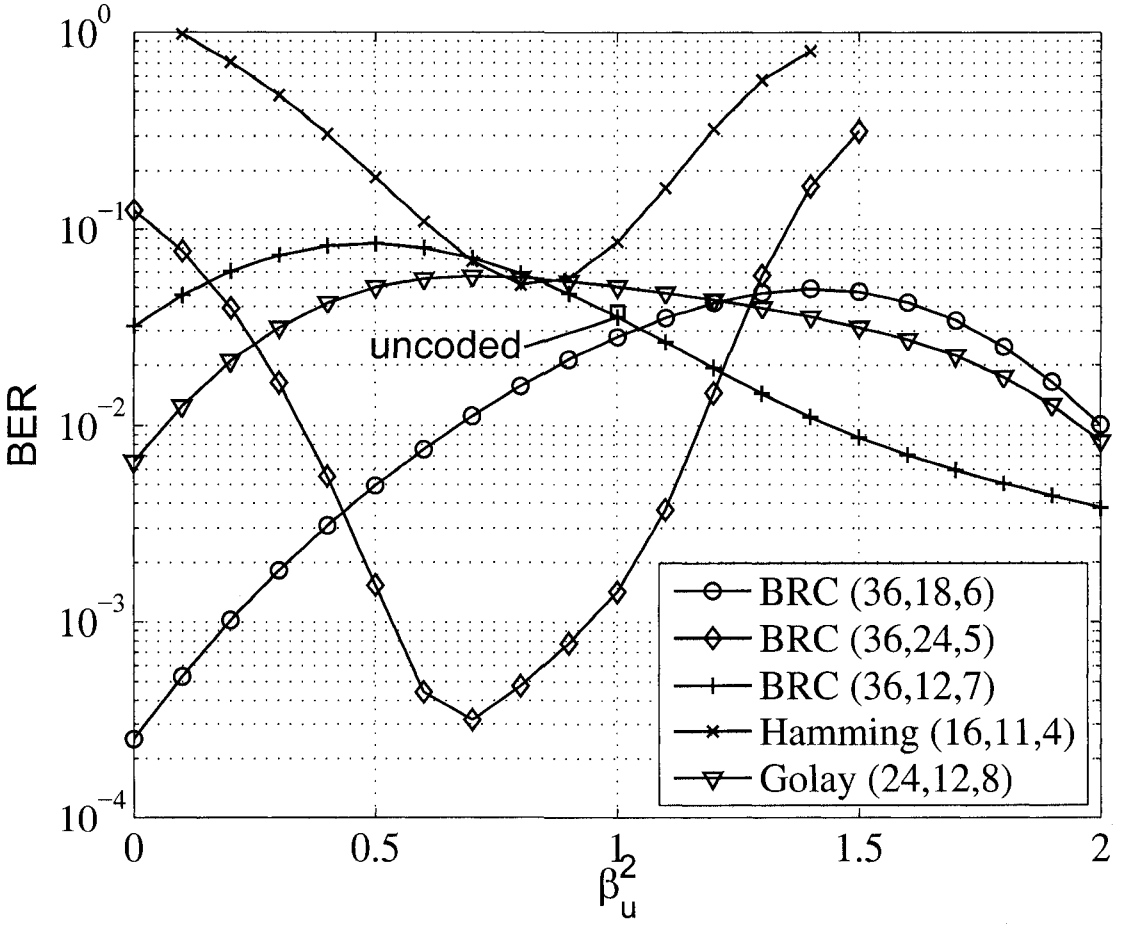

Figure 7.3: The BER union bound versus the energy, β_u^2, of the information bits over a AWGN channel, for SNR, $E_b/N_0 = 2$ dB.

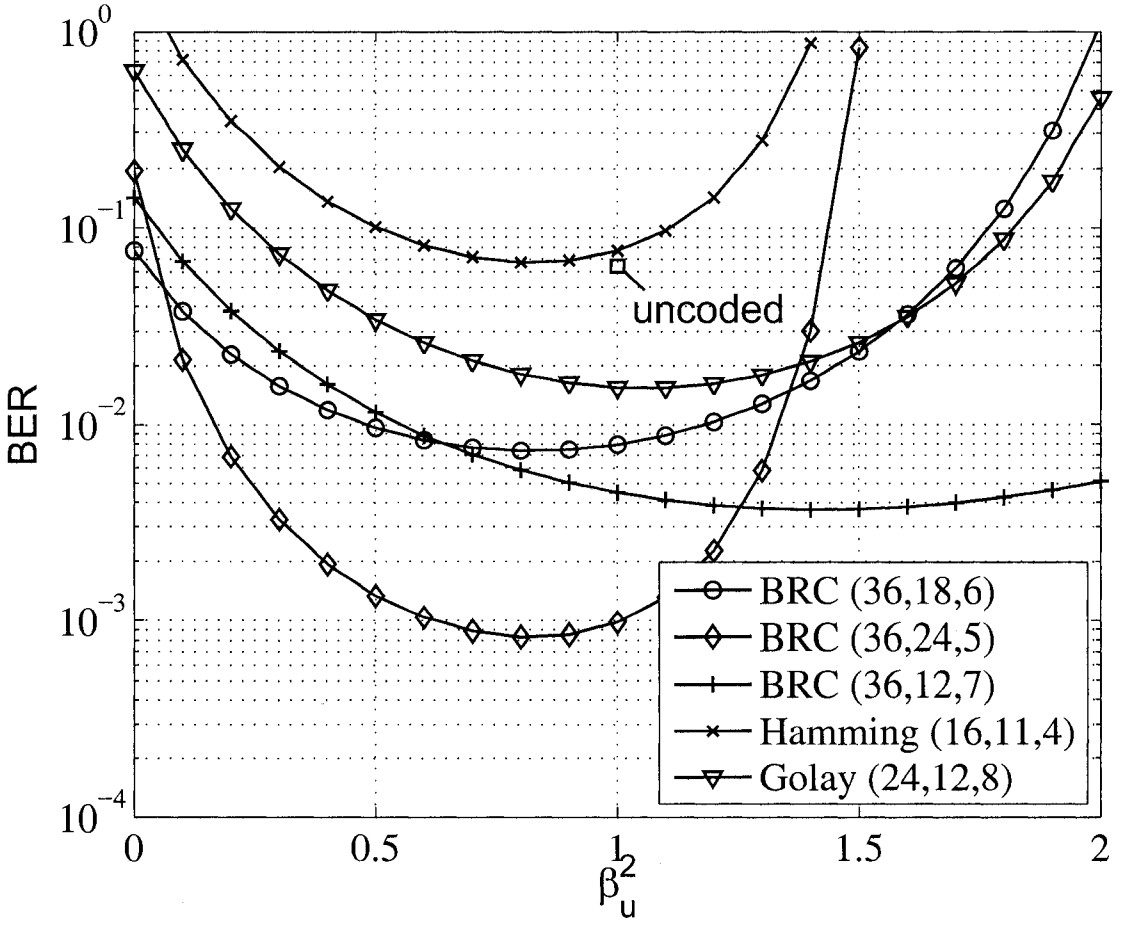

Figure 7.4: The BER union bound versus the energy, β_u^2, of the information bits over a Rayleigh fading channel, for SNR, $E_b/N_0 = 5$ dB.

7.2 A Cooperative Diversity Protocol With IBRC's and SPC Product Codes

7.2.1 Background

User cooperation is a promising concept that can improve network reliability, extend network coverage, and increase network throughput [144]. In general, the more information the users can share, the larger the cooperation gains. In cooperative networks, the nodes can share information using amplify-and-forward (AF) and decode-and-forward (DF) relaying techniques described in [144]. The usefulness of cooperation is often estimated using the probability of outage [144]. The probability of outage is defined as the probability that the transmission rate exceeds the channel capacity. Such probability can be often well approximated by the PER [17]. A protocol to combine channel coding and cooperation is proposed, for example, in [145] and [146]; particularly, the codewords are interleaved among the nodes to obtain coding and cooperative diversity gains. Cooperative protocols are usually designed for a given number of cooperating nodes and time slots [144]– [147]. A random space-time coding that decentralizes the cooperative protocols is proposed in [148]. The ML ML demodulation for user cooperation is studied in [149].

In this chapter, we consider a packet network where the packets are transmitted in dedicated orthogonal channels, and thus, all packets are received interference free. We propose a universal cooperative protocol for an arbitrary number of nodes and time slots to be used in uplink and downlink transmissions. The protocol combines three types of packets corresponding to the three protocol stages. The cooperating nodes listen to all transmitted packets. The codewords consist of all the packets received until the current time slot. A CRC code is used to detect uncorrectable transmission errors. The data packets are transmitted in Stage 1 of the protocol. In Stage 2, forward diversity and coding gain are achieved when source nodes employ forward error correction coding to transmit additional packets of parity bits corresponding to their own data packets. Coded and cooperative diversity is realized in Stage 3 of the protocol when the nodes transmit packets of parity bits obtained from all available data packets. Provided that the packets of parity bits in Stage 3 are generated assuming only successfully decoded data packets, the channel code corresponding to Stage 3 is random. The decoding of such a random code requires that the destination node has knowledge of which packets were successfully decoded in the other nodes in the previous stages. Alternatively, all the received data packets can be used to generate the packets of parity bits in Stage 3 of the protocol regardless whether the received packets were decoded successfully (i.e., the CRC

parity agrees) or not. In this case, the resulting code is non-random, and the transmission overhead to obtain knowledge of which packets were successfully decoded in Stage 1 and Stage 2 of the protocol can be avoided; however, error propagation can deteriorate the performance.

We assume that each node has one antenna, and that there are no scatterers surrounding the nodes. Then, the nodes communicate over a line-of-sight AWGN channel. The free-space path loss causes attenuation of the transmitted signals. A link budget analysis can be used to calculate the receiver SNR at a given distance from the transmitter antenna. We evaluate the PER improvement for the three protocol stages considering the stages as being independent. Also, the probability of not decoding a packet and the PER are assumed to be equal. We investigate the usefulness of cooperation for uplink and downlink transmissions for a particular number of nodes and network realization. We show that the proposed protocol can achieve diversity gain for particular locations of the nodes due to cooperation, and coding gain due to the use of forward error correction coding.

This section is organized as follows. A three stage protocol is described in Section 7.2.2. The system model is presented in Section 7.2.3. Performance analysis is carried out in Section 7.2.4. We obtain the PEP, and estimate the PER for coherent and non-coherent binary modulation schemes. The achievable coverage of the network for each of the protocol stages is investigated in Section 7.2.5. using numerical examples. The chapter is summarized in Section 7.3.

7.2.2 A Three Stage Protocol for Coded and Cooperative Diversity

Consider a network of $(N+1)$ nodes. One node represents an access point (AP), and the remaining N nodes are mobile terminals (MT's). We assume that the nodes can be time synchronized, and the propagation delays compensated to achieve time division multiple access. There are N orthogonal channels in each time slot corresponding to N MT's. In the uplink, each MT transmits L data packets to the AP. In the downlink, the AP transmits L data packets to each of the N MT's. In order to increase the network coverage and improve the network reliability, we allocate additional time slots to create coded diversity and cooperation. A CRC code is used to detect erroneous packets. In each node, a channel code is employed to generate packets of parity bits corresponding to the node data packets. Such parity packets are referred to as the horizontal parity, and they are transmitted in the forward diversity time slots. The cooperating nodes listen to all the transmitted packets, and can attempt to decode the received data packets. Then, using another channel code, the cooperative diversity is implemented by transmitting packets of parity bits created from each node's own data packets (in the uplink) as well as the other received data packets. These parity packets are referred

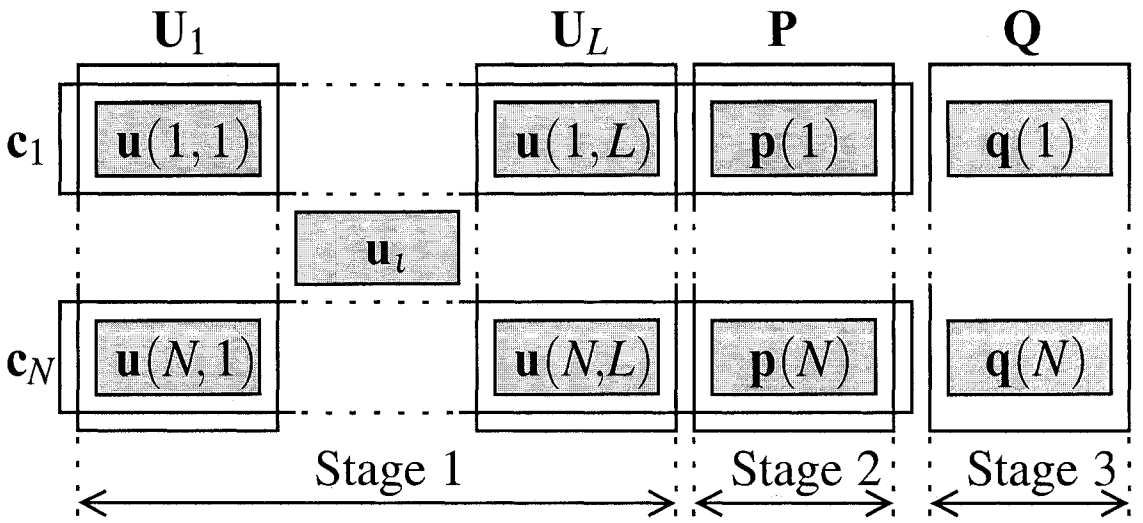

Figure 7.5: A three stage transmission protocol for N cooperating nodes.

to as the vertical parity, and they are transmitted in the cooperative diversity time slots.

Hence, we study a protocol for coded diversity and cooperation having a finite number of transmission stages, $S > 0$. During each stage, all nodes transmit the same type of packets in order to reduce the signaling overhead. The protocol considered in this chapter has, $S = 3$, stages, and is shown in Fig. 7.5. In Stage 1, the data packets, $\mathbf{u}(i,l)$, $i = 1,2,\cdots,N$, $l = 1,2,\cdots,L$, are transmitted over the L consecutive time slots. In Stage 2, one time slot is allocated for the parity bits, $\pi(i)$, of the horizontal channel code of rate, $L/(L+1)$. In Stage 3, another time slot is used to implement the cooperation. Particularly, a vertical channel code is used to generate the parity bits, $q(i)$. All packets are assumed to have equal length, K, bits. Hence, this protocol has a maximum throughput of, $KL/(L+2)$, information bits per packet; the throughput increases with L and is independent of N. Note also that the forward and cooperative diversity can be combined in one time slot, however, this case is not considered here.

Denote by q a generic index for one-dimensional packet indexing. Let $\mathcal{I}$ be the set of all, $(L+2)N$, packets, and $\mathcal{I}_{\mathrm{u}} \subseteq \mathcal{I}$ be the subset of all data packets; the cardinality, $|\mathcal{I}_{\mathrm{u}}| = LN$. Denote also, $\mathcal{I}_{\mathrm{u}} = \cup_{i=1}^{N} \mathcal{I}_{\mathrm{u}i}$, where $\mathcal{I}_{\mathrm{u}i}$ is the subset of data packets corresponding to the destination node, i, in the downlink, and the source node, i, in the uplink. The encodings in the three stages of the protocol in Fig. 7.5 are denoted as, $C_{[s]}$, $s = 1,2,3$, and they are described next.

Data Packets

Each data packet consists of, $K_{\rm u}=K-K_{\rm crc}$, information bits, and, $K_{\rm crc}$, CRC bits. The probability of an undetected erroneous packet is of the order, $2^{-K_{\rm crc}}$, and thus, it is neglected [150]. It is useful to select the CRC generating polynomial, such that all odd-weight error patterns are detected providing an overall parity check. Thus, for the source node, $i = 0, 1, \cdots, N$, the CRC codes, $\mathcal{C}_{[1]i} = (K, K_{\rm u}, d_{\rm crc})$, have rate, $K_{\rm u}/K$, the minimum Hamming distance, $d_{\rm crc} \leq K_{\rm crc}+1$, and the codewords, $\mathbf{u}_q$, $q \in \mathcal{I}_{{\rm u}i}$.

The code, $\mathcal{C}_{[1]i}$, can be decoded using Wagner decoding detailed in [151]; on average, we expect to correct at most $(d_{\rm crc}-1)$ bit errors. Note that the Wagner decoding rule is different from the Chase decoding rule [152]. While the Chase decoding selects the most reliable codeword searching over all possible combinations of the least reliable bits, the Wagner algorithm flips the least reliable bits until it finds the first valid codeword.

Forward Coded Diversity

Consider codewords, $\mathbf{c}_i = (\mathbf{u}(i,1), \cdots, \mathbf{u}(i,L), \pi(i))$, of the code, $\mathcal{C}_{[2]i}$, in Stage 2 of the protocol corresponding to the node i, for $i = 1, 2, \cdots, N$. The code, $\mathcal{C}_{[2]i} = (K(L+1), KL, d_{\min[2]i})$, is systematic, and has block length, $K(L+1)$, rate, $R_{[2]} = L/(L+1)$, minimum Hamming distance, $d_{\min[2]i}$, and the generator matrix, $\mathbf{G}_{[2]i} = [\mathbf{I}_{(LK)}|\mathbf{B}_{[2]i}]$, where $\mathbf{I}_{(LK)}$ is the $LK \times LK$ identity matrix, and $\mathbf{B}_{[2]i} \in \mathbb{Z}_2^{(LK,K)}$ is the parity check matrix. Thus, the horizontal parity packets, $\pi(i) = (\mathbf{u}(i,1), \cdots, \mathbf{u}(i,L))\mathbf{B}_{[2]i}$, are a linear combination of the data packets from a single source node.

The IBRC's [128] of rate, $L/(L+1)$, are well suited as the Stage 2 codes, $\mathcal{C}_{[2]i}$. In particular, for a given packet length, $K \geq K_0$, the minimum Hamming distance of IBRC's can be adapted to varying channel conditions to limit the number of unsuccessfully decoded packets. However, the complexity and power consumption of the encoding and decoding increases with the minimum Hamming distance, and thus, there exists an optimum $d_{\min[2]i}$ [153]. The minimum dimension, K_0, increases with the desired minimum Hamming distance [153]. Hence, consider the parity check matrix, $\mathbf{B}_{[2]i}$, of a systematic IBRC of rate, $L/(L+1)$, i.e.,

$$\mathbf{B}_{[2]i} = \left[\mathbf{A}^T_{[2]i1}|\mathbf{A}^T_{[2]i2}|\cdots|\mathbf{A}^T_{[2]iL}\right]^T$$

where $\mathbf{A}_{[2]il}$, for $l = 1, \cdots, L$, are $K \times K$ binary cyclic matrices generated by the vectors of

cyclic shifts, $\tilde{\mathbf{a}}_{[2]il}$, and $(\cdot)^T$ denotes the matrix transpose. For example, the cyclic shifts, $\tilde{\mathbf{a}}_{[2]il} = (0, 1, l+1)$, $l = 1, \cdots, L$, generate the IBRC of dimension, $K_0 \gg L$, having the minimum Hamming distance, $d_{\min[2]i} = 4$. The IBRC's can be decoded, for example, using the algorithm of [141].

Furthermore, if the CRC code in Stage 1 of the protocol provides an overall parity check for each data packet, then the single parity check (SPC) product code (SPCPC) [139] is particularly simple to implement. In this case, the parity check matrix, $\mathbf{B}_{[2]i} = \mathbf{1}$, i.e., the all-ones matrix. However, note that, for SPCPC's, the minimum Hamming distance, $d_{\min[2]i} = 4$, is fixed. The SPCPC can be efficiently decoded using an iterative soft decision decoding described in [139].

Cooperative Coded Diversity

In the uplink as well as in the downlink, the MT's listen to all transmitted packets, during Stage 1 and Stage 2 of the protocol. The MT's then attempt to decode the received data packets using knowledge of the CRC code, $\mathcal{C}_{[1]i}$, and the parity check matrices, $\mathbf{B}_{[2]i}$, for $i = 1, \cdots, N$. When only one time slot is allocated for cooperative diversity, the SPC code is particularly well-suited to generate the packets of vertical parity, $q(i)$. In this case, the vertical parity packets, $\mathbf{Q} \in \mathbb{Z}_2^{(N,K)}$, can be written as,

$$\mathbf{Q} = \mathbf{V}_{[3]}(\mathbf{U}_1^T, \cdots, \mathbf{U}_L^T)^T \tag{7.8}$$

where $\mathbf{V}_{[3]} \in \mathbb{Z}_2^{(N,LN)}$ is the parity check matrix; see Fig. 7.5. The rows of the matrix, $\mathbf{V}_{[3]}$, correspond to the nodes, $i = 1, \cdots, N$. The columns of the matrix, $\mathbf{V}_{[3]}$, correspond to the data packets, $q = 1, \cdots, NL$. Hence, the encoder of $\mathcal{C}_{[3]}$ is distributed among the cooperating nodes.

Assuming the SPC code, there are two strategies to generate the vertical parity packets. Either the parity bits, $\mathbf{Q}$, are generated using all the received data packets, or they are generated using only the successfully decoded data packets. The particular form of the matrix, $\mathbf{V}_{[3]}$, depends on the selected strategy. Consider the case when the parity bits, $\mathbf{Q}$, are generated from all the received data packets regardless whether they are decoded successfully or not. Then, we can use hard decisions of unsuccessfully decoded packets, however, the error propagation will deteriorate the performance. Alternatively, we can combine the AF and DF relaying. In particular, assume that cBPSK modulation is used for transmission, and let a mapping of coded bits, $c \in \mathbb{Z}_2$, to BPSK symbols, $\{-1, +1\}$, be, $c \mapsto (-1)^c$. In general, a modulo 2 sum, $c_1 \oplus c_2$, of bits, $c_1 \in \mathbb{Z}_2$, and, $c_2 \in \mathbb{Z}_2$, corresponds to a BPSK symbol, $(-1)^{c_1 \oplus c_2} = (-1)^{c_1 + c_2} = (-1)^{c_1}(-1)^{c_2}$, i.e., modulo 2 summation is equivalent to a product of the BPSK symbols. Also, in an AWGN channel, reliability of the bit decision is directly

proportional to the received BPSK symbol signal-plus-noise sample [17]. Hence, the parity bits of the SPC code can be generated by multiplying the BPSK symbols, $\{-1, +1\}$, corresponding to the DF relaying of the successfully decoded data packets, and the received BPSK symbols corresponding to the AF relaying of the unsuccessfully decoded data packets. In this case, the destination node does not need knowledge of which packets were successfully decoded in the other nodes during Stage 1 and Stage 2 of the protocol, and the matrix, $\mathbf{V}_{[3]}$, is non-random. However, the error propagation can deteriorate the performance, and, in general, analysis of systems with error propagation is difficult.

In this chapter, we investigate the strategy when the parity bits, $\mathbf{Q}$, in (7.8) are generated assuming only the successfully decoded data packets. Hence, let the code, $\mathcal{C}_{[3]}$, be a SPC code for successfully decoded data packets during Stage 1 and Stage 2 of the protocol. Then, the matrix, $\mathbf{V}_{[3]}$, in (7.8) is random, and has the elements, $[\mathbf{V}_{[3]}]_{iq} = 1$, if the i-th node can successfully decode the data packet, q, for $q = 1, 2, \cdots, NL$, and, $[\mathbf{V}_{[3]}]_{iq} = 0$, otherwise. The code, $\mathcal{C}_{[3]} = ((NL+1), NL, d_{\min[3]})$, has the rate, $R_{[3]} = NL/(NL+1)$, the codewords, $(\mathbf{U}_1, \cdots, \mathbf{U}_L, \mathbf{Q})$, and the random minimum Hamming distance, $d_{\min[3]} \geq 1$. Importantly, even though the matrix, $\mathbf{V}_{[3]}$, must be available at the destination node to facilitate decoding of the code, $\mathcal{C}_{[3]}$, knowledge of the matrix, $\mathbf{V}_{[3]}$, provides feedback information about the quality of the channels between the nodes; this can be used to select the minimum Hamming distance of the IBRC codes in Stage 2 of the protocol.

7.2.3 System Model

Assume that the nodes are distributed in a two-dimensional plane. The network topology is shown in Fig. 7.6. The node 0 at the origin is an AP. The other N nodes represent the MT's, and they are placed regularly on the circle of radius, d_{mt}, and with center at distance, d_{ap}, from the origin. Thus, the distances, d_{0j}, from the AP to the MT's, and, d_{ij}, between a pair of MT's, i, and, j, are,

$$\begin{aligned} d_{0j} &= \sqrt{d_{\mathrm{ap}}^2 + d_{\mathrm{mt}}^2 + 2 d_{\mathrm{ap}} d_{\mathrm{mt}} \cos\left(\frac{2\pi}{N}(j-1)\right)} \\ d_{ij} &= d_{\mathrm{mt}} \sqrt{2 - 2\cos\left(\frac{2\pi}{N}(i-j)\right)}. \end{aligned}$$

Provided that no significant scatterers are present in the area, the channels between any pair of nodes are line-of-sight, and they are modeled as Gaussian. Assuming limited mobility of the nodes,

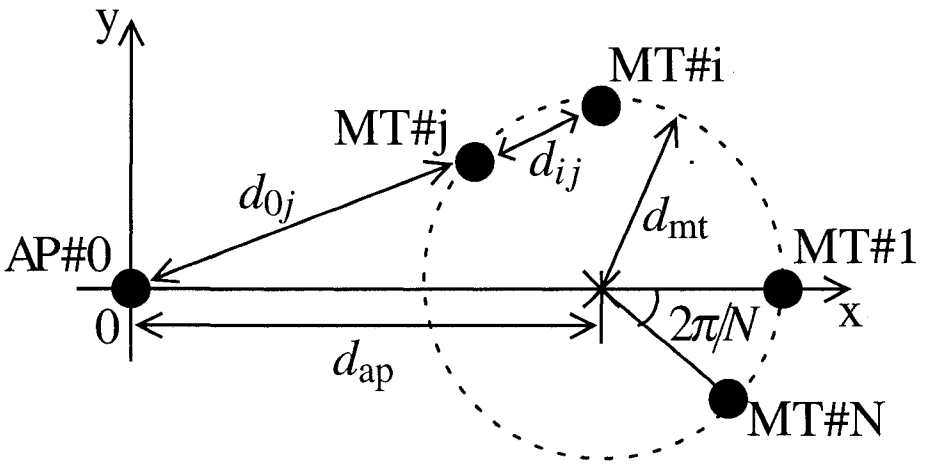

Figure 7.6: An example of the 2D network topology.

the distances between nodes are approximately constant, and so are the channel attenuations due to the free-space path loss. However, for short carrier wavelengths, even limited mobility causes random phase changes in the transmitted signals. Using equivalent complex envelopes in the baseband, the received signal in the node, j, corresponding to the packet, q, transmitted from the node, i, is,

$$\mathbf{y}_{qj} = |g_{ij}|\, \mathrm{e}^{\mathrm{j}\psi_{qij}} a_{qi} \mathbf{x}_{qi} + \mathbf{w}_{qj} \tag{7.9}$$

where $i, j = 0, 1, 2 \cdots, N$, $i \neq j$, and we assume column vectors by default. The channel attenuation, $|g_{ij}|$, represents a free-space path loss, ψ_{qij} is a random channel phase shift, a_{qi} sets the transmitter power for the q-th transmitted packet, $\mathbf{x}_{qi}$, and $\mathbf{w}_{qj}$ are the samples of a AWGN. The packet and nodes indices, q, i and j will be omitted if not necessary. The channel attenuations are modeled as the free-space path loss, i.e., [101],

$$|g_{ij}|^2 \approx \left(\frac{4\pi 100}{\lambda}\right)^{-2} \left(\frac{d_{ij}}{100}\right)^{-\mu} s_{\mathrm{ln}} \tag{7.10}$$

where $d_{ij} > 100$ is the distance from the transmitter antenna (in meters), $\lambda = 3 \cdot 10^8 / f_c$ is the carrier wavelength, f_c is the carrier frequency (in Hertz), and μ is the path loss exponent where, $1.5 \leq \mu \leq 4.0$, for the typical line-of-sight outdoor channels. A log-normal distributed random variable, s_{ln}, models the path loss variations, and we assume that it can be neglected. Note that the channel attenuation (7.10) is symmetric in both directions between the nodes, i, and, j. Assuming binary modulation, we define the SNR per encoded bit at the receiver to be, $\gamma_b = |g_{ij}|^2 a^2 E_b / N_0$,

where $E_b = \mathrm{E}[|\mathbf{x}_{qk}]\,|^2$ is the energy of the k-th binary symbol in the packet, $\mathbf{x}_q$, $k = 1, 2, \cdots, K$, $\mathrm{E}[\cdot]$ is expectation, and N_0 is the noise power spectral density. The AWGN's, $\mathbf{w}$, in (7.9) have independent real and imaginary parts of equal variance, $\sigma_w^2 = N_0/2$, per dimension. Denote, $\gamma_0 = E_b/N_0$, and denote by a_u^2, a_p^2, and a_q^2 the transmitter powers corresponding to the data packets, horizontal parity packets, and the vertical parity packets, respectively. The transmitter powers, a_u^2, a_p^2, and a_q^2 are assumed to be independent of the channel coefficients, g_{ij}. Thus, in order that the energy per bit, E_b, remain constant, one has that,

$$\begin{aligned} La_u^2 + a_p^2 + a_q^2 &= (L+2)E_b \quad \text{for MT, uplink} \\ La_u^2 + a_p^2 &= (L+2)E_b \quad \text{for AP, downlink} \\ a_q^2 &= (L+2)E_b \quad \text{for MT, downlink.} \end{aligned}$$

Furthermore and importantly, if the network mobility is sufficiently high in the duration of the transmission, one can assume random distribution of the nodes; for example, for Gaussian distributed nodes, the distances between nodes are Rayleigh or Ricean distributed. However, for low mobility networks, it is useful to evaluate the performance conditioned on the specific network realization to indicate locations of the nodes where the network reliability or the network throughput become unacceptable. In this case, the fading can be neglected, and the diversity gain is achieved by combining the signals transmitted from different nodes.

Modulation Schemes

In order to avoid phase tracking problems, and to simplify the receivers, we consider noncoherent BPSK (nBPSK) and differentially decoded differential BPSK (DBPSK). We also consider coherent BPSK (cBPSK) modulation as a reference. Hence, in general, denote by $\mathcal{I}$ the packet indices corresponding to the transmitted codeword, $\mathbf{x} = \{\cup_{q\in\mathcal{I}}\,\mathbf{x}_q\}$. In the destination node, assuming eq. (7.9), denote the received signal as, $\mathbf{y} = \{\cup_{q\in\mathcal{I}}\,\mathbf{y}_q\}$, and the corresponding channel coefficients as, $\mathbf{g} = \{\cup_{q\in\mathcal{I}}\,g_q\}$, where $g_q = |g_q|\,\mathrm{e}^{\mathrm{j}\psi_q}$, and the transmitted powers as, $\mathbf{a} = \{\cup_{q\in\mathcal{I}}\,a_q\}$. The conditional PDF of the received signal, $\mathbf{y}$, can be written as,

$$\begin{aligned} p(\mathbf{y}|\mathbf{g},\mathbf{a},\mathbf{x}) &= \prod_{q\in\mathcal{I}} p(\mathbf{y}_q|g_q,a_q,\mathbf{x}_q) \\ &= \prod_{q\in\mathcal{I}} \frac{1}{(\pi N_0)^K} \exp\left(-\frac{\|\mathbf{y}_q - g_q a_q \mathbf{x}_q\|^2}{N_0}\right) \end{aligned} \tag{7.11}$$

where $\|\cdot\|$ denotes the Euclidean norm of a vector. Then, the MLSD metric (in the log-likelihood domain), $\mathcal{M}_{\mathbf{x}}$, is the sum of the partial metrics, $\mathcal{M}_{\mathbf{x}_q}$, i.e., $\mathcal{M}_{\mathbf{x}} = \sum_{q\in\mathcal{I}} \mathcal{M}_{\mathbf{x}_q}$. The metric, $\mathcal{M}_{\mathbf{x}}$, is maximized over all possible transmitted codewords, $\mathbf{x}$, to obtain a maximum likelihood decision [17].

Consider cBPSK modulation. Using the PDF (7.11), the LLR's of binary symbols in the packet, $\mathbf{x}_q$, are, $\boldsymbol{\lambda}_q = \frac{4a_q}{N_0}\mathrm{Re}\{g_q^*\mathbf{y}_q\}$, where $(\cdot)^*$ is the complex conjugate. The partial metric is computed as, $\mathcal{M}_{\mathbf{x}_q} = a_q|g_q|\mathrm{Re}\{\,\mathrm{e}^{-\mathrm{j}\psi_q}\mathbf{x}_q^T\mathbf{y}_q\}$.

Assume that the phases, ψ_q, are uniformly distributed and constant over the packet duration. In order to avoid phase estimation, one can use nBPSK modulation with non-coherent detection. Thus, the PDF (7.11) is averaged over the phase, ψ_q, and we obtain [21], [16],

$$p(\mathbf{y}|g_q, a_q, \mathbf{x}_q) = \frac{1}{(\pi N_0)^K}\exp\left(-\frac{a_q^2|g_q|^2\,\|\mathbf{x}_q\|^2+\|\mathbf{y}_q^2\|}{N_0}\right) I_0\left(\frac{2a_q|g_q|\|\mathbf{x}_q^T\mathbf{y}_q|}{N_0}\right). \tag{7.12}$$

One can show that the partial metric corresponding to the PDF (7.12) is, $\mathcal{M}_{\mathbf{x}_q} = a_q|g_q|\|\mathbf{x}_q^T\mathbf{y}_q|$. If the phases, $\psi_q = \psi$, for all the packets, $q \in \mathcal{I}$, then the MLSD metric, $\mathcal{M}_{\mathbf{x}} = \left|\sum_{q\in\mathcal{I}} a_q|g_q|\,\mathbf{x}_q^T\mathbf{y}_q\right|$, [21], [16]. However, if the phase shifts, ψ_q, $q \in \mathcal{I}$, are changing from one packet to another, the partial metric, $\mathcal{M}_{\mathbf{x}_q}$, derived from (7.12) can only be used for very large packet length, $K \gg 1$, in order to obtain the phase averaging effect over the phases, $\{\cup_{q\in\mathcal{I}}\psi_q\}$. In this case, differential detection should generally be used.

Consider DBPSK modulation. We obtain the LLR values for differentially encoded symbols, $\mathbf{x}_{qk}$, $k = 1, 2, \cdots, K$, where the first symbol, x_{q1}, is a reference. Hence, the PDF of the decision variable, ξ_{qk}, after the differential detection, i.e., $\xi_{qk} = \mathrm{Re}\left\{y_{qk}y_{q(k-1)}^*\right\}$, is written as [154],

$$p(\xi_{qk}|a_q, |g_q|, x_{qk}) = \frac{\exp\left(\frac{2\xi_{qk}x_{qk}}{N_0}-\gamma_q\right)}{N_0}\begin{cases} Q_1(\sqrt{2\gamma_q}, \sqrt{8\xi_{qk}x_{qk}/N_0}) & \xi_{qk}x_{qk} > 0 \\ 1 & \xi_{qk}x_{qk} \le 0. \end{cases} \tag{7.13}$$

One can also obtain the CHF, $\Psi_{\xi_{qk}}(\mathrm{j}\omega) = \mathrm{E}[\exp(-\mathrm{j}\omega\xi_{qk})]$, of the decision variable, ξ_{qk}, i.e.,

$$\Psi_{\xi_{qk}}(\mathrm{j}\omega) = \frac{1}{1+\left(\frac{2\xi_{qk}x_{qk}\omega}{N_0}\right)^2}\exp\left(\frac{-4\mathrm{j}\gamma_q\xi_{qk}x_{qk}\omega/N_0}{1+\mathrm{j}2\xi_{qk}x_{qk}\omega/N_0}\right).$$

Then, the exact LLR of the binary symbol, x_{qk}, is given as,

$$\lambda_{qk} = \text{sign}\left(\frac{2\xi_{qk}}{N_0}\right)\left(4|\xi_{qk}|/N_0 + \log Q_1(\sqrt{2\gamma_q}, \sqrt{8|\xi_{qk}|/N_0})\right) \tag{7.14}$$

where γ_q is the SNR of the packet, q, and $Q_1(\cdot,\cdot)$ is the Marcum Q-function; see (A-9b). Note that, for large γ_q, the logarithmic term in the LLR (7.14) can be neglected; cf. the LLR expression for cBPSK modulation. Alternatively, one can use the received samples, $y_{q(k-1)}$, as the channel estimates to minimize the squared Euclidean norm, $\sum_{k=2}^{K} |y_{qk} - y_{q(k-1)}x_{qk}|^2$, [155]. Note also that, $\min_{x_{qk}} |y_{qk} - y_{q(k-1)}x_{qk}|^2 \propto \max_{x_{qk}} \text{Re}\left\{y_{qk}y^*_{q(k-1)}\right\} x_{qk} = \max_{x_{qk}} \xi_{qk}\, x_{qk}$. The decision variables, ξ_{qk}, are, in general, correlated, and we can show that the normalized correlation of, ξ_{qk}, and, $\xi_{q(k-1)}$, is equal to, $\frac{x_{qk}x_{q(k-1)}}{1/\gamma_q+2}$; thus, the correlation increases with the SNR. Assuming approximation of (7.13) for large values of SNR and differential detection, the partial metric is, $\mathcal{M}_{\mathbf{x}_q} = \sum_{k=2}^{K} \xi_{qk}\, x_{qk}$, [155].

Channel Estimation

Consider estimation of the variable, $h_q = a_q^2|g_q|^2$. The values of h_q are used to select the parity check matrices, $\mathbf{B}_{[2]i}$, at Stage 2 of the protocol in Fig. 7.5. Also, since the channel attenuation is a function of the distance from the transmitter antenna, one can use knowledge of h_q to determine distances between the nodes. For low mobility nodes, the channel is approximately constant over many packets, and thus, the estimator of h_q is chosen to be consistent [156], and simple to implement. Hence, for cBPSK modulation, conditioned on the transmitted sequence, $\mathbf{x}$, the ML estimator of h_q is [21],

$$\hat{h}_q = \frac{2}{K}\text{Re}\left\{\, \text{e}^{-\text{j}\hat{\psi}_{q_{\text{ML}}}} \mathbf{x}_q^T \mathbf{y}_q \right\}$$

where $\hat{\psi}_q = \arg(\mathbf{x}_q^T \mathbf{y}_q)$ is the ML estimator of ψ_q.

For nBPSK modulation, assume that the moments, $\text{E}[|y_{qK}|^m]$, $m \geq 1$, are constant for all packets and bits. Thus, for $m = 2$, $\text{E}\left[|y_{qK}|^2\right] = h_q + N_0$, and the moment estimator of h_q is [156],

$$\hat{h}_q = \frac{1}{K}\sum_{k=1}^{K} |y_{qk}|^2 - N_0 \tag{7.15}$$

where the values, N_0, are assumed to be known or can be estimated, for a given receiver. Furthermore, we can show that the estimator (7.15) has variance, $\text{var}\left[\hat{h}_q\right] = (2h_qN_0 + N_0^2)/K$.

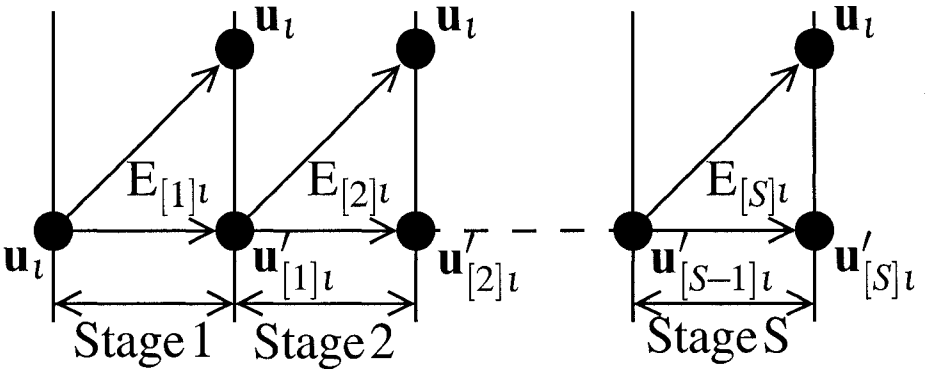

Figure 7.7: An equivalent channel model for the S transmission stages.

7.2.4 Performance Analysis

In general, in stage, s, the destination node decodes the transmitted packet, $\mathbf{u}_q$, or an incorrect packet, $\mathbf{u}'_{[s]q} \neq \mathbf{u}_q$. Thus, the transmission of packets, $\mathbf{u}_q$, from a source to a destination node can be modeled as concatenation of the S discrete channels with memory as shown in Fig. 7.7. Denote $\mathrm{E}_{[s]q}$ to be an error event that the destination node does not decode the packet, $\mathbf{u}_q$, in Stage s. Using the law of total probability, the PER at the destination node in Stage S can be evaluated as,

$$\begin{aligned}
\mathrm{PER}_{[S]} &= \frac{1}{|\mathcal{I}_\mathrm{u}|}\sum_{q\in\mathcal{I}_\mathrm{u}} \Pr\big(\cup_{s=1}^{S}\mathrm{E}_{[s]q}\big) \\
&= \frac{1}{|\mathcal{I}_\mathrm{u}|}\sum_{q\in\mathcal{I}_\mathrm{u}} \prod_{s=1}^{S} \Pr\big(\mathrm{E}_{[s]q}\big|\cup_{r=1}^{s-1}\mathrm{E}_{[r]q}\big) \\
&\leq \frac{1}{|\mathcal{I}_\mathrm{u}|}\sum_{q\in\mathcal{I}_\mathrm{u}} \prod_{s=1}^{S} \Pr\big(\mathrm{E}_{[s]q}\big) \qquad (7.16)
\end{aligned}$$

where $\Pr\big(\mathrm{E}_{[s]q}\big)$ denotes the probability of event $\mathrm{E}_{[s]q}$. Hence, if the data packet, q, is decoded in Stage $(s-1)$ of the protocol, then $\Pr\big(\mathrm{E}_{[s]q}\big|\cup_{r=1}^{s-1}\mathrm{E}_{[r]q}\big) = 0$. Inequality (7.16) follows assuming that the decoding of the protocol stages is independent. Also, we observe from (7.16) that the maximum diversity order of the protocol in Fig. 7.5 is given by the number of transmission stages, S.

We analyze the performance of the protocol stages in Fig. 7.5. Hence, assuming the destination node, i, and the channel codes, $\mathcal{C}_{[s]i}$, $s = 1, 2$, and 3 are linear, without loss of generality the all-zero codeword, $\mathbf{0}$, can be considered as transmitted. We can upper bound the PER of the code, $\mathcal{C}_{[s]i}$,

using a truncated union bound, i.e., [17],

$$\mathrm{PER}_{[s]i} \leq \sum_{\mathbf{c}\in\mathcal{L}_i(e_m)} \frac{\sum_{q\in\mathcal{I}_{\mathrm{u}i}} \tilde{\mathrm{I}}(\mathrm{w_H}(\mathbf{c}_q))}{|\mathcal{I}_{\mathrm{u}i}|} \mathrm{PEP}_{[s]i}(\mathbf{0}\mapsto\mathbf{c}) \tag{7.17}$$

where the indicator function, $\tilde{\mathrm{I}}(x)=1$, if $x>0$, and, $\tilde{\mathrm{I}}(x)=0$, otherwise, $\mathrm{PEP}_{[s]i}(\mathbf{0}\mapsto\mathbf{c})$ denotes the PEP that the all-zero codeword, $\mathbf{0}$, was transmitted, and the codeword, $\mathbf{c}=\{\cup_q \mathbf{c}_q\}$, is decoded at the destination node, i, and $\mathrm{w_H}(\mathbf{c}_q)$ is the Hamming weight of the packet, $\mathbf{c}_q$. The list, $\mathcal{L}_i(e_m) = \{\mathbf{c}\in\mathcal{C}_{[s]i} : \mathbf{c}\neq\mathbf{0}, \mathrm{w_H}(\mathbf{c}_q)\leq e_m, \forall q\in\mathcal{I}_{\mathrm{u}i}\}$, where e_m is the maximum number of bit errors in the packet, $\mathbf{c}_q$. The size of the list is, $|\mathcal{L}_i(e_m)| = \left(\sum_{e=0}^{e_m}\binom{K}{e}\right)^{|\mathcal{I}_{\mathrm{u}i}|} - 1$, where $\binom{K}{e}$ is the binomial coefficient, and $|\mathcal{I}_{\mathrm{u}i}|$ is the cardinality of $\mathcal{I}_{\mathrm{u}i}$.

Recall that, in Stage 3 of the protocol, a SPC code is employed for successfully decoded data packets to generate the packets of vertical parity bits for the cooperative diversity. In the downlink, the destination node, $i=1,2,\cdots,N$, is the MT, and it decodes the data packets, $\mathcal{I}_{\mathrm{u}i}$. In the uplink, the destination node, $i=0$, is the AP, and it decodes the data packets, $\mathcal{I}_{\mathrm{u}}$. Hence, denote $\mathrm{PER}_{[1]qi}$ and $\mathrm{PER}_{[2]qi}$ to be the probabilities of not decoding the data packet, q, in the node, $i=0,1,\cdots,N$, in Stage 1 and Stage 2 of the protocol, respectively. The probabilities, $\mathrm{PER}_{[1]qi}$, and, $\mathrm{PER}_{[2]qi}$, are functions of the SNR and the codes, $\mathcal{C}_{[1]i}$, and, $\mathcal{C}_{[2]i}$. Using (7.16) and the law of total probability, i.e., conditioned on the successful and unsuccessful decoding of the data packet, q, in the node, i, in Stage 1 of the protocol, the probability of not decoding the data packet, q, in Stage 2 of the protocol can be upper bounded as,

$$\mathrm{PER}'_{[2]qi} \leq \mathrm{PER}_{[2]qi}\mathrm{PER}_{[1]qi}. \tag{7.18}$$

Correspondingly, the probability, $\mathrm{PER}'_{[2]qi}$, assumes that the decoding in Stage 2 of the protocol depends on the success of the decoding in Stage 1. Then, the elements of the matrix, $\mathbf{V}_{[3]}$, are given as,

$$[\mathbf{V}_{[3]}]_{iq} = \begin{cases} 1 & \text{w.p. } (1-\mathrm{PER}'_{[2]qi}) \\ 0 & \text{w.p. } \mathrm{PER}'_{[2]qi}. \end{cases} \tag{7.19}$$

Note that, in the uplink, $[\mathbf{V}_{[3]}]_{iq}=1$, with probability (w.p.) 1, for the data packets, $q\in\mathcal{I}_{\mathrm{u}i}$, corresponding to the i-th source node. Also, if the i-th node does not participate in the cooperation, then the i-th row of the matrix, $\mathbf{V}_{[3]}$, has all components equal to 0.

Denote by $\mathrm{PER}_{[3]qi}(\mathbf{V}_{[3]})$ the PER of the random code, $\mathcal{C}_{[3]}$, in Stage 3 of the protocol corresponding to the data packet, q, and the destination node, i, conditioned on the parity check matrix,

$\mathbf{V}_{[3]}$. Note that the statistics of the random matrix, $\mathbf{V}_{[3]}$, are given by the PER's of Stage 1 and Stage 2 of the protocol, and also, that the PER, $\mathrm{PER}_{[3]qi}(\mathbf{V}_{[3]})$, is function of $\mathbf{V}_{[3]}$. Then, in the downlink, the overall PER, $\mathrm{PER}_{[3]}$, is the expected value over all realizations of the matrix, $\mathbf{V}_{[3]}$, the N destination nodes, and the corresponding L data packets, i.e.,

$$\mathrm{PER}_{[3]} = \frac{1}{N}\sum_{i=1}^{N}\frac{1}{|\mathcal{I}_{\mathrm{u}i}|}\sum_{q\in\mathcal{I}_{\mathrm{u}i}}\sum_{\mathbf{V}_{[3]}}\mathrm{PER}_{[3]qi}(\mathbf{V}_{[3]})\Pr(\mathbf{V}_{[3]})\,. \tag{7.20}$$

In the uplink, the overall PER, $\mathrm{PER}_{[3]}$, is the expected value over all realizations of the matrix, $\mathbf{V}_{[3]}$, and NL data packets, i.e.,

$$\mathrm{PER}_{[3]} = \frac{1}{|\mathcal{I}_{\mathrm{u}}|}\sum_{q\in\mathcal{I}_{\mathrm{u}}}\sum_{\mathbf{V}_{[3]}}\mathrm{PER}_{[3]q0}(\mathbf{V}_{[3]})\Pr(\mathbf{V}_{[3]})\,. \tag{7.21}$$

Importantly, note that evaluation of the PER, $\mathrm{PER}_{[3]}$, using (7.20) and (7.21) has dimension proportional to, $NL \gg 1$. In order to reduce the problem dimension and simplify the analysis, we define an auxiliary binary random vector, $\mathbf{D}_i \in \mathbb{Z}_2^{NL}$, for the destination node, i. The q-th component, $[\mathbf{D}_i]_q = 1$, if the data packet, q, is not decoded at the destination node, i, and, $[\mathbf{D}_i]_q = 0$, otherwise. Then, the components of $\mathbf{D}_i$ are,

$$[\mathbf{D}_i]_q = \begin{cases} 1 & \text{w.p. } \mathrm{PER}'_{[2]qi} \\ 0 & \text{w.p. } (1-\mathrm{PER}'_{[2]qi}). \end{cases} \tag{7.22}$$

Thus, in the downlink, for the i-th destination node, the i-th row of $\mathbf{V}_{[3]}$ is a binary complement of $\mathbf{D}_i$. Since the all-zero codeword is assumed transmitted, then, in the downlink, one can consider only a subset, $\mathcal{I}'_{\mathrm{u}} \subseteq \mathcal{I}_{\mathrm{u}}$, of $N' \leq NL$ data packets that cannot be successfully decoded at the destination node, i. The undecoded packets, $\mathcal{I}'_{\mathrm{u}}$, correspond to the non-zero components of the vector, $\mathbf{D}_i$. The cardinality, $|\mathcal{I}'_{\mathrm{u}}| = N'$, and thus, the dimension of the analysis is reduced to N'. Importantly, note that, for stronger codes, $\mathcal{C}_{[1]i}$, and, $\mathcal{C}_{[2]i}$, and larger values of SNR's, the probabilities, $\mathrm{PER}'_{[2]qi}$, and the values, N', are smaller. Particularly, for the i-th destination node, using eq. (7.22), we can show that the probability mass of N' is given by the generalized binomial distribution, i.e.,

$$\Pr(N'=n') = \sum_{\substack{\mathbf{D}_i \\ \sum_q[\mathbf{D}_i]_q=n'}}\prod_{q=1}^{NL}\left(\mathrm{PER}'_{[2]qi}\right)^{[\mathbf{D}_i]_q}\left(1-\mathrm{PER}'_{[2]qi}\right)^{1-[\mathbf{D}_i]_q} \tag{7.23}$$

and $\sum_{n'=0}^{NL} \Pr(N' = n') = 1$. The generalized binomial distribution is readily computed in the transform domain; see [157, Appendix C] and [158]. Hence and importantly, without loss of generality, $(NL - N')$ columns of the matrix, $\mathbf{V}_{[3]}$, corresponding to the successfully decoded packets in the destination node, i, (i.e., corresponding to the zero components of the vector, $\mathbf{D}_i$), can be removed; the resulting matrix is denoted as, $\mathbf{V}'_{[3]i} \in \mathbb{Z}_2^{(N,N')}$. Furthermore, assume downlink transmission, and let $\mathcal{I}'_{\mathrm{u}i} \subseteq \mathcal{I}'_{\mathrm{u}}$ be the data packets of the i-th destination node. Then, one can condition the PER in Stage 3 of the protocol on the matrix, $\mathbf{V}'_{[3]i}$, and the PER (7.20) can be efficiently evaluated as,

$$\mathrm{PER}_{[3]} = \frac{1}{N} \sum_{i=1}^{N} \frac{1}{|\mathcal{I}'_{\mathrm{u}i}|} \sum_{q \in \mathcal{I}'_{\mathrm{u}i}} \sum_{\mathbf{V}'_{[3]i}} \mathrm{PER}_{[3]iq}(\mathbf{V}'_{[3]i}) \Pr\left(\mathbf{V}'_{[3]i}\right). \tag{7.24}$$

In the uplink, we can use the vector, $\mathbf{D}_0$, to remove columns of the matrix, $\mathbf{V}_{[3]}$, corresponding to the successfully decoded packets in the AP, and obtain the matrix, $\mathbf{V}'_{[3]0}$. Then, assuming a subset, $\mathcal{I}'_{\mathrm{u}0} \subseteq \mathcal{I}_{\mathrm{u}}$, of $N' \leq NL$ data packets that cannot be successfully decoded in the AP, the PER (7.21) can be efficiently evaluated as,

$$\mathrm{PER}_{[3]} = \frac{1}{|\mathcal{I}'_{\mathrm{u}0}|} \sum_{q \in \mathcal{I}'_{\mathrm{u}0}} \sum_{\mathbf{V}'_{[3]0}} \mathrm{PER}_{[3]q0}(\mathbf{V}'_{[3]0}) \Pr\left(\mathbf{V}'_{[3]0}\right). \tag{7.25}$$

Thus, the dimension of the analysis is again reduced to N'. Finally, in this chapter, eqs. (7.24) and (7.25) are evaluated using computer simulations.

Pairwise Error Probabilities

In general, the PEP conditioned on the channel coefficients, $\mathbf{g}$, and the transmitter powers, $\mathbf{a}$, is evaluated as [17],

$$\mathrm{PEP}(\mathbf{x} \mapsto \mathbf{x}' | \mathbf{g}, \mathbf{a}) = \Pr(D_{\mathbf{x}\mathbf{x}'} < 0 | \tilde{\mathbf{g}}, \tilde{\mathbf{a}})$$

where $\mathbf{x} = \{\cup_{q \in \mathcal{I}} \mathbf{x}_q\}$ is the transmitted sequence corresponding to the codeword, $\mathbf{c} = \{\cup_{q \in \mathcal{I}} \mathbf{c}_q\}$, $\mathbf{x}' = \{\cup_{q \in \mathcal{I}} \mathbf{x}'_q\}$ is the decoded sequence (in the pairwise error event sense) corresponding to the codeword, $\mathbf{c}' = \{\cup_{q \in \mathcal{I}} \mathbf{c}'_q\}$, and $D_{\mathbf{x}\mathbf{x}'} = \sum_{q \in \mathcal{I}} D_{\mathbf{x}\mathbf{x}'q} = \mathcal{M}_{\mathbf{x}} - \mathcal{M}_{\mathbf{x}'}$ is the difference of the metric, $\mathcal{M}_{\mathbf{x}} = \sum_{q \in \mathcal{I}} \mathcal{M}_{\mathbf{x}q}$, and, $\mathcal{M}_{\mathbf{x}'} = \sum_{q \in \mathcal{I}} \mathcal{M}_{\mathbf{x}'q}$.

We consider cBPSK modulation as a reference. In particular, the PEP of cBPSK modulation

can be written as [82],

$$\mathrm{PEP}(\mathbf{x} \mapsto \mathbf{x}'|\mathbf{g}, \mathbf{a}) = Q\left(\sqrt{\sum_{q\in\mathcal{I}} \frac{a_q^2|g_q|^2}{2N_0} \left\|\mathbf{x}_q - \mathbf{x}'_q\right\|^2}\right)$$

where $\left\|\mathbf{x}_q - \mathbf{x}'_q\right\|^2 = 4\mathrm{w_H}(\mathbf{c}, \mathbf{c}')$, $\mathrm{w_H}(\mathbf{c}, \mathbf{c}')$ is the Hamming distance between the codewords, $\mathbf{c}$, and, $\mathbf{c}'$, and the Q-function, $Q(x) = (2\pi)^{-1/2}\int_x^\infty \exp(-t^2/2)\mathrm{d}t$, [21].

For nBPSK modulation, we assume that the phase shift is constant for all packets, $\mathcal{I}$, i.e., $\psi_q = \psi, \forall q \in \mathcal{I}$. We can follow reference [159] to obtain the PEP of nBPSK modulation. In particular, let the MLSD metric of the codeword, $\mathbf{x}'$, be, $\mathcal{M}_{\mathbf{x}'} = |\sum_{q\in\mathcal{I}} a_q|g_q|\mathbf{x}_q'^T(a_q|g_q|\mathbf{x}_q + \mathbf{w}_q)| = |N_t\rho_{\mathbf{x}\mathbf{x}'} + \sqrt{N_t}\mathbf{w}'|$ where $\mathbf{w}'$ is the vector of zero-mean AWGN's having variance, $\mathrm{E}\left[|w'_{qk}|^2\right] = N_0$, per dimension, and $k = 1, \cdots, K$. The normalized correlation and the total energy of the useful signal are given as, $\rho_{\mathbf{x}\mathbf{x}'} = \frac{1}{N_t}\sum_{q\in\mathcal{I}} a_q^2|g_q|^2\ \mathbf{x}_q'^T\mathbf{x}_q$, and, $N_t = K\sum_{q\in\mathcal{I}} a_q^2|g_q|^2$, respectively, where $\mathbf{x}_q'^T\mathbf{x}_q = K - 2\mathrm{w_H}(\mathbf{x}_q, \mathbf{x}'_q)$. Thus, the PEP of nBPSK modulation is [21, eq. (5-4-4)],

$$\mathrm{PEP}(\mathbf{x} \mapsto \mathbf{x}'|\mathbf{g}, \mathbf{a}) = Q_1(\frac{\tilde{a}}{2}, \frac{\tilde{b}}{2}) - \frac{1}{2}\exp\left(-\frac{\tilde{a}^2 + \tilde{b}^2}{8}\right) I_0\left(\frac{\tilde{a}\tilde{b}}{4}\right) \tag{7.26}$$

where the coefficients, $\tilde{a} = \sqrt{N_t\gamma_0(1 - \sqrt{1 - \rho^2_{\mathbf{x}\mathbf{x}'}})}$, and, $\tilde{b} = \sqrt{N_t\gamma_0(1 + \sqrt{1 - \rho^2_{\mathbf{x}\mathbf{x}'}})}$.

For differentially decoded DBPSK modulation, we have that, $D_{\mathbf{x}\mathbf{x}'q} = \frac{1}{2}\sum_{k=2}^{K}(y_{qk}y^*_{q(k-1)} + y^*_{qk}y_{q(k-1)})(x_{qk} - x'_{qk})$. In this case, the PEP is evaluated using the CHF of $D_{\mathbf{x}\mathbf{x}'q}$, as shown in [155]. We omit the packet index, q, for brevity, and obtain the CHF of $D_{\mathbf{x}\mathbf{x}'q}$. Hence, define the $2(K-1) \times 2(K-1)$ matrix,

$$\mathbf{F} = \begin{bmatrix} \mathbf{0} & \mathbf{\Delta}_{\mathbf{x}\mathbf{x}'} \\ \mathbf{\Delta}_{\mathbf{x}\mathbf{x}'} & \mathbf{0} \end{bmatrix}$$

where $\mathbf{\Delta}_{\mathbf{x}\mathbf{x}'} = \mathrm{diag}(x_2 - x'_2, \cdots, x_K - x'_K)^T$ is the diagonal matrix. Define also a complex-valued jointly Gaussian vector, $\mathbf{z} = (y_1, \cdots, y_{K-1}, y_2, \cdots, y_K)^T$, having the mean, $\bar{\mathbf{z}} = \mathrm{E}[\mathbf{z}] = ag\,(x_1, \cdots, x_{K-1}, x_2, \cdots, x_K)^T = ag\,\bar{\mathbf{x}}$, and the covariance,

$$\mathrm{E}\left[(\mathbf{z} - \bar{\mathbf{z}})(\mathbf{z} - \bar{\mathbf{z}})^{*T}\right] = N_0 \begin{bmatrix} \mathbf{I}_{(K-1)} & \mathbf{J}^T_{(K-1)} \\ \mathbf{J}_{(K-1)} & \mathbf{I}_{(K-1)} \end{bmatrix} = N_0\mathbf{\Sigma}$$

where the $(K-1)\times(K-1)$ matrix,

$$\mathbf{J}_{(K-1)} = \begin{bmatrix} 0 & 1 & \cdots & 0 \\ \vdots & & \ddots & \vdots \\ & & & 1 \\ 0 & & \cdots & 0 \end{bmatrix}.$$

Then, the CHF, $\Psi_{D_{\mathbf{x}\mathbf{x}'q}}(\mathrm{j}\omega) = \mathrm{E}\big[\exp(-\mathrm{j}\omega D_{\mathbf{x}\mathbf{x}'q})\big]$, of $D_{\mathbf{x}\mathbf{x}'q}$ can be written as [155],

$$\Psi_{D_{\mathbf{x}\mathbf{x}'q}}(\mathrm{j}\omega) = \frac{\exp\left(-a_q^2|g_q|^2\frac{1}{2}\mathrm{j}\omega\bar{\mathbf{x}}\mathbf{F}(\mathbf{I}+\frac{1}{2}N_0\mathrm{j}\omega\boldsymbol{\Sigma}\mathbf{F})^{-1}\bar{\mathbf{x}}\right)}{\det\left(\mathbf{I}+N_0\frac{\mathrm{j}\omega}{2}\boldsymbol{\Sigma}\mathbf{F}\right)}. \tag{7.27}$$

Correspondingly, conditioned on the sequences, $\mathbf{x}$, and, $\mathbf{x}'$, the values, $D_{\mathbf{x}\mathbf{x}'q}$, for packets, $q\in\mathcal{I}$, are independent, and thus, $\Psi_{D_{\mathbf{x}\mathbf{x}'}}(\mathrm{j}\omega) = \prod_{q\in\mathcal{I}}\Psi_{D_{\mathbf{x}\mathbf{x}'q}}(\mathrm{j}\omega)$. Finally, the PEP is computed using eq. (3) from [82], i.e.,

$$\mathrm{PEP}(\mathbf{x}\mapsto\mathbf{x}'|\mathbf{g},\mathbf{a}) = \frac{1}{2\pi}\int_{\tilde{c}-\mathrm{j}\infty}^{\tilde{c}+\mathrm{j}\infty}\frac{\Psi_{D_{\mathbf{x}\mathbf{x}'}}(\mathrm{j}\omega)}{\mathrm{j}\omega}\mathrm{d}\omega. \tag{7.28}$$

Note that the residue theorem cannot be used to compute (7.28) due to the essential singularity in (7.27); (in contrast, the essential singularity is removed in [155] since $\mathbf{z}$ has zero-mean in [155]). We evaluate the PEP (7.28) using Gauss-Chebyshev quadrature, i.e., [82],

$$\begin{aligned}\mathrm{PEP}(\mathbf{x}\mapsto\mathbf{x}'|\mathbf{g},\mathbf{a}) = \frac{1}{2Z}\sum_{z=1}^{Z}\big(&\mathrm{Re}\big\{\Psi_{D_{\mathbf{x}\mathbf{x}'}}(c(1+\mathrm{j}\tau_z))\big\}+\\ &+\tau_z\mathrm{Im}\big\{\Psi_{D_{\mathbf{x}\mathbf{x}'}}(c(1+\mathrm{j}\tau_z))\big\}\big)\end{aligned} \tag{7.29}$$

where $Z\gg 1$ and c are chosen for numerical convergence, and, $\tau_z = \tan((z-1/2)\pi/Z)$.

7.2.5 Numerical Examples

In the uplink, the MT's transmit and receive packets in all three stages while the AP only listens. In the downlink, the AP transmits packets in Stage 1 and Stage 2 of the protocol while the MT's listen, and in Stage 3, the MT's transmit and listen. Consider the link budget of a typical Wi-Fi system. The transmitter powers are 20–35 dBm for the AP, and 10–20 dBm for the MT. The typical noise figure for a low cost receiver is, say, 10 dB at the AP, and 13 dB at the MT. Let the minimum required SNR for the receiver (e.g., to detect the signal and acquire synchronization) be, 1 dB, for the AP, and, 3 dB, for the MT. Typical values of the background thermal noise are -175 dBm/Hz

Table 7.7: An example link budget for the AP and the MT.

	AP	MT
transmit power$^{(*)}$	20 dBm	
data rate$^{(*)}$	10 Mbps $\sim$ 10 MHz	
noise figure$^{(*)}$	10 dB	13 dB
thermal noise$^{(*)}$	-165 dBm/Hz	
path loss at 100m	-86.4 dB	
noise level at Rx	-85 dBm	-82 dBm
minimum SNR $\gamma_{b\min}{}^{(*)}$	1 dB	3 dB
receiver sensitivity	-84 dB	-79 dB
signal level at Rx	-66.4 dBm	
SNR γ_0 at 0m	105 dB	102 dB
SNR γ_b at 100m	18.6 dB	15.6 dB

to -165 dBm/Hz, and we assume a bandwidth of 10 MHz for a 10 Mbps (mega-bits per second) raw data rate (i.e., including the parity bits); thus, the spectral efficiency is 1 bit per second per Hertz. We can compute the required receiver sensitivity as the sum (in dB) of the background noise, the noise figure, and the minimum required SNR. An example of the link budget analysis to calculate the receiver SNR at a distance of 100m from the transmitter antenna of the AP and the MT, respectively, is given in Table 7.7. In Table 7.7, we assume that the path loss exponent, $\mu = 2$, and the wavelength, $\lambda = 0.06$m, corresponding to the carrier frequency, 5 GHz. An asterisk in the first column of Table 7.7 denotes input values; the other values are computed. For example, the noise level at the AP receiver is, $-165 + (10 \log_{10} 10^7) + 10 = -85$ dBm, the AP receiver sensitivity is, $-85 + 1 = -84$ dB, the signal level at the AP receiver is, $20 - 86.4 = -66.4$ dBm, and thus, the SNR at the AP receiver is, $-66.4 - (-85) = 18.6$ dB.

Assuming the parameters and the link budget analysis given in Table 7.7, and the path loss model (7.10), Fig. 7.8 shows the receiver SNR, $\gamma_b = |g|^2 \gamma_0$, where $|g|^2 \approx 2.28 \cdot 10^{-5} \cdot d^{-\mu}$, versus the distance, d, from the transmitter antenna, for $\mu = 2$, 3, and 4. The 3 dB difference between the AP and the MT receiver SNR's in Fig. 7.8 corresponds to the difference in the noise figures of the AP and the MT receivers. Note that the additional 2 dB difference in the minimum required SNR for the AP and the MT receivers results in downlink coverage of 600m, while the uplink coverage is only 550m, assuming equal uplink and downlink transmitter powers of 20 dBm. Hence, the receiver sensitivity is an important design parameter, and it is directly related to the achievable coverage of the network.

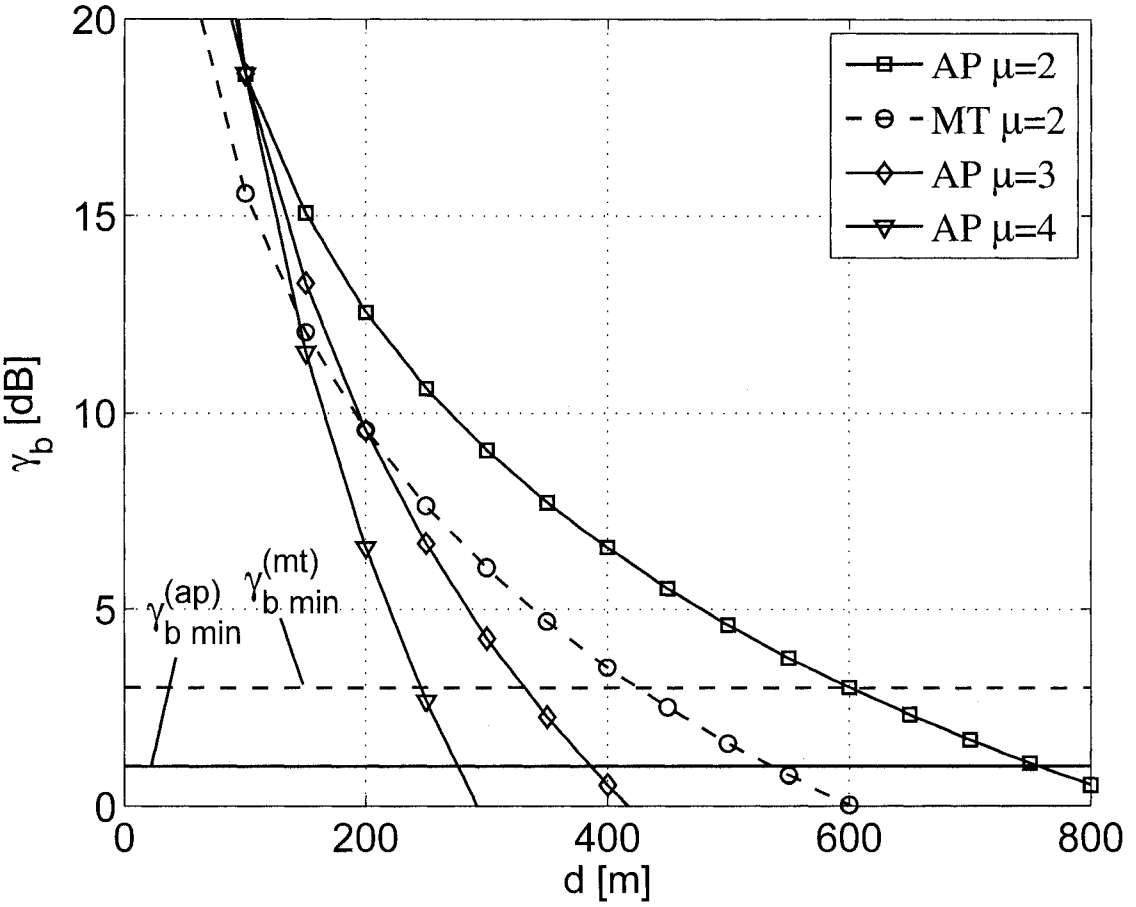

Figure 7.8: The uplink and downlink receiver SNR, γ_b, versus the distance, d.

In the sequel, we study the uplink and downlink PER performance versus the distance to evaluate the achievable network coverage at the three stages of the protocol in Fig. 7.5. In particular, the PER analysis in Stage 1 and Stage 2 of the protocol is considered independently; one can use eq. (7.18) to estimate the PER in Stage 2 of the protocol taking into account the possibility of the successful decoding already in Stage 1. The PER's, $\mathrm{PER}_{[1]i} = \mathrm{PER}_{[1]}$, and, $\mathrm{PER}_{[2]i} = \mathrm{PER}_{[2]}$, are obtained for the particular node, i, employing a truncated union bound (7.17). Also, using computer simulations, we estimate the PER for Stage 3 of the protocol at a particular destination node, i, assuming that Stage 2 of the protocol is represented by the PER's, $\mathrm{PER}_{[2]i}$; in this case, the decoding in Stage 1 is ignored. In general, we assume the packet length, $K = 24$, bits, and the network topology in Fig. 7.6, for $N = 4$ and 8 users, the distance, $d_{\mathrm{ap}} = 0$m and 400m, and for varying values of $d_{\mathrm{mt}} = d$.

PER of Stage 1

We assume the CRC generating polynomial, $z^6 + z^4 + z^3 + 1$, where z is a dummy variable [150]. Thus, we have, $K_{\mathrm{crc}} = 6$, CRC bits, and, $K_{\mathrm{u}} = 18$ ($K_{\mathrm{u}} = 17$, for differential encoding), information bits. Since the minimum Hamming distance, $d_{\mathrm{crc}} = 4$, this polynomial can detect all error patterns of weight, $1, 2, 3, 5, 7, 9, \cdots$. Fig. 7.9 shows the union bound (7.17) of the PER, $\mathrm{PER}_{[1]}$, for the uplink transmission. We assume, $Z = 128$, and, $c = 1/4$, in calculating the PEP's (7.29). The simulation results in Fig. 7.9 were obtained for the transmitter power, $a_u^2 = 1$, and Wagner decoding flipping the 7 least reliable bits, for cBPSK, nBPSK, differentially decoded DBPSK, and noncoherent binary frequency shift keying (nBFSK) modulations; the probability of bit-error for uncoded nBFSK modulation is given by [21, eq. (5-4-47)]. We observe from Fig. 7.9 that the CRC coding and Wagner decoding (with no packet retransmissions) improve the link coverage by 200m for cBPSK, and by 100m for nBFSK at $\mathrm{PER}_{[1]} = 10^{-2}$.

PER of Stage 2

Consider the IBRC's and the SPCPC's for Stage 2 of the protocol in Fig. 7.5. Let the transmission powers be, $La_u^2 + a_p^2 = (L+1)E_b$, so that, $a_u^2 < (1 + 1/L)E_b$, for the data packets, and, $a_p^2 < (1+L)E_b$, for the horizontal parity packets. We assume differentially detected DBPSK and that neither the CRC bits nor any decoding in Stage 1 are employed. Fig. 7.10 compares the truncated union bound (7.17) for the PER, $\mathrm{PER}_{[2]}$, of the IBRC's and the SPCPC's versus the distance, d, for $d_{\min} = 4$, and $L = 1$ and 2 data packets. The parity check matrix of the IBRC's, for $d_{\min} = 4$, is

given in Section II.B. Note that the data packets employing the SPC coding and DBPSK modulation contain, $K_{\rm u} = 22$, information bits, while $K_{\rm u} = 23$ for information bits in data packets using the IBRC's. We observe from Fig. 7.10 that reducing the power, a_u^2, while increasing the power, a_p^2, improves the link coverage for the IBRC's, however, the improvement monotonically decreases with L. On the other hand, the optimum transmission power distribution for the SPCPC's is uniform, i.e., $a_u^2 = a_p^2$.

The PER truncated union bounds for the IBRC's of rate, $R = 1/2$ (i.e., $L = 1$), and $R = 2/3$ (i.e., $L = 2$), and $d_{\min} = 5$ and 7, are shown in Fig. 7.11. The parity check matrix of the IBRC's is generated by the cyclic shifts, $(0, 1, 2, 4)$, for $L = 1$ and $d_{\min} = 5$, $(0, 1, 2, 4, 5, 7)$, for $L = 1$ and $d_{\min} = 7$, $(0, 1, 2, 4)$ and $(0, 1, 5, 8)$, for $L = 2$ and $d_{\min} = 5$, and $(0, 1, 2, 4, 5, 7)$ and $(0, 1, 5, 8, 9, 14)$, for $L = 2$ and $d_{\min} = 7$. We observe from Fig. 7.11 that reducing the power, a_u^2, while increasing $d_{\min}$ and L significantly improves the achievable coverage. For example, the coverage of 370m for the IBRC of $R = 1/2$, $a_u^2 = 1.0$, and $d_{\min} = 5$, is increased to 470m for the IBRC of $R = 2/3$, $a_u^2 = 0.5$, and $d_{\min} = 7$, for $\text{PER}_{[2]} = 10^{-2}$. Note also that, in general, the power optimized IBRC's outperform the SPCPC's, for the same $d_{\min}$.

PER of Stage 3

Exact analytical evaluation of the performance for Stage 3 of the protocol in Fig. 7.5 is particularly difficult. Thus, MC simulation, and the truncated union bound are used to obtain the expected PER averaged over the realizations of $\mathbf{V}'_{[3]i}$, for a particular destination node, i. As an example, assume differentially detected DBPSK modulation, and the IBRC of rate $R = 1/2$, and $d_{\min} = 5$ from Fig. 7.11. The values of $\text{PER}_{[2]}$ are obtained using interpolation and the curves in Fig. 7.11. For each network realization, we generate 1000 matrices, $\mathbf{V}_{[3]}$, using (7.19). In turn, using N' and $\mathbf{D}_i$, we obtain the matrix, $\mathbf{V}'_{[3]i}$, and generate the N' data packets having equally probable bits, 0, and 1, and total Hamming weight at least 1, since the all-zero codeword is transmitted. Furthermore, in order to reduce the computer simulation run time, we assume that the data packets have the weight, $e_m = 1$, and that there are $K_{\rm u}^{N'}$ such packets having the same PEP.

Fig. 7.12 shows an estimate of the PER truncated union bound for the uplink and downlink transmissions, for $d_{\rm ap} = 0$m, and 400m, and transmitter power, $a_q^2 = 1$, and energy per bit, $E_b = 1$, for both the AP and the MT's. In the downlink, we assume that the destination node is at distance, $d_{\rm ap} + d_{\rm mt}$, from the AP. We observe from Fig. 7.12 that the downlink cooperation is more efficient than the uplink cooperation for both values of $d_{\rm ap}$. Although the network coverage is improved with

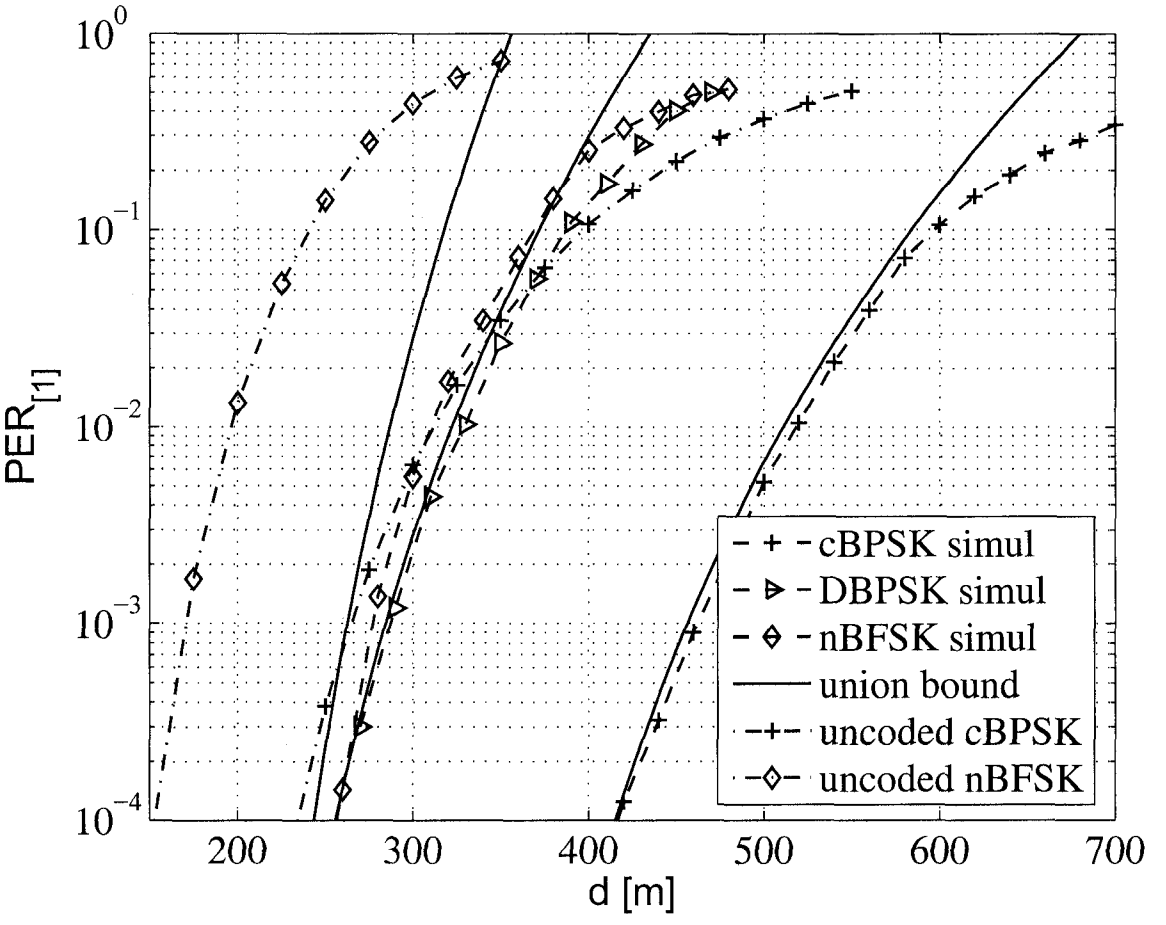

Figure 7.9: The PER of Stage 1 of the protocol using the CRC code, and Wagner decoding.

the number of cooperating nodes, the improvement is significantly more dependent on the specific network realization. We observe from Fig. 7.11 and Fig. 7.12 that cooperation can improve the coverage of Stage 2 from 370m to $(d_{\text{ap}}+180) = 580$m in the downlink, and $(d_{\text{ap}}+100) = 500$m in the uplink, for $\text{PER}_{[2]} = \text{PER}_{[3]} = 10^{-2}$. Note also that the cooperation gain is increasing towards smaller values of the target PER. In particular, for smaller values of $\text{PER}_{[2]}$, more information can be shared among the nodes, and the larger the coding gain of the product code, $\mathcal{C}_{[3]i}$. Also, the overall PER is improved by cooperation in the areas where $\text{PER}_{[3]} < 1$; cf. eq. (7.16).

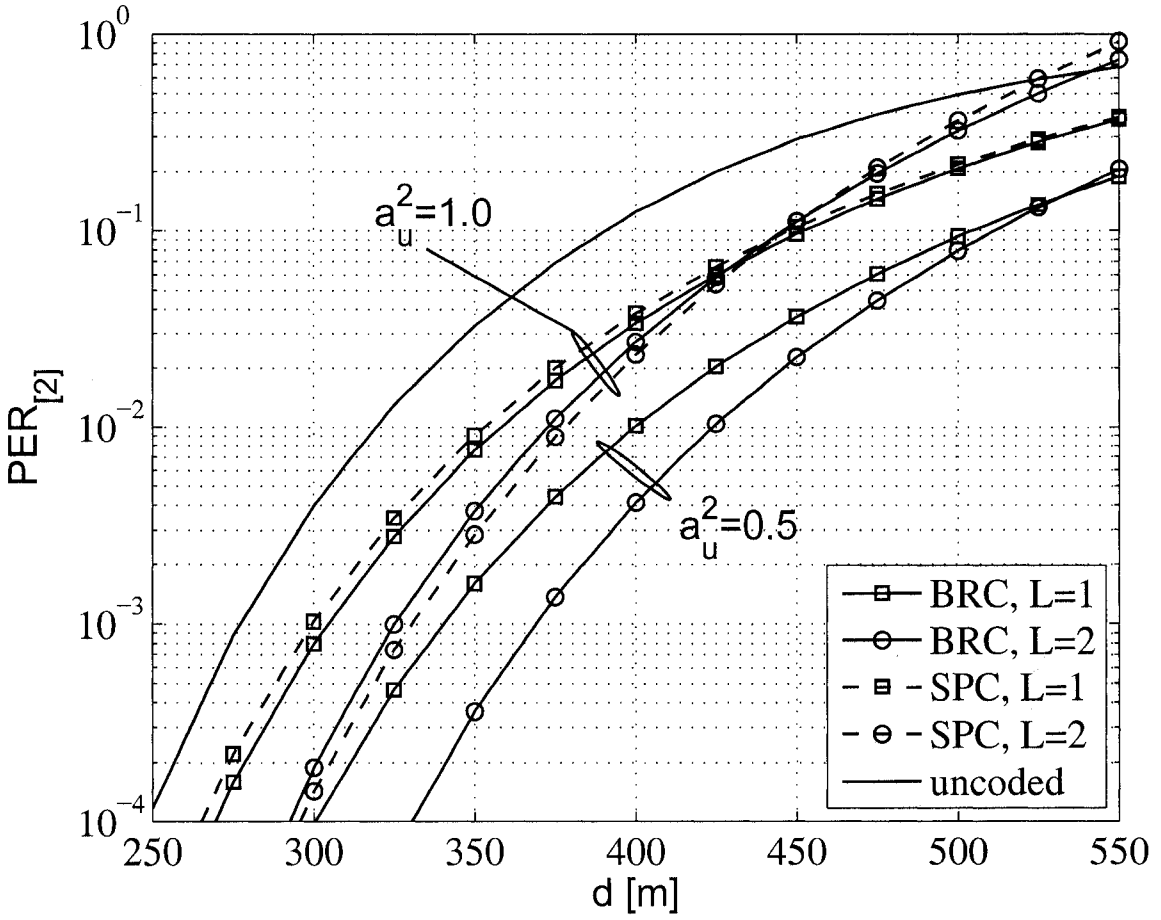

Figure 7.10: The PER truncated union bound for the IBRC's and the SPCPC's used in Stage 2 of the protocol.

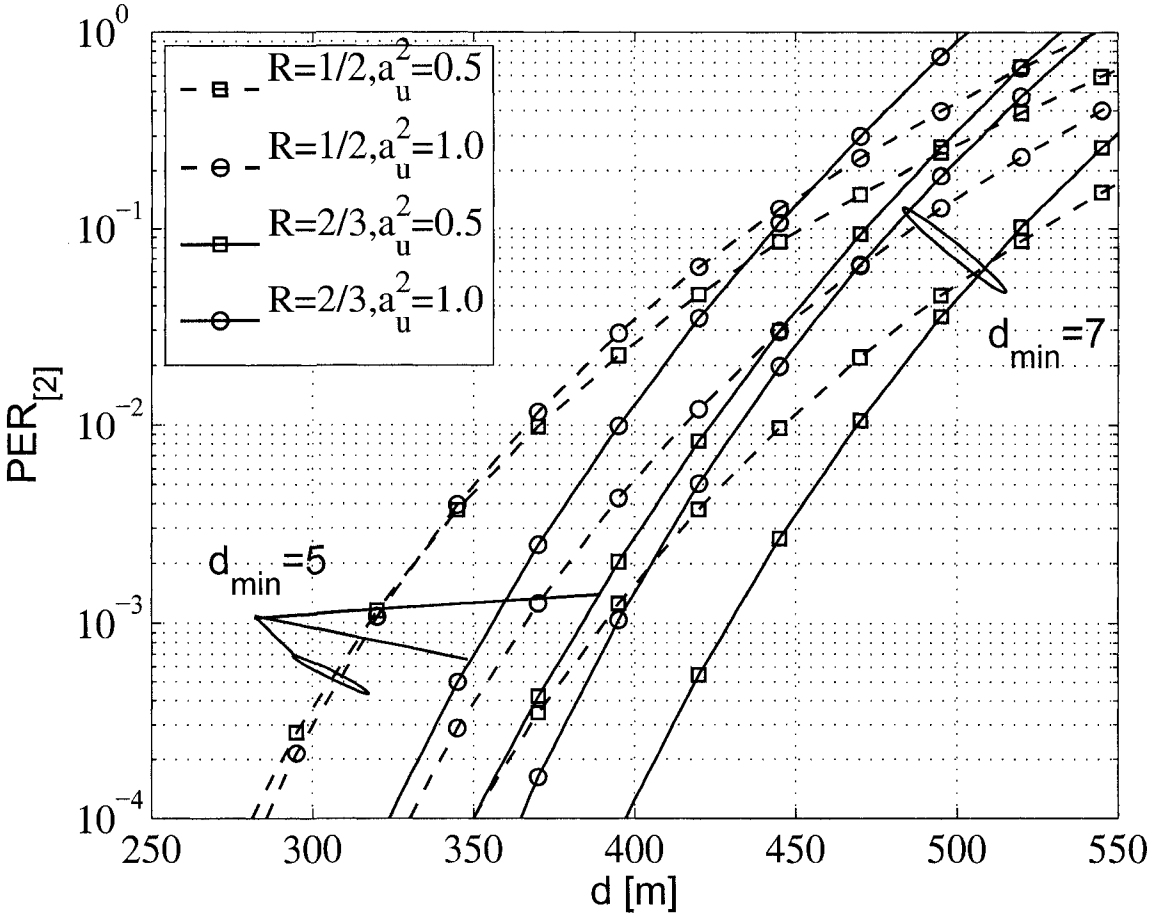

Figure 7.11: The PER truncated union bound for the IBRC's used in Stage 2 of the protocol.

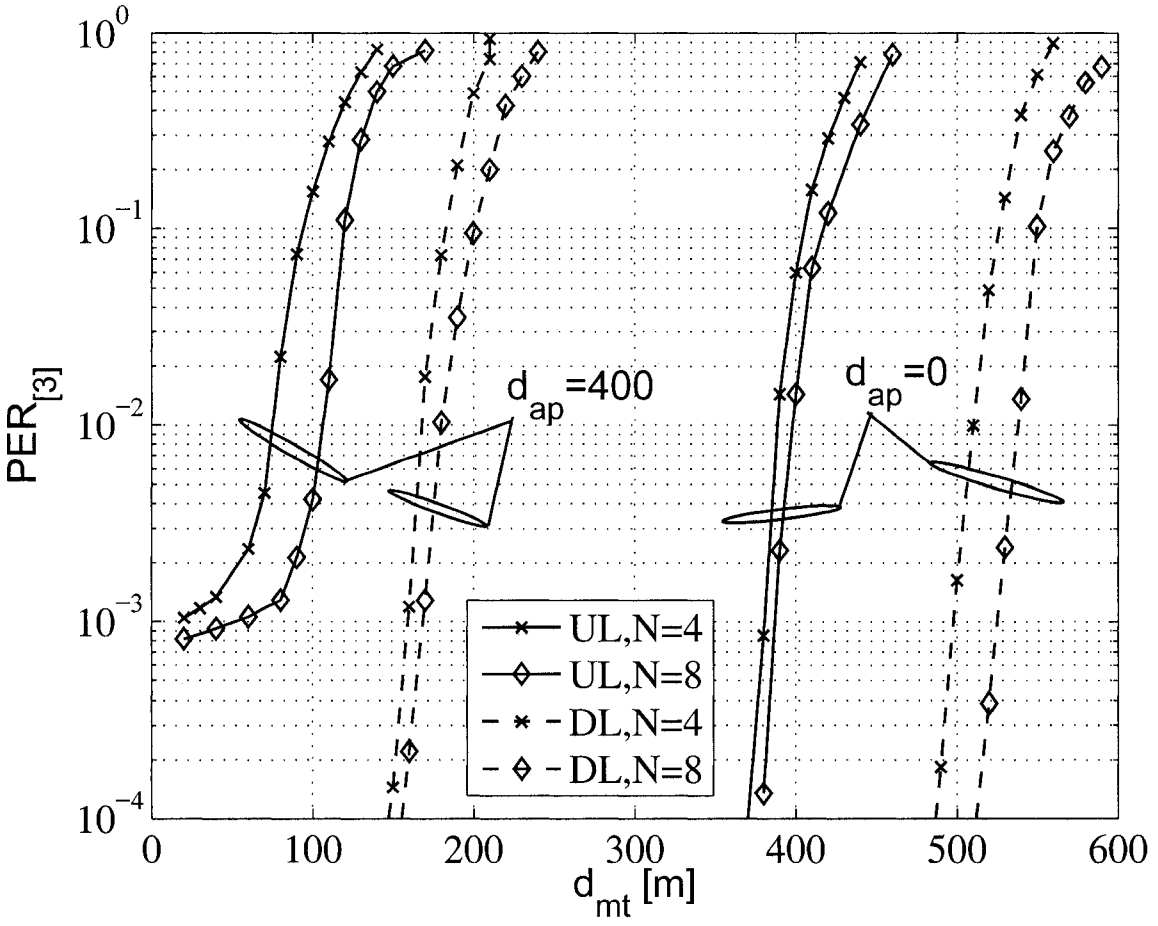

Figure 7.12: An estimate of the PER truncated union bound for a random code, $\mathcal{C}_{[3]}$, in Stage 3 of the protocol.

7.3 Summary

A novel class of multidimensional IBRC's was proposed. Properties of binary cyclic matrices useful to the design of IBRC's were discussed. Two optimization problems to design multidimensional IBRC's assuming either the constraint length or the constraint weight were presented. The constraint on the weights was shown to make searching for good codes significantly easier. It was also proved that permutation of bits in other dimensions can increase the minimum Hamming distance of the code without increasing the transmission bandwidth. This is especially useful for concatenation of 1D binary codewords. Examples of non-systematic 1D, 2D and 3D IBRC's were presented. Applications of IBRC's were considered and their performance was analyzed using a union bound of the BER. Particularly, IBRC's were investigated for adaptive coding, turbo product coding, retransmission and multihop routing and block differential encoding. It was observed that non-recursive block differential encoding of IBRC's increases the overall coding rate with the number of differentially encoded blocks while the code minimum Hamming distance remains constant. Finally, the transmitter energy distribution over a codeword was optimized in order to improve the BER.

In the second part, a three stage network protocol that improves network coverage was proposed. It was shown that the PER is a product of the PER's corresponding to the protocol stages. The PER's were conditioned on the specific network realization assuming that the channel attenuations are proportional to the free-space path loss. A realistic link budget was used to estimate the achievable network coverage. Noncoherent modulation schemes were considered in order to simplify the receivers. Examples of a CRC code for Stage 1, and IBRC's and SPCPC's well-suited for Stage 2 of the protocol were investigated. Particularly, minimum Hamming distance of the IBRC's can be adapted to channel attenuation. Cooperation among the nodes was implemented using a random vertical encoding. It was observed that the cooperation gains are strongly dependent on the specific network realization, both in the uplink and in the downlink, and less dependent on the number of cooperating nodes. For the parameters considered, the downlink cooperation was found to be more efficient than the uplink cooperation.

The channels between nodes were assumed to be Gaussian, and thus, the performance improvement is due to coding gain rather than fading diversity gain. On the other hand, for moderate decoding complexity, Stage 2 of the protocol allows exploiting diversity of the fading channel improving the reliability and coverage of Stage 1 of the protocol. Stage 3 of the protocol can improve the reliability and coverage further, but at the cost of increased decoding complexity and signal-

ing overhead. Note also that the number of time slots allocated for each of the protocol stages is arbitrary (i.e., can be zero), and it is a design parameter for the specific network scenario.

Chapter 8

A Hypergeometric Analysis of Diversity Combining Schemes and SNR Adaptive Receivers

In this chapter, we investigate a hypergeometry of objects in K dimensions. The results of hypergeometry are then applied to optimize dimension of the SNR adaptive receivers.

8.1 Background

Many practical problems in communication and information theory involve entities in K dimensions. For example, information transmitted from a source to a destination has to propagate over a noisy communication channel. Such channels make the information transmission unreliable, and thus, the communication channels are often deliberately formed in K dimensions in order to improve the transmission reliability or to increase the channel throughput. The transmission reliability is improved provided that the K channel dimensions (or degrees of freedom) are used to create transmission diversity in time, in frequency, and in spatial domains [160], [161]. Thus, motivated by the K-dimensional problems of information transmission, we investigate the hypergeometry of some objects in K dimensions. In particular, we consider the K-dimensional sphere, polytope, cube, scaled polytope and the scaled cube. We observe that the volume and the surface area of these objects is not monotonic in dimension, but reaches a maximum, and then, decrease towards zero. This fact appears not to be explicitly stated otherwise. For example, Weisstein [162] comments on

the monotonicity of the surface area of the unit radius hypersphere:

"Strangely enough, the hypersurface area reaches a maximum and then decreases towards 0 *as* n *increases. The point of maximal hyper-surface area satisfies* $\frac{\mathrm{d}S_n}{\mathrm{d}n} = \frac{\pi^{n/2}[\ln \pi - \Psi_0(\frac{1}{2}n)]}{\Gamma(\frac{1}{2}n)} = 0$, *where* $\Psi_0(x) \equiv \Psi(x)$ *is the digamma function. This cannot be solved analytically for* n, *but the numerical solution is* $n = 7.25695$ *(Sloane's A074457; Wells 1986, p. 67). As a result, the seven-dimensional hypersphere has maximum hyper-surface area (Le Lionnais 1983; Wells 1986, p. 60)."* see also, [163], [164, p. 58], and [165]

Furthermore, diversity combining schemes (DCS's) are often used to exploit multiple received copies of the transmitted signal at a fraction of the complexity cost of forward error correction codes. The maximum number of receiver antennas is usually determined by the receiver physical constraints and the cost of radio-frequency signal processing units. Hence, one can optimize the number of receiver antennas to reduce the implementation cost and complexity and to obtain a sufficient diversity gain. In general, a particular DCS is selected for a given channel estimation complexity. However, literature on optimum receiver dimensionality is scarce; for example, the optimum repetition diversity is investigated in [125]. On the other hand, references on performance analysis of DCS's are plentiful. For example, performance analysis of DCS's can be found in [66] and references therein.

This chapter is organized as follows. In Section 8.2, results presented in [166] are recalled and generalized to other K-dimensional objects. In particular, we elaborate on an important observation that the dimension corresponding to the maximum volume and to the maximum surface area depends on the radius of the object being considered. Thus, we solve the maximization problem in the discrete domain, and we obtain a dimension maximizing the volume and the surface area as a function of the radius; this is proved in two theorems. We also consider monotonicity of the p-norm, in general. In Section 8.3, we introduce a system model and assume partitioning of the SNR into a finite number of sub-intervals to realize adaptive signal processing using a bank of subchannel detectors. We then define several performance measures. In Section 8.4, we describe DCS's using a hypergeometry of objects in K dimensions. In particular, we consider MRC, EGC, SC and HS/MRC schemes to obtain a K-dimensional sphere, scaled polytope, cube and sphere, respectively. In Section 8.5, numerical examples are used to confirm non-monotonicity of the performance measures versus dimension as predicted by the hypergeometry. Finally, the chapter is summarized in Section 8.6.

8.2 Hypergeometry

Denote a real vector space in K dimensions as $\mathcal{R}^K$, for $K = 1, 2, \cdots$, and let the vector, $\mathbf{g} = (g_1, g_2, \cdots, g_K) \in \mathcal{R}^K$. Recall the definition of the l_p norm of the vector, $\mathbf{g} \in \mathcal{R}^K$, in (A-10), i.e., $l_p \geq 0$, for $p > 0$. In general, we assume that the distances in $\mathcal{R}^K$ correspond to the l_2 norm; for example, radius and edge length are defined using the l_2 norm. We define the following K-dimensional objects, i.e.,

$$\begin{aligned} \mathrm{S}_K(a) &= \{\mathbf{g} \in \mathcal{R}^K : \|\mathbf{g}\|_2 \leq a\} \\ \mathrm{P}_K(a) &= \{\mathbf{g} \in \mathcal{R}^K : \|\mathbf{g}\|_1 \leq a\} \\ \mathrm{C}_K(a) &= \{\mathbf{g} \in \mathcal{R}^K : \|\mathbf{g}\|_\infty \leq a\} \end{aligned}$$

where $\mathrm{S}_K(a)$ is the sphere of radius, a, $\mathrm{P}_K(a)$ is the polytope of radius, a, and $\mathrm{C}_K(a)$ is the cube of edge length, $2a$. Note that, for $K = 2$, $\mathrm{P}_2(a)$ corresponds to the cube, $\mathrm{C}_2(a/\sqrt{2})$, rotated by $\pi/4$ radians. Using the Pythagorean theorem, it is straightforward to show that the polytope, $\mathrm{P}_K(a)$, of radius, a, has edge length, $a\sqrt{K}$, and the cube, $\mathrm{C}_K(a)$, of edge length, $2a$, has radius (i.e., the distance between the origin and any of the vertices), $a/\sqrt{K}$. Let $\mathrm{P}'_K(a)$ denote the polytope of edge length, a, and $\mathrm{C}'_K(a)$ to be the cube of radius, a, i.e.,

$$\mathrm{P}'_K(a) = \{\mathbf{g} \in \mathcal{R}^K : \frac{1}{\sqrt{K}} \|\mathbf{g}\|_1 \leq a\} \tag{8.1a}$$

$$\mathrm{C}'_K(a) = \{\mathbf{g} \in \mathcal{R}^K : \sqrt{K} \|\mathbf{g}\|_\infty \leq a\}. \tag{8.1b}$$

In addition, denote the corresponding $(K-1)$-dimensional surfaces of the K-dimensional sphere, polytope, cube, scaled polytope and the scaled cube, respectively, as,

$$\begin{aligned} \hat{\mathrm{S}}_K(a) &= \{\mathbf{g} \in \mathcal{R}^K : \|\mathbf{g}\|_2 = a\} \\ \hat{\mathrm{P}}_K(a) &= \{\mathbf{g} \in \mathcal{R}^K : \|\mathbf{g}\|_1 = a\} \\ \hat{\mathrm{C}}_K(a) &= \{\mathbf{g} \in \mathcal{R}^K : \|\mathbf{g}\|_\infty = a\} \\ \hat{\mathrm{P}}'_K(a) &= \{\mathbf{g} \in \mathcal{R}^K : \frac{1}{\sqrt{K}} \|\mathbf{g}\|_1 = a\} \\ \hat{\mathrm{C}}'_K(a) &= \{\mathbf{g} \in \mathcal{R}^K : \sqrt{K} \|\mathbf{g}\|_\infty = a\}. \end{aligned}$$

In order to simplify the notation, let $\mathrm{O}_K(a)$ represent an object having the surface, $\hat{\mathrm{O}}_K(a)$, i.e.,

$$\begin{aligned}\mathrm{O}_K(a) &\in \{\mathrm{S}_K(a), \mathrm{P}_K(a), \mathrm{C}_K(a), \mathrm{P}'_K(a), \mathrm{C}'_K(a)\} \\ \hat{\mathrm{O}}_K(a) &\in \{\hat{\mathrm{S}}_K(a), \hat{\mathrm{P}}_K(a), \hat{\mathrm{C}}_K(a), \hat{\mathrm{P}}'_K(a), \hat{\mathrm{C}}'_K(a)\}.\end{aligned}$$

Then, $\lim_{a\to 0} \mathrm{O}_K(a) = \emptyset_K$ is an empty object having zero volume, and, $\lim_{a\to\infty} \mathrm{O}_K(a) = \mathcal{R}^K$.

8.2.1 Properties of the l_p Norm

We prove the following theorem on monotonicity of the l_p norm and the scaled l'_p norm.

Theorem 8.1 *Let* $\mathbf{g} = (g_1, g_2, \cdots, g_K) \in \mathcal{R}^K$, *and* $p > 0$. *The* l_p *norm,* $\|\mathbf{g}\|_p$, *and the scaled* l'_p *norm,* $\frac{1}{\sqrt{K}}\|\mathbf{g}\|_p$, *are monotonically increasing in dimension,* K, *and monotonically decreasing in the norm-order,* p.

Proof: The theorem is proved by induction. Consider first the l_p norm. Given the vector, $\mathbf{g}$, let the vector, $\mathbf{g}' = (\mathbf{g}, g_{K+1})$. For $p < \infty$, one has that, $\|\mathbf{g}'\|_p = \left(\|\mathbf{g}\|_p^p + |g_{K+1}|^p\right)^{1/p}$, and thus, $\|\mathbf{g}'\|_p \geq \|\mathbf{g}\|_p$. If $p = \infty$, then $\max_{k=1,\cdots,K}|g_k| \leq \max_{k=1,\cdots,K+1}|g_k|$, and thus, $\|\mathbf{g}\|_p \leq \|\mathbf{g}'\|_p$, for $\forall \mathbf{g} \in \mathcal{R}^K$, $\forall g_{K+1} \in \mathcal{R}$, and $\forall p > 0$. Consider now the scaled l'_p norm. Given the vector, $\mathbf{g}$, we need to show that, $\frac{\|\mathbf{g}'\|_p}{\sqrt{K+1}} \geq \frac{\|\mathbf{g}\|_p}{\sqrt{K}}$. Hence, for $p < \infty$, we have that, $\frac{\|\mathbf{g}'\|_p}{\sqrt{K+1}} = \frac{\left((\|\mathbf{g}\|_p)^p + |g'_{K+1}|^p\right)^{1/p}}{\sqrt{K+1}}$, and after some manipulations, $|g_{K+1}|^p \geq \|\mathbf{g}\|_p^p \left((\sqrt{1+1/K})^p - 1\right)$. Thus, whether the $(K+1)$-th component, g_{K+1}, increases the l'_p norm depends on the l_P norm, $\|\mathbf{g}\|_p$, and on the sequence, $\xi_K(p) = (\sqrt{1+1/K})^p - 1$. Since, for any $p > 0$, the sequence, $\xi_K(p)$, is decreasing with dimension, K, the probability that, $|g_{K+1}|^p \geq \|\mathbf{g}\|_p^p \xi_K(p)$, is increasing. Thus, the l'_p norm increases with dimension K in the probability sense. Similarly, for $p = \infty$, we have that, $\|\mathbf{g}'\|_\infty \geq \|\mathbf{g}\|_\infty \sqrt{1+1/K}$. Since the sequence, $\sqrt{1+1/K}$, is decreasing, the probability that, $g_{K+1} \geq \|\mathbf{g}\|_p \sqrt{1+1/K}$, is increasing, and thus, the l'_∞ norm is increasing with K in the probability sense.

Finally, we show that the l_p norm, $\|\mathbf{g}\|_p$, is decreasing with p. Thus, taking the derivative of $\|\mathbf{g}\|_p$, one has that,

$$\frac{\mathrm{d}}{\mathrm{d}p}\|\mathbf{g}\|_p = \frac{\|\mathbf{g}\|_p^{(1-p)}}{p^2}\sum_{k=1}^{K}|g_k|^p \log\left(\frac{|g_k|^p}{\sum_{k'=1}^{K}|g_{k'}|^p}\right).$$

Since $\log x < 0$, for $x < 1$, we have that, $\frac{\mathrm{d}}{\mathrm{d}p} \|\mathbf{g}\|_p < 0$, for $\forall \mathbf{g} \in \mathcal{R}^K$, and thus, the norm, $\|\mathbf{g}\|_p$, is a decreasing function of p, for $p > 0$. ■

Furthermore, it is useful to determine the conditions when one K-dimensional object is contained inside another K-dimensional object. We can prove the following inequalities for $\mathbf{g} \in \mathcal{R}^K$, i.e.,

$$\|\mathbf{g}\|_\infty \leq \|\mathbf{g}\|_2 \leq \|\mathbf{g}\|_1 \tag{8.2a}$$

$$\frac{1}{\sqrt{K}} \|\mathbf{g}\|_1 \leq \|\mathbf{g}\|_2 \tag{8.2b}$$

$$\|\mathbf{g}\|_2 \leq \sqrt{K} \|\mathbf{g}\|_\infty \tag{8.2c}$$

$$\|\mathbf{g}\|_\infty \gtrless \frac{1}{\sqrt{K}} \|\mathbf{g}\|_1 \tag{8.2d}$$

where the operator, $\gtrless$, denotes the case when either of the operands can be larger. We observe from (8.2a) that, without any scaling, l_1 is the largest norm. On the other hand, if l_∞ is not scaled, and l_1 is scaled by $1/\sqrt{K}$, then l_2 is the largest norm; see (8.2b). Also, if $\|\mathbf{g}\|_\infty \leq a$, then, $\frac{1}{K} \|\mathbf{g}\|_1 \leq a$. Hence, we can determine the maximum radius of an object to be contained inside another object of the given radius; this condition is *necessary*, but *not sufficient* for one object to be inside another object. Hence, the maximum radius, a^*, of the polytope (of the cube) to be contained inside the sphere of radius, a, is,

$$a^* = \max_{\mathbf{g}} \|\mathbf{g}\|_p \text{ s.t. } \|\mathbf{g}\|_2 \leq a \tag{8.3}$$

where $p = 1$ ($p = \infty$). Using the method of Lagrange multipliers, and noting the symmetry of (8.3) [54], one obtains that the vector, $\mathbf{g}^*$, that solves (8.3), is given by all permutations of the components of the vector, $(a/\sqrt{m}, \cdots, a/\sqrt{m}, 0, \cdots, 0)$, where m is the number of non-zero components; thus, for $m = 1, 2, \cdots, K$, we have that, $\|\mathbf{g}^*\|_2 = a$, $\|\mathbf{g}^*\|_1 = a\sqrt{m}$, and $\|\mathbf{g}^*\|_\infty = a/\sqrt{m}$. Hence, for $m = 1$ ($m = K$), the polytope (the cube) has the maximum radius, $a^* = a$ (the edge length, $2a^* = 2a/\sqrt{K}$) in order to be fully contained inside the sphere. Similarly, the sphere contained inside the polytope (the cube) of radius, a (the edge length, $2a$), has the maximum radius, $a^* = a/\sqrt{K}$, ($a^* = a$).

8.2.2 Volume and Surface Area

Denote $\mathrm{V}[\mathrm{O}_K(a)]$ to be the volume, and $\mathrm{A}\left[\hat{\mathrm{O}}_K(a)\right]$ to be the surface area of the K-dimensional object, $\mathrm{O}_K(a)$. We investigate monotonicity of the volume, $\mathrm{V}[\mathrm{O}_K(a)]$, and of the surface area,

$\mathrm{A}\left[\hat{\mathrm{O}}_K(a)\right]$, versus dimension, K. Hence, in general, for $p > 0$, using spherical coordinates in K dimensions, the volume of the object, $\mathrm{O}_K(a)$, is computed as,

$$\mathrm{V}[\mathrm{O}_K(a)] = \int\limits_{\|\mathbf{g}\|_p \leq a} \mathrm{d}\mathbf{g} = \int_0^a \mathrm{A}\left[\hat{\mathrm{O}}_K(1)\right] t^{K-1} \mathrm{d}t = \mathrm{A}\left[\hat{\mathrm{O}}_K(1)\right] \frac{a^K}{K} \tag{8.4}$$

where $\mathrm{A}\left[\hat{\mathrm{O}}_K(1)\right]$ is the surface area of the unit radius object, $\mathrm{O}_K(1)$, and $\mathrm{A}\left[\hat{\mathrm{O}}_K(1)\right] t^{K-1}$ is the $(K-1)$-dimensional surface area of the object, $\mathrm{A}[\mathrm{O}_K(t)]$, of radius, t. Correspondingly, the surface area of the object, $\mathrm{O}_K(a)$, is,

$$\mathrm{A}\left[\hat{\mathrm{O}}_K(a)\right] = \frac{\mathrm{dV}[\mathrm{O}_K(a)]}{\mathrm{d}a} = \mathrm{A}\left[\hat{\mathrm{O}}_K(1)\right] a^{K-1} = \mathrm{V}[\mathrm{O}_K(a)] \frac{K}{a}.$$

Hence, knowledge of $\mathrm{A}\left[\hat{\mathrm{O}}_K(1)\right]$ is sufficient to evaluate the volume and the surface area of any object, $\mathrm{O}_K(a)$. Also, given the dimension, K, and the volume, $\mathrm{V}[\mathrm{O}_K(a)]$, or the surface area, $\mathrm{A}\left[\hat{\mathrm{O}}_K(a)\right]$, one can compute the radius, a, as,

$$\begin{aligned} a &= \left(K \frac{\mathrm{V}[\mathrm{O}_K(a)]}{\mathrm{A}\left[\hat{\mathrm{O}}_K(1)\right]} \right)^{1/K} \\ a &= \left(\frac{\mathrm{A}\left[\hat{\mathrm{O}}_K(a)\right]}{\mathrm{A}\left[\hat{\mathrm{O}}_K(1)\right]} \right)^{1/(K-1)} . \end{aligned}$$

Note that, if $a \leq 1$, the limit, $\lim_{K \to \infty} \frac{a^K}{K} = 0$. Furthermore, for any dimension, K, the volume and the surface area are finite provided that the radius is finite; i.e., if $0 < a < \infty$, then, $0 < \mathrm{V}[\mathrm{O}_K(a)] < \infty$, and, $0 < \mathrm{A}\left[\hat{\mathrm{O}}_K(a)\right] < \infty$. Hence, given the radius, a, we investigate whether there exists dimension, K^*, such that, $\mathrm{V}[\mathrm{O}_{K_1}(a)] \leq \mathrm{V}[\mathrm{O}_{K_2}(a)]$, for $K_1 \leq K_2 \leq K^*$, and, $\mathrm{V}[\mathrm{O}_{K_1}(a)] \geq \mathrm{V}[\mathrm{O}_{K_2}(a)]$, for $K^* \leq K_1 \leq K_2$; a similar conjecture can be made for the surface area. Furthermore, we conjecture that the volume, $\mathrm{V}[\mathrm{O}_K(a)]$, and the surface area, $\mathrm{A}\left[\hat{\mathrm{O}}_K(a)\right]$, reach a maximum for dimension, $K = K^*$, and then decrease toward zero as K increases while the radius, a, is constant. This observation appears not to be well known in the literature, [167]. Noting that the dimension, K^*, of the maximum volume and of the maximum surface area depend on the radius, a, we prove the following two theorems.

Theorem 8.2 *The volume,* $\mathrm{V}[\mathrm{O}_K(a)]$, *of the* K*-dimensional object,* $\mathrm{O}_K(a)$, *of constant radius,* a,

reaches a maximum for dimension, $K^* = K$, if $\nu_{K-1} < a < \nu_K$, and, $K^* \in \{K, K+1\}$, if $a = \nu_K$, where

$$\nu_K = \begin{cases} \frac{\mathrm{A}\left[\hat{\mathrm{O}}_K(1)\right]}{\mathrm{A}\left[\hat{\mathrm{O}}_{K+1}(1)\right]} \left(\frac{K+1}{K}\right) & K = 1, 2, \cdots \\ 0 & K \leq 0 \end{cases}$$

and importantly, provided that the sequence, ν_K, is monotonically increasing with K.

Proof: Recall that, $\mathrm{V}[\mathrm{O}_K(a)] = \mathrm{A}\left[\hat{\mathrm{O}}_K(1)\right] \frac{a^K}{K}$. If $\mathrm{V}[\mathrm{O}_K(a)] \geq \mathrm{V}[\mathrm{O}_{K+1}(a)]$, then one has that, $\mathrm{V}[\mathrm{O}_{K+1}(a)] > \mathrm{V}[\mathrm{O}_{K+2}(a)]$, since $\mathrm{V}[\mathrm{O}_K(a)] \geq \mathrm{V}[\mathrm{O}_{K+1}(a)]$ is equivalent to the condition, $\frac{\mathrm{A}\left[\hat{\mathrm{O}}_K(1)\right]}{\mathrm{A}\left[\hat{\mathrm{O}}_{K+1}(1)\right]} \left(\frac{K+1}{K}\right) = \nu_K \geq a$, and $\mathrm{V}[\mathrm{O}_{K+1}(a)] > \mathrm{V}[\mathrm{O}_{K+2}(a)]$ is equivalent to the condition, $\frac{\mathrm{A}\left[\hat{\mathrm{O}}_{K+1}(1)\right]}{\mathrm{A}\left[\hat{\mathrm{O}}_{K+2}(1)\right]} \left(\frac{K+2}{K+1}\right) = \nu_{K+1} > a$, and the first condition implies the second, for any dimension, $K = 1, 2, \cdots$. Consequently, by induction, since ν_K is assumed to be a monotonically increasing sequence, the volume, $\mathrm{V}[\mathrm{C}_K(a)]$, is a monotonically decreasing sequence, for $K > K^*$. Similarly, we can show that, if $\mathrm{V}[\mathrm{O}_K(a)] \geq \mathrm{V}[\mathrm{O}_{K-1}(a)]$, then $\mathrm{V}[\mathrm{O}_{K-1}(a)] > \mathrm{V}[\mathrm{O}_{K-2}(a)]$, and, $a \geq \nu_{K-1}$. Consequently, by induction, and using an assumption that the sequence, ν_K, is monotonically increasing, the volume, $\mathrm{V}[\mathrm{C}_K(a)]$, is a monotonically increasing sequence, for $K = 1, 2, \cdots, K^*$. Hence, $\mathrm{V}[\mathrm{O}_{K-1}(a)] < \mathrm{V}[\mathrm{O}_K(a)] > \mathrm{V}[\mathrm{O}_{K+1}(a)]$ is equivalent to $\nu_{K-1} < a < \nu_K$, and $\mathrm{V}[\mathrm{O}_K(a)]$ is a global maximum, and $K^* = K$. Finally, the global maximum with equality, $\mathrm{V}[\mathrm{O}_K(a)] = \mathrm{V}[\mathrm{O}_{K+1}(a)]$, occurs when $a = \nu_K$, and, $K^* \in \{K, K+1\}$. ■

Theorem 8.3 *The surface area, $\mathrm{A}\left[\hat{\mathrm{O}}_K(a)\right]$, of the K-dimensional object, $\mathrm{O}_K(a)$, of constant radius, a, reaches a maximum for dimension, $K^* = K$, if $\mu_{K-1} < a < \mu_K$, and, $K^* \in \{K, K+1\}$, if $a = \mu_K$, where*

$$\mu_K = \nu_K \frac{K}{K+1} = \begin{cases} \frac{\mathrm{A}\left[\hat{\mathrm{O}}_K(1)\right]}{\mathrm{A}\left[\hat{\mathrm{O}}_{K+1}(1)\right]} & K = 1, 2, \cdots \\ 0 & K \leq 0 \end{cases}$$

and importantly, provided that the sequence, μ_K, is monotonically increasing with K.

Proof: The proof follows along the same lines as the proof of Theorem 8.2. ■

Importantly, since ν_K and μ_K are monotonically increasing sequences, we have the following corollary of Theorem 8.2 and Theorem 8.3.

Corollary 8.4 *Let K_i^* denote the dimension of the maximum volume or the maximum surface area corresponding to radius, a_i, for $i = 1$ and 2, and $a_1 < a_2$, then, $K_1^* \leq K_2^*$.*

Since $\mu_K = \nu_K \frac{K}{K+1}$, the monotonically increasing sequence, ν_K, implies the monotonically increasing sequence, μ_K. Strictly speaking, the opposite statement does not hold; since $\frac{K+1}{K}$ is the

monotonically decreasing sequence, the monotonically increasing sequence, μ_K, does not imply the monotonically increasing sequence, ν_K. Also, according to Theorem 8.3, if $\lim_{K\to\infty}\nu_K = \infty$, then, for any radius, $0 < a < \infty$, the volume, $\mathrm{V}[\mathrm{O}_K(a)]$, reaches the maximum value. Similarly, the condition, $\lim_{K\to\infty}\mu_K = \infty$, guarantees that, for any radius, $a > 0$, there exists a maximum value of the surface area, $\mathrm{A}\left[\hat{\mathrm{C}}_K(a)\right]$. Note also that, if $a = \nu_K$ ($a = \mu_K$), the maximum volume (the maximum surface area) occurs at two consecutive values of dimension.

Particularly, consider the K-dimensional sphere of radius, a. Using spherical coordinates, we obtain that, $\mathrm{A}\left[\hat{\mathrm{S}}_K(1)\right] = 2\pi^{K/2}/\Gamma\left(\frac{K}{2}\right)$, where $\Gamma(\cdot)$ is the gamma function [168]. Hence, the volume and the surface area of the sphere, $\mathrm{S}_K(a)$, are [22], [23],

$$\begin{aligned}\mathrm{V}[\mathrm{S}_K(a)] &= \frac{2\pi^{K/2}}{\Gamma\left(\frac{K}{2}\right)}\frac{a^K}{K}\\ \mathrm{A}\left[\hat{\mathrm{S}}_K(a)\right] &= \frac{2\pi^{K/2}}{\Gamma\left(\frac{K}{2}\right)}a^{K-1}.\end{aligned}$$

We have the following lemma.

Lemma 8.5 *Let, K_V^*, and, K_A^*, denote the dimension that correspond to the maximum volume, $\mathrm{V}\left[\mathrm{S}_{K_V^*}(a)\right] = \max_K \mathrm{V}[\mathrm{S}_K(a)]$, and the maximum surface area, $\mathrm{A}\left[\hat{\mathrm{S}}_{K_A^*}(a)\right] = \max_K \mathrm{A}\left[\hat{\mathrm{S}}_K(a)\right]$, of the sphere, $\mathrm{S}_K(a)$, respectively. Then, for $a > 1/2$, one has that, $K_V^* = K_A^* - 2$, and the sequences defined in Theorem 8.2 and Theorem 8.3, $\mu_K = \nu_{K-2}$.*

Proof: Note that $\Gamma\left(\frac{K}{2}\right) = \left(\frac{K}{2}-1\right)!$ if K is even, where $K! = K(K-1)\cdots 2\cdot 1$, and $\Gamma\left(\frac{K}{2}\right) = \frac{\sqrt{\pi}(K-2)!!}{2^{K/2-1/2}}$ if K is odd, where $K!! = K(K-2)\cdots 5\cdot 3\cdot 1$. Hence, $\nu_K = \frac{\Gamma((K+1)/2)}{\sqrt{\pi}\Gamma(K/2)}\left(\frac{K+1}{K}\right) = \mu_K\left(\frac{K+1}{K}\right)$, and we have that, $\mu_K = \nu_{K-2}$. Consequently, $K_V^* = K_A^* - 2$. ■

For example, while the unit radius ($K = 7$)-dimensional sphere has the maximum surface area, the unit radius sphere has the maximum volume for dimension, $K = 5$. We have the following corollary of Lemma 8.5.

Corollary 8.6 *For the sphere in $K \geq 3$ dimensions (equivalently, having the radius, $a > 1/2$), the dimension of the maximum surface area, $K^* = K$, and of the maximum volume, $K^* = K - 2$, if $\mu_{K-1} < a < \mu_K$. Similarly, if $a = \mu_K$, then for $K \geq 3$, the dimension of the maximum surface area, $K^* \in \{K, K+1\}$, and of the maximum volume, $K^* \in \{K-2, K-1\}$, if $\mu_{K-1} < a < \mu_K$.*

Consider the polytope, $\mathrm{P}_K(a)$. The surface area of the unit radius polytope, $\mathrm{P}_K(1)$, can be obtained recursively, i.e., $\mathrm{A}\left[\hat{\mathrm{P}}_K(1)\right] = 2^K/(K-1)!$. Thus, the volume and the surface area of the

K-dimensional polytope, $\mathrm{P}_K(a)$, are,

$$\begin{aligned} \mathrm{V}[\mathrm{P}_K(a)] &= \tfrac{2^K}{K!}\, a^K \\ \mathrm{A}\Big[\hat{\mathrm{P}}_K(a)\Big] &= \tfrac{2^K}{(K-1)!}\, a^{K-1}. \end{aligned} \tag{8.5}$$

Note that the polytope volume can be written as,

$$\mathrm{V}[\mathrm{P}_K(a)] = \prod_{k=1}^{K} \frac{2a}{k}$$

indicating that the polytope can be viewed as a cube having edges of length, $\frac{2a}{k}$, $k = 1, 2, \cdots, K$. We have the following lemma.

Lemma 8.7 *Let K_V^* and K_A^* be the dimensions corresponding to the maximum volume, $\mathrm{V}\Big[\mathrm{P}_{K_V^*}(a)\Big] = \max_K \mathrm{V}[\mathrm{P}_K(a)]$, and the maximum surface area, $\mathrm{A}\Big[\hat{\mathrm{P}}_{K_A^*}(a)\Big] = \max_K \mathrm{A}\Big[\hat{\mathrm{P}}_K(a)\Big]$, of the polytope, $\mathrm{P}_K(a)$, respectively. Then, for $a > 1/2$, one has that, $K_V^* = K_A^* - 1$, and the sequences defined in Theorem 8.2 and Theorem 8.3, $\mu_K = \nu_{K-1}$.*

Proof: Since, $\nu_K = \frac{K+1}{2}$, and, $\mu_K = \frac{K}{2}$, we have that, $\mu_K = \nu_{K-1}$. Consequently, $K_V^* = K_A^* - 1$. ■

For the scaled polytope (8.1a), we substitute the radius, $a/\sqrt{K}$, into (8.5). Thus, the surface area of the unit radius scaled polytope is, $\mathrm{A}\Big[\hat{\mathrm{P}}'_K(1)\Big] = \frac{2^K}{\sqrt{K^K}(K-1)!}$, and the volume and the surface area of the K-dimensional scaled polytope, $\mathrm{P}'_K(a)$, are,

$$\begin{aligned} \mathrm{V}\big[\mathrm{P}'_K(a)\big] &= \frac{2^K}{\sqrt{K^K}K!}\, a^K \\ \mathrm{A}\Big[\hat{\mathrm{P}}'_K(a)\Big] &= \frac{2^K}{\sqrt{K^{K-1}}(K-1)!}\, a^{K-1}. \end{aligned}$$

Using Theorem 8.2 and Theorem 8.3, we can show that the volume and the surface area of the scaled polytope, $\mathrm{P}'_K(a)$, reach a maximum value for a particular value of dimensionality.

The surface area of the cube, $\mathrm{C}_K(1)$, having edge length, 2, is, $\mathrm{A}\Big[\hat{\mathrm{C}}_K(1)\Big] = K2^K$. Hence, the volume and the surface area of the K-dimensional cube, $\mathrm{C}_K(a)$, are,

$$\begin{aligned} \mathrm{V}[\mathrm{C}_K(a)] &= 2^K a^K \\ \mathrm{A}\Big[\hat{\mathrm{C}}_K(a)\Big] &= K2^K a^{K-1}. \end{aligned} \tag{8.6}$$

Chapter 8

A Hypergeometric Analysis of Diversity Combining Schemes and SNR Adaptive Receivers

In this chapter, we investigate a hypergeometry of objects in K dimensions. The results of hypergeometry are then applied to optimize dimension of the SNR adaptive receivers.

8.1 Background

Many practical problems in communication and information theory involve entities in K dimensions. For example, information transmitted from a source to a destination has to propagate over a noisy communication channel. Such channels make the information transmission unreliable, and thus, the communication channels are often deliberately formed in K dimensions in order to improve the transmission reliability or to increase the channel throughput. The transmission reliability is improved provided that the K channel dimensions (or degrees of freedom) are used to create transmission diversity in time, in frequency, and in spatial domains [160], [161]. Thus, motivated by the K-dimensional problems of information transmission, we investigate the hypergeometry of some objects in K dimensions. In particular, we consider the K-dimensional sphere, polytope, cube, scaled polytope and the scaled cube. We observe that the volume and the surface area of these objects is not monotonic in dimension, but reaches a maximum, and then, decrease towards zero. This fact appears not to be explicitly stated otherwise. For example, Weisstein [162] comments on

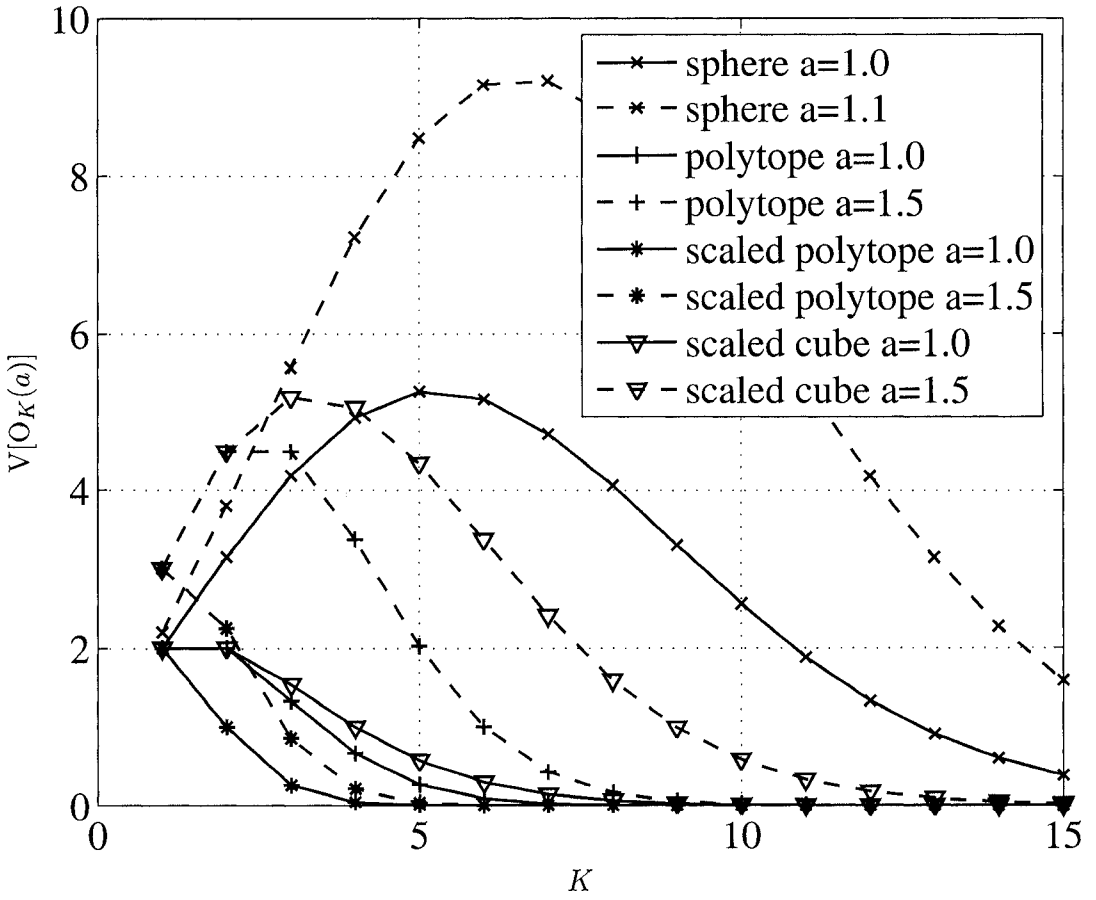

Figure 8.1: The volume, $\mathrm{V}[\mathrm{O}_K(a)]$, of the sphere, polytope, scaled polytope, and the scaled cube versus dimension, K.

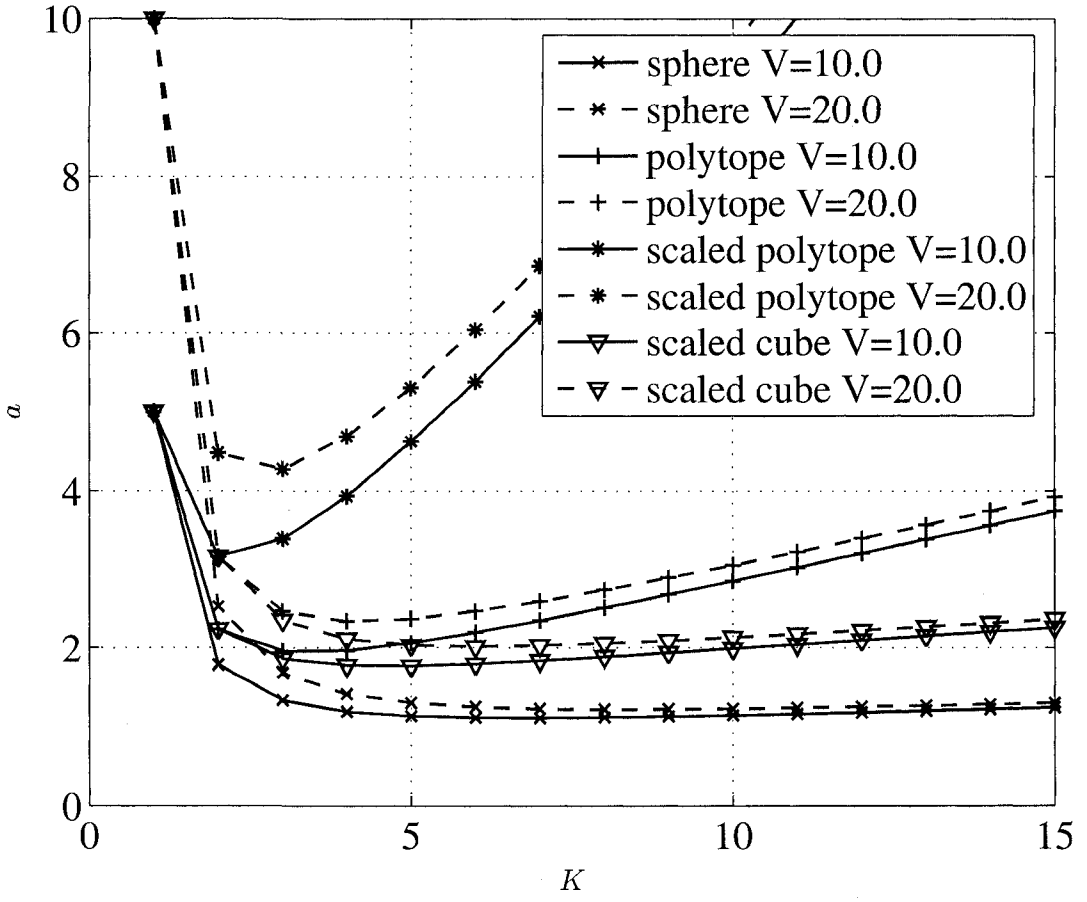

Figure 8.2: The radius, a, of the constant volume sphere, polytope, scaled polytope, and the scaled cube versus dimension, K.

the following K-dimensional objects, i.e.,

$$\begin{aligned}
\mathrm{S}_K(a_1, a_2) &= \{\mathbf{g} \in \mathbb{R}^K : a_1 \leq \|\mathbf{g}\|_2 \leq a_2\} \\
\mathrm{P}_K(a_1, a_2) &= \{\mathbf{g} \in \mathbb{R}^K : a_1 \leq \|\mathbf{g}\|_1 \leq a_2\} \\
\mathrm{P}'_K(a_1, a_2) &= \{\mathbf{g} \in \mathbb{R}^K : a_1 \leq \frac{1}{\sqrt{K}} \|\mathbf{g}\|_1 \leq a_2\} \\
\mathrm{C}_K(a_1, a_2) &= \{\mathbf{g} \in \mathbb{R}^K : a_1 \leq \|\mathbf{g}\|_\infty \leq a_2\}
\end{aligned}$$

where $\mathrm{S}_K(a_1, a_2)$ is a hollow sphere of radii, a_1, and, a_2, $\mathrm{P}_K(a_1, a_2)$ is a hollow polytope of radii, a_1, and, a_2, $\mathrm{P}'_K(a_1, a_2)$ is a hollow scaled polytope of radii, a_1, and, a_2, and $\mathrm{C}_K(a_1, a_2)$ is a hollow cube of edge lengths, $2a_1$, and, $2a_2$. Denote, $a_2 = a$, and, $a_1 = \kappa a$, where $0 \leq \kappa \leq 1$. The volume of hollow K-dimensional objects can be computed using (8.4), i.e.,

$$\mathrm{V}[\mathrm{O}_K(a\kappa, a)] = \mathrm{A}\Big[\hat{\mathrm{O}}_K(1)\Big] \frac{a^K(1 - \kappa^K)}{K}.$$

Thus, if $\kappa = 0$, the cavity is removed, and, if $\kappa = 1$, the object has zero volume. For hollow K-dimensional objects having $\kappa > 0$, we can extend Theorem 2 as follows.

Theorem 8.8 *Given a constant radius, $a > 0$, and, $0 \leq \kappa \leq 1$, the volume, $\mathrm{V}[\mathrm{O}_K(a\kappa, a)]$, reaches a maximum for dimension, $K^* = K$, if $o_{K-1}(\kappa) < a < o_K(\kappa)$, and, $K^* \in \{K, K+1\}$, if $a = o_K(\kappa)$, where*

$$o_K(\kappa) = \begin{cases} \left(\frac{\mathrm{A}[\hat{\mathrm{O}}_K(1)]}{\mathrm{A}[\hat{\mathrm{O}}_{K+1}(1)]}\right)\left(\frac{K+1}{K}\right)\left(\frac{1-\kappa^K}{1-\kappa^{K+1}}\right) & K = 1, 2, \cdots \\ 0 & K \leq 0 \end{cases}$$

and importantly, provided that the sequence, $o_K(\kappa)$, is monotonically increasing with K.

Proof: Note that, $\frac{K+1}{K}$, and, $\frac{1-\kappa^K}{1-\kappa^{K+1}}$, are increasing sequences. Hence, equivalently, the first-order difference, $\mathrm{A}\Big[\hat{\mathrm{O}}_K(1)\Big] - \mathrm{A}\Big[\hat{\mathrm{O}}_{K+1}(1)\Big]$, must be an increasing sequence in order that the sequence, $o_K(\kappa)$, be increasing. Note that, $\mathrm{V}[\mathrm{O}_K(a\kappa, a)] \geq \mathrm{V}[\mathrm{O}_{K+1}(a\kappa, a)]$, is equivalent to the condition, $o_K(\kappa) \geq a$, and, $\mathrm{V}[\mathrm{O}_{K-1}(a\kappa, a)] \leq \mathrm{V}[\mathrm{O}_K(a\kappa, a)]$, is equivalent to the condition, $o_{K-1}(\kappa) \leq a$. Thus, provided that $o_K(\kappa)$ is a monotonically increasing sequence, and, $o_{K-1}(\kappa) \leq a \leq o_K(\kappa)$, then dimension K corresponds to the maximum volume, and, $K^* = K$. Similarly, we can show that, if $a = o_K(\kappa)$, then $K^* \in \{K, K+1\}$. ■

For example, for $\mathrm{C}_K(a\kappa, a)$, the sequence, $o_K(\kappa) = \frac{1}{2}\frac{1-\kappa^K}{1-\kappa^{K+1}}$, so that, $\lim_{K\to\infty} o_K(\kappa) = \frac{1}{2}$. Thus, if $a < \frac{1}{2}$, the volume of a hollow cube reaches a maximum value for a particular dimension, $1 \leq K^* < \infty$.

Finally, it is also useful to consider a discrete K-dimensional space, $\mathbb{Z}_Q^K$, where $\mathbb{Z}_Q = \{0, \cdots, Q-1\}$. We can define a discrete hollow sphere as,

$$\mathrm{S}_{\mathrm{d}K}(a_1, a_2) = \{\mathbf{g} \in \mathbb{Z}_Q^K : a_1 \leq w_{\mathrm{H}}(\mathbf{g}) \leq a_2\} \tag{8.7}$$

where the Hamming weight, $w_{\mathrm{H}}(\mathbf{g}) = \sum_{k=1}^{K} g_k$. The discrete hollow sphere has the volume, $V[\mathrm{S}_{\mathrm{d}K}(a_1, a_2)] = \sum_{k=a_1}^{a_2} \binom{(Q-1)K}{k}$, where $\binom{a}{b}$ denotes the binomial coefficient.

In the following sections, we use a hypergeometry of objects in K dimensions to analyze and optimize SNR adaptive receivers for K-dimensional received signals.

8.3 System Model

Assume symbol samples of the equivalent complex envelopes in the baseband. Groups of m independent and identically distributed data bits, $\mathbf{b}$, are Gray mapped to uncoded M-ary square QAM or M-ary PSK modulation symbols, x, where $M = 2^m$. The modulation constellation, $X = \{(2i - \sqrt{M} + 1) + \mathrm{j}(2j - \sqrt{M} + 1); i, j = 0, 1, \cdots, \sqrt{M} - 1\}$, for M-ary square-QAM, and, $X = \{\mathrm{e}^{\mathrm{j}\,2\pi i/M}; i = 0, 1, \cdots, M-1\}$, for M-ary PSK, where the imaginary unit, $\mathrm{j} = \sqrt{-1}$, [21]. Scaling of the modulation constellation by the factor, $\sqrt{3/(2M-2)}$, for M-ary square QAM, and, 1, for M-ary PSK, sets the average transmitted energy, $E_s = \mathrm{E}[|x|^2]$, of symbols, x, to unity. The symbols, x, are transmitted over slowly flat fading channels to the receiver having K antennas; the receiver structure is shown in Fig. 8.3. The channel coefficient corresponding to the i-th receiver antenna can be written as, $h_i = g_i\,\mathrm{e}^{\mathrm{j}\phi_i}$, where g_i is the channel fading amplitude, and ϕ_i is the channel fading phase, and $i = 1, 2, \cdots, K$. Denote, $h = g\,\mathrm{e}^{\mathrm{j}\phi}$, to be the channel coefficient at the output of the combiner. Hence, assuming coherent combining, the received signal at the input to the detector is,

$$y = gx + w \tag{8.8}$$

where $g = \mathrm{e}^{-\mathrm{j}\phi}h$, and w is the sample of an AWGN having zero-mean and variance, $\sigma_w^2 = \mathrm{E}[|w|^2] = 2N_0$, and N_0 denotes the one-sided noise power spectral density. Then, the SNR at the detector input is, $\gamma = |h|^2\gamma_b = g^2\gamma_b$, where the SNR per bit, $\gamma_b = E_b/N_0$, and $E_b = E_s/m$.

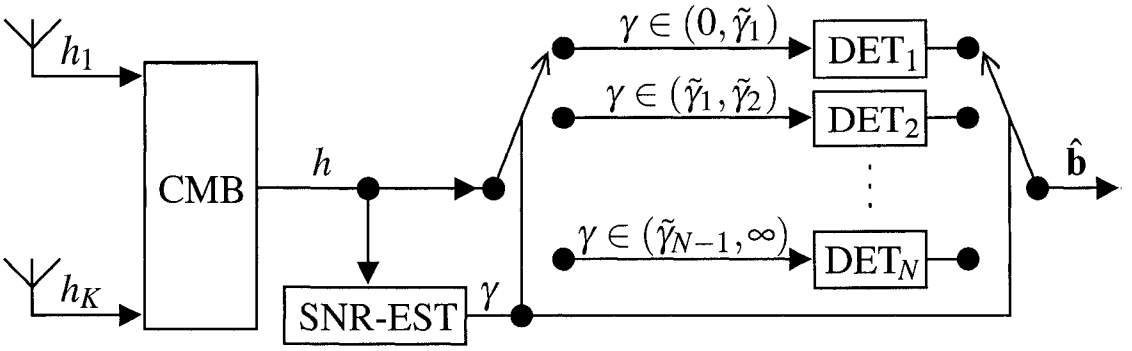

Figure 8.3: The system model and structure of a generic diversity combining SNR adaptive receiver.

Adaptive signal processing in the receiver is realized by a bank of N subchannel detectors; see Fig. 8.3. Thus, assuming perfect SNR estimation, the SNR values, $\gamma \in (0, \infty)$, are quantized to N intervals in order to select one of the N detectors to process the received signal, y, and to provide final decisions, $\hat{\mathbf{b}}$, on the transmitted bits, $\mathbf{b}$. Hence, we define disjoint SNR intervals, $\Omega_n = (\tilde{\gamma}_{n-1}, \tilde{\gamma}_n)$, $n = 1, 2, \cdots, N$, where $\tilde{\gamma}_0 = 0 < \tilde{\gamma}_1 < \cdots < \tilde{\gamma}_{N-1} < \tilde{\gamma}_N = \infty$. Thus, if $\gamma \in \Omega_n$, then, $g^2 \in (\tilde{\gamma}_{n-1}/\gamma_b, \tilde{\gamma}_n/\gamma_b)$, and $g \in \left(\sqrt{\tilde{\gamma}_{n-1}/\gamma_b}, \sqrt{\tilde{\gamma}_n/\gamma_b}\right)$. Note that, if $N = 1$, then $\Omega_1 = (0, \infty)$, and the receiver has one conventional symbol-by-symbol detector. For $N > 1$, the receiver adapts the decision strategy for different values of γ. In particular, the first detector corresponding to $\gamma < \tilde{\gamma}_1$ can be used to declare an outage when the detected symbol would be unreliable. Also, it is required that, $\gamma > \tilde{\gamma}_1$, in order the receiver can synchronize, and always, $\gamma < \tilde{\gamma}_{N-1}$, due to physical constraints in the input receiver circuits; thus one has that, $N \geq 3$, in order to accurately model any practical receiver. For example, reference [169] reports the dynamic range of the path strength to be usually 20–30 dB. Furthermore, if there exists a feedback channel from the receiver to the transmitter, then different modulation constellations and the corresponding detectors can be used for each SNR interval, Ω_n, [170]. For coded systems, less complex detectors can often be employed at larger values of SNR. For systems with interference, the detection can be adapted according to whether the system is interference limited or noise limited.

In general, the SNR partitioning creates N erasure subchannels. The received signal corresponding to the n-th erasure subchannel of the n-th detector is denoted as,

$$y(\Omega_n) = \begin{cases} y & \gamma \in \Omega_n \\ \text{erasure} & \gamma \notin \Omega_n. \end{cases} \tag{8.9}$$

We investigate symbol-by-symbol detectors operating over erasure subchannels using the following performance measures.

8.3.1 Performance Measures

Let $f_g(g)$, $f_{g^2}(g^2)$ and $f_\gamma(\gamma)$ be the PDF's of g, g^2, and γ, respectively. Recall that, $\gamma = g^2\gamma_b$, and thus [53],

$$f_\gamma(\gamma) = \frac{1}{\gamma_b} f_{g^2}(\frac{\gamma}{\gamma_b}) = \frac{1}{2\sqrt{\gamma\gamma_b}} f_g(\sqrt{\frac{\gamma}{\gamma_b}}).$$

In general, denote $\mathcal{M}(\gamma)$ to be an instantaneous performance measure. Assuming the n-th erasure subchannel, i.e., the SNR, $\gamma \in \Omega_n = (\tilde{\gamma}_{n-1}, \tilde{\gamma}_n)$, the average performance measure, $\bar{\mathcal{M}}(\gamma_b; \Omega_n)$, for the n-th detector is evaluated as,

$$\begin{aligned} \bar{\mathcal{M}}(\gamma_b; \Omega_n) &= \int_{\tilde{\gamma}_{n-1}}^{\tilde{\gamma}_n} \mathcal{M}(\gamma) f_\gamma(\gamma) \, \mathrm{d}\gamma \\ &= \int_{\tilde{\gamma}_{n-1}/\gamma_b}^{\tilde{\gamma}_n/\gamma_b} \mathcal{M}\left(g^2\gamma_b\right) f_{g^2}(g^2) \, \mathrm{d}g^2 \\ &= \int_{\sqrt{\tilde{\gamma}_{n-1}/\gamma_b}}^{\sqrt{\tilde{\gamma}_n/\gamma_b}} \mathcal{M}\left(g^2\gamma_b\right) \, f_g(g) \, \mathrm{d}g. \end{aligned} \tag{8.10}$$

Importantly, note that the PDF, $f_\gamma(\gamma)$, corresponding to the n-th erasure subchannel, i.e., for $\gamma \in \Omega_n$, is *not* normalized by the factor, $\int_{\tilde{\gamma}_{n-1}}^{\tilde{\gamma}_n} f_\gamma(\gamma)\mathrm{d}\gamma$, and thus, $\int_{\Omega_n} f_\gamma(\gamma)\mathrm{d}\gamma \neq 1$. Consequently, the probability mass contained in the volume corresponding to $\gamma \in \Omega_n$ is a function of dimension, K, and using Theorem 8.8, we have the following conjecture.

Conjecture 8.9 *The average performance measure, $\bar{\mathcal{M}}(\gamma_b; \Omega_n)$, corresponding to the n-th erasure subchannel reaches a maximum for a particular value of dimension.*

In particular, let $\mathrm{P}_\epsilon(\gamma)$ be the instantaneous BER. The average BER, $\bar{\mathrm{P}}_\epsilon(\gamma_b; \Omega_n)$, is computed using (8.10), and the overall average BER of the receiver is,

$$\bar{\mathrm{P}}_\epsilon(\gamma_b) = \sum_{n=1}^{N} \bar{\mathrm{P}}_\epsilon(\gamma_b; \Omega_n) \, .$$

The probability of outage, P_{out}, is defined as the probability that SNR, $\gamma \in \Omega_1$. Thus, the first detector is selected with probability, $\mathrm{P}_{\text{out}} = \Pr(\gamma \in \Omega_1)$. This definition can be generalized to consider the probability that the n-th detector is selected, i.e., $\mathrm{P}_{\text{det}}(\Omega_n) = \Pr(\gamma \in \Omega_n)$, and, $\mathrm{P}_{\text{out}} = \mathrm{P}_{\text{det}}(\Omega_1)$. Hence, in this case, $\mathcal{M}(\gamma) = 1$, and using (8.10), the probability of selecting the

detector, n, is,

$$\begin{aligned} \mathrm{P}_{\mathrm{det}}(\Omega_n) &= F_\gamma(\tilde{\gamma}_n) - F_\gamma(\tilde{\gamma}_{n-1}) \\ &= F_{g^2}(\tilde{\gamma}_n/\gamma_b) - F_{g^2}(\tilde{\gamma}_{n-1}/\gamma_b) \\ &= F_g(\sqrt{\tilde{\gamma}_n/\gamma_b}) - F_g(\sqrt{\tilde{\gamma}_{n-1}/\gamma_b}) \end{aligned}$$

where $F_\gamma(\gamma) = \int_0^\gamma f_\gamma(u)\mathrm{d}u$, $F_{g^2}(g^2) = \int_0^{g^2} f_{g^2}(u)\mathrm{d}u$, and $F_g(g) = \int_0^g f_g(u)\mathrm{d}u$ are the CDF's. Note also that, $\sum_{n=1}^N \mathrm{P}_{\mathrm{det}}(\Omega_n) = 1$.

The channel capacity of a Gaussian channel having an unconstrained (Gaussian) input, $\mathrm{C}(\gamma)$, and having 2-PSK modulation symbols at its input, $\mathrm{C}_{2\mathrm{psk}}(\gamma)$, respectively, is computed as, [21], [171],

$$\mathrm{C}(\gamma) = \log_2(1+\gamma) \tag{8.11a}$$

$$\mathrm{C}_{2\mathrm{psk}}(\gamma) = 1 - \int_{-\infty}^{\infty} f_w(w) \log_2\left(1 + \mathrm{e}^{-4\gamma(1+w)}\right) \mathrm{d}w \tag{8.11b}$$

where $f_w(w) = \sqrt{\frac{\gamma}{\pi}}\,\mathrm{e}^{-\gamma w^2}$ is the PDF of a zero-mean Gaussian noise. The average channel capacity is computed using (8.10). The overall average channel capacity between the transmitter input and the receiver output is,

$$\begin{aligned} \bar{\mathrm{C}}(\gamma_b) &= \sum_{n=1}^{N} \bar{\mathrm{C}}(\gamma_b;\Omega_n) \\ \bar{\mathrm{C}}_{2\mathrm{psk}}(\gamma_b) &= \sum_{n=1}^{N} \bar{\mathrm{C}}_{2\mathrm{psk}}(\gamma_b;\Omega_n). \end{aligned}$$

8.4 A Hypergeometric View of Diversity Combining

We describe DCS's using a hypergeometry of objects in K dimensions. In general, all DCS's require some knowledge of the channel coefficients. The more knowledge of the channel coefficients is available, the better the performance of the DCS's [66]. We assume perfect channel estimation. Then, the channel fading amplitude, g, in (8.8) for MRC, EGC, SC and HS/MRC diversity, respectively, can be written as,

$$g \overset{(\mathrm{MRC})}{=} \sqrt{\sum_{i=1}^{K} g_i^2} \tag{8.12a}$$

$$g \overset{\text{(EGC)}}{=} \frac{1}{\sqrt{K}} \sum_{i=1}^{K} g_i \tag{8.12b}$$

$$g \overset{\text{(SC)}}{=} \max_{i=1,\cdots,K} g_i \tag{8.12c}$$

$$g \overset{\text{(HS/MRC)}}{=} \sqrt{\sum_{i=1}^{L} g_{(i)}^2} \tag{8.12d}$$

where $L \leq K$ is the number of selected branches having the largest fading amplitudes, and $g_{(i)}$ denotes the i-th largest fading amplitude, so that, $g_{(1)} \geq g_{(2)} \geq \cdots \geq g_{(K)}$. Thus, the output channel fading amplitude, g, and its statistics are a function of the number of diversity branches, K. Note also that MRC scheme requires knowledge of the K channel fading amplitudes and phases, EGC scheme requires knowledge of K channel fading phases, and the SC scheme requires knowledge of K channel fading amplitudes. Hence, we observe that the output channel amplitudes (8.12a)–(8.12d) for MRC, EGC, SC and HS/MRC diversity are given by the l_2, l_1', l_∞ and l_2 norms, respectively, of the complex valued channel coefficients vector, $\mathbf{h} = (h_1, h_2, \cdots, h_K)$, since $|h_i| = g_i$, for $i = 1, 2, \cdots, K$. We have the following theorem.

Theorem 8.10 *Assuming an arbitrary joint PDF of the branch channels fading coefficients,* $\mathbf{h}$*, the output channel amplitude of MRC, SC and HS/MRC diversity is always increased by adding more receiver antennas. On the other hand, additional receiver antennas for EGC diversity increase the output channel amplitude with increasing probability.*

Proof: The proof follows using mathematical induction and Theorem 8.1. ■

Note that no co-phasing is assumed in the conditions of Theorem 8.10. Yet, assuming that $\gamma = g^2\gamma_b$, and that γ_b is a non-decreasing function of the number of diversity branches, then, for any branch channels fading statistics, the output SNR of DCS's is monotonically increasing with the number of diversity branches. Assuming a linear DCS and perfect channel estimation, l_2 is the largest achievable value of the combiner output channel amplitude [172]; see inequalities (8.2a)–(8.2c). On the other hand, whether EGC or SC diversity has larger output channel amplitude depends on a specific channel realization; see inequality (8.2d). Note also that, for all DCS's considered, since the output channel fading amplitude, g, increases with K, so does its expected value, $\mathrm{E}[g]$. Then, provided that the instantaneous performance measure is monotonically improving with g, and using Jensen's inequality, an upper (or lower) bound of the expected (average) performance measure is monotonically improving with K.

the following K-dimensional objects, i.e.,

$$\begin{aligned}
\mathrm{S}_K(a_1, a_2) &= \{\mathbf{g} \in \mathbb{R}^K : a_1 \leq \|\mathbf{g}\|_2 \leq a_2\} \\
\mathrm{P}_K(a_1, a_2) &= \{\mathbf{g} \in \mathbb{R}^K : a_1 \leq \|\mathbf{g}\|_1 \leq a_2\} \\
\mathrm{P}'_K(a_1, a_2) &= \{\mathbf{g} \in \mathbb{R}^K : a_1 \leq \frac{1}{\sqrt{K}} \|\mathbf{g}\|_1 \leq a_2\} \\
\mathrm{C}_K(a_1, a_2) &= \{\mathbf{g} \in \mathbb{R}^K : a_1 \leq \|\mathbf{g}\|_\infty \leq a_2\}
\end{aligned}$$

where $\mathrm{S}_K(a_1, a_2)$ is a hollow sphere of radii, a_1, and, a_2, $\mathrm{P}_K(a_1, a_2)$ is a hollow polytope of radii, a_1, and, a_2, $\mathrm{P}'_K(a_1, a_2)$ is a hollow scaled polytope of radii, a_1, and, a_2, and $\mathrm{C}_K(a_1, a_2)$ is a hollow cube of edge lengths, $2a_1$, and, $2a_2$. Denote, $a_2 = a$, and, $a_1 = \kappa a$, where $0 \leq \kappa \leq 1$. The volume of hollow K-dimensional objects can be computed using (8.4), i.e.,

$$\mathrm{V}[\mathrm{O}_K(a\kappa, a)] = \mathrm{A}\Big[\hat{\mathrm{O}}_K(1)\Big] \frac{a^K(1 - \kappa^K)}{K}.$$

Thus, if $\kappa = 0$, the cavity is removed, and, if $\kappa = 1$, the object has zero volume. For hollow K-dimensional objects having $\kappa > 0$, we can extend Theorem 2 as follows.

Theorem 8.8 *Given a constant radius, $a > 0$, and, $0 \leq \kappa \leq 1$, the volume, $\mathrm{V}[\mathrm{O}_K(a\kappa, a)]$, reaches a maximum for dimension, $K^* = K$, if $o_{K-1}(\kappa) < a < o_K(\kappa)$, and, $K^* \in \{K, K+1\}$, if $a = o_K(\kappa)$, where*

$$o_K(\kappa) = \begin{cases} \left(\frac{\mathrm{A}[\hat{\mathrm{O}}_K(1)]}{\mathrm{A}[\hat{\mathrm{O}}_{K+1}(1)]}\right)\left(\frac{K+1}{K}\right)\left(\frac{1-\kappa^K}{1-\kappa^{K+1}}\right) & K = 1, 2, \cdots \\ 0 & K \leq 0 \end{cases}$$

and importantly, provided that the sequence, $o_K(\kappa)$, is monotonically increasing with K.

Proof: Note that, $\frac{K+1}{K}$, and, $\frac{1-\kappa^K}{1-\kappa^{K+1}}$, are increasing sequences. Hence, equivalently, the first-order difference, $\mathrm{A}\Big[\hat{\mathrm{O}}_K(1)\Big] - \mathrm{A}\Big[\hat{\mathrm{O}}_{K+1}(1)\Big]$, must be an increasing sequence in order that the sequence, $o_K(\kappa)$, be increasing. Note that, $\mathrm{V}[\mathrm{O}_K(a\kappa, a)] \geq \mathrm{V}[\mathrm{O}_{K+1}(a\kappa, a)]$, is equivalent to the condition, $o_K(\kappa) \geq a$, and, $\mathrm{V}[\mathrm{O}_{K-1}(a\kappa, a)] \leq \mathrm{V}[\mathrm{O}_K(a\kappa, a)]$, is equivalent to the condition, $o_{K-1}(\kappa) \leq a$. Thus, provided that $o_K(\kappa)$ is a monotonically increasing sequence, and, $o_{K-1}(\kappa) \leq a \leq o_K(\kappa)$, then dimension K corresponds to the maximum volume, and, $K^* = K$. Similarly, we can show that, if $a = o_K(\kappa)$, then $K^* \in \{K, K+1\}$. ■

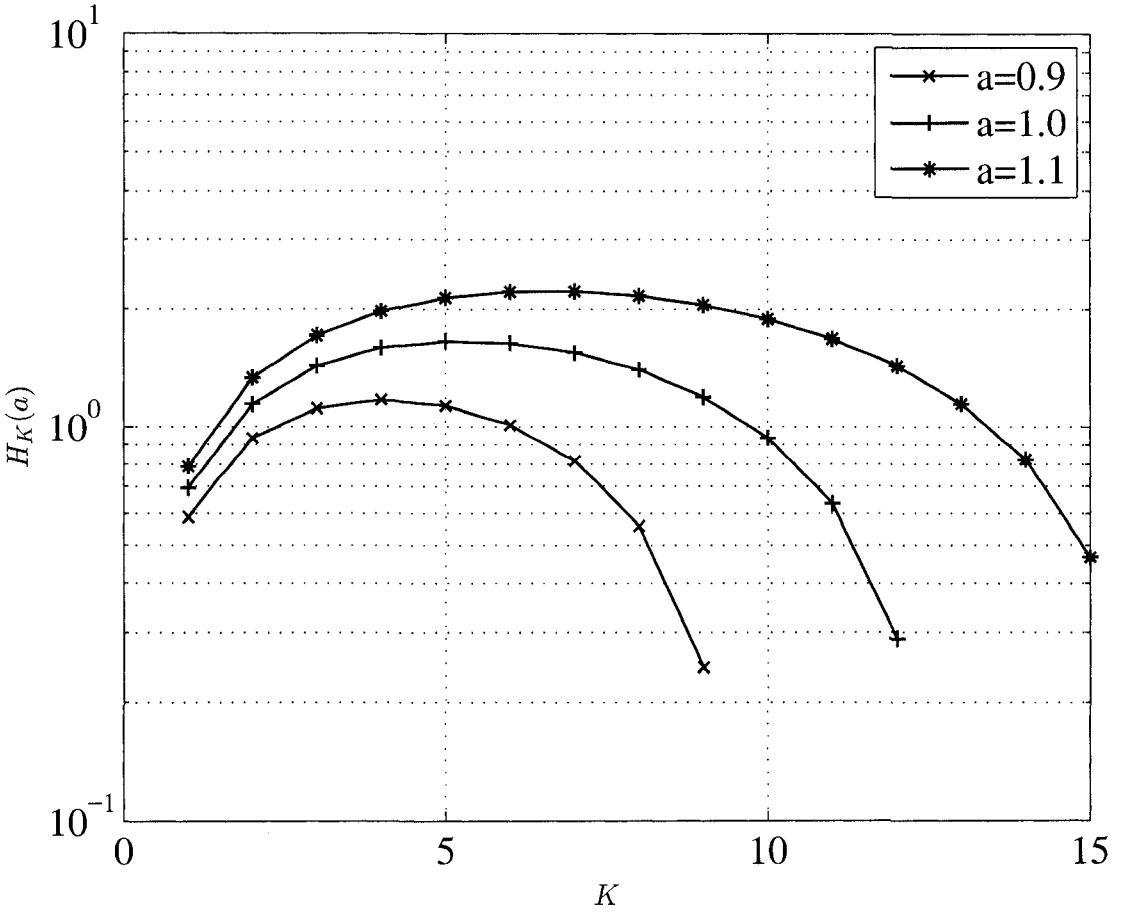

Figure 8.4: The entropy, $H_K(a) = \log \mathrm{V}[\mathrm{S}_K(a)]$, of a uniform distribution over a sphere, $\mathrm{S}_K(a)$, versus dimension, K.

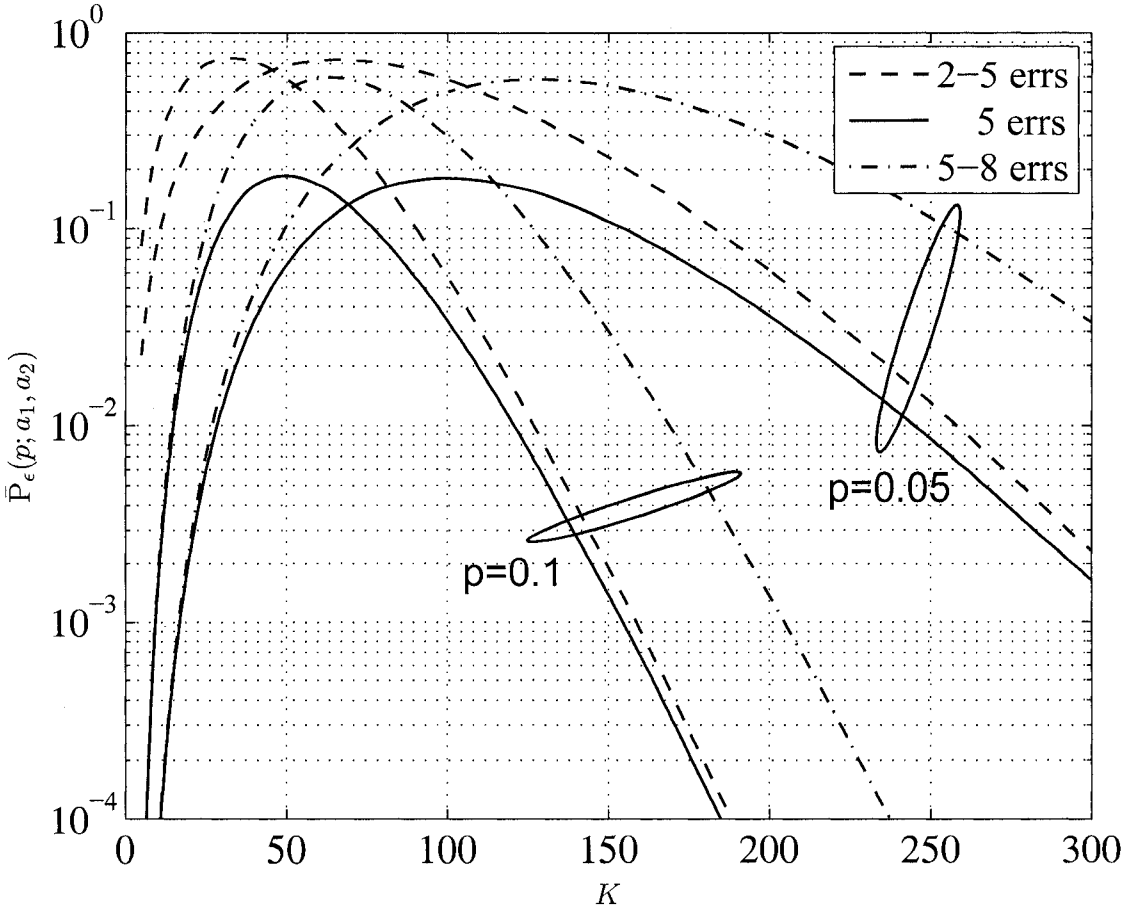

Figure 8.5: The probability of at least a_1 and at most a_2 errors in a sequence of K bits with crossover probability, p.

corresponds to the discrete hollow sphere (8.7) and is written as,

$$\bar{\mathrm{P}}_\epsilon(p; a_1, a_2) = \sum_{i=a_1}^{a_2} \binom{K}{i} p^i (1-p)^{K-i}. \tag{8.13}$$

The probability (8.13) versus dimension, K, is plotted in Fig. 8.5, for $p = 0.05$, and $p = 0.1$. We observe from Fig. 8.5 that, for example, the detector with 2–5 errors is an order of magnitude more likely to be selected over the detector having 5–8 errors, for dimensions, $K > 150$.

In general, the average BER, $\bar{\mathrm{P}}_\epsilon(\gamma_b; \Omega_n)$, can be efficiently evaluated using the Prony approximation of the conditional BER, i.e., $\mathrm{P}_\epsilon(\gamma) = \sum_{j=1}^{q} \tilde{A}_j \, \mathrm{e}^{-\tilde{a}_j \gamma}$, where $\tilde{A}_i$ and $\tilde{a}_i$ are positive real constants, and $q \geq 1$, [70]. Assuming that the MGF, $\Phi_g(t)$ of g, or, $\Phi_{g^2}(t)$ of g^2, is known, then we

can show that the average BER is evaluated as,

$$\begin{aligned}\bar{\mathrm{P}}_\epsilon(\gamma_b;\Omega_n) &= \sum_{j=1}^{q}\frac{\tilde{A}_j}{2\pi\mathrm{j}}\int_{c-\mathrm{j}\infty}^{c+\mathrm{j}\infty}\Phi_g(t)I_g(t,\tilde{a}_j\gamma_b;\Omega_n)\mathrm{d}t \\ &= \sum_{j=1}^{q}\frac{\tilde{A}_j}{2\pi\mathrm{j}}\int_{c-\mathrm{j}\infty}^{c+\mathrm{j}\infty}\Phi_{g^2}(t)I_{g^2}(t,\tilde{a}_j\gamma_b;\Omega_n)\mathrm{d}t\end{aligned} \tag{8.14}$$

where $t = c + \mathrm{j}\omega$ is a dummy variable, $c, \omega \in \mathbb{R}$, and the integrals,

$$\begin{aligned}I_g(t,a;\Omega_n) &= \int_{\sqrt{\tilde{\gamma}_{n-1}/\gamma_b}}^{\sqrt{\tilde{\gamma}_n/\gamma_b}} \mathrm{e}^{-gt-ag^2}\mathrm{d}g \\ &= \sqrt{\frac{\pi}{a}}\,\mathrm{e}^{\frac{t^2}{4a}}\left(Q\left(\sqrt{2a\frac{\tilde{\gamma}_{n-1}}{\gamma_b}}+\frac{t}{2a}\right)-Q\left(\sqrt{2a\frac{\tilde{\gamma}_n}{\gamma_b}}+\frac{t}{2a}\right)\right) \\ I_{g^2}(t,a;\Omega_n) &= \int_{\tilde{\gamma}_{n-1}/\gamma_b}^{\tilde{\gamma}_n/\gamma_b} \mathrm{e}^{-g^2t-ag^2}\mathrm{d}g^2 \\ &= \frac{1}{a+t}\left(\mathrm{e}^{-\frac{\tilde{\gamma}_{n-1}}{\gamma_b}(a+t)}-\mathrm{e}^{-\frac{\tilde{\gamma}_n}{\gamma_b}(a+t)}\right)\end{aligned}$$

and $Q(x) = \frac{1}{\sqrt{2\pi}}\int_x^\infty \mathrm{e}^{-u^2/2}\mathrm{d}u$ is the Q-function. The integrals in (8.14) are efficiently computed using a Gauss-Chebyshev numerical quadrature [46]. For example, assume K independent Ricean distributed branch fading amplitudes [21] having 2 degrees of freedom, unit variance per dimension, and the Rice factor, 3 dB. Fig. 8.6 shows the average BER for MRC, EGC and SC diversity, and 2-PSK modulation having the conditional BER, $\mathrm{P}_\epsilon(\gamma) \approx 0.204\,\mathrm{e}^{-1.504\gamma} + 0.105\,\mathrm{e}^{-1.024\gamma}$, and the SNR, $\gamma_b = -3\,\mathrm{dB}$. We observe from Fig. 8.6 that, for all DCS's, the average BER is monotonically decreasing for $\gamma \in (0,\infty)$. However, the BER reaches a maximum value before decreasing towards 0, if the lower limit of γ is greater than 0.

Assuming the parameters of the branch fading channels as in Fig. 8.6, the probability, $\mathrm{P}_{\mathrm{det}}(\Omega_n)$, that $\gamma \in \Omega_n$, versus the number of receiver antennas, K, is shown in Fig. 8.7. We observe from Fig. 8.7 that, for shorter intervals, Ω_n, the maximum of $\mathrm{P}_{\mathrm{det}}(\Omega_n)$ becomes more pronounced.

The average channel capacity is computed as,

$$\begin{aligned}\bar{\mathrm{C}}(\gamma_b;\Omega_n) &= \frac{1}{2\pi\mathrm{j}}\int_{c-\mathrm{j}\infty}^{c+\mathrm{j}\infty}\Phi_g(t)J_g(t,\gamma_b;\Omega_n)\mathrm{d}g \\ \bar{\mathrm{C}}(\gamma_b;\Omega_n) &= \frac{1}{2\pi\mathrm{j}}\int_{c-\mathrm{j}\infty}^{c+\mathrm{j}\infty}\Phi_{g^2}(t)J_{g^2}(t,\gamma_b;\Omega_n)\mathrm{d}g^2\end{aligned}$$

where the integrals,

$$\begin{aligned}J_g(t,\gamma_b;\Omega_n) &= \int_{\sqrt{\tilde{\gamma}_{n-1}/\gamma_b}}^{\sqrt{\tilde{\gamma}_n/\gamma_b}}\mathrm{C}(\gamma_b g^2)\,\mathrm{e}^{-gt}\mathrm{d}g \\ J_{g^2}(t,\gamma_b;\Omega_n) &= \int_{\tilde{\gamma}_{n-1}/\gamma_b}^{\tilde{\gamma}_n/\gamma_b}\mathrm{C}(\gamma_b g^2)\,\mathrm{e}^{-g^2t}\mathrm{d}g^2\end{aligned}$$

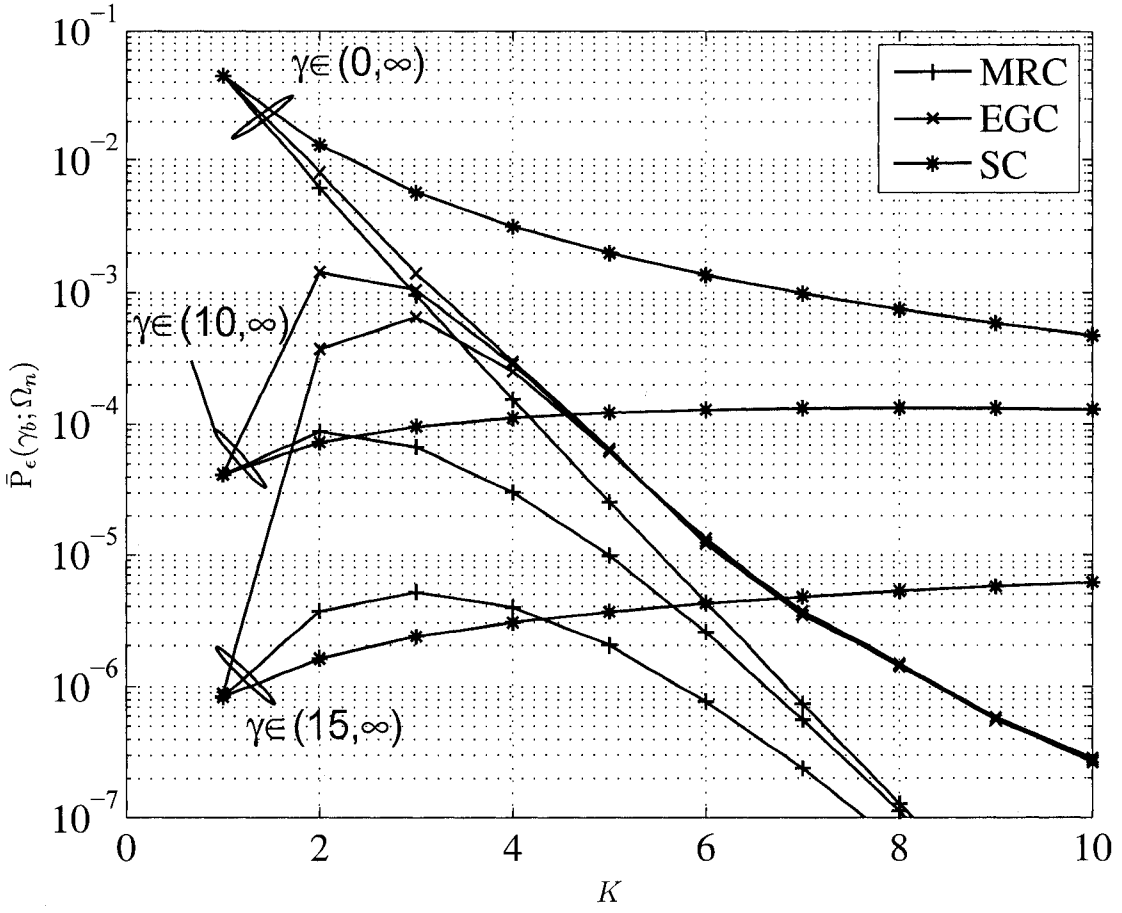

Figure 8.6: The average BER versus the number of receiver antennas, K, for 2-PSK modulation with MRC, EGC and SC diversity over generalized Ricean fading channels.

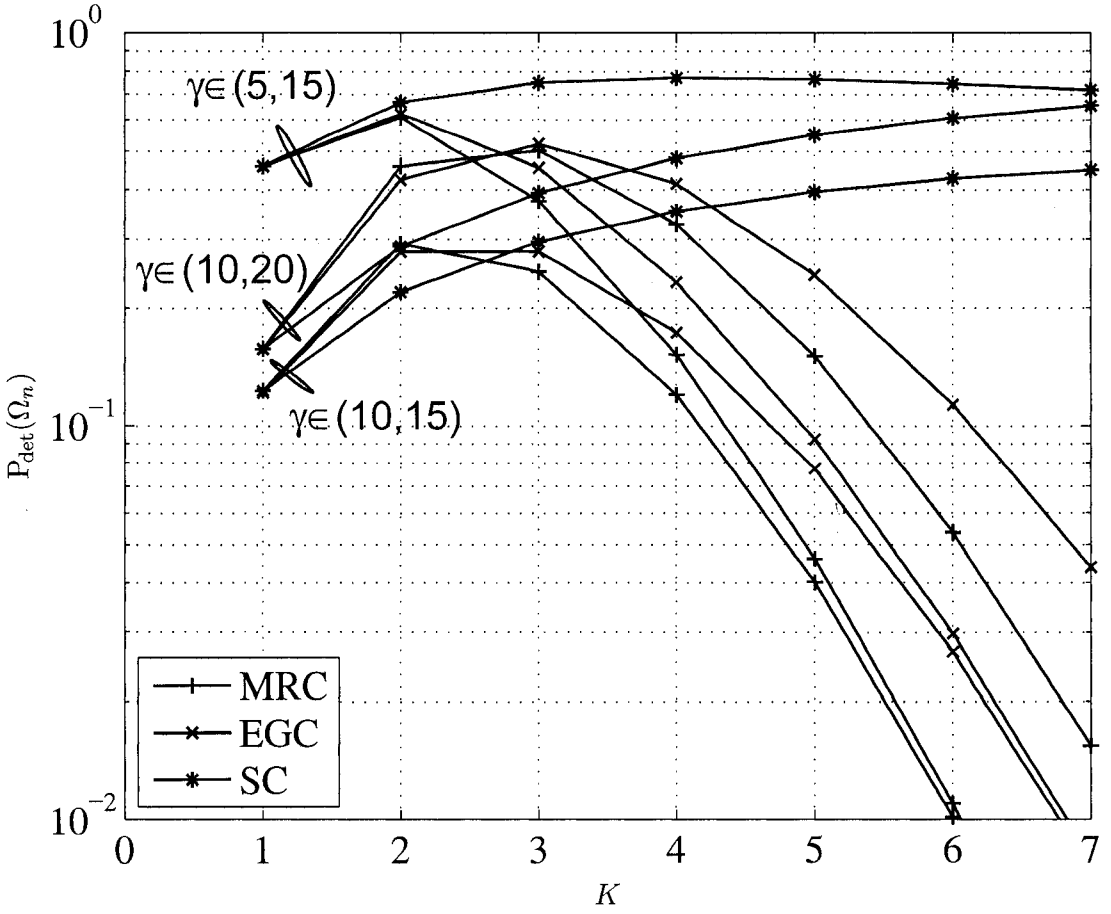

Figure 8.7: The probability, $\mathrm{P_{det}}(\Omega_n)$, versus the number of receiver antennas, K, for MRC, EGC and SC diversity over generalized Ricean fading channels.

and the conditional channel capacity, $\mathrm{C}(\gamma)$, for unconstrained Gaussian input and 2-PSK input, respectively, is given by (8.11a) and (8.11b). A closed-form expression for the partial MGF of the channel capacity, $\mathrm{C}(\gamma)$, can be obtained for the case of unconstrained Gaussian input, i.e.,

$$\begin{aligned}&\int_0^b \log_2(1+g^2)\,\mathrm{e}^{-g^2 t}\mathrm{d}g^2 = \\ &\quad = \tfrac{\mathrm{e}^t}{t\log(2)}\left(\Gamma\left(0,t\right)-\Gamma\left(0,t+bt\right)\right) - \tfrac{\mathrm{e}^{-bt}}{t}\log_2(1+b)\end{aligned}$$

where $\Gamma\left(\cdot,\cdot\right)$ is the incomplete gamma function [168]. Assuming again the branch fading statistics as in Fig. 8.6 and Fig. 8.7, the average channel capacities, $\bar{\mathrm{C}}(\gamma_b;\Omega_n)$, and, $\bar{\mathrm{C}}_{2\mathrm{psk}}(\gamma_b;\Omega_n)$, corresponding to the unconstrained Gaussian input and 2-PSK input, respectively, are shown in Fig. 8.8 and Fig. 8.9. In Fig. 8.8, the symbols '1' and '2' correspond to the case of $\gamma \in (20,25)$ and $\gamma \in (20,30)$, respectively. Importantly, we observe from Fig. 8.8 and Fig. 8.9 that the DCS maximizing the average subchannel capacity depends on the number of receiver antennas as well as the choice of the SNR interval, Ω_n.

Consider a MIMO channel having independent and identically distributed channel coefficients. Let the number of transmitter antennas be equal to the number of receiver antennas and denoted as K. Provided that the channel coefficients are zero-mean and complex Gaussian, then, for $\gamma \in \Omega_n$ and unconstrained Gaussian inputs, the channel capacity is evaluated as [175],

$$\bar{\mathrm{C}}_{K\times K}(\gamma_b;\Omega_n) = \int_{\tilde{\gamma}_{n-1}/\gamma_b}^{\tilde{\gamma}_n/\gamma_b} \log(1+g^2\gamma_b)\frac{(g^2)^{K-1}}{(K-1)!}\,\mathrm{e}^{-g^2}\mathrm{d}g^2.$$

Fig. 8.10 shows the capacity of a Gaussian $K \times K$ MIMO channel for several choices of the SNR interval, Ω_n, and $\gamma_b = 0\,\mathrm{dB}$. We can again observe from Fig. 8.10 that constraining the values of SNR creates an optimum in the number of transmitter and receiver antennas, for which the MIMO channel capacity is maximized.

Finally, note also that comparing the average BER in Fig. 8.6 and the average channel capacity in Fig. 8.8–Fig. 8.10 illustrate a general trade-off between reliability and throughput of a communication subchannel [161]. In particular, either the subchannel dimension is selected to minimize the average BER, or the subchannel dimension maximizes the average channel capacity.

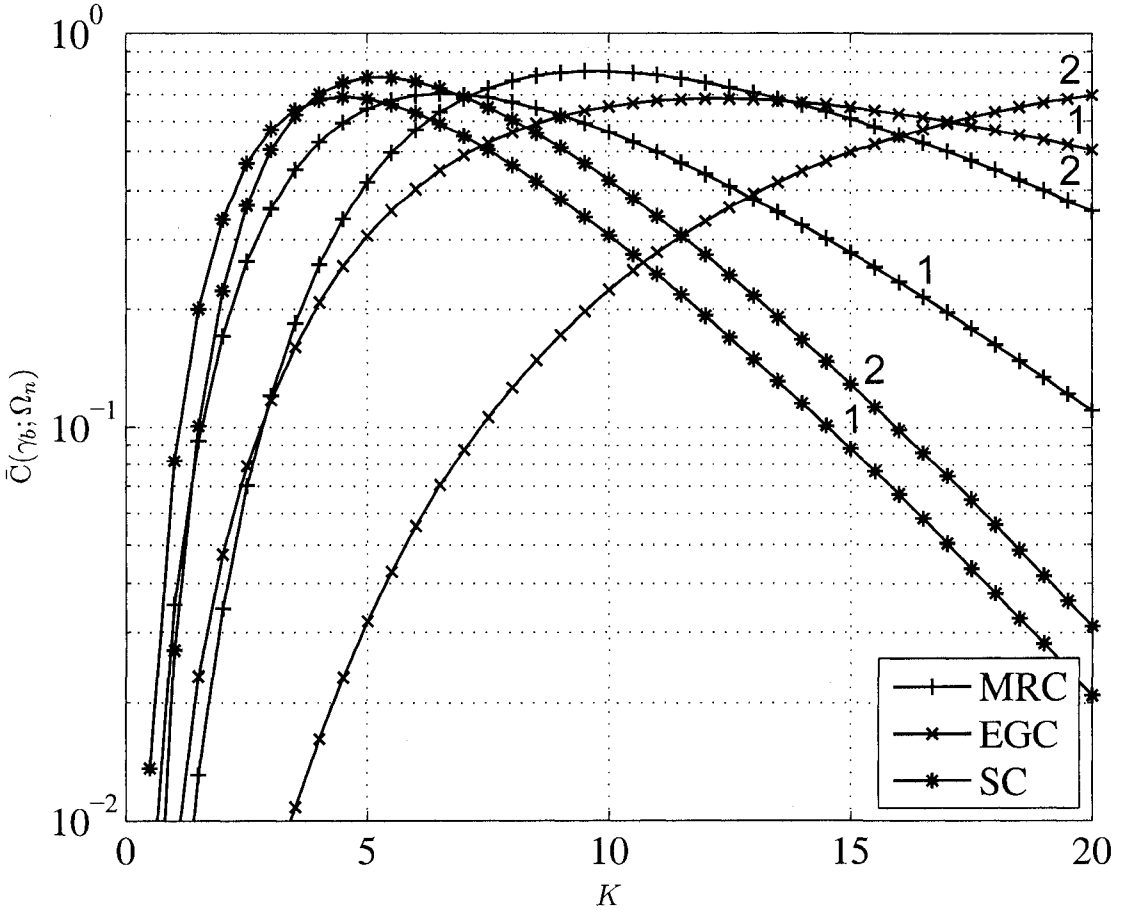

Figure 8.8: The average channel capacity, $\bar{\mathrm{C}}(\gamma_b;\Omega_n)$, versus the number of receiver antennas, K, for MRC, EGC and SC diversity over generalized Ricean fading channels.

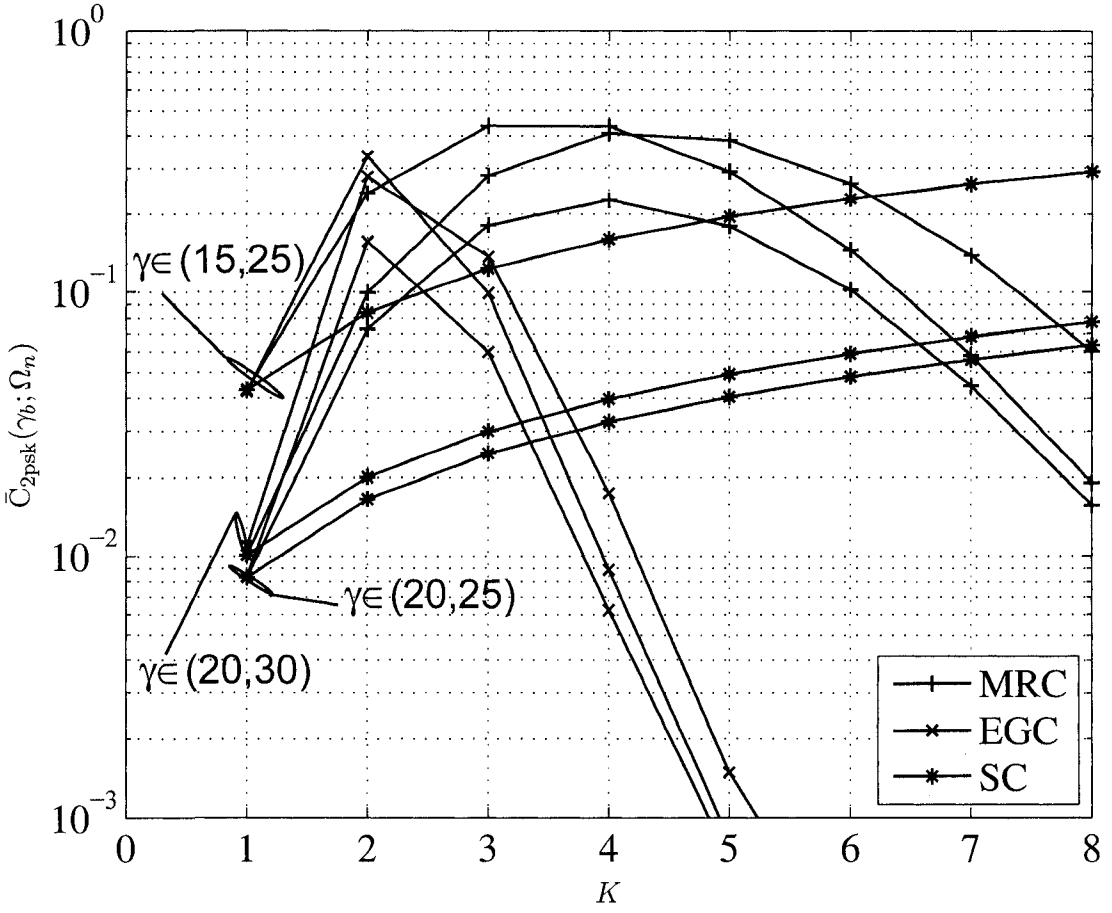

Figure 8.9: The average channel capacity, $\bar{C}_{2psk}(\gamma_b;\Omega_n)$, versus the number of receiver antennas, K, for MRC, EGC and SC diversity over generalized Ricean fading channels.

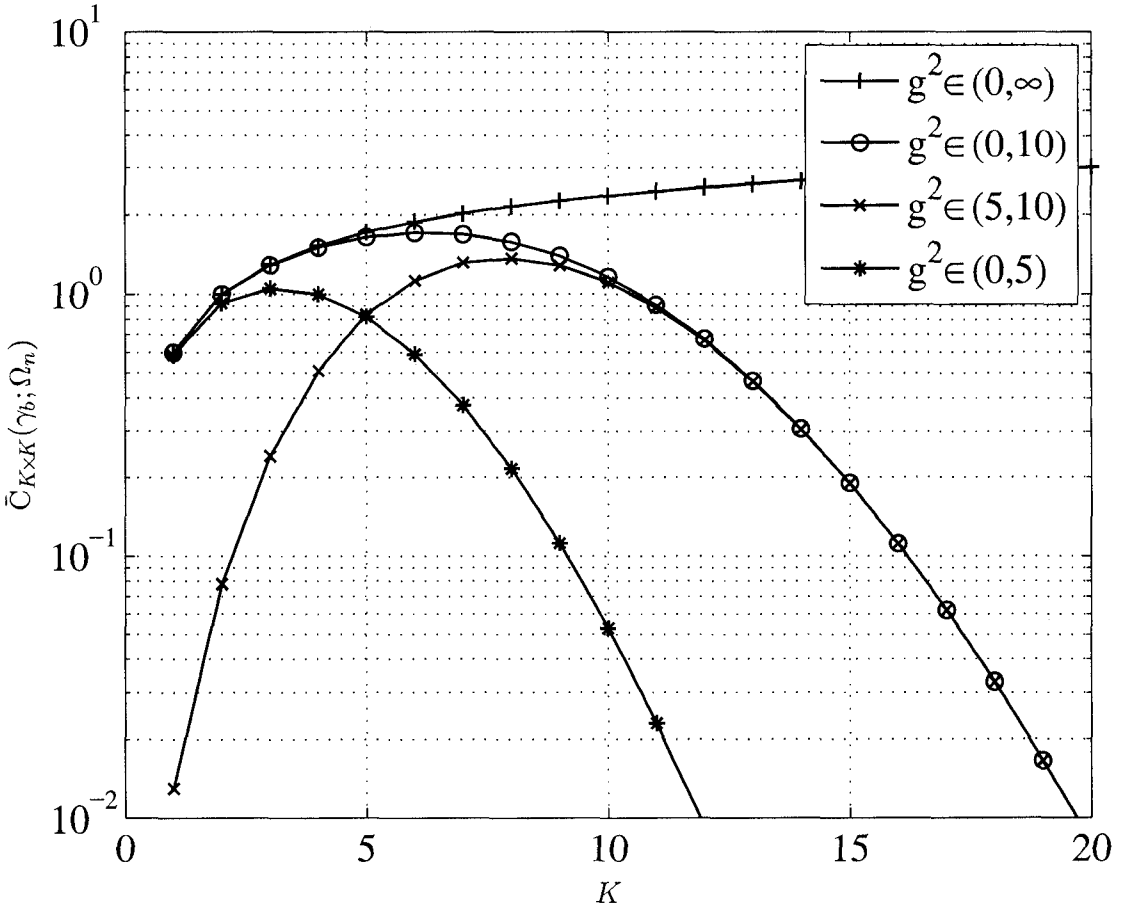

Figure 8.10: The average channel capacity, $\bar{C}_{K\times K}(\gamma_b;\Omega_n)$, of a Gaussian $K \times K$ MIMO channel versus the equal number of transmitter and receiver antennas, K.

8.6 Summary

The K-dimensional sphere, polytope, cube, scaled polytope, and the scaled cube were studied. It was proved that the l_p norm and the scaled l'_p norm are monotonically increasing in dimension, K, while monotonically decreasing in the norm-order, p. It was also proved that the volume and the surface area of objects under consideration reach a maximum value for a particular dimension, and then, the volume and the surface area decrease toward zero. The dimension maximizing the volume and the surface area was obtained as a function of the radius. These results provide important insights into diverse problems in digital communications such as the error rate estimation of block codes using importance sampling [167], and the properties of DCS's. In particular, SNR adaptive receivers employing a bank of symbol-by-symbol subchannel detectors and a K branch diversity combining front-end operating over erasure subchannels were investigated. Several DCS's were described using a hypergeometry of objects in K dimensions. Hence, it was proved that, at least in probability, the combiners output channel fading amplitudes are increased by using additional receiver antennas, for any distribution of branch channel fadings. Furthermore, average performance measures such as the average BER, the probability of selecting a particular subchannel and the average channel capacity corresponding to erasure subchannels were conjectured to reach a maximum for a particular dimension and the subchannel selected. The conjecture was then confirmed using numerical examples. The results indicate that the receiver dimension (e.g., the sequence length and the number of receiver antennas) and the SNR partitioning have significant impact on the average performance measures corresponding to a particular subchannel, and in turn, on the overall complexity of the SNR adaptive receivers.

Chapter 9

Conclusions and Future Work

In this final chapter, we draw conclusions, summarize the major results of the thesis, and also, provide suggestions for future work.

9.1 Conclusions

We studied techniques for efficient performance evaluation of wireless communications systems. In the first part of the thesis, novel performance evaluation techniques were proposed in order to improve efficacy of the performance analysis, so that the analysis becomes simpler, is applicable to more complex system models, and also, is easier to be verified. In the second part of the thesis, the efficient performance evaluation techniques were used to obtain novel design guidelines.

As evidenced by numerical examples in this thesis, semi-analytical techniques appear to be the most efficient approach to performance analysis of wireless communications systems. In particular, provided that some parts of the system model can be described analytically, then these parts do not have to be simulated, potentially saving large amount of computations. For example, the SR simulation technique can decide on the decoded sequence analytically avoiding running a computationally expensive decoder. The Prony approximation method requires knowledge of the conditional probability of error at only a small number of SNR values; such knowledge can be obtained using computer simulation, and then, the average probability of error is computed analytically.

Furthermore, selection of the system model was shown to be critical for obtaining the performance analysis efficiently. This was illustrated for the case of DCS's over correlated fading channels where the channel modeling was used to transform correlated branches into independent branches. Importantly, note that the system model for efficient performance analysis and the system model

following actual implementation can be very distinct. While precise knowledge of the input, output and the latent parameters values is available at any time at any place in the course of simulation, such knowledge is often missing or is impossible to be obtained in real implementation. Hence, exploiting all the available knowledge in the course of simulation can result in significant reduction of simulation run-times; however, one has to make sure that the analysis remains unbiased.

Two examples of obtaining the design guidelines from the efficient performance analysis were illustrated for the case of BRC's and the case of SNR adaptive receivers. In particular, initially, the exact BER of binary Hamming codes was evaluated using their recursive structure. Then, the recursive structure and the cyclic parity matrix were used to propose a family of multidimensional binary block codes referred to as BRC's. Also, theoretical analysis of the SR simulation gain revealed that the volume of hypersphere reaches a maximum for a particular value of dimension. This observation was used to obtain an optimum dimension of the SNR adaptive receivers.

In general, the system model and the performance evaluation technique should be chosen for a particular system at hand, and the application being considered. The complexity of communications systems is constantly increasing. Novel design guidelines are important to sustain the progress of technology. Hence, we conjecture that the research area of efficient performance evaluation techniques, perhaps underestimated until very recently, will become much more important in near future. Furthermore, development of efficient performance evaluation techniques should complement advancements of efficient signal processing algorithms.

The main results presented in this thesis can be summarized as follows.

1. Sample rejection is an easy-to-implement computer simulation technique for binary coded systems operating over quantized AWGN channels and ISI channels.

2. Modified FD can be more efficient for simulations of coded schemes over ISI channels and near-MLSD than the VA.

3. The Prony approximation method is an efficient semi-analytical technique for evaluation of the average error rates of digital modulations over slowly fading channels.

4. Prony approximation is a generalization of the Chernoff bound and the MGF method.

5. A linear correlation channel model, and a fading amplitude channel model using vector norm superposition of the impinging plane waves are well-suited for efficient performance evaluation of DCS's having correlated branches.

6. Decorrelation and orthogonalization of the diversity branches prior to combining can be used to restore some of the diversity gain lost due to the correlations between branches.

7. The rank and determinant design criteria of space-time-frequency block codes are valid not only for the Chernoff bound of the PEP, but also for the exact PEP.

8. Binary Hamming codes can be constructed recursively, and their coding gain does not increase monotonically with SNR.

9. Extended binary Hamming codes attain the Hamming bound.

10. Binary repetition codes having variable block length and variable minimum Hamming distance are well-suited for adaptive coding, turbo product coding, retransmission and multihop routing and block differential encoding.

11. Binary repetition codes and block differential encoding can be used to arbitrarily increase the coding rate while the minimum Hamming distance remains constant.

12. Binary repetition codes in multiple dimensions can be used to increase the minimum Hamming distance of concatenated 1D codes without increasing the transmission bandwidth.

13. Transmitter energy distribution over the codewords of BRC's can be optimized to improve the BER.

14. Distributed SPC codes can be used to implement coded cooperation among the network nodes in the uplink and downlink transmission.

15. The cooperation gains are strongly dependent on the specific network realization, and are less dependent on the number of cooperating nodes.

16. The volume and the surface area of some K-dimensional objects reach a maximum, and then, decrease towards zero.

17. The average performance measures of SNR adaptive receivers reach a maximum, and then, decrease towards zero, i.e., there exists an optimum receiver dimension.

9.2 Future Work

We outline the directions of possible future research.

1. The SR simulation technique should be considered for non-binary modulation schemes, multipath fading (time-varying) channels, and iterative decoding schemes.

2. In some cases, the SR simulation technique can provide design guidelines for the decoding schemes.

3. The Prony approximation method can be considered for evaluation of the average error rates for systems with additive interference, e.g., multiuser and intersymbol interference.

4. Prony approximation should be investigated for use in multiple dimensions, i.e., for cases where the error rates have to be averaged over several random processes.

5. Distributions and parameters of the linear correlation channel model and the vector norm plane wave superposition channel model have to be chosen in order to match the performance analysis and real measurements of DCS's assuming the existing correlated channel models.

6. Efficient channel models for systems with correlated co-channel interference should be developed.

7. Semi-analytical methods should be developed for efficient performance evaluation of various bits-to-symbol and symbol-to-subcarrier and antenna mappings for coded MIMO-OFDM systems.

8. The SISO decoding techniques suitable for multidimensional BRC's should be investigated.

9. The performance analysis of coded cooperation schemes using BRC's and SPC codes should be extended to fading channels.

10. The proof that the volume and the surface area of K-dimensional objects reach a maximum should be extended to a general case of the l_p-norm where $p \in \mathbb{Z}$, and then, $p \in \mathbb{R}$, $p > 0$.

11. The dimension that minimizes radius for constant volume and constant surface area objects in K dimensions should be derived.

12. Further applications of the results of hypergeometry to wireless communications systems should be considered.

References

[1] R. Lucky, "Is "industrial research" an oxymoron?," *IEEE Spectrum Mag.*, p. 56, Sept. 2003.

[2] R. Gallager, "The golden years of information theory," the Kailath Lecture, http://isl.stanford.edu/kailathlecture/, 2005.

[3] M. K. Simon, S. M. Hinedi, and W. C. Lindsey, *Digital Communication Techniques: Signal Design and Detection*. Prentice Hall, 1995.

[4] C. E. Shannon, "A mathematical theory of communications," *The Bell System Technical Journal*, vol. 27, pp. 379–423, 623–656, Oct. 1948.

[5] K. S. Shanmugam and P. Balaban, "A modified Monte-Carlo simulation technique for the evaluation of error rate in digital communication systems," *IEEE Trans. Commun.*, vol. COM-28, no. 11, pp. 1916–1924, Nov. 1980.

[6] P. J. Smith, M. Shafi, and H. Gao, "Quick simulation: A review of importance sampling techniques in communications systems," *IEEE J. Select. Areas Commun.*, vol. 15, no. 4, pp. 597–613, May 1997.

[7] P. M. Hahn and M. C. Jeruchim, "Developments in the theory and application of importance sampling," *IEEE Trans. Commun.*, vol. COM-35, no. 7, pp. 706–714, July 1987.

[8] M. A. Herro and J. M. Nowack, "Simulated Viterbi decoding using importance sampling," *IEE Proc.-F*, vol. 135, no. 2, pp. 133–142, Apr. 1988.

[9] J. S. Sadowsky, "A new method for Viterbi decoder simulation using importance sampling," *IEEE Trans. Commun.*, vol. 38, no. 9, pp. 1341–1351, Sept. 1990.

[10] N. C. Beaulieu, E. Biglieri, and M. Lai, "Sample rejection and importance sampling in the simulation of multidimensional signaling systems," *IEE Proc.-I*, vol. 140, no. 6, pp. 445–452, Dec. 1993.

[11] R. G. McKay, M. Shafi, and C. J. Carlisle, "Trellis-coded modulation on digital microwave radio systems — simulations for multipath fading channels," in *Proc. GLOBECOM*, 1988, vol. 1, pp. 239–243.

[12] K. B. Letaief and K. Muhammad, "An efficient new technique for accurate bit error probability estimation of ZJ decoders," *IEEE Trans. Commun.*, vol. 43, no. 6, pp. 2020–2027, June 1995.

[13] X. Ma, X. Zhang, H. Yu, and A. Kavčić, "Optimal quantization for soft-decision decoding revisited," in *Proc. ISITA*, 2002, pp. 1–3.

[14] J. A. Heller and I. M. Jacobs, "Viterbi decoding for satellite and space communication," *IEEE Trans. Commun. Tech.*, vol. COM-19, no. 5, pp. 835–848, Oct. 1971.

[15] W. Feller, *An Introduction to Probability Theory and Its Applications*, 3rd ed., vol. I. Wiley, 1968.

[16] G. L. Stuber, *Principles of Mobile Communication*, 2nd ed. Kluwer Academic, 2001.

[17] S. Benedetto and E. Biglieri, *Principles of Digital Transmission with Wireless Applications*, 2nd ed. Kluwer Academic, 1999.

[18] S. Lin and D. J. Costello, *Error Control Coding: Fundamentals and Applications*. Prentice-Hall, 1983.

[19] M. Rouanne and D. J. Costello, "An algorithm for computing the distance spectrum of trellis codes," *IEEE J. Select. Areas Commun.*, vol. 7, no. 6, pp. 929–940, Aug. 1989.

[20] A. Papoulis and S. U. Pillai, *Probability, Random Variables, and Stochastic Processes*, 4th ed. McGraw-Hill, 2002.

[21] J. G. Proakis, *Digital Communications*, 3rd ed. McGraw-Hill, 1995.

[22] D. M. Y. Sommerville, *An Introduction to the Geometry of n Dimensions*. New York: Dover, 1958.

[23] H. S. M. Coxeter, *Regular Polytopes*, 3rd ed. New York: Dover, 1973.

[24] 3GPP TR 26.201 V. 5.0.0, "AMR wideband speech codec; frame structure," Technical specification, Mar. 2001.

[25] 3GPP TS 25.212 V. 5.6.0, "Multiplexing and channel coding (FDD)," Technical specification, Sept. 2003.

[26] 3GPP TS 145.003 V. 5.8.0, "Digital cellular telecommunications system (Phase 2+); channel coding," Technical specification, June 2003.

[27] J. A. Heller, "Feedback decoding of convolutional codes," in *Advances in Commun. Syst.* 1975, vol. 4, pp. 261–278, A. J. Viterbi Ed., Academic Press, New York.

[28] J. B. Anderson and S. Mohan, "Sequential coding algorithms: A survey and cost analysis," *IEEE Trans. Commun.*, vol. COM-32, no. 2, pp. 169–176, Feb. 1984.

[29] A. J. Viterbi and J. K. Omura, *Principles of Digital Communication and Coding*. McGraw-Hill, 1979.

[30] A. Demosthenous, C. Verdier, and J. Taylor, "A new architecture for low power analogue convolutional decoders," in *IEEE Proc. Int. Symp. Circuits and Systems*, 1997, pp. 37–40.

[31] D. W. Waters and J. R. Barry, "The Chase family of detection algorithms for multiple-input multiple-output channels," in *Proc. GLOBECOM*, 2004, vol. 4, pp. 2635–2639.

[32] D. Haccoun and S. Kallel, "Application of multiple path sequential decoding for intersymbol interference reduction problem," *IEE Proc.-I*, vol. 138, no. 1, pp. 21–31, Feb. 1991.

[33] F. Xiong, A. Zerik, and E. Shwedyk, "Sequential sequence estimation for channels with intersymbol interference of finite or infinite length," *IEEE Trans. Commun.*, vol. 38, no. 6, pp. 795–804, June 1990.

[34] S. Ohno and G. B. Giannakis, "ML sequence estimation for long ISI channels with controllable complexity," in *Proc. ICC*, 2004, vol. 5, pp. 2782–2786.

[35] S. M. Ross, *Simulation*, 3rd ed. Academic Press, 2002.

[36] H. V. Poor, *An Introduction to Signal Detection and Estimation*, 2nd ed. Springer-Verlag, 1998.

[37] H. Zamiri-Jafarian and S. Pasupathy, "Complexity reduction of the MLSD/MLSDE receiver using the adaptive state allocation algorithm," *IEEE Trans. Wireless Commun.*, vol. 1, no. 1, pp. 101–111, Jan. 2002.

[38] H. Vikalo, B. Hassibi, and U. Mitra, "Sphere-constrained ML detection for channels with memory," in *Asilomar Conf. Sig., Syst. and Comp.*, 2003, vol. 1, pp. 672–676.

[39] ITU-R Recommendations, "Guidelines for evaluation of radio transmission technologies for IMT-2000," Vol. 2000 – M Series, Part 2, 1997.

[40] M. Schwartz, W. R. Bennett, and S. Stein, *Communication Systems and Techniques*. McGraw-Hill, 1966.

[41] A. Annamalai, C. Tellambura, and V. K. Bhargava, "A general method for calculating error probabilities over fading channels," *IEEE Trans. Commun.*, vol. 53, no. 5, pp. 841–852, May 2005.

[42] M. A. Smadi and V. K. Prabhu, "Efficient moment-based method for error rate calculations using the Beaulieu series," *IEE Proc. – Comm.*, vol. 153, no. 3, pp. 349–354, June 2006.

[43] M. Kavehrad and M. Joseph, "Maximum entropy and the method of moments in performance evaluation of digital communications systems," *IEEE Trans. Commun.*, vol. COM-34, no. 12, pp. 1183–1189, Dec. 1986.

[44] J. K. Cavers and P. Ho, "Analysis of the error performance of trellis-coded modulations in Rayleigh fading channels," *IEEE Trans. Commun.*, vol. 40, no. 1, pp. 74–83, Jan. 1992.

[45] E. Biglieri, G. Caire, G. Taricco, and J. Ventura-Traveset, "Simple method for evaluating error probabilities," *Electron. Lett.*, vol. 32, no. 3, pp. 191–192, Feb. 1996.

[46] E. Biglieri, G. Caire, G. Taricco, and J. Ventura-Traveset, "Computing error probabilities over fading channels: a unified approach," *European Trans. Telecommun.*, vol. 9, no. 1, pp. 15–25, Jan.–Feb. 1998.

[47] C. Tellambura and A. Annamalai, "Further results on the Beaulieu series," *IEEE Trans. Commun.*, vol. 48, no. 11, pp. 1774–1777, Nov. 2000.

[48] M. K. Simon and M.-S. Alouini, *Digital Communication over Fading Channels: A Unified Approach to Performance Analysis*. Wiley, 2000.

[49] K. Schumacher and J. J. O'Reilly, "Relationship between the saddlepoint approximation and the modified Chernoff bound," *IEEE Trans. Commun.*, vol. 38, no. 3, pp. 270–272, Mar. 1990.

[50] S. D. Foss, "A method of exponential curve fitting by numerical integration," *Biometrics*, vol. 26, no. 1–4, pp. 815–821, 1970.

[51] J. M. Varah, "On fitting exponentials by nonlinear least squares," *SIAM J. Scien. Comp.*, vol. 6, no. 1, pp. 30–44, Jan. 1985.

[52] M. R. Osborne and G. K. Smyth, "A modified Prony algorithm for exponential function fitting," *SIAM J. Scien. Comp.*, vol. 16, no. 1, pp. 119–138, Jan. 1995.

[53] A. Papoulis and S. U. Pillai, *Probability, Random Variables and Stochastic Processes*, 4th ed. McGraw Hill, 2002.

[54] S. Boyd and L. Vandenberghe, *Convex Optimization*. Cambridge University Press, 2004.

[55] T. M. Apostol, *Mathematical Analysis*, 2nd ed. Addison-Wesley, 1974.

[56] W. H. Press, S. A. Teukolsky, W. T. Vetterling, and B. P. Flannery, *Numerical Recipes in C*, 2nd ed. Cambridge University Press, 1997.

[57] K. Cho and D. Yoon, "On the general ber expression of one- and two-dimensional amplitude modulations," *IEEE Trans. Commun.*, vol. 50, no. 7, pp. 1074–1080, July 2002.

[58] P. J. Lee, "Computation of the bit error rate of coherent PSK with Gray code bit mapping," *IEEE Trans. Commun.*, vol. 34, no. 5, pp. 488–491, May 1986.

[59] M. Chiani, D. Dardari, and M. K. Simon, "New exponential bounds and approximations for the computation of error probability in fading channels," *IEEE Trans. Wireless Commun.*, vol. 2, no. 4, pp. 840–845, July 2003.

[60] P. O. Börjesson and C.-E. W. Sundberg, "Simple approximations of the error function Q(x) for communications applications," *IEEE Trans. Commun.*, vol. COM-27, no. 3, pp. 639–643, Mar. 1979.

[61] G. Corazza and G. Ferrari, "New bounds for the Marcum Q-function," *IEEE Trans. Inform. Theory*, vol. 48, no. 11, pp. 3003–3008, Nov. 2002.

[62] I. S. Gradshteyn and I. M. Ryzhik, *Table of Integrals, Series, and Products*, 6th ed. Academic Press, 2000.

[63] P. Loskot and N. C. Beaulieu, "Maximum ratio combining with arbitrary correlated generalized Ricean branches," in *Proc. WCNC*, 2004, vol. 1, pp. 333–338.

[64] G. F. P. Lombardo and M. M. Rao, "MRC performance for binary signals in Nakagami fading with general branch correlation," *IEEE Trans. Commun.*, vol. 47, no. 1, pp. 44–52, Jan. 1999.

[65] O. C. Ugweje and V. A. Aalo, "Performance of selection diversity system in correlated Nakagami fading," in *Proc. VTC*, 1997, vol. 3, pp. 1488–1492.

[66] M. K. Simon and M.-S. Alouini, *Digital Communication over Fading Channels*, 2nd ed. John Wiley & Sons, 2004.

[67] X. Dong and N. C. Beaulieu, "Optimal maximal ratio combining with correlated diversity branches," *IEEE Commun. Lett.*, vol. 6, no. 1, pp. 22–24, Jan. 2002.

[68] M.-S. Alouini, A. Scaglione, and G. B. Giannakis, "PCC: Principal components combining for dense correlated multipath fading environments," in *Proc. VTC*, 2000, vol. 5, pp. 2510–2517.

[69] H. A. David, *Order Statistics*, 2nd ed. John Wiley & Sons Inc., 1981.

[70] P. Loskot and N. C. Beaulieu, "Average error rate evaluation of digital modulations in slow fading by Prony approximation," in *Proc. ICC*, 2004, vol. 6, pp. 3353–3357.

[71] G. P. Efthymoglou, T. Piboongungon, and V. Aalo, "Error rates of M-ary signals with multichannel reception in Nakagami-m fading channels," *IEEE Commun. Lett.*, vol. 10, no. 2, pp. 100–102, Feb. 2006.

[72] R. A. Monzingo and T. W. Miller, *Adaptive Arrays*. John Wiley & Sons Inc., 1980.

[73] Q. T. Zhang and H. G. Lu, "A general analytical approach to multi-branch selection combining over various spatially correlated fading channels," *IEEE Trans. Commun.*, vol. 50, no. 7, pp. 1066–1073, July 2002.

[74] M. Z. Win and J. H. Winters, "Analysis of hybrid selection/maximal-ratio combining in rayleigh fading," *IEEE Trans. Commun.*, vol. 47, no. 12, pp. 1773–1776, Dec. 1999.

[75] R. K. Mallik and M. Z. Win, "Analysis of hybrid selection/maximal-ratio combining in correlated Nakagami fading," *IEEE Trans. Commun.*, vol. 50, no. 8, pp. 1372–1383, Aug. 2002.

[76] X. Zhang and N. C. Beaulieu, "Performance analysis of generalized selection combining in generalized correlated Nakagami-m fading," *IEEE Trans. Commun.*, vol. 54, no. 11, pp. 2103–2112, Nov. 2006.

[77] A. M. D. Turkmani, "Performance evaluation of a composite microscopic plus macroscopic diversity system," *IEE Proc.-I*, vol. 138, no. 1, pp. 15–20, Feb. 1991.

[78] L. C. Choo and T. T. Tjhung, "BER performance of DQPSK in Nakagami fading with selection diversity and maximal-ratio combining," *IEEE Trans. Commun.*, vol. 48, no. 10, pp. 1618–1621, Oct. 2000.

[79] Y. Ma and S. Pasupathy, "Efficient performance evaluation for generalized selection combining on generalized fading channels," *IEEE Trans. Wireless Commun.*, vol. 3, no. 1, pp. 29–34, Jan. 2004.

[80] Y. Ma and S. Pasupathy, "Theoretical diversity improvement in GSC(N,L) receiver with nonidentical fading statistics," *IEEE Trans. Commun.*, vol. 53, no. 6, pp. 1027–1035, June 2005.

[81] R. A. Horn and C. R. Johnson, *Matrix Analysis*. Cambridge Univ. Press, 1990.

[82] G. Taricco and E. Biglieri, "Exact pairwise error probability of space-time codes," *IEEE Trans. Inform. Theory*, vol. 48, no. 2, pp. 510–513, Feb. 2002.

[83] M. K. Simon and H. Jafarkhani, "Performance evaluation of super-orthogonal space-time trellis codes using a moment generating function-based approach," *IEEE Trans. Sign. Proc.*, vol. 51, no. 11, pp. 2379–2751, Nov. 2003.

[84] Y. Gong and K. B. Letaief, "An efficient space-frequency coded OFDM system for broadband wireless communications," *IEEE Trans. Commun.*, vol. 51, no. 12, pp. 2019–2029, Dec. 2003.

[85] Y. Li, J. C. Chuang, and N. R. Sollenberger, "Transmitter diversity for OFDM systems and its impact on high-rate data wireless networks," *IEEE J. Select. Areas Commun.*, vol. 17, no. 7, pp. 1233–1243, July 1999.

[86] H. Bölcskei, M. Borgmann, and A. J. Paulraj, "Impact of the propagation environment on the performance of space-frequency coded MIMO-OFDM," *IEEE J. Select. Areas Commun.*, vol. 21, no. 3, pp. 427–439, Apr. 2003.

[87] M. Fozunbal, S. W. McLaughlin, and R. W. Schafer, "On space-time-frequency coding over MIMO-OFDM systems," *IEEE Trans. Wireless Commun.*, vol. 4, no. 1, pp. 320–331, Jan. 2005.

[88] W. Su, Z. Safar, and K. J. R. Liu, "Towards maximum achievable diversity in space, time, and frequency: performance analysis and code design," *IEEE Trans. Wireless Commun.*, vol. 4, no. 4, pp. 1847–1857, July 2005.

[89] IEEE 802.16 Broadband Wireless Working Group, "IEEE standard for local and metropolitan area networks, Part 16: Air interface for fixed broadband wireless access systems," 2001.

[90] G. Caire, G. Taricco, and E. Biglieri, "Bit-interleaved coded modulation," *IEEE Trans. Inform. Theory*, vol. 44, no. 3, pp. 927–946, May 1998.

[91] V. Tarokh, N. Seshadri, and A. R. Calderbank, "Space-time codes for high data rate wireless communication: performance criterion and code construction," *IEEE Trans. Inform. Theory*, vol. 44, no. 2, pp. 744–765, Mar. 1998.

[92] J. Wang, M. K. Simon, M. P. Fitz, and K. Yao, "On the performance of space-time codes over spatially correlated Rayleigh fading channels," *IEEE Trans. Commun.*, vol. 52, no. 6, pp. 877–881, June 2004.

[93] M. Gharavi-Alkhansari and A. B. Gershman, "Exact symbol-error probability analysis for orthogonal space-time block codes: Two- and higher dimensional constellations cases," *IEEE Trans. Commun.*, vol. 52, no. 7, pp. 1068–1073, July 2004.

[94] Y. Li, P. H. W. Fung, Y. Wu, and S. Sun, "Bit-interleaved coded modulation in linear dispersion coded MIMO system over spatially correlated Rician fading channel," in *Proc. GLOBECOM*, 2004, vol. 1, pp. 5–9.

[95] A. Chindapol and J. A. Ritcey, "Design, analysis, and performance evaluation for BICM-ID with square QAM constellations in Rayleigh fading channels," *IEEE J. Select. Areas Commun.*, vol. 19, no. 5, pp. 944–957, May 2001.

[96] Y. He, B. Z. G. Zhu, Z. Zhang, and X. Li, "The performance of STBC coded MIMO-OFDM system based on turbo product codes," in *Proc. WCNM*, 2005, vol. 1, pp. 653–656.

[97] I. Lee, A. M. Chan, and C.-E. W. Sundberg, "Space-time bit-interleaved coded modulation for OFDM systems," *IEEE Trans. Sign. Proc.*, vol. 52, no. 3, pp. 820–825, Mar. 2004.

[98] E. Akay and E. Ayanoglu, "Achieving full frequency and space diversity in wireless systems via BICM, OFDM, STBC, and Viterbi decoding," *IEEE Trans. Commun.*, vol. 54, no. 12, pp. 2164–2172, Dec. 2006.

[99] L. Dossi, G. Tartara, and F. Tallone, "Statistical analysis of measured impulse response functions of 2.0 GHz indoor radio channels," *IEEE J. Select. Areas Commun.*, vol. 14, no. 3, pp. 405–410, Apr. 1996.

[100] J. G. Proakis, *Digital Communications*, 4th ed. McGraw-Hill, 2001.

[101] V. Erceg, K. S. Hari, M. Smith, D. Baum, K. Sheikh, C. Tappenden, J. Costa, C. Bushue, A. Sarajedini, R. Schwartz, D. Branlund, T. Kaitz, and D. Trinkwon, "Channel models for fixed wireless applications," IEEE 802.16 Broadband Wireless Access, IEEE 802.16.3c-01/29r4, 2001.

[102] M. Russell and G. L. Stüber, "Interchannel interference analysis of OFDM in a mobile environment," in *Proc. VTC*, 1995, vol. 2, pp. 820–824.

[103] H. Shin and J. H. Lee, "Performance analysis of space-time block codes over keyhole Nakagami-m fading channels," *IEEE Trans. Vehic. Tech.*, vol. 53, no. 2, pp. 351–362, Mar. 2004.

[104] K. Chugg, A. Anastasopoulos, and X. Chen, *Iterative Detection*. Kluwer Academic, 2001.

[105] J. Hagenauer, E. Offer, and L. Papke, "Iterative decoding of binary block and convolutional codes," *IEEE Trans. Inform. Theory*, vol. 42, no. 2, pp. 429–445, Mar. 1996.

[106] R. W. Hamming, "The Bell System Technical Journal," *Bell Syst. Tech. J.*, vol. XXVI, no. 2, pp. 147–160, Apr. 1950.

[107] Bluetooth SIG, *Specification of the Bluetooth System*, "Core system package," Version 1.2, Vol. 2, Nov. 4, 2004.

[108] K. Thaller and A. Steininger, "A transparent online memory test for simultaneous detection of functional faults and soft errors in memories," *IEEE Trans. on Reliab.*, vol. 52, no. 4, pp. 413–422, Dec. 2003.

[109] C. Desset and A. Fort, "Selection of channel coding for low-power wireless systems," in *Proc. VTC*, 2003, vol. 3, pp. 1920–1924.

[110] H. Nickl, J. Hagenauer, and F. Burkert, "Approaching Shannon's capacity limit by 0.27 db using simple Hamming codes," *IEEE Commun. Lett.*, vol. 1, no. 5, pp. 130–132, Sept. 1997.

[111] S. B. Wicker, *Error Control Systems for Digital Communication and Storage*. Prentice Hall, 1995.

[112] H.-F. Lu, P. V. Kumar, and E.-H. Yang, "On the input-output weight enumerators of product accumulate codes," *IEEE Commun. Lett.*, vol. 8, no. 8, pp. 520–522, Aug. 2004.

[113] M. Plotkin, "Binary codes with specified minimum distance," *IRE Trans. Inform. Theory*, pp. 445–450, Sept. 1960.

[114] N. J. A. Sloane and D. S. Whitehead, "New family of single-error correcting codes," *IEEE Trans. Inform. Theory*, vol. IT-16, no. 6, pp. 717–719, Nov. 1970.

[115] C. L. Liu, B. G. Ong, and G. R. Ruth, "A construction scheme for linear and non-linear codes," *Discrete Math.*, vol. 4, pp. 171–184, 1973.

[116] F. J. MacWilliams and N. J. A. Sloane, *The Theory of Error-Correcting Codes*. North-Holland Publ., 1977.

[117] S. Benedetto and G. Montorsi, "Unveiling turbo codes: Some results on parallel concatenated coding schemes," *IEEE Trans. Inform. Theory*, vol. 42, no. 2, pp. 409–428, Mar. 1996.

[118] G. G. Apple and P. A. Wintz, "Exact determination of probability of bit error for perfect single error correcting codes," in *Proc. Hawaii Int. Conf. Syst. Sci.*, 1970, pp. 922–924.

[119] D. Torrieri, "Information-bit, information-symbol, and decoded-symbol error rates for linear block codes," *IEEE Trans. Commun.*, vol. 36, no. 5, pp. 613–617, May 1988.

[120] J. H. van Lint, *Coding Theory, Lecture Notes in Mathematics*. Springer-Verlag, 1971.

[121] P. K. Vitthaladevuni and M.-S. Alouini, "A tight upper bound on the BER of linear systematic block codes," *IEEE Commun. Lett.*, vol. 8, no. 5, pp. 299–301, May 2004.

[122] I. M. Jacobs, "Practical applications of coding," *IEEE Trans. Inform. Theory*, vol. IT-20, no. 3, pp. 305–310, May 1974.

[123] V. M. Jovanović and S. Z. Budišin, "On the coding gain of linear binary block codes," *IEEE Trans. Commun.*, vol. COM-32, no. 5, pp. 635–638, May 1984.

[124] M. R. Best, A. E. Brouwer, F. J. MacWilliams, A. M. Odlyzko, and N. J. Sloane, "Bounds for binary codes of length less than 25," *IEEE Trans. Inform. Theory*, vol. IT-24, no. 1, pp. 81–93, Jan. 1978.

[125] A. A. Ali, "Optimum time diversity for channels subject to pulse-burst interference," *IEE Proc. – Comm.*, vol. 143, no. 1, pp. 43–46, Feb. 1996.

[126] A. A. Ali and I. A. Al-Kadi, "On the use of repetition coding with binary digital modulations on mobile channels," *IEEE Trans. Vehic. Tech.*, vol. 38, no. 1, pp. 14–18, Feb. 1989.

[127] P. Loskot and N. C. Beaulieu, "A family of rate $1/2$ modified binary block repetition codes," in *Asilomar Conf. Sig., Syst. and Comp.*, 2004, vol. 2, pp. 1985–1989.

[128] P. Loskot and N. C. Beaulieu, "A family of low-complexity binary linear codes for Bluetooth and BLAST signaling applications," *IEEE Commun. Lett.*, vol. 9, no. 12, pp. 1061–1063, Dec. 2005.

[129] M. Karlin, "New binary coding results by circulants," *IEEE Trans. Inform. Theory*, vol. IT-15, no. 1, pp. 81–92, Jan. 1969.

[130] H. H. Ma and J. K. Wolf, "On tail biting convolutional codes," *IEEE Trans. Commun.*, vol. COM-34, no. 2, pp. 104–111, Feb. 1986.

[131] I. E. Bocharova, M. Handlery, R. Johannesson, and B. D. Kudryashov, "Tailbiting codes obtained via convolutional codes with large active distance-slopes," *IEEE Trans. Inform. Theory*, vol. 48, no. 9, pp. 2577–2587, Sept. 2002.

[132] P. Ståhl, J. B. Anderson, and R. Johannesson, "Optimal and near-optimal encoders for short and moderate-length tail-biting trellises," *IEEE Trans. Inform. Theory*, vol. 45, no. 7, pp. 2562–2571, Nov. 1999.

[133] C. Weiß, C. Bettstetter, and S. Riedel, "Code construction and decoding of parallel concatenated tail-biting codes," *IEEE Trans. Inform. Theory*, vol. 47, no. 1, pp. 366–386, Jan. 2001.

[134] O. Milenkovic, I. B. Djordjevic, and B. Vasic, "Block-circulant low-density parity-check codes for optical communication systems," *IEEE J. Select. Topics Quantum Elect.*, vol. 10, no. 2, pp. 294–299, Mar./Apr. 2004.

[135] L. Chen, J. Xu, I. Djurdjevic, and S. Lin, "Near-shannon-limit quasi-cyclic low-density parity-check codes," *IEEE Trans. Commun.*, vol. 52, no. 7, pp. 1038–1042, July 2004.

[136] J. Xu, L. Chen, L. Zeng, L. Lan, and S. Lin, "Construction of low-density parity-check codes by superposition," *IEEE Trans. Commun.*, vol. 53, no. 2, pp. 243–251, Feb. 2005.

[137] J. Li, K. R. Narayanan, and C. N. Georghiades, "Product accumulate codes: A class of codes with near-capacity performance and low decoding complexity," *IEEE Trans. Inform. Theory*, vol. 50, no. 1, pp. 31–46, Jan. 2004.

[138] M. Yang, W. E. Ryan, and Y. Li, "Design of efficiently encodable moderate-length high-rate irregular LDPC codes," *IEEE Trans. Commun.*, vol. 52, no. 4, pp. 564–571, Apr. 2004.

[139] D. M. Rankin and T. A. Gulliver, "Single parity check product codes," *IEEE Trans. Commun.*, vol. 49, no. 8, pp. 1354–1362, Aug. 2001.

[140] S. Rajpal, D. J. Rhee, and S. Lin, "Multidimensional trellis coded phase modulation using a multilevel concatenation approach part I: Code design," *IEEE Trans. Commun.*, vol. 45, no. 1, pp. 64–72, Jan. 1997.

[141] M. P. C. Fossorier and S. Lin, "Soft-input soft-output decoding of linear block codes based on ordered statistics," in *Proc. GLOBECOM*, 1998, vol. 5, pp. 2828–2833.

[142] R. M. Pyndiah, "Near-optimum decoding of product codes: Block turbo codes," *IEEE Trans. Commun.*, vol. 46, no. 8, pp. 1003–1010, Aug. 1998.

[143] L. Tolhuizen and S. B. adn E. Hekstra-Nowacka, "Union bounds on the performance of product codes," in *Proc. ISIT*, 1998, p. 267.

[144] J. N. Laneman, D. N. C. Tse, and G. W. Wornell, "Cooperative diversity in wireless networks: Efficient protocols and outage behavior," *IEEE Trans. Inform. Theory*, vol. 50, no. 12, pp. 3062–3080, Dec. 2004.

[145] T. E. Hunter, S. Sanayei, and A. Nostratinia, "Outage analysis of coded cooperation," *IEEE Trans. Inform. Theory*, vol. 52, no. 2, pp. 375–391, Feb. 2006.

[146] T. E. Hunter and A. Nosratinia, "Diversity through coded cooperation," *IEEE Trans. Wireless Commun.*, vol. 5, no. 2, pp. 1–7, Feb. 2006.

[147] S. Yang and J. C. Belfiore, "A novel two-relay three-slot amplify-and-forward cooperative scheme," in *Proc. CISS*, 2006, vol. 1, pp. 1–6.

[148] B. S. Mergen and A. Scaglione, "Randomized space-time coding for distributed cooperative communication: Franctional diversity," in *Proc. ICASSP*, 2006, vol. 4, pp. IV–677–IV–680.

[149] D. Chen and J. N. Laneman, "Noncoherent demodulation for cooperative diversity in wireless systems," in *Proc. GLOBECOM*, 2004, vol. 1, pp. 31–35.

[150] P. Koopman and T. Chakravarty, "Cyclic redundancy code (CRC) polynomial selection for embedded networks," in *Proc. DSN*, 2004, pp. 145–154.

[151] R. A. Silverman and M. Balser, "Coding for a constant data rate source," *IRE Trans. Inform. Theory*, vol. PG IT-4, no. 4, pp. 50–63, Sept. 1954.

[152] D. Chase, "A class of algorithms for decoding block codes with channel measurement information," *IEEE Trans. Inform. Theory*, vol. IT-18, no. 1, pp. 170–181, Jan. 1972.

[153] P. Loskot and N. C. Beaulieu, "A family of low complexity adaptive binary linear block codes," in *Proc. GLOBECOM*, 2006.

[154] G. L. Stüber, "Soft decision direct-sequence DPSK receivers," *IEEE Trans. Vehic. Tech.*, vol. 37, no. 3, pp. 151–157, Aug. 1988.

[155] P. Ho and D. K. P. Fung, "Error performance of interleaved trellis-coded PSK modulations in correlated rayleigh fading channels," *IEEE Trans. Commun.*, vol. 40, no. 12, pp. 1800–1809, Dec. 1992.

[156] S. M. Kay, *Fundamentals of Statistical Signal Processing: Estimation Theory*, vol. I. Prentice Hall, 1993.

[157] N. C. Beaulieu and C. Leung, "On the performance of three suboptimum detection schemes for binary singaling," *IEEE Trans. Commun.*, vol. COM-33, no. 3, pp. 241–245, Mar. 1985.

[158] N. C. Beaulieu, "Comment on 'calculating binomial probabilities when the trial probabilities are unequal'," *J. Stat. Computation and Simul.*, vol. 20, no. 4, pp. 327–328.

[159] R. Knopp and H. Leib, "M-ary phase coding for the noncoherent AWGN channel," *IEEE Trans. Inform. Theory*, vol. 40, no. 6, pp. 1968–1984, Nov. 1994.

[160] D. Tse and P. Viswanath, *Fundamentals of Wireless Communication*. Cambridge Univ. Press, 2005.

[161] L. Zheng and D. N. C. Tse, "Diversity and multiplexing: A fundamental tradeoff in multiple-antenna channels," *IEEE Trans. Inform. Theory*, vol. 5, no. 49, pp. 1073–1096, May 2003.

[162] E. W. Weisstein, "Hypersphere," From *MathWorld* – A Wolfram Web Resource, http://mathworld.wolfram.com/Hypersphere.html.

[163] N. J. A. Sloane, "Sequences A072478, A072479, and A074457 in 'The On-Line Encyclopedia of Integer Sequences'," http://www.research.att.com/~njas/sequences/.

[164] F. L. Lionnais, *Les nombres remarquables*. Paris: Hermann, 1983.

[165] D. Wells, *The Penguin Dictionary of Curious and Interesting Numbers*. Penguin, 1986.

[166] P. Loskot and N. C. Beaulieu, "On monotonicity of the hypersphere volume and area," *J. Geom.*, 2007, to appear.

[167] P. Loskot and N. C. Beaulieu, "Sample rejection for efficient simulation of binary coding schemes over quantized additive white Gaussian noise channels," *IEEE Trans. Commun.*, vol. 53, no. 7, pp. 1145–1154, July 2005.

[168] M. Abramowitz and I. A. Stegun, *Handbook of Mathematical Functions with Formulas, Graphs, and Mathematical Tables*. Dover, 1974.

[169] H. Suzuki, "A statistical model for urban radio propagation," *IEEE Trans. Commun.*, vol. COM-25, no. 7, pp. 673–680, July 1977.

[170] A. Goldsmith and S.-G. Chua, "Variable-rate variable-power MQAM for fading channels," *IEEE Trans. Commun.*, vol. 45, no. 10, pp. 1218–1230, Oct. 1997.

[171] G. Ungerboeck, "Channel coding with multilevel/phase signals," *IEEE Trans. Inform. Theory*, vol. IT-28, no. 1, pp. 55–67, Jan. 1982.

[172] D. G. Brennan, "Linear diversity combining techniques," *Proc. IRE*, vol. 47, pp. 1075–1102, June 1959.

[173] S. Krusevac, P. B. Rapajic, R. A. Kennedy, and P. Sadeghi, "Mutual coupling effect on thermal noise in multi-antenna wireless communication systems," in *Proc. Austral. Comm. Th. Workshop*, 2005, pp. 209–214.

[174] T. M. Cover and J. A. Thomas, *Elements of information theory*, 2nd ed. John Wiley & Sons, 1991.

[175] I. E. Telatar, "Capacity of multi-antenna Gaussian channels," *European Trans. Telecommun.*, vol. 10, no. 6, pp. 585–595, Nov./Dec. 1999.

[176] A. M. Mathai and S. B. Provost, *Quadratic Forms in Random Variables*, 1st ed. Marcel Dekker, 1992.

[177] N. L. Johnson and S. Kotz, *Distributions in Statistics: Continuous Multivariate Distributions*, 1st ed. John Wiley & Sons, Inc., 1972.

[178] G. L. Turin, "The characteristic function of hermitian quadratic forms in complex normal variables," *Biometrika*, vol. 47, pp. 199–201, June 1960.

Appendix A

Definitions of functions are provided.

The MGF of RV, X, [66]

$$\Phi_X(t) = \mathrm{E}\left[\mathrm{e}^{xt}\right] = \int_{\mathrm{dom}(X)} f_x(x)\,\mathrm{e}^{xt}\,\mathrm{d}x \tag{A-1a}$$

the inverse MGF of RV, X,

$$f_X(x) = \frac{1}{2\pi\mathrm{j}} \int_{c-\mathrm{j}\omega}^{c+\mathrm{j}\omega} \Phi_X(t)\,\mathrm{e}^{-xt}\mathrm{d}t \tag{A-1b}$$

where $t = c + \mathrm{j}\omega$, and $c, \omega \in \mathbb{R}$, and c is chosen in the region of convergence

the upper incomplete MGF of RV, X,

$$\phi_X(t, x) = \int_x^{\infty} f_x(x)\,\mathrm{e}^{xt}\,\mathrm{d}x \tag{A-1c}$$

Q-function [21, (2-1-97)]

$$\begin{aligned} Q(x) &= \frac{1}{\sqrt{2\pi}} \int_x^{\infty} \mathrm{e}^{-t^2/2}\mathrm{d}t \\ &= \frac{1}{2}\mathrm{erfc}\left(\frac{x}{\sqrt{2}}\right) \end{aligned} \tag{A-2}$$

and the alternative form [66]

$$Q(x) = \frac{1}{\pi} \int_0^{\pi/2} \exp\left(-\frac{x^2}{2\sin^2\phi}\right) \mathrm{d}\phi$$

gamma function (Euler's integral form) [62, 8.310], [168, p. 255]

$$\Gamma(z) = \int_0^{\infty} t^{z-1}\,\mathrm{e}^{-t}\mathrm{d}t \tag{A-3}$$

where $\mathrm{Re}\{z\} > 0$, and

$$\Gamma\left(\frac{n}{2}\right) = \begin{cases} (n/2-1)! & n \text{ is even} \\ \frac{\sqrt{\pi}(n-2)!!}{2^{n/2-1/2}} & n \text{ is odd} \end{cases}$$

where $n!! = \frac{n!}{2^{n/2-1/2}(n/2-1/2)!} = n(n-2)\cdots 5\cdot 3\cdot 1$

upper incomplete gamma function [168]

$$\Gamma(z,x) = \int_x^\infty t^{z-1}\,\mathrm{e}^{-t}\mathrm{d}t \tag{A-4a}$$

for $z \in \mathbb{R}$, and

$$\Gamma(n,x) = \Gamma(n)\,\mathrm{e}^{-x}\sum_{k=0}^{n-1}\frac{x^k}{k!} \tag{A-4b}$$

for $n \in \mathbb{Z}$, $n \geq 0$

n-th order modified Bessel function of the first kind [21, (2-1-120)], [168]

$$I_n(z) = \frac{1}{\pi}\int_0^\pi \mathrm{e}^{z\cos(\theta)}\cos(n\theta)\mathrm{d}\theta \tag{A-5a}$$

$$= \sum_{k=0}^\infty \frac{\left(\frac{x}{2}\right)^{n+2k}}{k!\Gamma(n+k+1)} \tag{A-5b}$$

where $n \in \mathbb{Z}$, $n \geq 0$, and $z \geq 0$

beta function [62, 8.38]

$$B(a,b) = \frac{\Gamma(a)\,\Gamma(b)}{\Gamma(a+b)} \tag{A-6}$$

incomplete beta function [55]

$$\beta_z(a,b) = \int_0^z u^{a-1}(1-u)^{b-1}\mathrm{d}u \tag{A-7}$$

hypergeometric functions [21, (2-1-134)], [55]

$${}_1F_1(a,b;x) = \sum_{k=0}^\infty \frac{\Gamma(a+k)\,\Gamma(b)\,x^k}{\Gamma(a)\,\Gamma(b+k)\,k!} \tag{A-8a}$$

$${}_2F_1\left(\frac{n}{2}+\frac{1}{2},\frac{1}{2};\frac{3}{2};x\right) = \frac{1}{B(\frac{1}{2},1)}\int_0^1 u^{-\frac{1}{2}}(1-u\,x)^{-(\frac{n}{2}+\frac{1}{2})}\mathrm{d}u \tag{A-8b}$$

where $b \neq 0, -1, -2, \cdots$, and $B(\cdot,\cdot)$ is the beta function (A-6)

n-th order Marcum Q-function [21, (2-1-122)]

$$Q_n(a,b) = Q_1(a,b) + \mathrm{e}^{(a^2+b^2)/2} \sum_{k=1}^{m-1} \left(\frac{b}{a}\right)^k I_k(ab) \tag{A-9a}$$

where

$$Q_1(a,b) = \mathrm{e}^{-(a^2+b^2)/2} \sum_{k=0}^{\infty} \left(\frac{a}{b}\right)^k I_k(ab) \tag{A-9b}$$

and $b > a > 0$

p-th vector norm, l_p, of the vector, $\mathbf{a} = (a_1, a_2, \cdots, a_n)$

$$\|\mathbf{a}\|_p = \begin{cases} \left(\sum_{i=1}^n |a_i|^p\right)^{1/p} & 0 < p < \infty \\ \max\limits_{i=1,2,\cdots,n} |a_i| & p \to \infty \end{cases} \tag{A-10}$$

Kronecker delta

$$\delta_{a-b} = \begin{cases} 1 & a = b \\ 0 & \text{otherwise} \end{cases} \tag{A-11}$$

and equivalently, $\delta_{ab} = \delta_{a,b} = \delta_{(a-b)0} = \delta_{a-b}$, for $a, b = \cdots, -1, 0, 1, \cdots$

modulo operation

$$\mathrm{mod}_a(b) = b - \left\lfloor \frac{b}{a} \right\rfloor a \tag{A-12}$$

for $a, b = \cdots, -1, 0, 1, \cdots$

binomial coefficient

$$\binom{b}{a} = \begin{cases} \frac{b!}{a!(b-a)!} & b \geq a \geq 0 \\ 0 & \text{otherwise} \end{cases} \tag{A-13}$$

for $a, b = \cdots, -1, 0, 1, \cdots$

signum function

$$\mathrm{sign}(x) = \begin{cases} 1 & x > 1 \\ 0 & x = 0 \\ -1 & x < 0 \end{cases} \tag{A-14}$$

Heaviside (unit-step) function

$$\eta(x) = \begin{cases} 1 & x \geq 0 \\ 0 & x < 0 \end{cases} \tag{A-15}$$

Appendix B

The GCQ rule to invert the MGF, $\Phi_X(t) = \int_0^\infty \mathrm{e}^{tx} f_X(x)\mathrm{d}x$, of the random variable, X, is obtained. Hence, let an auxiliary complex-valued variable, $t = c + \mathrm{j}\omega$, where $c, \omega \in \mathbb{R}$. Then, for $\omega = c\sqrt{1-u^2}/u$, one has that [66],

$$\begin{aligned} f_X(x) &= \frac{1}{2\pi\mathrm{j}} \int_{c-\mathrm{j}\omega}^{c+\mathrm{j}\omega} \Phi_X(t)\, \mathrm{e}^{-xt}\mathrm{d}t \\ &= \frac{1}{2\pi} \int_{-\infty}^{\infty} \Phi_X(c+\mathrm{j}\omega)\, \mathrm{e}^{-x(c+\mathrm{j}\omega)}\mathrm{d}\omega \\ &= \frac{1}{2\pi} \int_{-1}^{1} \Phi_X\left(c + \mathrm{j}c\frac{\sqrt{1-u^2}}{u}\right) \mathrm{e}^{-x\left(c+\mathrm{j}c\frac{\sqrt{1-u^2}}{u}\right)} \frac{c\,\mathrm{d}u}{u^2\sqrt{1-u^2}} \\ &\approx \frac{1}{2\nu} \sum_{l=1}^{\nu} \Phi_X\left(c(1+\mathrm{j}\tau_l)\right)\, \mathrm{e}^{-xc(1+\mathrm{j}\tau_l)} c\,(1+\tau_l^2) \end{aligned}$$

where $\nu \gg 1$, $\tau_l = \tan((l-1/2)\pi/\nu)$, and c is chosen in the region of convergence, i.e., $\max \mu^- < c < \min \mu^+$, where μ^+ and μ^- denote the positive and negative residues of $\Phi_X(t)\,\mathrm{e}^{-xt}$, respectively.

Appendix C

The statistics of the Ricean distributed amplitude, $g \geq 0$, and the non-central chi-square distributed squared amplitude, g^2, are summarized. The PDF's are written as, [21]

$$f_g(g) = \begin{cases} \frac{g^{n-1}}{2^{n/2-1}\sigma^n \Gamma\left(\frac{n}{2}\right)} \mathrm{e}^{-g^2/2\sigma^2} & s = 0 \\ \frac{g^{n/2}}{\sigma^2 s^{n/2-1}} \mathrm{e}^{-(g^2+s^2)/2\sigma^2} I_{n/2-1}\left(\frac{gs}{\sigma^2}\right) & s > 0 \end{cases} \tag{C-1a}$$

$$f_{g^2}(g^2) = \frac{1}{2g} f_g(g) \quad s \geq 0 \tag{C-1b}$$

where n denotes the number of degrees-of-freedom, σ^2 is the variance per dimension, $\Gamma(\cdot)$ is the gamma function, and $I_n(\cdot)$ is the n-th order modified Bessel function of the first kind; see Appendix A. Using the infinite series representation (A-5b), one can express the CDF's as,

$$F_g(g) = \begin{cases} 1 - \frac{\Gamma\left(n/2, g^2/2\sigma^2\right)}{\Gamma(n/2)} & s = 0 \\ \mathrm{e}^{-s^2/2\sigma^2} \sum_{k=0}^{\infty} \frac{(s/\sigma)^{2k}}{k!\, 2^k \Gamma(n/2+k)} \left(\Gamma\left(k+\frac{n}{2}\right) - \Gamma\left(k+\frac{n}{2}, g^2/2\sigma^2\right)\right) & s > 0 \end{cases} \tag{C-2a}$$

$$F_{g^2}(g^2) = F_g(g) \quad s \geq 0 \tag{C-2b}$$

where $\Gamma(\cdot,\cdot)$ is the incomplete gamma function; see (A-4a). The upper incomplete MGF's, $\phi_g(t,x)$, and, $\phi_{g^2}(t,x)$, can be derived as (see Appendix A),

$$\phi_g(t,x) = \sum_{k=0}^{\infty} \frac{\mathrm{e}^{-s^2/2\sigma^2}}{2^{k-1}} \left(\frac{s}{\sigma}\right)^{2k} \int_{x/\sqrt{2}\sigma}^{\infty} \mathrm{e}^{-u^2+\sqrt{2}\sigma t\, u} u^{n-1+2k} \mathrm{d}u \tag{C-3a}$$

$$\phi_{g^2}(t,x) = \mathrm{e}^{\frac{s^2 t}{1-2\sigma^2 t}} (1-2\sigma^2 t)^{-n/2} Q_{n/2-1}\left(\frac{s/\sigma}{\sqrt{1-2\sigma^2 t}}, \frac{\sqrt{x(1-2\sigma^2 t)}}{\sigma}\right) \tag{C-3b}$$

where $Q_n(\cdot,\cdot)$ is the n-th order Marcum Q-function; see (A-9a). The MGF's, $\Phi_g(t)=\mathrm{E}\left[\mathrm{e}^{gt}\right]$, and, $\Phi_{g^2}(t)=\mathrm{E}\left[\mathrm{e}^{g^2t}\right]$, can be obtained as [21] (see Appendix A),

$$\Phi_g(t) = \begin{cases} \mathrm{e}^{-s^2/2\sigma^2}\left({}_1F_1\left(\frac{n}{2},\frac{1}{2},\frac{t^2\sigma^2}{2}\right)+\sqrt{2}\sigma t\frac{\Gamma(n/2+1/2)}{\Gamma(n/2)}{}_1F_1\left(\frac{n}{2}+\frac{1}{2},\frac{3}{2},\frac{t^2\sigma^2}{2}\right)\right) & s=0 \\ \mathrm{e}^{-s^2/2\sigma^2}\sum_{k=0}^{\infty}\frac{(s^2/2\sigma^2)^k}{k!}\left({}_1F_1\left(k+\frac{n}{2},\frac{1}{2},\frac{t^2\sigma^2}{2}\right)+\right. & \\ \left.\sqrt{2}\sigma\, t\frac{\Gamma(k+n/2+1/2)}{\Gamma(k+n/2)}{}_1F_1\left(k+\frac{n+1}{2},\frac{3}{2},\frac{t^2\sigma^2}{2}\right)\right) & s>0 \end{cases} \tag{C-4a}$$

$$\Phi_{g^2}(t) = (1-2\sigma^2t)^{-n/2}\exp\left(\frac{t\,s^2}{1-2\sigma^2t}\right) \qquad s\geq 0 \tag{C-4b}$$

where t is a complex dummy variable, $t=c+\mathrm{j}\omega$, and $c,\omega\in\mathbb{R}$ are real numbers, and ${}_1F_1(\cdot,\cdot,\cdot)$ is the hypergeometric function; see (A-8a).

Appendix D

The MGF's of two transformed RV's are obtained assuming knowledge of the MGF, $\Phi_X(t)$, of the RV, X. In particular, the MGF of the RV, $Y = \tilde{a}X + \tilde{b}$, where $\tilde{a}, \tilde{b} \in \mathbb{R}$ are constants, is, $\Phi_Y(t) = \mathrm{E}\Big[\,\mathrm{e}^{(\tilde{a}x+\tilde{b})t}\Big] = \mathrm{e}^{\tilde{b}t}\Phi_Y(\tilde{a}t)$.

Consider also the RV, $Y = \tilde{a}X^2$, for $\tilde{a} > 0$. Recall that [53],

$$f_Y(y) = \begin{cases} \frac{1}{2\sqrt{\tilde{a}y}}\left(f_X\left(\sqrt{y/\tilde{a}}\right) + f_X\left(-\sqrt{y/\tilde{a}}\right)\right) & x \in \mathbb{R} \\ \frac{1}{2\sqrt{\tilde{a}y}}\, f_X\left(\sqrt{y/\tilde{a}}\right) & x \geq 0. \end{cases}$$

Correspondingly,

$$f_Y(y) = \begin{cases} \frac{1}{\pi \mathrm{j}}\frac{1}{2\sqrt{y\tilde{a}}}\int_{c-\mathrm{j}\omega}^{c+\mathrm{j}\omega} \Phi_X(t)\cosh(t\sqrt{y/\tilde{a}})\mathrm{d}t & x \in \mathbb{R} \\ \frac{1}{2\pi \mathrm{j}}\frac{1}{2\sqrt{y\tilde{a}}}\int_{c-\mathrm{j}\omega}^{c+\mathrm{j}\omega} \Phi_X(t)\,\mathrm{e}^{-t\sqrt{y/\tilde{a}}}\mathrm{d}t & x \geq 0. \end{cases}$$

One has that, for $\mathrm{Re}\{r\} < 0$,

$$\begin{aligned} 2\int_0^\infty \mathrm{e}^{r\tilde{a}u^2}\cosh(su)\mathrm{d}u &= \sqrt{\tfrac{\pi}{-\tilde{a}r}}\,\mathrm{e}^{-\frac{s^2}{4\tilde{a}r}} \\ \int_0^\infty \mathrm{e}^{r\tilde{a}u^2 - su}\mathrm{d}u &= \sqrt{\tfrac{\pi}{-\tilde{a}r}}\,\mathrm{e}^{-\frac{s^2}{4\tilde{a}r}}Q\Big(\tfrac{s}{\sqrt{-2\tilde{a}r}}\Big). \end{aligned}$$

After some manipulations, the MGF, $\Phi_Y(t) = \mathrm{E}\Big[\,\mathrm{e}^{\tilde{a}x^2 t}\Big]$, is,

$$\Phi_Y(t) = \begin{cases} \frac{1}{\sqrt{\pi}\mathrm{j}}\int_{c-\mathrm{j}\infty}^{c+\mathrm{j}\infty} \Phi_X(2\sqrt{-\tilde{a}t}u)\,\mathrm{e}^{u^2}\mathrm{d}u & x \in \mathbb{R} \\ \frac{1}{\sqrt{\pi}\mathrm{j}}\int_{c-\mathrm{j}\infty}^{c+\mathrm{j}\infty} \Phi_X(2\sqrt{-\tilde{a}t}u)\,\mathrm{e}^{u^2}Q(\sqrt{2}u)\,\mathrm{d}u & x \geq 0 \end{cases}$$

where $u = c + \mathrm{j}\omega$, $u, \omega \in \mathbb{R}$, $\mathrm{Re}\{t\} < 0$.

Appendix E

We obtain the correlation coefficient, $\rho_{\tilde{W}_i\tilde{W}_j}$, of the i-th and j-th diagonal elements, $\tilde{W}_i$, and, $\tilde{W}_j$, of the non-central Wishart matrix, $\tilde{\mathbf{W}}$ (cf. Appendix F). Assume that all columns of the matrix, $\mathbf{G}$, have the same covariance matrix, so that, $\mathbf{C_G} = 2m\mathbf{C_g}$. Then, for $i, j = 1, \cdots, K$, we evaluate the moments,

$$\begin{aligned}
\mathrm{E}\Big[\tilde{W}_i\tilde{W}_j\Big] &= \frac{\partial^2}{\partial s_i \partial s_j}\,\Phi_{\tilde{\mathbf{W}}}(\mathbf{S})\big|_{\mathbf{S=0}} \\
\mathrm{E}\Big[\tilde{W}_i\Big] &= \frac{\partial}{\partial s_i}\,\Phi_{\tilde{\mathbf{W}}}(\mathbf{S})\big|_{\mathbf{S=0}} \\
\mathrm{E}\Big[\tilde{W}_i^2\Big] &= \frac{\partial^2}{\partial s_i^2}\,\Phi_{\tilde{\mathbf{W}}}(\mathbf{S})\big|_{\mathbf{S=0}}
\end{aligned}$$

and substituting into the definition of $\rho_{\tilde{W}_i\tilde{W}_j}$, one obtains that,

$$\begin{aligned}
\rho_{\tilde{W}_i\tilde{W}_j} &= \frac{\mathrm{E}\Big[(\tilde{W}_i - \mathrm{E}\Big[\tilde{W}_i\Big])(\tilde{W}_j - \mathrm{E}\Big[\tilde{W}_j\Big])\Big]}{\sqrt{\mathrm{E}\Big[(\tilde{W}_i - \mathrm{E}\Big[\tilde{W}_i\Big])^2\Big]\,\mathrm{E}\Big[(\tilde{W}_j - \mathrm{E}\Big[\tilde{W}_j\Big])^2\Big]}} \\
&= \frac{[\mathbf{C_G}]_{ij}[\mathbf{C_G}]_{ji} + [\bar{\mathbf{M}}_{\mathbf{G}}]_{ij}[\mathbf{C_G}]_{ji} + [\bar{\mathbf{M}}_{\mathbf{G}}]_{ji}[\mathbf{C_G}]_{ij}}{\sqrt{[\mathbf{C_G}]_{ii}([\mathbf{C_G}]_{ii} + 2[\bar{\mathbf{M}}_{\mathbf{G}}]_{ii})[\mathbf{C_G}]_{jj}([\mathbf{C_G}]_{jj} + 2[\bar{\mathbf{M}}_{\mathbf{G}}]_{jj})}}
\end{aligned}$$

where $\bar{\mathbf{M}}_{\mathbf{G}} = \bar{\mathbf{G}}\bar{\mathbf{G}}^T$, $\bar{\mathbf{G}} = \mathrm{E}[\mathbf{G}]$, and $[\cdot]_{ij}$ is the matrix element corresponding to the i-th row and the j-th column.

Appendix F

We derive the MGF of a non-central Wishart matrix, $\tilde{\mathbf{W}} \in \mathbb{R}^{K\times K}$, [176]. In general, let, $\tilde{\mathbf{W}} = \mathbf{G}\mathbf{G}^T$, where $\mathbf{G} = [\mathbf{g}_1, \mathbf{g}_2, \cdots, \mathbf{g}_{2m}] \in \mathbb{R}^{K\times 2m}$ is the real-valued jointly Gaussian matrix having the columns, $\mathbf{g}_i$, $i = 1, \cdots, 2m$, and the means, $\bar{\mathbf{G}} = \mathrm{E}[\mathbf{G}] = [\bar{\mathbf{g}}_1, \bar{\mathbf{g}}_2, \cdots, \bar{\mathbf{g}}_{2m}]$. The vectors, $\mathbf{g}_i$, are assumed to be mutually uncorrelated, and thus, independent. Then, using lemma (L3) in Appendix G, the covariance matrix of $\mathbf{G}$ can be written as,

$$\mathbf{C}_{\mathbf{G}} = \mathrm{E}\big[(\mathbf{G} - \bar{\mathbf{G}})(\mathbf{G} - \bar{\mathbf{G}})^T\big] = \sum_{i=1}^{2m} \mathbf{C}_{\mathbf{g}_i}$$

where $\mathbf{C}_{\mathbf{g}_i} = \mathrm{E}\big[(\mathbf{g}_i - \bar{\mathbf{g}}_i)(\mathbf{g}_i - \bar{\mathbf{g}}_i)^T\big]$ is the covariance matrix of the vector, $\mathbf{g}_i$. The PDF of $\mathbf{G}$ is given as [100],

$$p_{\mathbf{G}}(\mathbf{G}) = \prod_{i=1}^{2m} p_{\mathbf{g}_i}(\mathbf{g}_i) = \prod_{i=1}^{2m} \frac{\exp\left(-\frac{1}{2}(\mathbf{g}_i - \bar{\mathbf{g}}_i)^T \mathbf{C}_{\mathbf{g}_i}(\mathbf{g}_i - \bar{\mathbf{g}}_i)\right)}{\sqrt{(2\pi)^K \det(\mathbf{C}_{\mathbf{g}_i})}}.$$

Correspondingly, using again lemma (L3) in Appendix G, one has that the MGF of $\tilde{\mathbf{W}}$ is,

$$\Phi_{\tilde{\mathbf{W}}}(\mathbf{S}) = \mathrm{E}\Big[\,\mathrm{e}^{\mathrm{tr}\{\mathbf{S}\tilde{\mathbf{W}}\}}\Big] = \prod_{i=1}^{2m} \mathrm{E}\Big[\,\mathrm{e}^{\mathbf{g}_i \mathbf{S} \mathbf{g}_i^T}\Big] \tag{F-1}$$

where $\mathbf{S} = \mathrm{diag}(s_1, s_2, \cdots, s_K)$ is a diagonal matrix of dummy variables, s_i. Substituting the PDF, $p_{\mathbf{G}}(\mathbf{G})$, into eq. (F-1), we get,

$$\mathrm{E}\Big[\,\mathrm{e}^{\mathrm{tr}\{\mathbf{S}\tilde{\mathbf{W}}\}}\Big] = \prod_{i=1}^{2m} \int_{\mathbb{R}^K} f_1(\mathbf{g}_i) f_2(\bar{\mathbf{g}}_i - \mathbf{g}_i) \mathrm{d}\mathbf{g}_i \tag{F-2}$$

where $f_1(\mathbf{g}_i) = \sqrt{(2\pi)^K \det\left(\frac{1}{2}\mathbf{S}^{-1}\right)}\, p_{\mathbf{g}_i}(\mathbf{g}_i)$, and $f_2(\mathbf{g}_i) = p_{\mathbf{g}_i}(\mathbf{g}_i + \bar{\mathbf{g}}_i)$. Thus, eq. (F-2) is a product of $2m$ convolutions of the functions $f_1(\mathbf{g}_i)$ and $f_2(\mathbf{g}_i)$. Since the convolution of two PDF's

gives the distribution of a sum of two independent random variables [53], and the sum of two independent jointly Gaussian random vectors is a Gaussian random vector with covariance matrix given by the sum of individual covariance matrices, one has that,

$$\Phi_{\tilde{\mathbf{W}}}(\mathbf{S}) = \prod_{i=1}^{2m} \frac{\exp\left(\bar{\mathbf{g}}_i^T(\mathbf{I} - 2\mathbf{S}\mathbf{C}_{\mathbf{g}_i})^{-1}\mathbf{S}\bar{\mathbf{g}}_i\right)}{\sqrt{\det(\mathbf{I} - 2\mathbf{S}\mathbf{C}_{\mathbf{g}_i})}}. \tag{F-3}$$

Furthermore, assuming that all columns of the matrix, $\mathbf{G}$, have the same covariance matrix, $\mathbf{C}_{\mathbf{g}_i} = \mathbf{C}_{\mathbf{g}}$, for $\forall i = 1, \cdots, 2m$, then $\mathbf{C}_{\mathbf{G}} = 2m\mathbf{C}_{\mathbf{g}}$, and using lemma (L1) in Appendix G, the PDF of $\mathbf{G}$ can be written as [177, Ch. 38, eq. (46)],

$$p_{\mathbf{G}}(\mathbf{G}) = \frac{\text{etr}\{-\frac{1}{2}\mathbf{C}_{\mathbf{G}}^{-1}(\mathbf{G} - \text{E}[\mathbf{G}])(\mathbf{G} - \text{E}[\mathbf{G}])^T\}}{(2\pi)^{Km}\det(\mathbf{C}_{\mathbf{G}})^m}.$$

Then, the MGF expression (F-3) can be simplified, and we obtain,

$$\Phi_{\tilde{\mathbf{W}}}(\mathbf{S}) = \frac{\text{etr}\{\bar{\mathbf{G}}^T(\mathbf{I} - 2\mathbf{S}\mathbf{C}_{\mathbf{G}})^{-1}\mathbf{S}\bar{\mathbf{G}}\}}{\det(\mathbf{I} - 2\mathbf{S}\mathbf{C}_{\mathbf{G}})^m}. \tag{F-4}$$

Finally, note that there is yet another form of the MGF (F-4) in the literature; particularly, [176, eq. (6.3.2)] and [177, Ch. 38, eq. (47)], however, both these expressions can be rearranged into the more compact form (F-4) by applying lemma (L4) in Appendix G. Also, for $s_1 = s_2 = \cdots = s_K = s$, and $m = 1$, one can obtain the MGF of a quadratic form, $\mathbf{g}^H\mathbf{A}\mathbf{g}$, where $\mathbf{g}$ is the jointly Gaussian complex-valued random vector, and the complex-valued matrix, $\mathbf{A}$, must be Hermitian [82, eq. (15)], [178]; however, the derivation in this appendix is simpler than the procedure used in [178].

Appendix G

The matrix lemmas are summarized. In general, consider the real-valued matrices, $\mathbf{A} \in \mathbb{R}^{m \times n}$, and, $\mathbf{B} \in \mathbb{R}^{m \times n}$. Then, we have the following matrix lemmas, [81].

(L1) $\mathrm{tr}\{\mathbf{A}\mathbf{B}^T\} = \mathrm{tr}\{\mathbf{B}\mathbf{A}^T\}$ where $\mathrm{tr}\{\cdot\}$ denotes the trace of the matrix

(L2) (Cauchy-Schwartz inequality) $\mathrm{tr}\{\mathbf{A}\mathbf{B}^T\}^2 \leq |\mathrm{tr}\{\mathbf{A}\mathbf{A}^T\}|\,|\mathrm{tr}\{\mathbf{B}\mathbf{B}^T\}|$ where $|\cdot|$ is the absolute value

(L3) $\mathbf{A}\mathbf{A}^T = \sum_{i=1}^{n} \mathbf{a}_i \mathbf{a}_i^T$ where $\mathbf{a}_i$ is the i-th column of $\mathbf{A}$, and $\mathbf{A}^T\mathbf{A} = \sum_{i=1}^{m} \mathbf{a}_i^T \mathbf{a}_i$ where $\mathbf{a}_i$ is the i-th row of $\mathbf{A}$

(L4) (Woodbury matrix identity) let $m = n$, and $\mathbf{A}$ and $\mathbf{B}$ be invertible, then $(\mathbf{I} + \mathbf{B}\mathbf{A})^{-1} = \mathbf{I} - (\mathbf{I} + (\mathbf{A}\mathbf{B})^{-1})^{-1}$

(L5) $\mathrm{E}_{\mathbf{B}}\left[\left\|\mathbf{A}\mathbf{B}^T\right\|^2\right] = \frac{1}{n}\|\mathbf{A}\|^2 \mathrm{E}_{\mathbf{B}}\left[\|\mathbf{B}\|^2\right]$, and $\mathrm{E}_{\mathbf{B}}\left[\left\|\mathbf{B}\mathbf{A}^T\right\|^2\right] = \frac{1}{m}\|\mathbf{A}\|^2 \mathrm{E}_{\mathbf{B}}\left[\|\mathbf{B}\|^2\right]$ where $\mathrm{E}_{\mathbf{B}}[\cdot]$ is expectation over the distribution of $\mathbf{B}$, and $\|\mathbf{A}\|$ is the Frobenius norm of the matrix, $\mathbf{A}$

Appendix H

The IOWE matrix, $\mathbf{A}_{(\text{iowe})}^{\mathscr{H}_{m+1}}$, of the $\mathscr{H}_{m+1} = (n_2, k_2, 3)$ code given $\mathbf{A}_{(\text{iowe})}^{\mathscr{H}_m}$ of the $\mathscr{H}_m = (n_1, k_1, 3)$ code is derived. Denote the i-th column and the j-th row of the matrix, $\mathbf{A}$, by $\text{col}(\mathbf{A})_i$ and $\text{row}(\mathbf{A})_j$, respectively, and the diagonal matrix with elements given by the vector, $\mathbf{a}$, as $\text{diag}(\mathbf{a})$. Let the vector, $\mathbf{T}_i = \left(\binom{i}{0}, \binom{i}{1}, \cdots, \binom{i}{i}\right)$, be the i-th row of the Pascal triangle. Let $\mathbf{x}$ be an arbitrary binary vector of length n_1 bits and weight w_x. Given $\mathbf{x}$, $\mathscr{C}(\mathbf{x}) = \{\mathbf{x} \circ \mathbf{y}, \mathbf{y} \in \mathbb{Z}_2^{n_1}\}$ is a $(2n_1, n_1, 2)$ code having the IOWE matrix

$$\text{col}\big(\mathbf{A}_{(\text{iowe})}(w_x)\big)_j = \begin{cases} \text{col}\big([\mathbf{T}_{w_x}^T \otimes \text{diag}(\mathbf{T}_{n_1 - w_x})]\big)_{(j-w_x)/2} \\ \qquad \text{if } j = w_x, w_x+2, \cdots, 2n_1 - w_x \\ \mathbf{0}_{(n_1+1,1)} \quad \text{otherwise} \end{cases}$$

for $j = 0, 1, \cdots, 2n_1$. Depending on parity $\pi(\mathbf{y})$ being even or odd, we can write $\mathbf{A}_{(\text{iowe})}(w_x) = \mathbf{A}_{(\text{iowe})}^{\text{e}}(w_x) + \mathbf{A}_{(\text{iowe})}^{\text{o}}(w_x)$ where

$$\text{row}\Big(\mathbf{A}_{(\text{iowe})}^{\text{e}}(w_x)\Big)_i = \begin{cases} \text{row}\big(\mathbf{A}_{(\text{iowe})}(w_x)\big)_i & i - \text{even} \\ \mathbf{0}_{(1,2n_1+1)} & \text{otherwise} \end{cases}$$

$$\text{row}\Big(\mathbf{A}_{(\text{iowe})}^{\text{o}}(w_x)\Big)_i = \begin{cases} \text{row}\big(\mathbf{A}_{(\text{iowe})}(w_x)\big)_i & i - \text{odd} \\ \mathbf{0}_{(1,2n_1+1)} & \text{otherwise} \end{cases}$$

for $i = 0, 1, \cdots, k$. Let $\mathbf{x} = (\mathbf{x}_1, \mathbf{x}_2)$ be the codeword of $\mathscr{H}_m = (n_1, k_1, 3)$ where $\mathbf{x}_1$ are information bits of weight, w_{x_1}, and $\mathbf{x}_2$ are the corresponding parity bits of weight, w_{x_2}. Using Theorem 6.1, the codewords of $\mathscr{H}_{m+1}$ are obtained by concatenation of the two codes, $\mathscr{C}_1(\mathbf{x}_1) = \{(\mathbf{x}_1 \circ \mathbf{y}_1), \mathbf{y}_1 \in \mathbb{Z}_2^{k_1}\}$, and, $\mathscr{C}_2(\mathbf{x}_2) = \{(\mathbf{x}_2 \circ \mathbf{y}_2), \mathbf{y}_2 \in \mathbb{Z}_2^{n_1 - k_1}\}$, and appending the parity bit, $\pi(\mathbf{y}_1) + \pi(\mathbf{y}_2)$. We can express the corresponding IOWE matrices of the codes $\mathscr{C}_1(\mathbf{x}_1)$ and $\mathscr{C}_2(\mathbf{x}_2)$

as,

$$\begin{aligned}\mathbf{A}_{(\text{iowe})}(w_{x_1}) &= \mathbf{A}^{\text{e}\mathscr{C}_1}_{(\text{iowe})}(w_{x_1}) + \mathbf{A}^{\text{o}\mathscr{C}_1}_{(\text{iowe})}(w_{x_1}) \\ \mathbf{A}_{(\text{iowe})}(w_{x_2}) &= \mathbf{A}^{\text{e}\mathscr{C}_2}_{(\text{iowe})}(w_{x_2}) + \mathbf{A}^{\text{o}\mathscr{C}_2}_{(\text{iowe})}(w_{x_2}).\end{aligned}$$

Then, using Claim 6.3, and summing over all input-output weights of the Hamming code $\mathscr{H}_m$, the IOWE matrix of the $\mathscr{H}_{m+1}$ code is

$$\left[\mathbf{A}^{\mathscr{H}_{m+1}}_{(\text{iowe})}\right]_{o,w} = \sum_{u=0}^{k_1}\sum_{v=0}^{n_1}\left[\mathbf{A}^{\mathscr{H}_m}_{(\text{iowe})}\right]_{u,v}\left[\mathbf{A}^{(\mathscr{C}_1,\mathscr{C}_2,\pi)}_{(\text{iowe})}(u,v)\right]_{o,w}$$

for $o = 0, 1, \cdots, k_2$, and $w = 0, 1, \cdots, n_2$, where

$$\begin{aligned}\mathbf{A}^{(\mathscr{C}_1,\mathscr{C}_2,\pi)}_{(\text{iowe})}(u,v) &= \{\text{diag}\Big(\mathbf{1}_{(1,k_1+n_1+1)}\mathbf{A}^{\text{e}\mathscr{C}_1}_{(\text{iowe})}(u)\Big) \otimes \mathbf{A}^{\text{e}\mathscr{C}_2}_{(\text{iowe})}(v-u) \\ &\quad + \text{diag}\Big(\mathbf{1}_{(1,k_1+n_1+1)}\mathbf{A}^{\text{o}\mathscr{C}_1}_{(\text{iowe})}(u)\Big) \otimes \mathbf{A}^{\text{o}\mathscr{C}_2}_{(\text{iowe})}(v-u)\} \otimes (1,0) \\ &\quad + \{\text{diag}\Big(\mathbf{1}_{(1,k_1+n_1+1)}\mathbf{A}^{\text{e}\mathscr{C}_1}_{(\text{iowe})}(u)\Big) \otimes \mathbf{A}^{\text{o}\mathscr{C}_2}_{(\text{iowe})}(v-u) \\ &\quad + \text{diag}\Big(\mathbf{1}_{(1,k_1+n_1+1)}\mathbf{A}^{\text{o}\mathscr{C}_1}_{(\text{iowe})}(u)\Big) \otimes \mathbf{A}^{\text{e}\mathscr{C}_2}_{(\text{iowe})}(v-u)\} \otimes (0,1).\end{aligned}$$

The computationally efficient expression (6.1) can be obtained by further manipulations and using Claim 6.4 and Corollary 6.5.

Vita

Pavel Loskot

EDUCATION

University of Alberta Edmonton, Canada	Ph.D. Student	Electrical and Computer Engineering January 2002 – present
Czech Technical University Prague, Czech Republic	M.Sc. (honors)	Radioelectronics September 1996 – June 1998
Czech Technical University Prague, Czech Republic	B.Sc. (honors)	Biomedical Engineering September 1992 – June 1996

WORK EXPERIENCE

Swansea University Swansea, United Kingdom	Lecturer	January 2007 – present
Centre for Wireless Comm. Oulu, Finland	Research Scientist	September 1999 – December 2001
Czech Technical University Prague, Czech Republic	Research Assistant Teaching Assistant	September 1998 – June 1999

AWARDS

Alberta Ingenuity and *i*CORE Scholarship	May 2003 – December 2006
Mary Louise Imrie Graduate Student Award	May 2004

PUBLICATIONS

[1] P. Loskot and N. C. Beaulieu, "On monotonicity of the hypersphere volume and area," *Journal of Geometry*, to appear.

[2] P. Loskot and N. C. Beaulieu, "A family of low-complexity binary linear codes for Bluetooth and BLAST signaling applications,". *IEEE Communications Letters*, vol. 9, pp. 1061–1063, December 2005.

[3] P. Loskot and N. C. Beaulieu, "Sample rejection for efficient simulation of binary coding schemes over quantized additive white Gaussian noise channels," *IEEE Transactions on Communications*, vol. 53, pp. 1145–1154, July 2005.

[4] D. P. Wiens, N. C. Beaulieu and P. Loskot, "The exact distribution of the sum of the largest $N - K$ out of N normal random variables with differing means," *Statistics*, vol. 40, pp. 165–173, April 2006.

[5] P. Loskot and N. C. Beaulieu, "The input-output weight enumeration of binary Hamming codes," *European Transactions on Telecommunications*, vol. 17, no. 4, pp. 483–488, July/Aug. 2006.

[6] P. Loskot and N. C. Beaulieu, "A hypergeometric analysis of diversity combining schemes and SNR adaptive receivers," submitted to *IEEE Transactions on Information Theory*, June 2007.

[7] P. Loskot and N. C. Beaulieu, "Prony and polynomial approximations for evaluation of the average probability of error over slowly fading channels," submitted to *IEEE Transactions on Vehicular Technology*, June 2007.

[8] P. Loskot and N. C. Beaulieu, "Binary repetition codes and their applications," submitted to *IEEE Transactions on Wireless Communications*, July 2007.

[9] P. Loskot and N. C. Beaulieu, "Binary block repetition codes and SPC product codes for coded and cooperative diversity systems," submitted to *IEEE Transactions on Communications*, July 2007.

[10] P. Loskot and N. C. Beaulieu, "A unified approach to computing error probabilities of diversity combining schemes over correlated fading channels," submitted to *IEEE Transactions on Communications*, July 2007.

[11] P. Loskot and N. C. Beaulieu, "Performance analysis of coded MIMO-OFDM systems over arbitrary correlated generalized Ricean fading channels," submitted to *IEEE Transactions on Communications*, July 2007.

[12] P. Loskot and N. C. Beaulieu, "Further results on Prony approximation for evaluation of the average probability of error," submitted to *IEEE International Conference on Communications, ICC 2008*, Beijing, China, 19–23, 2008.

[13] P. Loskot and N. C. Beaulieu, "A hypergeometric view on diversity combining schemes and SNR adaptive receivers," submitted to *IEEE International Conference on Communications, ICC 2008*, Beijing, China, 19–23, 2008.

[14] P. Loskot and N. C. Beaulieu, "Polynomial approximations for average error rate evaluations over slowly fading channels," *The 6th International Conference on Information, Communications and Signal Processing, ICICS 2007*, December 10–13, 2007, to appear.

[15] P. Loskot and N. C. Beaulieu, "A novel fading amplitude model and performance analysis of diversity combining schemes," *ChinaCom 2007*, Shanghai, China, August 22–24, 2007, to appear.

[16] P. Loskot and N. C. Beaulieu, "Binary block repetition codes and SPC product codes for coded and cooperative diversity systems," *IEEE International Conference on Communications, ICC 2007*, Glasgow, United Kingdom, June 24–28, 2007, to appear.

[17] P. Loskot and N. C. Beaulieu, "Some results on monotonicity of volume and surface area of objects in K dimensions," *The 10th Canadian Workshop on Information Theory, CWIT 2007*, Edmonton, Canada, pp. 188–192, June 6–8, 2007.

[18] P. Loskot and N. C. Beaulieu, "Multidimensional binary repetition codes," *IEEE Wireless Communications and Networking Conference, WCNC 2007*, Kowloon, Hong Kong, pp. 692–697, March 11–15, 2007.

[19] P. Loskot and N. C. Beaulieu, "A family of low complexity adaptive binary linear block codes," *IEEE GLOBECOM*, San Francisco, CA, pp. 1–6, November 27–December 1, 2006.

[20] P. Loskot and N. C. Beaulieu, "Performance analysis of coded MIMO-OFDM systems over generalized Ricean fading channels," *Canadian Conference on Electrical and Computer Engineering, CCECE 2006*, Ottawa, Canada, pp. 1634–1639, May 7–10, 2006.

[21] P. Loskot and N. C. Beaulieu, "Sample rejection for efficient simulation of intersymbol interference channels with MLSD," *IEEE Wireless Communications and Networking Conference, WCNC 2005*, New Orleans, Louisiana, pp. 911–916, March 13–17, 2005.

[22] P. Loskot and N. C. Beaulieu, "A recursive structure of binary Hamming codes," *The 38th Asilomar Conf. on Signals, Systems, and Computers*, Pacific Grove, CA, pp. 1136–1140, November 7–10, 2004.

[23] P. Loskot and N. C. Beaulieu, "A family of rate 1/2 modified binary block repetition codes," *The 38th Asilomar Conf. Signals, Systems, and Computers*, Pacific Grove, CA, pp. 1985–1989, November 7–10, 2004.

[24] P. Loskot and N. C. Beaulieu, "Maximum ratio combining with arbitrary correlated generalized Ricean branches," *IEEE Wireless Communications and Networking Conference, WCNC 2004*, Atlanta, Georgia, pp. 333–338, March 21–25, 2004.

[25] P. Loskot and N. C. Beaulieu, "Average error rate evaluation of digital modulations in slow fading by Prony approximation," *IEEE International Conference on Communications, ICC 2004*, Paris, France, pp. 3353–3357, June 20–24, 2004.

[26] P. Loskot and N. C. Beaulieu, "Efficient simulation of multidimensional communication systems by sample rejection," *IEEE International. Conference on Communications, ICC 2004*, Paris, France, pp. 2240–2245, June 20–24, 2004.

[27] P. Loskot, "Efficient techniques for performance analysis of communications systems," invited talk, VTT Technical Research Centre of Finland, Oulu, Finland, June 19, 2007.

[28] P. Loskot, "Computer simulations of coding schemes using sample rejection," Poster in *Alberta Ingenuity Workshop*, University of Alberta, Edmonton, Canada, March 5, 2004.

[29] P. Loskot, "Adaptive transmission schemes and cross-layer design," invited talk, Czech Technical University of Prague, January 10, 2003.